INVESTIGATION OF EMISSION CHARACTERISTICS AND DEVELOPMENT OF CONTROL TECHNIQUES TOWARDS COOKING OIL FUMES

HAN SHUWEN

PhD

The Hong Kong Polytechnic University

2024

The Hong Kong Polytechnic University

Department of Civil and Environmental Engineering

Investigation of Emission Characteristics and Development of Control Techniques Towards Cooking Oil Fumes

Han Shuwen

A thesis submitted in partial fulfillment of the requirements for the degree of Doctor of Philosophy

August 2023

CERTIFICATE OF ORIGINALITY

I hereby declare that this thesis is my own work and that, to the best of my knowledge and belief, it reproduces no material previously published or written, nor material that has been accepted for the award of any other degree or diploma, except where due acknowledgement has been made in the text.

______________________ (Signed)

Han Shuwen (Name of Student)

ABSTRACT

Air pollution has emerged as one of the most critical environmental challenges worldwide, particularly in heavily populated urban areas where human activities are concentrated. Cooking oil fumes (COFs) are the exhaust emission gases produced from the mixture of cooking oils, raw food materials and condiments with complicated physical and chemical transformations including decomposition, oxidation, and polymerization in high temperature conditions from the cooking processes. In this study, the analysis results of the five different types of cooking methods, i.e., stir-frying, pan-frying, deep-frying, boiling and steaming from the in-lab cooking simulation kitchen revealed the $PM_{2.5}$ concentration trend of stir-frying (381.66 μg/m^3) > deep-frying (235.88 μg/m^3) > pan-frying (146.87 μg/m^3) > boiling (88.13 μg/m^3) > steaming (38.58 μg/m^3). OC was found to be the dominant component with the proportions of 39.3% - 49.3% and high OC/EC ratios were obtained in all these cooking sources. Carcinogenic PAHs were also detected in $PM_{2.5}$ sampling which accounted for 29% to 49% of the total detected PAHs, indicating the existence of potential carcinogenic health risks. While the concentration trend of the total VOCs was observed as deep-frying (1166.2 μg/m^3) > pan-frying (937.0 μg/m^3) > stir-frying (897.3 μg/m^3) > boiling (692.4 μg/m^3) > steaming (133.4 μg/m^3), indicating the oil-based cooking methods emitted higher concentrations of $PM_{2.5}$ and VOCs than those from water-based cooking styles.

A field study of the COFs from four common commercial restaurants including Chinese fast food (CFF), Western fast food (WFF), Cantonese cuisine (CAN) and Chongqing hot pot (CHP) were investigated, and the concentrations of $PM_{2.5}$ in decreasing order were 269.85 μg/m^3, 232.11 μg/m^3, 199.95 μg/m^3, and 85.69 μg/m^3 for CAN, CFF, WFF, and CHP. The dominant cooking methods could be confirmed by the ratios of OC/EC and diagnostic analysis of PAHs. The VOC emission levels and composition profiles from the four restaurants were consistent with their major cooking methods with significant high VOC emissions of hexane, ethylene, and formaldehyde. Significant adverse environmental effects on the formation of O_3 and secondary organic aerosols were revealed by the results of their high chemical reactivity, OFP, and SOAFP. The highest unit formation rates for ozone and SOA were obtained from CAN as 5.55 g OFP/g VOCs and WFF as 2.17 g SOAFP/ g VOCs. In addition, health risk assessment by inhalation exposure suggested that significant carcinogenic risks existed to kitchen staff in all the restaurants and to the customers of CHP in particular.

Given the mitigation demands of the COFs due to their detrimental effects on environment and health, two promising control strategies by applying high gravity rotating packed bed scrubber and photocatalytic nanomaterial were investigated. The $PM_{2.5}$ and TVOC removal efficiency of the scrubber could be as high as 86% and 74%, respectively, as suggested by the results from the field trails, and the L_{OH}, OFP and SOAFP all exhibited superior improvement of 62.95%, 60.35%, and 61.05%, respectively. The successfully synthesized insulator-based STO/SCO nano-heterojunction was demonstrated to have degradation capabilities towards low-concentrated gaseous pollutants of NO and HCHO with removal efficiency of 44% and 40% respectively. And it could serve as a supplementary measure for degradation of excessive gaseous pollutants after scrubber.

In summary, this thesis presents the characterization and evaluation of the COFs from various scenarios, which provides a comprehensive emission inventory in Hong Kong and Asian areas. Moreover, novel control strategies were developed based on the features of COFs with satisfactory purification performance and promising application potential.

THE NOVELTY OF THIS STUDY

Air pollution has risen to become a severe global environmental concern, especially in densely populated cities where human activities are prevalent. Emissions of cooking oil fumes (COFs), which are the byproducts of the complex physical and chemical interactions during cooking processes, contribute a significant part to urban air pollution. The composition of COFs is extremely complicated, consisting of various compounds including fatty acids, aldehydes, ketones, esters, alcohols, hydrocarbons, and polycyclic aromatic hydrocarbons. And these chemical compounds can also potentially impact human health and the environment. In is urgently needed to fully understand the characteristics of COFs and develop efficient control methods. Although there were a few studies focused on the emissions from cooking processes, most of them were based on simulated processes in laboratory with limited cooking methods and scenarios. In this thesis, a systematical characterization of COFs from different cooking methods and various commercial kitchens focusing on the common cooking styles in Asia were conducted in Hong Kong for the first time. In addition, two promising COFs control methods including high gravity rotating packed bed (HiGee) scrubber and functional nanomaterials were developed and creatively applied in lab study and field trails.

The novelty of this thesis includes but is not confined to the following aspects:

(i) The concentrations and detailed chemical compositions of the $PM_{2.5}$ and VOCs were determined for all five common cooking methods in Hong Kong including stir-frying, deep-frying, pan-frying, boiling and steaming for the first time. The characteristic results provided the updated anthropogenic emission inventory and complemented the baseline for source identification of urban air pollution.

(ii) Evaluation of the COFs from four integrated commercial kitchens in Hong Kong were conducted systematically and both the environmental and health impacts were well assessed. These results pointed out the critical pollution situations and further guided the design and development of effective control techniques.

(iii) The high gravity rotating packed bed scrubber was creatively selected and developed for the application of COFs emission control. The developed surfactant made by the mixture of span 80 and Tween 80 were proven to be effective in removing both $PM_{2.5}$ pollutants and TVOC in field trails for the first time with the removal efficiency of 86% and 74%, respectively. The improvement of the environmental impacts was also confirmed by studying the L_{OH}, OFP and SOAFP in the application in real cooking processes.

(iv) Insulator-based STO/SCO nano-heterojunctions constructed by using the CN self-sacrificing hydrothermal synthesis method have been applied for the first time to purify the representative COF pollutants of NO and HCHO. A certain level of oxygen vacancies and the internal electric field were found to be formed at the interface of the insulator-based STO/SCO heterojunction, which maximized the utilization of solar energy to excite photocarriers and enhanced the transfer efficiency on its surface. The detected abundant ROS was generated by the combined effects of efficient photocarriers and stimulative O_2 activation, which enhanced the photo-degradation of NO and HCHO. The developed functional nanomaterial served as a supplementary to the HiGee scrubber in focus on the gaseous pollutants from the COF emissions as well.

PUBLICATIONS ARISING FROM THE THESIS

Journal Publications

1. **Han, S.**, Tan, Y., Gao, Y., Li, X., Ho, S.S.H., Wang, M. and Lee, S.C.*, 2023. Volatile organic compounds at a roadside site in Hong Kong: Characteristics, chemical reactivity, and health risk assessment. Science of The Total Environment, p.161370.

2. **Han, S.**, Li, X., Tan, Y., Huang, Y., Wu, Z., Wang, M., Ho, W. and Lee, S.C.*, 2023. In-situ self-sacrificed fabrication of insulator-based SrTiO3/SrCO3 heterojunction interface for gaseous HCHO and NO photocatalytic degradation. Applied Surface Science, 612, p.155806.

3. **Han, S.**, Tan, Y., Li, X., Ho, S.S.H., and Lee, S.C.*, Characterization and risk assessment of PM2.5-related air pollutants of cooking emissions from different cooking methods. Submitted to Science of The Total Environment.

4. Tan, Y., **Han, S.**, Chen, Y., Wu, Z. and Lee, S.C.*, 2023. Long-term variation and evaluation of air quality across Hong Kong. Journal of Environmental Sciences, 127, pp.284-294.

5. Tan, Y., **Han, S.**, Chen, Y., Zhang, Z., Li, H., Li, W., Yuan, Q., Li, X., Wang, T. and Lee, S.C.*, 2021. Characteristics and source apportionment of volatile organic compounds (VOCs) at a coastal site in Hong Kong. Science of The Total Environment, 777, p.146241.

6. Li, X., **Han, S.**, Wang, P., Mei, H., Ning, Z., Dong, F., Cui, L., Huang, Y., Wang, T., Leu, S.Y. and Wang, M., 2023. Application of roadside air purifiers in urban street

canyons: A pilot-scale study in Hong Kong. Science of The Total Environment, p.168671.

7. Li, X., Wang, P., **Han, S.**, Huang, Y., Ho, W., Ho, S.S.H., Lee, S.C.* and Wang, M., 2023. Development and application of photocatalytic coating for roadside NOx mitigation in Hong Kong. Chinese Chemical Letters, p.108709.

8. Li, X., Huang, Y., Ho, W., **Han, S.**, Wang, P., Lee, S.C.* and Zhang, Z., 2023. Modulation of Sulfur Vacancies at ZnIn2S4-δ/g-C3N4 Heterojunction Interface for Successive CH Secession in Photocatalytic Gaseous Formaldehyde Complete Oxidation. Applied Catalysis B: Environmental, p.123048.

9. Wang, M., Zhang, Z., Yuan, Q., Li, X., **Han, S.**, Lam, Y., Cui, L., Huang, Y., Cao, J. and Lee, S.C.*, 2022. Slower than expected reduction in annual PM2. 5 in Xi'an revealed by machine learning-based meteorological normalization. Science of The Total Environment, 841, p.156740.

10. Wang, M., Duan, Y., Xu, W., Wang, Q., Zhang, Z., Yuan, Q., Li, X., **Han, S.**, Tong, H., Huo, J. and Chen, J., Gao, S., Wu, Z., Cui, L., Huang, Y., Xiu, G., Cao, J., Fu, Q.*, Lee, S.C.* 2022. Measurement report: Characterisation and sources of the secondary organic carbon in a Chinese megacity over 5 years from 2016 to 2020. Atmospheric Chemistry and Physics, 22(19), pp.12789-12802.

11. Wei, W., Wang, M., Yuan, Q., Zhang, Z., Li, X., **Han, S.**, Duan, Y., Fu, Q. and Lee, S.C., 2023. Comprehensive Assessment of Pollution Sources and Health Impacts in Suburban Area of Shanghai. Toxics, 11(7), p.552.

Patent Applications

1. **Han, S.W.**, Tan, Y., Li, X.W., Lee S.C.* OIL FUME PURIFICATION DEVICE AND MOBILE KITCHENHAVING THE SAME, Hong Kong Invention Patent Application, HK30082971
2. **韩舒文,** 谈琰, 李欣蔚, 李顺诚* 油烟净化装置及带有该油烟净化装置的移动式厨房, 中国实用新型专利，ZL202320371074.0
3. Tan, Y., **Han, S.W.**, Lee, S.C.* WALK-IN TYPE AIR POLLUTION SIMULATION REACTION CHAMBER, Hong Kong Invention Patent Application, HK30040962

Conference Presentations

1. **Han, S.W.**, Tan, Y., Lee, S.C.*, Characterization and Evaluation of Long-term Air Quality Across Urban Hong Kong, EGU 2023, Vienna, Austria
2. **Han, S.W.**, Tan, Y., Lee, S.C.*, Emission Source Characteristics and Health Risk Assessment of Fine Particulate Matter from Different Commercial Cooking Methods, Dust 2023, Bari, Italy
3. **Han, S.W.**, Tan, Y., Lee, S.C.*, Development and Evaluation of High Gravity Technology for Control of Cooking Oil Fume Emissions, A&WMA ACE 2023, Orlando, United States

ACKNOWLEDGEMENTS

I would like to express the deepest gratitude to my supervisor, Professor LEE Shun-cheng, who is an erudite, patient and kind scientist. I want to thank him for providing me with the opportunity for Ph.D. study, giving me all the necessary resources during my research period, encouraging me when I was trapped in tight corners, and mentoring for lifelong development. I must say that it is so lucky for me to have such a nice supervisor during my 3-year PhD journey.

I want to give my special thanks to Dr. LEU Shao-yuan in supporting me for the final period of my PhD study. I would also like to thank Prof. GUO Hai, our air lab in-charge, who provided me with suggestions for the design and conduction of experiments and Prof. WANG Tao in assisting with academic courses and research works. I would also like to thank the technicians from our laboratory, Mr. Jazz CHAN, Mr. David LEUNG, Mr. W.S. LAM, and Ms. Celine CHE for their technical support.

I must thank my friend for their guidance and support. Many thanks to Ms. LI Xinwei, who helped me with writing and reviewing papers and gave me valuable suggestions on experiment works. Thanks to Dr. YUAN Min-hao, Dr. Steven HO, Mr. Joseph Law, Dr. ZHANG Zhuozhi, Ms. YUAN Qi, and Dr. WANG Meng for their kind assistance and great support. I would like to give my gratitude to all my group mates who helped me in completing my research.

Incredibly special thanks to Dr. TAN Yan, who provided me continuous support from academic work to daily life. I wish to extend sincere thanks to her company for such a long time. Auld Lang Syne.

I want to take the time to thank my parents. Thank my mother, who always listens to me and encourages me. Thank my father, who always enlightens me and supports me. I cannot finish my studies without their selfless and devoted love.

I am grateful for the valuable comments from the reviewers, Prof. TSAI Jiun-Horng and Prof. HUANG Haibao for the improvement of the thesis.

Finally, I hope to thank the arrangement and sites support from canteens, restaurants, kitchens, and SAO of PolyU. I also would like to acknowledge the financial support from The Hong Kong Polytechnic University, the University Grants Committee, and the Environment and Conservation Fund of the Government of Hong Kong SAR (Project No.: ECF 2019-63).

TABLE OF CONTENTS

LIST OF FIGURES

LIST OF TABLES

LIST OF ABBREVIATIONS

2,3-DHN	2,3-dihydroxynaphthalene
AE	Anion Equivalent
AT	Averaging Time
BL	Boiling
CAN	Cantonese Cuisine
CB	Valence Band
CE	Cation Equivalent
CFF	Chinese Fast Food
CHP	Chongqing Hot Pot
CMC	Critical Micelle Concentration
CN	g-C_3N_4
COF	Cooking Oil Fume
C-PAHS	Carcinogenic PAHs
CRS	Certified Reference Standard
DF	Deep-frying
DFT	Density Functional Theory
DMPO	5,5′-dimethyl-1-pirroline-N-oxide
DNPH	2,4-dinitrophenylhydrazine
EC	Elemental Carbon
EC	Exposure Concentration
ED	Exposure Duration
ED-XRF	Energy Dispersive X-Ray Fluorescence
EF	Exposure Frequency
EI	Electron Impact
EIS	Electrochemical Impedance Spectroscopy
EP	Electrostatic Precipitators
ESR	Electron Spin-Resonance spectroscopy
ET	Exposure Time
FAC	Fraction Aerosol Coefficient
FT-IR	Fourier-Transform Infrared Spectroscopy
G/L	Gas-to-Liquid
HCHO	Formaldehyde
HiGee	High Gravity Rotating Packed Beds
HLB	Hydrophilic-Lipophilic Balance

HM-PAHs	High Molecular Weight PAHs
HPLC	High-performance Liquid Chromatography
HQ	Hazard Quotient
HR-TEM	High-Resolution Transmission Electron Microscopy
ILCR	Incremental Lifetime Cancer Risk
IRIS	Integrated Risk Information System
IUR	Inhalation Unit Risk
LM-PAHs	Low Molecular Weight PAHs
LOD	Limit of Detection
LQL	Lower Quantifiable Limit
MDEA	N-methyl diethanolamine
MDL	Method Detection Limit
MEK	2-butanone
MIR	Maximum Incremental Reactivity
MM-PAHs	Middle Molecular Weight PAHs
MOF	Metal-Organic Framework
MSD	Mass Selective Detector
MW	Molecular Weight
NAAQS	National Ambient Air Quality Standards
ND	Nanometer Diamond
NIST	National Institute of Standards and Technology
NOX	Oxide of Nitrogen
OC	Organic Carbon
OEHHA	Office of Environmental Health Hazard Assessment
OFP	Ozone Formation Potential
OV	Oxygen Vacancy
OVOC	Oxygenated Volatile Organic Compound
PAD	Photodiode Array Detector
PAH	Polycyclic Aromatic Hydrocarbons
PAM	Potential Aerosol Mass
PDS	Phthalocyanine Sulfonate
PF	Pan-frying
PFA	Perfluoro Alkoxy Alkane
PL	Photoluminescence
PM	Particulate Matter
PM_{10}	Inhalable Particulates

$PM_{2.5}$	Fine Particulates
ppb	part per billion
ppm	part per million
RfC	Inhalation Reference Concentration
RPB	Rotating Packed Bed
rpm	Revolutions Per Minute
SCO	Strontium Carbonate
SE-GC/MS	Solvent Extraction-Gas Chromatography/Mass Spectrometry
SEM	Scanning Electron Microscopy
SF	Stir-frying
SIM	Selective Ion Monitoring
SOA	Secondary Organic Aerosol
SOAFP	Secondary Organic Aerosol Formation Potential
SRM	Standard Reference Material
ST	Steaming
STO	Strontium Titanate
TD	Thermo-Desorption
TETA	Triethylenetetramine
TOR	Thermal/Optical Reflectance
TPD	Temperature-Programmed Desorption
TSP	Total Suspended Particulates
TV	Toxicity Value
TVOC	Total Volatile Organic Carbon
VB	Conduction Band
VOC	Volatile Organic Compound
WFF	Western Fast Food
XPS	X-ray Photoelectron Spectroscopy
XRD	X-ray Diffraction

Chapter 1 Introduction

1.1 Background of This Study

Air pollution has emerged as one of the most critical environmental challenges worldwide, particularly in heavily populated urban areas where human activities are concentrated. Cooking, one of the fundamental human activities and necessities, generates significant amounts of air pollutants through both food heating and fuel combustion processes, which have detrimental effects on air quality and human health. Cooking oil fumes (COFs) are the exhaust emission gases produced from the mixture of cooking oils, raw food materials and condiments with complicated physical and chemical transformations including decomposition, oxidation, and polymerization in elevated temperature conditions from the cooking processes.

COFs together with industrial and vehicular emissions have been identified as the top three largest air pollution sources in urban areas (Tao et al., 2023). In addition, COFs have also been considered as the most major contributor to indoor air pollution with significant odour issues and severe human health concerns (Hung et al., 2007). COF emissions constitute various complex toxic pollutants including particulate matters (PMs), polycyclic aromatic hydrocarbons (PAHs), heavy metals and gaseous pollutants, such as volatile organic compounds (VOCs), and oxides of nitrogen (NO_X) (Abdullahi, Delgado-Saborit, & Harrison, 2013; Chen, Zhao, & Zhao, 2018). The emission characteristics of cooking oil fumes may vary significantly according to the types of cuisines, cooking styles, added ingredients and fuels (Peng et al., 2017). In addition, these complex chemical compounds in COFs could not only lead to the deterioration of atmospheric environment, e.g., formation of excessive ozone (O_3) and secondary organic aerosol (SOA) (Tan et al., 2021; Ziemann & Atkinson, 2012), but also contribute to severe human health impacts involving tissue inflammation, respiratory diseases and even lung cancer (Lee & Gany, 2013; Peng et al., 2017). Therefore, effective control of both the particulate and gaseous emissions from COFs has been of great demand for the concerns of environment protection and human health risks (Amouei Torkmahalleh et al., 2017; D. Zhao & X.-Y. You, 2021).

In Hong Kong, there were over 17,000 food and beverage establishments and about 220,000 practitioners involved in the food services industry (CSD, 2023). Thus, cooking emissions, especially those from commercial restaurants and kitchens, should be taken with seriously in densely populated developed cities. However, some of the COFs studies focused on the laboratory-based emission characteristics with single variation factor of oils, which could not reflect the actual cooking emissions. Limited studies revealed the real-world emissions characteristics of cooking oil fumes while most of them were conducted in home kitchens, where the cooking time was short and chemical composition was simple. Therefore, a systematic study of the COF emissions from different real cooking processes and commercial restaurants is needed, which helps supplement the anthropogenic emission inventory. In this study, detailed characteristics of COF emissions from five kinds of cooking styles (i.e., stir-frying, deep-frying, pan-frying, boiling and steaming) and four kinds of restaurants with various cuisines (i.e., Chinese fast food, Western fast food, Cantonese cuisine and Chongqing hotpot) will be investigated. Besides, further environmental and atmospheric influences and health impacts from cooking processes will be assessed based on their emission concentrations.

On the other hand, given the mitigation demands of the COFs pollution due to their detrimental environmental and health effects, novel control strategies are urgently needed.

After reviewing the existing control methods for the cooking emissions, two promising control techniques by applying high gravity rotating packed bed scrubber and photocatalytic heterojunction nanomaterial to deal with the particulate and gaseous pollutants in emission gas stream. The working principle and performance of COFs purification will be studied by the in-lab characterization analysis, activity test, model simulation and on-site removal efficiency trails. In summary, this study will provide a comprehensive cooking emission inventory in Hong Kong and Asian areas, as well as effective control strategies which could be applied in commercial kitchens.

1.2 Research Objectives

In view of the research gaps and shortage of studies stated above, the present study attempts to investigate the detailed characteristics of cooking oil fumes and their impacts through on-site sampling campaigns. In addition, the development of effective control techniques is included to tackle the pollution issues raised by COFs emissions. The major objectives of this study include:

1) To study the detailed emissions characteristics of both gaseous pollutants and particulate matters from various cooking methods and different commercial restaurants in Hong Kong;
2) To evaluate the environmental and atmospheric influences and health risk impacts raised by the emission of cooking oil fumes;
3) To develop the high gravity rotating packed bed scrubber in removal of both gaseous and particulate pollutants simultaneously and to evaluate its actual COF removal efficiency through in-kitchen field trail tests;

4) To design and synthesize novel photocatalytic nanomaterials in degradation of gaseous pollutants from cooking activities and to explore its purification mechanism and efficiency.

1.3 Outline of the Thesis

This thesis comprises a total of eight chapters, and the details of each chapter are described as follows:

Chapter 1 provides the research background and main objectives of this study.

Chapter 2 presents a brief literature review on the emission characteristics of cooking oil fumes, existing COFs control techniques, principles and development of high gravity rotating packed bed system, as well as the fabrication and application of nanomaterials in air pollution control.

Chapter 3 describes the adopted methodologies in this thesis, including the sampling methods, chemical characterization methods, activity measurement and efficiency evaluation techniques, and model configurations.

Chapter 4 discusses the analytical results of fine particulate matters ($PM_{2.5}$) and gaseous pollutants (VOCs) of the collected COFs samples from different cooking methods conducted in simulated kitchens.

Chapter 5 focuses on the COFs emission features from the real kitchens with diverse types of cuisines, and their associated environmental impacts and human health influences, including ozone formation potential, secondary organic aerosol formation and health risks through inhalation exposure.

Chapter 6 presents the investigation of operation conditions and liquid absorbents of the high gravity rotating packed bed scrubber device and evaluates the removal efficiency for COFs from the trial tests in real kitchens.

Chapter 7 shows the design, synthesis, test, and model exploration of the novel heterojunction nanomaterials in phototactically degradation of specified VOCs and NO pollutants from the COFs.

Chapter 8 summarizes the major findings of this study and provides limitations and suggestions for future studies on the COFs characterization and control works.

Chapter 2 Literature Review

2.1 Overview of the Cooking Oil Fumes

Cooking oil fumes (COFs) are the mixed smokes generated during the cooking process, which have very complex chemical compositions and pose significant hazards to both human health and the environment (Arı et al., 2020; Hou et al., 2018; Yang et al., 2020). The COFs can be divided into particulate pollutants and gaseous pollutants in terms of their morphology. Particulate pollutants are composed of inorganic elements, organic matters, water-soluble ions, and carbon elements, among which heavy metals and PAHs can cause severe health impacts and element carbon may cause atmospheric and climate influences (Zhao, Chen, & Zhao, 2019). The main component of gaseous pollutants is volatile organic compounds (VOCs), including alkanes, alkenes, aromatic hydrocarbons, and aldehydes (H. L. Wang et al., 2018). The VOCs in cooking fumes can react with strong oxidants such as O_3 and ·OH in the atmosphere to form secondary organic aerosols (Garmash et al., 2020). In the presence of NO_X, complicated reactions can occur to form photochemical smog, which is one of the major sources of ozone pollution and has significant negative impacts on the environment (He et al., 2019; X. F. Huang et al., 2020). At the same time, the impact of toxic VOCs from cooking fumes on human health cannot be ignored. Long-term exposure to the environment with cooking oil fumes can affect the respiratory and immune systems of the human body. Evidence from epidemiological study show that cooking oil fumes have a certain risk of causing cancers as well (Svedahl, Hilt, & Svendsen, 2020).

2.1.1 Particulate Emissions

Particulate matter (PM) is a significant indicator of atmospheric environmental pollution and is commonly used to quantitatively evaluate the degree of atmospheric pollution. According to the definition of aerodynamic equivalent diameter in ambient air, particulate matter in the atmospheric environment can be divided into total suspended particulates (TSP), inhalable particulates (PM_{10}), and fine particulates ($PM_{2.5}$), which refer to the diameters less than or equal to 100 µm, 10 µm, and 2.5 µm, respectively (USEPA).

The particle size from the cooking oil fumes is relatively small, mainly consisting of fine particulates ($PM_{2.5}$) (Wallace, 2006). The particle size and concentration of particulate matter from cooking oil fumes are also different, which is significantly affected by temperature, type of food, and type of oil, with major particle sizes ranging from 10-100 nm (Y. C. Li et al., 2015). Wan et al. (2011) studied the emission characteristics of ultrafine particles during in-house cooking periods in Hong Kong. The most emitted particulate matter was ultrafine particles, accounting for more than 80% of the total number of particles, which is more than 10 times the concentration of ambient background. Source apportionment results showed that cooking emission contributed about 52.5% and 43.2% to personal exposure concentrations and residential indoor concentrations, respectively (Ozkaynak *et al.,* 1996).

Emission of particles from different cooking styles including frying, barbeque, oven cooking, sautéing and toasting were compared (Wallace, Lance *et al.,* 2006), showing the frying method generated most particulate emissions. In another study (Buonanno, Morawska and Stabile, 2009) two types of common energies (gas stove and electrical pan) was used to in residential cooking process, and the emission results demonstrated more fine particles emitted by using the gas stove.

1）OC/EC Emissions

The fine particle emission of the cooking oil fumes mainly contains carbonaceous particles, including elemental carbon (EC) and organic carbon (OC) (See & Balasubramanian, 2008) due to the rich contents of carbon element in raw food and oil. And organic carbon is the predominant component in cooking oil fumes (Abdullahi, Delgado-Saborit, & Harrison, 2013; Kleeman et al., 2008). A comparison of different cooking methods showed that those processes using oil, such as frying, released higher concentrations of both EC and OC than those using less oil, such as boiling and steaming. See and Balasubramanian (2008) found that the highest emissions release of EC and OC was attributed to deep frying in their simulations cooking experiments. In another study of cooking emissions (Y. C. Li et al., 2015), more organic carbon (OC) contents and higher OC/EC ratios in meat roasting and cafeteria frying samples suggested that oils usage and raw materials with high-fat contents might significantly affect the $PM_{2.5}$ and OC emissions. At the same time, cooking activity was shown to be a minor source for elemental carbon (EC) with its relative low contents in all samples.

2）Inorganic Compounds Emissions

Metal content exists in the cooking oil fumes and its contributing sources includes raw food materials, additives, edible oils and even biomass burning (Acciai et al., 2017; Zhao, Chen, & Zhao, 2019). In some previous research results, Cu, Fe, Mn, and Zn were found in vegetables and meats (Kawashima & Soares, 2003; Lombardi-Boccia, Lanzi, & Aguzzi, 2005), while Cu, Zn, and Cd were detected in fish. Na and K are likely emitted from the salt used in cooking and oil-based meat cooking, respectively (Acciai et al., 2017). Certain elements, including Cr, Fe, Cu and Ni, may derive from cooking appliances, such as pans and spatulas (Zhao et al., 2019). These heavy metals can be toxic and may be located on the surface of particles, which may potentially cause inflammation, heart and lung disease, or even DNA damage (Lu et al., 2015). Particle-bound water-soluble ions, including Na^+, K^+, NO_2^-, Mg^{2+}, Ca^{2+}, Cl^-, NO_3^-, and SO_4^{2-}, have also been identified in cooking oil fumes (Hsieh et al., 2011). Their concentrations may vary significantly among different cooking methods and conditions (Zhao et al., 2019). As reported in the previous research, the source of SO_4^{2-} might be the water used in cooking process (Y. C. Li et al., 2015), NO_3^- might generate from nitrogen oxides produced by fuel or biomass burning, and Na+ and Cl– mainly emitted from the added salt (Wang et al., 2015).

3）PAHs Emissions

PAHs are organic compounds containing two or more benzene rings. Incomplete combustion or pyrolysis of organic compounds under high heating temperature may produce PAHs during the cooking process (Chen et al., 2019). Studies compared emissions from different cooking styles revealed that Chinese cooking usually had high PAHs emissions due to stir-fry technique and high cooking temperature (Li et al., 2003; Wei See, Karthikeyan, & Balasubramanian, 2006). In terms of cooking methods, deep-frying, stir-frying, and pan-frying that involve high cooking temperature with the use of oil were found to produce more PAHs (Schauer et al., 2001). In addition, the raw materials used, and the ingredients added also affect the emission concentration of PAHs. Food with higher fat was found producing more PAHs than low fat food (Schauer et al., 2002). Oils used frequently by Chinese cooking including lard oil, soya bean oil and peanut oil were examined in terms of PAHs emission (Wu et al., 1998). Fortmann compared the PAHs emission from heating untreated oils including canola oil, olive oil, corn oil, peanut oil and vegetable oil (Roy, Peter, & Russ, 2021). Although PAHs make up only a small portion of cooking particles (Schauer et al., 2002), they have received significant attention since some of the PAHs are carcinogenic and the potential exposure through inhalation to human beings.

2.1.2 Gaseous Emissions

The chemical compositions of the gaseous emissions from COFs are quite complicated, which can be divided into two major types including trace gases and VOCs (Yi et al., 2019). VOCs mainly derive from the raw food materials heating process, while the trace gases, such as CO, CO_2, and NO_X, also come from fuel or biomass burning beside cooking process (Chen, Zhao, & Zhao, 2018). There are over 300 different kinds of VOCs compounds in the COFs, including alkanes, alkenes, aldehydes, alcohol, aromatic, fatty acids and heterocyclic compounds (Tao et al., 2023). In a study of the COFs from typical home kitchens in Hong Kong with two kinds of fuels of town gas and liquified petroleum gas (Huang et al., 2011), it was found that the proportion of alkanes was 53% - 95% of the total VOCs, and the average concentration ranges of formaldehyde, benzene, toluene, and xylene were 60.4 - 151.0 $\mu g/m^3$, 1.3 - 9.7 $\mu g/m^3$, 27.6 - 40.2 $\mu g/m^3$, and 5.9 - 7.1 $\mu g/m^3$, respectively. Moreover, no carcinogenic compounds such as benzene, acetaldehyde or formaldehyde were detected in these fuels or combustion emissions, confirming that these substances were completely generated from cooking processes. Xiang et al. (2017) studied and assessed the impact factors of the emission of carbonyl compounds in different Chinese cooking process, results demonstrated that the cooking methods, types of oils and ingredients all had relevant impacts on the emission characteristics of carbonyl compounds. Among all these different cooking methods, the highest emission concentration of carbonyl compounds was from barbecue (1.60 μg/kg), followed by frying (1.53 μg/kg), teppanyaki (1.22 μg/kg), and stir-frying (0.70 μg/kg). By comparing the cooking oils and raw food materials, the use of sunflower oil produced the highest emission level of carbonyl, and more carbonyl compounds were released from the meat cooking process than vegetables cooking. Lee et al. (2020) simulated the cooking process of meat grilling with both pork belly and ribs, determining their main VOCs emissions were alkanes and aromatic hydrocarbons. It was also found that benzene, ethyl acetate, and hexene were the main VOCs emitted during the barbecue of pork belly, while the major VOCs emitted from pork ribs were butane, ethyl acetate, and dodecane.

In addition to these studies of COFs from the above real or simulated kitchens, Abdullahi, Delgado-Saborit and Harrison (2013) investigated the emission characteristics of VOCs by heating different types of vegetable oils, determining the VOC contents from oil heating are mainly alkanes, aldehydes, alcohols, ketones, and organic acids. When the heating temperature exceeded the smoke point of the oil, the VOCs emission would increase sharply due to the breakup of the internal chemical structures. In 2019, the COFs generated from 5 kinds of common cooking oils were studied in a lab-based heating apparatus under different temperature conditions (D. C. Zhang et al., 2019). A total of 55 organic compounds, including aldehydes, hydrocarbons, and benzene series, were identified from the emissions of oil heating. The total concentration of VOCs from the cooking oil fumes of these edible oils at the temperature of 270 °C was ranked as follows: canola (81.0 mg/m^3) > soybean (75.5 mg/m^3) > peanut (70.9 mg/m^3) > corn (60.3 mg/m^3) > lard (20.5 mg/m^3), indicating that vegetable oils rich in unsaturated fatty acids might produce more VOCs.

2.1.3 Environmental and Health Impacts

Cooking oil fumes contain many particulate pollutants, organic compounds, and hazardous matters, which not only have a direct impact on the environment, but also cause secondary pollutants in reducing the ambient air quality. Due to their complex composition and wide existence, cooking oil fumes pose influence on both outdoor atmospheric environments and human health impacts.

1）Atmospheric Environment Impacts

The discharged liquid and solid phases of the COFs can form primary particles directly and become $PM_{2.5}$ after complex physical and chemical processes. While the emitted gaseous substances, which are mainly VOCs, will form secondary organic aerosols (SOAs) through photooxidation processes and gas/particle partitioning processes (Rosales et al., 2022), as shown in Fig 2-1. SOAs are important components of atmospheric $PM_{2.5}$, which contain oxygen functional groups with strong polarity, hygroscopicity and solubility, thereby affecting or participating in atmospheric extinction to reduce atmospheric visibility and form haze (Zheng et al., 2021).

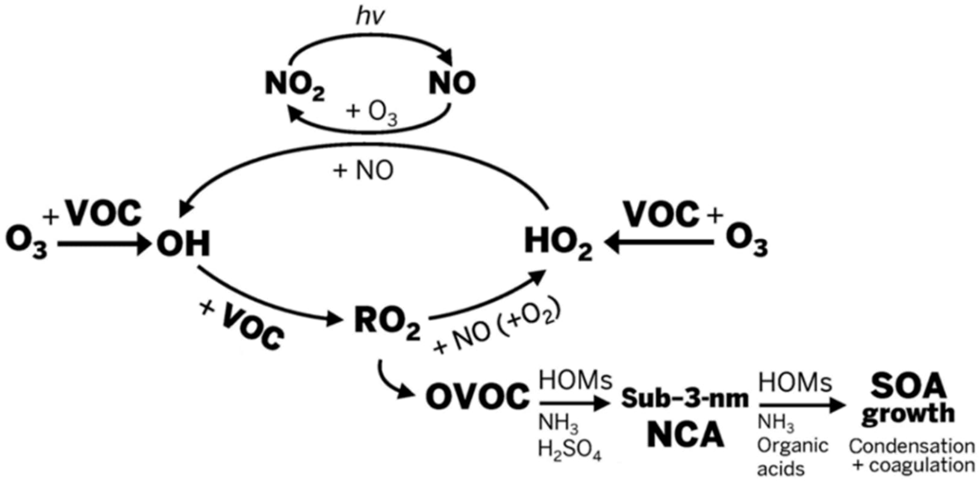

Figure 2-1 Schematic of SOA formation by atmospheric VOCs (Rosales et al., 2022)

The formation of SOA from gas-phase emissions of cooking process has been investigated through in-lab oil heating or simulation experiments. Five different kinds of vegetable oils, including corn, canola, sunflower, peanut, and olive oils were heated and then injected into a potential aerosol mass (PAM) chamber to simulate the formation of SOA (Liu et al., 2017). Results suggested that the production efficiencies of SOA from heated cooking oils in increasing order were peanut oil, olive oil, canola oil, corn oil, and sunflower oil, and the primary precursors for SOA formation were found to be related to the contents of monounsaturated fat and omega-6 fatty acids in the oils. Takhar, Li and Chan (2021) found that the chemical compositions of cooking SOA changed with increasing photochemical aging, with an increase in average oxidation state and a decrease in average carbon number, which suggested that fragmentation reactions were key processes in the oxidative aging of cooking emissions. The researchers also estimated that aldehyde precursors from cooking emissions accounted for many of the oxidation products and SOA formation.

In addition to the strong SOA formation potentials, COFs can contribute to the formation of ozone in the atmosphere as well (Atamaleki et al., 2021). Ozone is formed when VOCs react with nitrogen oxides (NO_X) in the presence of sunlight (Koppmann, 2020), and its typical ozone formation cycles are shown in Fig 2-2.

H. L. Wang et al. (2018) investigated the COFs from different Chinese cuisines, showing that the largest ozone formation potential (OFP) was from the alkenes which accounted for 6.8–97.0% of total OFP. In another study, Song et al. (2022) found that the estimation of ozone formation potential (OFP) was consistent with the emission rate of pollutants from COFs, where aromatic and alkenes were identified as dominant precursors for ozone formation in meat-related dishes. And Kung Pao chicken was found to emit the most pollutants and produce the highest amount of ozone formation with an estimated rate of 21.12 ± 19.45 mg/min. In addition, the types of oils, seasonings, and dishes were all demonstrated to have influences on the OFP, where soybean oil had the highest OFP of 1.84 mg/g oil/h and trichlorethylene was the largest contributor (Son et al., 2022).

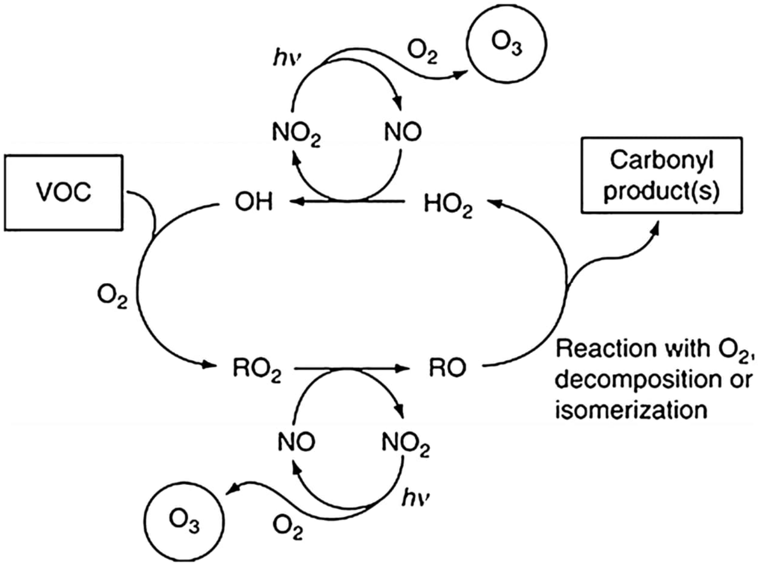

Figure 2-2 Schematic of ozone formation by atmospheric VOCs (Koppmann, 2020)

Due to the large number of $PM_{2.5}$ and VOCs in COFs, if they are not effectively purified or controlled before being discharged into the atmosphere, it can participate in atmospheric chemical reactions and contribute to secondary pollutants such as SOA and ozone, thereby aggravating the atmospheric environmental pollution.

2）Human Health Impacts

Cooking oil fumes contain fine particles, VOCs, and PAHs, which can remain stable in indoor air for a long time. Long-term exposure to pollutants from cooking oil fumes can increase the risk of cardiovascular, respiratory and lung diseases, and cooking oil fumes contain substances such as polycyclic aromatic hydrocarbons, heterocyclic compounds, and nitrosamines, which are known carcinogens and can cause cancer (Wang et al., 2017).

Epidemiological studies have confirmed that occupational workers who are exposed to cooking oil fumes for long periods of time have a much higher incidence of chronic and polar respiratory diseases (Juntarawijit & Juntarawijit, 2017). Studies have shown that the incidence of lung cancer among non-smoking women in China ranked first in the world (Yu et al., 2006). The main health hazards of cooking oil fumes are reflected in the following aspects:

a) Lung Damage

Human is exposed to cooking oil fumes through breathing and pollutants can directly enter lungs through the respiratory tract, causing oxidative stress reactions in respiratory and lung cells, which may damage lung tissue cells and increase the incidence of lung cancer. Tung et al. (2001) studied the biological effects of COFs produced by heating grape seed oil on human lung epithelial cells. The results showed that exposure to cooking oil substances significantly reduced the growth of human lung epithelial cells, which increased the secretion of TGFb1 in cells and induced oxidative stress reactions in CL3 lung epithelial cells. Wang et al. (2019) found the synergistic effects on the incidence of lung cancer by exposure to COFs and genetic polymorphism. Every 1-hour exposure to COFs would increase the incidence of lung cancer by 17%. In addition, exposure to COFs had a potential harmful cumulative effect, and reduced human lung function significantly after 2-day exposure by measuring the biomarkers of lung function and respiratory inflammation (Du et al., 2017).

b) Blood Poisoning

COFs can also affect the function of various organs under the effect of blood circulation after entering through the human respiratory system. Yamashita et al. (2011) studied the effects of fine particles on the metabolism of pregnant mice and found that fine particles with the size of 70 nm could pass through the barrier of blood-brain and placenta, which would enter the fetus of pregnant mice and endanger their normal development. Amegah et al. (2012) found that there was an exposure-response relationship between indoor air quality during pregnancy and weight of infant. The birth weight could reduce by 243 g when using charcoal as fuel for cooking at home, possibly because gaseous pollutants such as CO produced by fuel combustion could bind to hemoglobin and pass through the placenta, reducing maternal oxygen transport and limiting the ability of the placenta in nutrients supply.

c) Reproductive Disease

Organic compounds in COFs can disrupt the cell cycle and toxic compounds can cause biological effects such as chromosomal damage and gene mutations, which will alter the genetic materials within cells. Dung, Wu and Yen (2006) studied the COFs produced by heating soybean oil, sunflower oil, and lard and found that the methanol extracts of COFs could attack the 8th carbon atom of guanine in DNA molecules of human lung cancer epithelial type II cells to form 8-hydroxy-2-deoxyguanosine, causing significant oxidative damage and genetic toxicity. Moreover, cells exposed to trans-2,4-decadienal compounds in COFs demonstrated a significant increase in DNA synthesis and cell proliferation, and enhanced expression and release of pro-inflammatory cytokines TNF-a and IL-1b in cells (Chang, Lo, & Lin, 2005).

d) Cardiovascular Damage

The main component of cooking oil smoke is fine particles with a proportion of more than 60%, which are major risk factors for the incidence and death of cardiovascular diseases. The incidence risk of cardiovascular disease is positively correlated with the concentration (Rajagopalan, Al-Kindi, & Brook, 2018), and long-term exposure to environments with low $PM_{2.5}$ concentrations is more harmful than short-term exposure to environments with high concentrations (Brook et al., 2010). Studies have shown that the biological mechanism of blood clotting induced by exposure to $PM_{2.5}$ is one of the reasons for the increase in cardiovascular disease, and the coagulation effects induced by particles mainly include platelet activation, thrombus formation, and fibrinolysis inhibition (Chen et al., 2020; Miller & Newby, 2020; Robertson & Miller, 2018). Yatera et al. (2008) used animal models to study the effects of exposure to particles on cardiac function, proving that fine particles can promote monocytes to enter atherosclerotic plaques. Peters et al. (2004) pointed out that short-term exposure to an environment with a high mass concentration of $PM_{2.5}$ for several hours would increase the risk of myocardial infarction in the human body.

2.2 Development and Application of Technologies for Control of Cooking Oil Fumes

The technology used to purify grease particles is a crucial component of the exhaust COFs system in commercial kitchens (D. F. Zhao & X. Y. You, 2021). Common methods used in the catering industry include filtration, mechanical separation, electrostatic deposition, and washing and absorption. Each of these methods will be separately discussed in detail below.

2.2.1 Filtration

Filtration is a widely used method for removing grease particles from COFs in commercial kitchens. This approach is popular due to its small space requirements and provision of large filtering area. The principle of filtration is by using inertial collision, interception, and diffusion to remove particles ranging in size from 1.0 μm to 4.0 μm (Bian et al., 2018). COFs filters are typically made from fibrous materials and can be divided into two categories based on their structure: nonwoven and woven (or knitted) (Ye et al., 2007). Filter materials can include synthetic fibers, glass fibers, combination fibers, and other materials. Filtration is highly effective at removing grease particles from COFs, with removal efficiencies generally exceeding 80%. It can also help remove gaseous contaminants (Sheng et al., 2020). However, the adsorption capacity of the filter material will decrease over time, and the pressure drop will increase as the filter becomes clogged.

2.2.2 Mechanical Separation

Mechanical separation is a common method for purifying COFs that relies on the density difference between grease particles and air. This method uses inertia collision, centrifugal separation, and gravity sedimentation to remove grease particles from the air (Risto & Panu, 2016). Common mechanical separators include cyclonic filters, baffle filters, and dynamic grease separators. Baffle filters work by causing grease particles to collide with the filter surfaces and stick to them. These filters are typically installed in the exhaust hood above the cooking equipment, at the inlet opening of the exhaust system air duct. However, their separation efficiency for particles smaller than 4 μm is almost zero, and their maximum separation efficiency for grease particles larger than 10 μm is only about 35% (Shevchenko, 2012).

2.2.3 Electrostatic Deposition

Electrostatic deposition is a process that uses electro hydrodynamics to purify COFs. This method charges grease particles using corona discharge and collects them using induced electrostatic forces. Electrostatic precipitators are the most mature and widely used devices for this purpose, and they can achieve ultra-low emissions of fine particles. They have the advantages of low resistance and easy cleaning (Mizuno, 2000; Tian, Mo, & Li, 2018; Tu, Song, & Yao, 2017). Electrostatic precipitators can be divided into single-stage and two-stage types, based on the mode of particle charging and the arrangement of separation areas (S. S. Li et al., 2019). The two-stage electrostatic precipitator has multiple collecting plates to improve separation efficiency and small plate spacing to reduce its size (Zou, Wu, & Huang, 2010). As a result, it is more effective at removing oil mist in factories, kitchens, and ship cabins (S. S. Li et al., 2019).

2.2.4 Washing and Absorption

Washing and absorption, also known as the wet method, is a process that uses a specific gas distribution device to mix COFs containing grease particles with an absorption liquid. During this process, the grease particles transfer from the gas phase to the liquid phase through physical or chemical reactions with the absorbent. This method can be divided into spray type, liquid film, and vent wash exhaust hood, depending on the mode of gas-liquid contact (He, Yuan, & Yuan, 2009). The purification efficiency of washing and absorption is generally high (Xiong & Zhang, 2009), and it can also reduce the temperature of the COFs to prevent the risk of fire (He, Yuan, & Yuan, 2009).

2.2.5 Real-world Application of COFs Control Facilities

In addition to these technologies discussed above, the actual control facilities based on these different technologies are listed in Table 2-1. These are the commonly installed devices in commercial restaurants and kitchens in Hong Kong while electrostatic precipitators (EP) are the most frequent in the market due to its low cost, occupied small space, easy maintenance, and relative high purification efficiency (Kang et al., 2021).

However, EP can hardly remove gaseous pollutants from COFs as the electrostatic field could only be applied to those particulate matters passing through. Similar to EP, wet scrubber which uses water or surfactant to wash away the COFs can also be used alone to handle the cooking emissions, which has good particulate removal efficiency and limited gaseous purification capability (Hsieh et al., 2011). EP and wet scrubber are suitable for major cooking scenarios, but for some areas with strict requirements and those cooking industries with series polluted cooking processes, the control of gaseous and odour emissions still needs to be considered. UV/O_3 and activated carbon facilities are designed for purification of gaseous pollutants such as VOCs, which should always be used with EP or wet scrubber in series. UV/O_3 can generate strong oxidants to fully degrade VOCs, while VOCs adsorption happens on the surface of activated carbon. All these COFs control devices need regular maintenance to ensure the normal operation and effectiveness. In addition, due to their adopted technologies, hazardous by-products such as ozone and VOCs are generated in EP and UV/O_3 treatment processes, which then emit to atmosphere and contribute to the worsening of air quality.

Table 2-1 Comparison of different existing cooking emission control technologies

Facilities	**EP (Electrostatic Precipitators)**	**Wet Scrubber**	**UV/O_3**	**Activated Carbon**
Mechanism	Electrostatic charge	Absorption	Chemical oxidation	Adsorption
Usability	Most used	Can be used alone or with EP in large site	Must be used with EP and/or wet scrubber	Must be used with EP and/or wet scrubber
PM removal	70-90%	50-70%	Less	Less
Gas removal	Less	30-60%	80-90%	60-90%

Cost	Low	Low	High	High
Maintenance	Discharge electrodes and collection plates	Scrubbing solution and filters	Replace of UV lamp	Replace of activated carbon
By-products generation	O_3 and VOCs	N/A	O_3 and VOCs	N/A

2.3 High Gravity Rotating Packed Bed Technology

High gravity rotating packed bed (RPB, or HiGee) was first proposed by Pilo and Dahlbeck in a granted patent in 1963 (Wilhelm & Wilhelm, 1960), but it did not attract much interest at that time. Till 1981, the technology was further developed and marketed by Ramshaw and Mallinson at the New Science Group in Imperial Chemical Industries (Ramshaw, 1979), which was created to carry out distillation and absorption. The application of enhanced acceleration in RPBs was observed to profoundly improve the mass transfer process and severed for process intensification in chemical engineering. As shown in Fig. 2-3, the publications related to HiGee technology in the past 30 years were categorized by different research subjects, which demonstrate that scientists across the world studied and optimized the operation of the HiGee system and applied it to different areas beyond chemical engineering, such as nanomaterial synthesis, wastewater treatment and air purification.

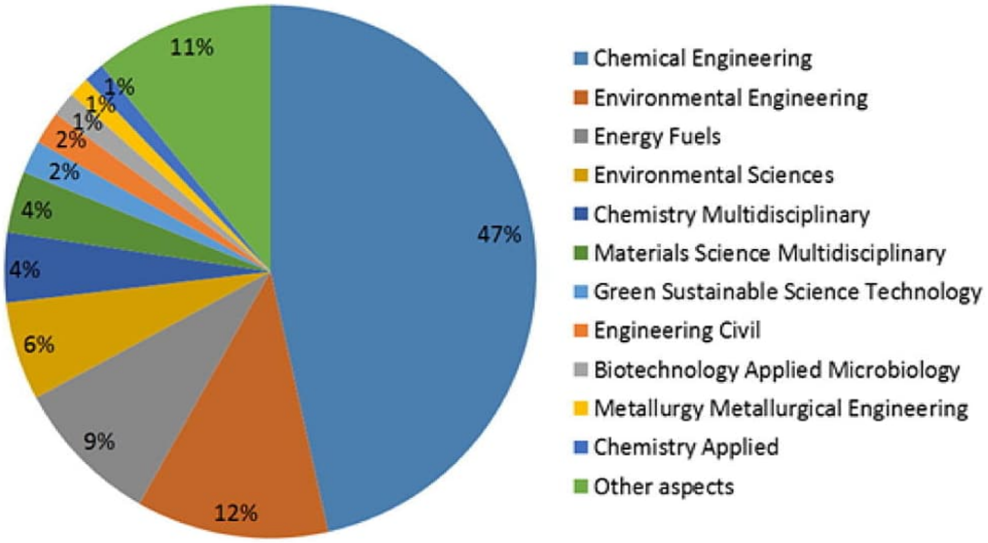

Figure 2-3 Distribution of literature publications by research field on high gravity rotating packed beds

2.3.1 Design and Working Principles

High gravity rotating packed beds, also known as HiGee systems, use rotational energy to generate high centrifugal force and increase inter-phase mass transfer compared to conventional columns. A typical HiGee system consists of an outside casing, packed bed, liquid spray distributor, gas/liquid inlet/outlet, and a drive motor. The liquid stream enters through a stationary distributor and is fed into the inner periphery of the HiGee in the form of jets or droplets (Rao, Bhowal, & Goswami, 2004). The liquid then attaches to the inner packing of the rotor and experiences intense impingement due to the relative velocity between the liquid and packing (Yi et al., 2009). At the same time, gas enters from the outer casing and flows radially inwards in a countercurrent direction due to the imposed pressure gradient. Under the centrifugal force, the liquid flows within the packing become thin films, tiny droplets, and rivulets (Burns & Ramshaw, 1996), decreasing mass transfer resistance and increasing gas/liquid interfacial area (Chen et al., 2010). As a result, mass transfer enhancement can be achieved in a HiGee system compared to conventional columns (Chen & Shao, 2003). These features lead to a significant reduction in the size of the processing system and allow for higher gas/liquid flow ratios due to its lower tendency to flooding.

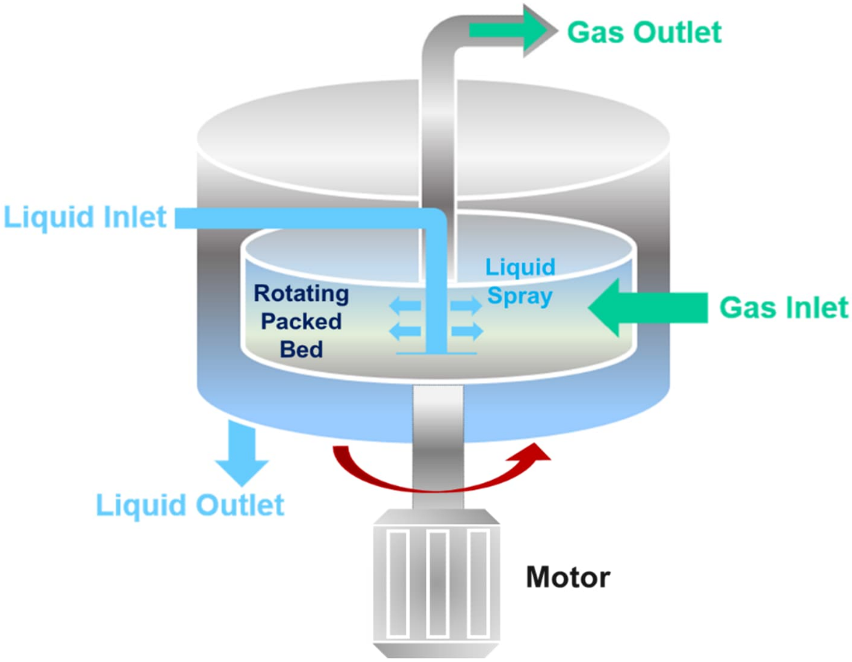

Figure 2-4 Schematic of a typical high gravity rotating packed beds system

2.3.2 Features of HiGee System

The high gravity rotating packed bed system has the following features in practical applications:

1) Compared with the conventional used plate column and packed column, the height of mass transfer unit can be reduced by 1-2 orders of magnitude, the mass transfer coefficient can be increased by 1-3 orders of magnitude, and the size of the equipment can be reduced by more than 10 times, under the same operating conditions.

2) Both the gas and liquid flux can be greatly improved thus treatment capacities can be increased without producing any liquid flooding.
3) The vacancy rate in packing beds is basically over 90%, which is much larger than the ordinary packed column. This will lead to a lower pressure drop and less energy consumption in HiGee system.
4) The liquid holding capacity is relatively small, and the liquid retention time in the rotor is very short, which makes it suitable for handling some heat-sensitive, expensive, or toxic materials.
5) Due to its smaller size, light weight, and easy location arrangement, it can be used on occasions where height or space is limited.
6) It is also suitable for ships, aircraft, and other moving objects as it is hardly influenced by vibration and bumps.
7) HiGee system occupies less space area, which help to save a lot of infrastructure investment and can be used for update and renovation work.
8) The maintenance cost is low, as the packing layer has a self-cleaning effect, which is not easy to scale or clog.
9) Rotating packed bed is easy to open and stop, and it can achieve stability in a few minutes showing its wide range of applications and operation flexibility.

2.3.3 Application Scenarios

High gravity rotating packed bed system has been widely applied in different scenarios mainly in chemical engineering due to its excellent performance on mass transfer process. Some of the typical real-world applications and reported research studies around the world are listed below.

1）Gas purification

The study and application on removal of a series of common air pollutants including H_2S, SO_2, NO_X, CO_2, NH_3, VOCs and particles has been conducted by using the high gravity rotating packed bed technology (Guo et al., 2019).

a) H_2S

Qi, Liu and Jiao (2008) reported that they used the Na_2CO_3 as the reactant under the binuclear catalyst of cobalt-phthalocyanine sulfonate (PDS) to remove the H_2S from coke oven gas using wet oxidation process in the rotating packed bed system. The removal rate of H_2S could reach as high as 99.8%, and the average removal rate was 90.15%, which showed the flexibility of using HiGee technology for both fine and bulk removal of H_2S on-site. In another study of H_2S removal in a fertilizer factory (Ximin, Jiaoping, & Shuanghong, 2008), hindered amine was used as adsorption solution. The outlet concentration could achieve the same level as the conventional desulfurizing tower stably with less steam consumption showing considerable economic benefits. Figure 2-5 displays the actual appearance of desulfurization using a high gravity rotating packed bed system in one chemical factory.

b) SO_2

The RPBs were developed to remove SO_2 with different reactant solutions. As reported by Chen et al. (2012), SO_2 from the tail gas of production lines of sulfuric acid were removed by RPBs system using ammonia-based solution with the averaged desulfurization efficiency of over 97%. In another similar application (Xu et al., 2013), the SO_2 removal efficiency could reach up to 98.8% with higher gas-to-liquid (G/L) ratio than conventional packed bed system, thus saving more operational space. At the same time, ammonium sulfate precipitates produced from the absorption of SO_2 by ammonium buffer solution were then recycled and utilized as fertilizers.

Figure 2-5 Photo of the actual appearance of high gravity rotating packed bed system for desulfurization in a chemical factory (Guo et al., 2019)

c) CO_2

CO_2 emissions make up a significant portion of greenhouse gases, it is critical to develop carbon capture, utilization, and storage technologies to meet the carbon neutrality targets. HiGee technology could provide promising short-term solutions, this concept was first realized in 2007 by using N-methyldiethanolamine (MDEA) and Triethylenetetramine (TETA) mixed solution as adsorbent for power plants to treat CO_2 with volume fraction about 5%-8% (Xing, Liu, & Cui, 2007). In 2012, Chang et al. (2012) proposed high gravity enhanced micro-mixing and mass transfer for carbonation (HiGCarb) process, it was used in steel plants (Pan et al., 2015; Pan et al., 2013) and petrochemical industry (Pan et al., 2017) in Taiwan. The HiGCarb process can achieve CO_2 removal efficiency of over 90% (Pan et al., 2015) and the largest scale of captured CO_2 was around 600 kg/day (Pan et al., 2017). In addition, modeling work on HiGee CO_2 capture system suggested the top two critical factors affecting the capture efficiency were the rotor speed and solution flow rate (Borhani, Oko, & Wang, 2018), which had food agreement with experimental results and provided thermotical support for system improvement.

d) NO_X

NO_X emission is a major pollutant from industrial process and fossil fuel combustion. It was first treated by carbamide as the absorbent, the removal efficiency of over 96% was achieved by two RPBs in series (Liu et al., 2007). When compared to traditional towers, the use of an RPB can result in a reduction of nearly 75% in equipment investment and a decrease of about 79% in operation costs. Li et al. (2010) developed and applied the HiGee in denitrification in industry area by using nitric acid solution as absorbent. At the same time, ozone was added as oxidizer for oxidation of HNO_2 to stable HNO_3 in liquid phase, and the detailed chemical mechanism was illustrated in Figure 2-6. The developed equipment can reach 90% removal efficiency with useful byproduct of nitic acid, which are suitable for real applications.

e) NH_3

Ammonia (NH_3) is a colorless gas that has a strong, unpleasant odor. It is considered an air pollutant and is primarily emitted by petrochemical, agricultural, and chemical industries. These industries include the synthetic ammonia industry, ammonium carbonate industry, ammonium nitrate industry, and nitro phosphate fertilizer industry. In 2006, HiGee technique had been applied to treat the NH_3 from the flue gas of a nitrophosphate fertilizer factory in China (Meng et al., 2008). A new type of RPB, equipped with radial corrugated packing, has been developed that can achieve both deamination and dehumidification simultaneously. This technique can achieve a deamination rate of up to

92% and a dehumidification rate of around 60%, while the large amount of collected ammonia and water can be easily recycled, making a significant contribution to reducing emissions and conserving energy.

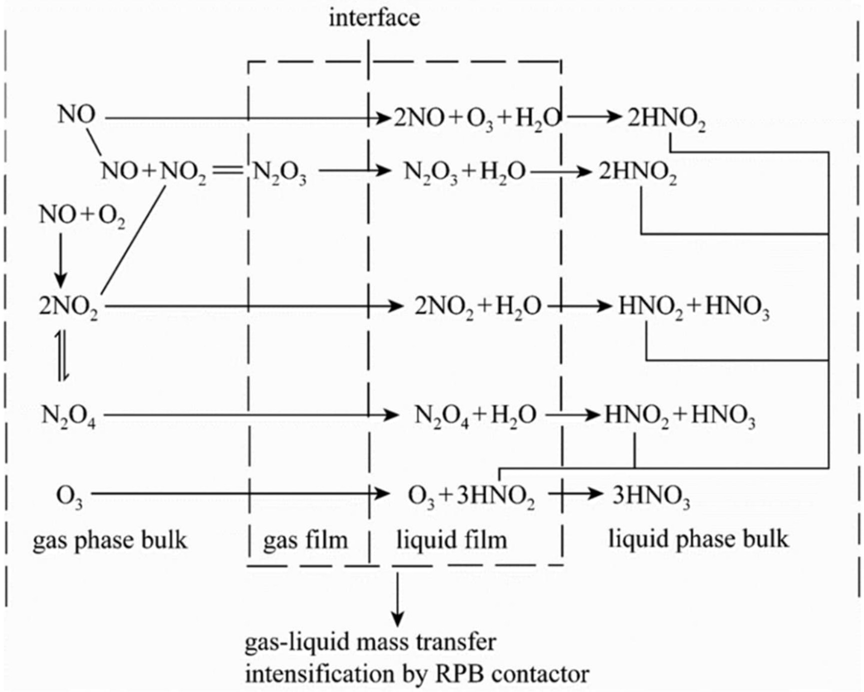

Figure 2-6 Mechanism of NO_X absorption into acid solution with the presence of O_3 in high gravity rotating packed bed system (Li et al., 2010)

f) VOCs

Traditional methods for purifying VOCs include adsorption, absorption, condensation, and membrane separation. However, these methods have several drawbacks, such as lengthy processing times, high energy consumption, and the potential for secondary pollution. Qu et al. (2011) applied HiGee in the VOC purification since 2010, and the developed system can be used to purify and recycle acetic acid (CH_3COOH), acetone (CH_3COCH_3), ethyl acetate ($CH_3COOC_2H_5$), etc. In a typical process of purifying acetic acid (CH_3COOH) gas, water is used as an absorbent. After the concentration of CH_3COOH

in the absorbent exceeds 70%, the used absorbent will be transferred to a rectification tower, where the purity of the CH_3COOH could be greater than 99%. By returning the recycling solution to the previous process, pollution can be reduced, and operation costs can be decreased as well.

g) Particulate matters

The HiGee scrubber PM collection technique is a newly designed method that combines the components of a cyclone, filter, mechanical rotation collector, and water dust scrubber to fully utilize their features and advantages (Guo et al., 2019). This system can be installed in series after existing treatment facilities to enhance purification effects. It can remove both hydrophilic and hydrophobic particulates with a higher purification capacity than an electrostatic precipitator (Jiao, Liu, & Zhang, 2005). Additionally, the floor area of the equipment is only 1/4 that of an electrostatic precipitator, resulting in lower equipment investment and capital expenditure. The removal efficiency is comparable to that of a venturi scrubber, but the pressure drop is only 1/6 and the energy consumption is only 17% of a venturi scrubber under the same purification conditions. These advanced features make the HiGee system efficient and economical for PM removal in real-world applications.

2）Wastewater treatment

Due to the pressing need to improve the efficiency and cost-effectiveness of wastewater treatment, the use of HiGee technology in this field has attracted interest and attention globally. Higee technology can be applied in various ways, either as a standalone system or in combination with other treatment technologies. When used to enhance wastewater treatment, Higee technology can achieve high mass transfer rates, shorter processing times, smaller equipment volumes, and lower energy consumption compared to traditional treatment systems (Jiao et al., 2017). Air stripping driven by RPB has been widely applied to purify wastewater containing volatile compounds by mass transferring from liquid to gas phase, including ammonia striping (Jiao et al., 2005; Yuan et al., 2016), acrylonitrile removal (Xue, Liu, & Jiao, 2016) and so on. As HiGee technique could provide more reaction opportunity between liquid and gas phases, ozone and radical related reactive process has been combined with HiGee system (Ge et al., 2016). H_2O_2 (Zeng et al., 2013), Fe (II) (Zeng et al., 2012) and Fenton solution (Wei et al., 2015) were added as oxidants to accelerate the conversion rate from O_3 to ·OH and to further decompose organic pollutants. In addition, the RPB system was also combined with electrochemical treatment to integrate with multi-concentric cylindrical electrodes, which not only enhanced the mass transfer but also helped to reduce the bubbling effect (Lao, Ramshaw, & Yeung, 2011; Mandin et al., 2007). Recently, Mosleh et al. (2016) developed a new catalytic rotating packed bed with visible blue LED around the reactor, and the final photocatalytic degradation rate of toluidine blue and auramine-O were 99.37% and 98.44, respectively. These results demonstrated the economical features by adapting rotating packed bed with higher efficiency and larger treatment capacities.

3）Nanomaterial preparation

Reactive precipitation is considered an effective method for mass-producing nanoparticles due to its low cost and ease of scaling up. However, the conventional precipitation process, typically carried out in a stirred tank or column reactor, can result in inconsistent product quality and varying particle size and morphology between batches. Using a Higee as an innovative reactor for synthesizing nanoparticles through precipitation has become a promising technology, thanks to its greatly enhanced mass transfer and micromixing efficiency (Zhao, Shao, & Chen, 2010). As the size of the nanoparticles could be well controlled for inorganic products and easy application in bulk production, the HiGee technology has been rapidly applied in chemical and petroleum industries (Chen et al., 2004). Besides, the production of pharmaceutical nanomaterials by high-gravity technique has been explored intensively (Chen & Shao, 2003; Shen, Chen, & Zhong, 2004), such as danazol (Zhao et al., 2009) and cefuroxime axetile (Chen et al., 2006). Nano-sized drug particles prepared using HiGee have been shown to have significantly improved bioactivities compared to commercially available particles including faster dissolution rates (Zhao et al., 2009), reduced need for complex solubilizers (Zhong et al., 2005), and higher fine particle fractions (Hu et al., 2008).

2.4 Application of Nanomaterials for Degradation of Gaseous Emissions from Cooking Oil Fumes

2.4.1 Application of Photocatalytic Nanomaterials for Pollutants Degradation

Photocatalysis is an effective and environment-friendly technology widely applied for gaseous pollutants removal such as NOx and HCHO with low economic consumption and little generated secondary pollutions (X. Li et al., 2022; Natarajan, Thampi, & Tayade, 2018; Zhang et al., 2021). Cooking oil fumes contain a variety of types of VOCs mainly including hydrocarbons, aldehydes and ketones, acids and esters, and alcohol pollutants with complex compositions and human toxicity (Lin & Bai, 2016; Sun et al., 2019). Compared with normal polluted flue gases with single-component or fixed species of VOCs, there are enhanced difficulties and uncertainties in catalytic oxidation and purification of flue gas from COFs. In addition, the catalytic activity, degradation stability, lifetime, and other properties of the photocatalyst also need higher requirements. Different photocatalysts like metal catalysts, non-metal catalysts, and metal-organic frameworks

(MOFs) have been investigated to deal with the VOCs in both indoor and outdoor environments.

The Ag-Ag-BrTiO$_2$ nanocomposite photocatalyst prepared by a simple deposition-precipitation method was used for the degradation of benzene and acetone in indoor and outdoor environments. And due to the synergistic photocatalysis between Ag-AgBr and P25, the photocatalytic activity and stability of Ag-AgBr-TiO$_2$ nanocomposites were higher than those of industrial TiO$_2$ (P25) in degrading benzene and acetone (Zhang et al., 2011). As for the VOCs of acetone, acetaldehyde, and toluene, Bianchi et al. (2014) compared the photocatalytic degradation performance of four industrial TiO$_2$ powders (two nanoscale and two microscale materials). The adsorption of acetone, acetaldehyde, or toluene on the surface of TiO$_2$ was proven to be a key factor affecting subsequent photocatalytic activity. The Ti-OH-Ti bridging clusters play a key role in promoting the photocatalytic activity of both nanoscale and microscale TiO$_2$, and the more Ti-OH-Ti bridging cluster groups there are, the higher the efficiency of photocatalytic degradation. In another study, the all-solid-state core-shell structured Z-scheme Bi@β-Bi$_2$O$_3$/g-C$_3$N$_4$ heterojunction is prepared by in-situ deposition and oxidation methods, where the metal Bi acts as a bridge for shuttling electrons between β-Bi$_2$O$_3$ and g-C$_3$N$_4$ (Lan et al., 2020). The developed Z-scheme heterojunction had good visible light degradation ability for 2,3-dihydroxynaphthalene (2,3-DHN) with a degradation rate of 87.0%. In 2019, Liu et al. (2019) designed a ZnO/ND photocatalyst, which effectively alleviated the photocorrosion problem of ZnO by controlling the morphology and exposed crystal planes of ZnO and adjusting the surface treatment method of nanometer diamond (ND). The test results showed that toluene with the concentration of 50 ppb could be completely removed within 2 hours under UV-365 light irradiation. Therefore, these newly designed various kinds of photocatalyst exhibit potential industrial and commercial application values in reducing VOCs emissions.

2.4.2 Design and Development of Heterojunction Photocatalyst

Traditionally, photocatalysts are semiconductors (such as TiO_2 and g-C_3N_4) (Huang et al., 2019; Nikokavoura & Trapalis, 2018) and some noble conductors (plasmonic metals, such as Au and Ag) (Yu et al., 2019; Ziashahabi et al., 2019). Compared with the above relatively rare and expensive semiconductors and plasmonic metals, earth-abundant insulators have great properties such as cheap price, stable chemical property and easy fabrication (Dong et al., 2017; Schiavoni et al., 2016). However, insulators have suffered application obstacles due to their great large band gaps which are hard to be excited, compared to those of semiconductors. On the other hand, the wide band gaps could offer excellent redox ability and prevent the combination of electron-hole pairs which are favorable in participating the photocatalytic reactions (R. Li et al., 2015). Recently, various strategies have been developed to modify the wide-gap insulators in solving the bottleneck problem, among which, constructing heterostructures has shown rising interest (Parul et al., 2020). The blending of different materials including semiconductors and insulators for the formation of heterojunctions could promote the efficiency of light utilization and capacity of redox reactions (Dong et al., 2018; Xue et al., 2019).

As a natural abundant semiconductor, strontium titanate ($SrTiO_3$, STO) is a cubic perovskite with superior photocatalytic redox potential and provide a higher efficiency in photocatalytic process than TiO_2 (Zhang, Yu, & Yi, 2017). Insulator strontium carbonate ($SrCO_3$, SCO) is developed as catalysts or co-catalysts and displays superior photocatalytic activity for NOx removal (Hodjati et al., 2000; Kobayashi et al., 2018). Considering the unique features of $SrTiO_3$ and $SrCO_3$, fabrication of $SrTiO_3/SrCO_3$ heterojunction has been confirmed as an effective way to combine the merits of each component and to accelerate the transmission and separation of photo-generated carriers to improve photocatalytic efficiency. Thus, several strategies have been adopted to construct $SrTiO_3/SrCO_3$ heterojunction in order to improve the adsorption ability and optical absorption (Jin et al., 2018; Márquez-Herrera et al., 2014). Nevertheless, all these mentioned synthesis methodologies normally require two or more steps and addition of carbonate sources or noble metals. Herein, developing functional heterostructure with a green and simple preparation method remains challenging.

Chapter 3 Methodology

In this chapter, the methodologies applied will be detailed described. In order to investigate characteristics and control strategies of the cooking emissions, sampling work, chemical analysis, efficiency and activity tests will be included.

3.1 Sampling Sites and Configurations

In this study, both in-lab cooking simulation tests and cooking scenarios in commercial kitchens/restaurants will be conducted. The cooking simulation test will focus on the investigation of different common cooking methods, while the on-site trials will target on the integrated cooking exhausts from various cooking processes in the commercial restaurants. The summary of the studied in-lab cooking methods and selected types of restaurants are listed in the below Table 3-1 and Table 3-2, which illustrate the 5 different types of cooking methods and 4 kinds of common restaurants in Hong Kong, respectively, with detailed information of space, number of stoves, the usage of oil, energy, ingredients and their represent dishes. The detailed basic information including kitchen room volume, air change rate and background concentrations of our designed simulation kitchens was used to estimate the emission rates (in mg/min) of these major pollutants from different cooking styles.

The on-site sampling and high gravity rotated packed bed test system are configured as displayed in Fig. 3-1. In this system setup, it includes 24 components with different roles, and it can be further divided into 4 functional sections. The item 1-5, 9 and 10 represent the typical and existing duct system for the exhaust of cooking oil fumes, while the item 6-8 in the green box shows the developed HiGee RPB scrubber equipment for the purification of cook exhaust, and the sampling point (item11) are located at the inlet and outlet duct of the scrubber. The red box (item 12-18) and blue box (item 19-24) demonstrate the sampling system to collect the particulate matters and gaseous chemicals from cooking exhaust, respectively. And the detailed description and operation will be discussed in the following sections.

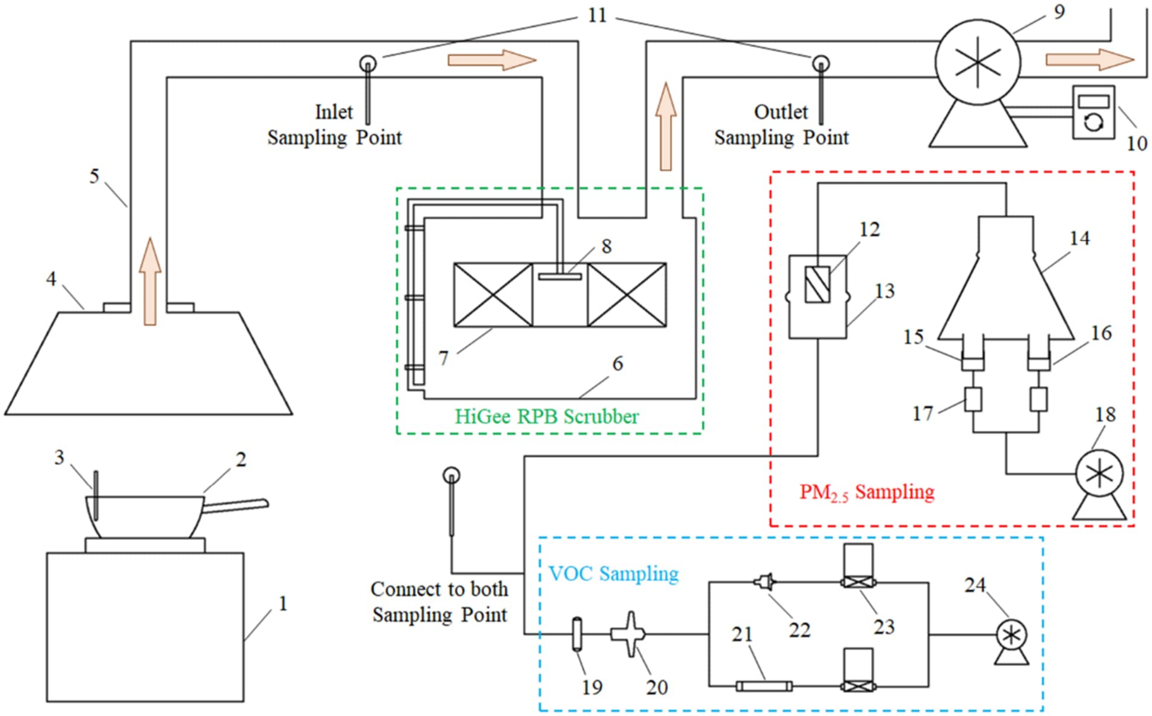

Figure 3-1 Schematic chart of the HiGee RPB scrubber system integrated with cooking exhaust system for cooking oil fumes and the setup of particulate and gaseous pollutants sampling system

The components in the figure are illustrated below. 1. Cooking bench, 2. Pan, 3. Temperature Sensor, 4. Exhaust fume hood, 5. Flue duct, 6. Casing of the HiGee RPB scrubber, 7. Rotating packed bed, 8. Washing liquid nozzle, 9. Exhaust fan, 10. Variable frequency drive for exhaust fan, 11. Inlet and outlet sampling points of scrubber system, 12. $PM_{2.5}$ cyclone cutter, 13. Inlet stilling chamber, 14. Plenum, 15. Quartz filter holder,

16. Teflon- membrane filter holder, 17. Flow meter, 18. Sampling pump, 19. Particle filter, 20. Ozone scrubber (Potassium Iodide), 21. VOC sorbent tube, 22. DNPH-Silica cartridge, 23. Mass flow controller, 24. Sampling pump.

A series of samples from cooking oil fumes were collected in the very front of the exhaust duct before any purification system to reflect the actual concentrations of the cooking processes. In addition, to study the purification efficiency of the developed scrubber, another series of samples were collected at the outlet of the HiGee scrubber to determine the efficiency of the purification system. For the sampling work in the lab simulation kitchen, the sampling duration was fixed to 90 mins with continuous cooking activities for all kinds of cooking methods. While the duration of the sampling work was adjusted to 3 hours in each real kitchen and the actual sampling time was also correlated to their designated working periods (i.e., peak cooking hours) of each restaurant. In a typical sampling experiment, 2 sets of $PM_{2.5}$ samples and 1 set of VOC tube and DNPH cartridge were collected from the sampling point. In addition, 1 set of blank samples was collected for each scenario when no cooking activities were carried out to determine the background status and for the QA/QC verification.

Table 3-1 Summary of different types of cooking methods included in this study (in-lab simulated kitchen test)

Type of Cooking	Abbr.	Type of Ingredient	Type of Oil	Type of Energy	Main Dishes	Basic Information of Simulated Kitchen
Stir-Frying	SF	Vegetable, Pork, Beef	Soybean Oil	Electric	Stir-fried Shrimps with Scrambled Eggs	Total room volume: 60 m^3 Air exchange rate during cooking period: 20 Air Change per Hour (ACH) Background concentrations: $PM_{2.5}$: 25 ug/m^3 TVOC: 30 ug/m^3
Pan-Frying	PF	Beef, Chicken, Egg, Sausage	Soybean Oil/Butter	Electric	Beef Steak	
Deep-Frying	DF	Chicken, Fish, Potato	Palm Oil	Electric	Fried Chicken	
Boiling	BL	Rice, Pork, Vegetable	Animal Oil (Beef Tallow)	Electric	Porridge	
Steaming	ST	Rice, Meat	Soybean Oil	Electric	Rice	

Table 3-2 Summary of different types of commercial restaurants included in this study

Restaurant Styles	Abbr.	Major Cooking Methods	Type of Oil	Type of Energy	Typical Dishes	Space (m^2)	No. of Stoves
Chinese Fast Food	CFF	Stir-frying, Boiling, Steaming	Soybean Oil, Peanut Oil	Town Gas, Electrical	Stir-fried Shrimps with Scrambled Eggs	100	10 (6 Gas, 4 Electrical)
Western Fast Food	WFF	Pan-frying, Deep-frying	Soybean Oil	Town Gas, Electrical	Hamburger, French fires	30	5 (2 Gas, 3 Electrical)
Cantonese Cuisine	CAN	Stir-frying, Steaming	Soybean Oil, Peanut Oil	Town Gas, Electrical	Dim Sum, BBQ Pork, Steamed Soup	80	8 (4 Gas, 4 Electrical)
Chongqing Hot Pot	CHP	Boiling	Animal Oil (Beef Tallow)	Electrical	Spicy Boiled Beef Tripe	150	15 (All Electrical)

3.2 Sampling and Chemical Analysis

3.2.1 Fine Particulate Matters ($PM_{2.5}$) Sampling

The DRI MEDVOL Particle sampler (Fraser et al., 2002) was used in this study to collect $PM_{2.5}$ samples. As shown in Fig. 3-2, it consists of an inlet stilling chamber, a $PM_{2.5}$ cyclone cutter, a conical plenum, open faced filter packs and a air vacuum pump. The $PM_{2.5}$ cyclone cutter (Bendix, Model: 240) operates at the fixed flow rate of 113 L/min, which removes particles larger than 2.5 micrometers in aerodynamic diameter from the inlet air stream. The desired air flow is provided by a pump (GAST, Model: 1023 ¾ HP carbon-vane vacuum pump, US), and the flowrate is continuously monitored and logged by a mass flow meter (TSI, Model: 4030E, US). The inner surface of the plenum is coated with nitric acid treated Perfluoro alkoxyalkane (PFA) Teflon, and its conical shape diffuses the airflow and minimizes the effect of particle deposition. 47-mm Teflon-membrane filters and 47-mm quartz-fiber filters can be placed in the filter holder based on the sampling arrangement and the targeted pollutants. All these filters are placed inside the PetriSlides prior to and after sampling and collected samples are stored in a preservation container at −25 °C before analysis.

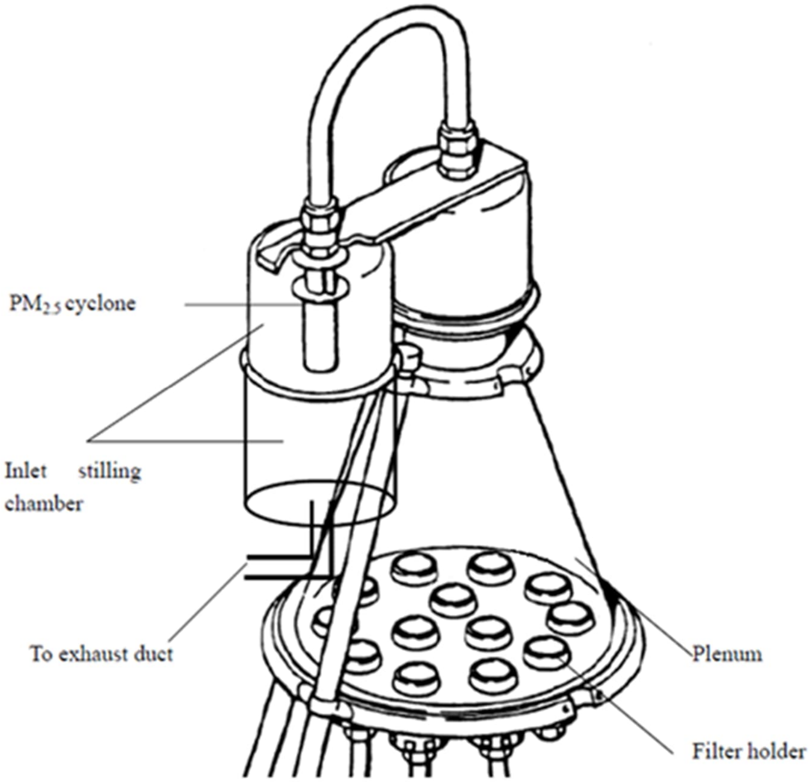

Figure 3-2 Schematic drawing and components of the DRI MEDVOL air particulate matters sampler

3.2.2 VOCs Sampling

A multi-bed stainless steel adsorbent tube (mass capacity of 380 mg with bed length of 60 mm, 5 mm i.d., and 6 mm o.d.), combining Tenax TA (35–60 mesh), Carbograph 1 TD (40–60 mesh) and Carboxen 1003 (40–60 mesh) (Markes, Model: C3-DXXX-5266, UK), is used to collect the target VOCs. Prior to sampling, the adsorbent tubes are cleaned for 20 mins at 330 °C in a thermal conditioner (Markes, Model: TC20, UK) with a purge of high-purity nitrogen gas (99.9999% purity) at a rate of 50 mL min^{-1}. Both ends of these pre-conditioned tubes are sealed with Difflok caps (Markes, UK) and stored in a preservation container at −10 °C for a maximum of 14 days. A diaphragm gas pump (KNF, Model: N84.3, Germany) was used to collect the gas samples and a mass flow controller (SevenStar, Model: CS-200A, China) to regulate the flow rate at 50 mL/min. A particle filter and an ozone scrubber (Waters Corporation, Model: Sep-Pak; US) were connected to the very front of the sampling tube to avoid the influence from particulate matters and ambient ozone. In addition, an inline dryer was installed after the adsorption tube to eliminate the water contents and ensure the accuracy of the mass flow controller, and two identical adsorption tubes were connected in series to check the situation of VOC breakthrough regularly.

3.2.3 OVOCs Sampling

Carbonyl samples were collected using 2,4-dinitrophenylhydrazine (DNPH) cartridges (Waters, Model: Sep-Pak DNPH-silica, US) at the flow rate of 0.7 L/min controlled by a mass flow controller (SevenStar, Model: CS-200A, China) with the same diaphragm gas pump. The sampling tube, particle filter and ozone scrubber were shared with the VOC sampling system as illustrated in Fig. 3-1. As VOCs sampling, an inline dryer was also adopted after the DNPH cartridges and breakthrough situation for OVOCs was checked regularly as well.

3.2.4 Online Measurement Equipment

In order to obtain the full picture of each cooking scenario and to evaluate the purification efficiency, additional real-time monitoring equipment and portable sensors were applied in the experiment. The Q-Trak (TSI, Model: 7575, US) and DustTrak II (TSI, Model: 8532, US) were used to measure the real-time environment conditions and $PM_{2.5}$ concentrations, respectively, which were installed at the sampling points of cooking exhaust air duct and data was captured during the whole sampling periods. In addition, a handheld total volatile organic carbon (TVOC) monitor (Honeywell, ppbRAE-3000, US) and a newly developed moveable mini air station (Sapiens, Model: MAS-AF300, China) were used to measure the indoor ambient environment and other pollutants during cooking periods. The detailed information was demonstrated in previous study in Hong Kong (Che et al., 2020) and these measured parameters includes TVOC, $PM_{2.5}$, PM_{10}, NO, NO_2, O_3, CO and CO_2. The accuracy of the air station was validated in the laboratory and all the data was stored with a time interval of 1 min.

3.2.5 Gravity Analysis

Teflon-membrane filter samples were used to report the mass concentrations as the Teflon-membrane filter media is relatively stable from the influence of relative humidity on its mass. As discussed in our previous study (Gao et al., 2015), the filter samples were equilibrated in a temperature (25.0 ± 1.0 °C) and humidity (40.0 ± 1.0%) controlled environment chamber for at least 24 hours prior to the first weighing of the sample. The mass of filter sample was determined by a microbalance with sensitivity of ± 1 μg (Sartorius AG, Model MC5, Germany). A second weighing was conducted after another 24-hour sample equilibration following the first weighing. Consecutive weighing with intervals of at least 24 hours was conducted until the mass difference between the two weighing results is less than 15 μg. The average of the two results was used to report the $PM_{2.5}$ mass concentration.

3.2.6 $PM_{2.5}$-bound Chemical Analysis

1）Carbon Analysis

Organic carbon (OC) and elemental carbon (EC) are determined by 0.5 cm^2 punches prepared from each of the sample filters. A DRI model 2001 carbon analyzer (Atmoslytic Inc., Calabasas, CA, USA) is used for these determinations following the IMPROVE_A thermal/optical reflectance (TOR) protocol (Chow et al., 2007). The sample aliquot is heated in a series of steps to determine the concentrations of four OC fractions (OC1, OC2, OC3, and OC4) in a helium atmosphere and OP (pyrolyzed carbon fraction) and three EC fractions (EC1, EC2, and EC3) in a 2% O_2/ 98% He atmosphere. The analyzer is calibrated with known quantities of methane (CH_4) each day of use. The IMPROVE protocol defined OC as OC1, + OC2 + OC3+ OC4 + OP and EC as EC1 + EC2 + EC3 - OP. Replicate analyses are performed at a frequency of one per group of 10 samples. The relative deviation of replicate analysis is < 5% for TC (total carbon, the sum of OC and EC), and < 10% for OC and EC. The Method Detection Limits (MDLs) represent the best sensitivity of the method and should always be less than or equal to the lower quantifiable limits (LQLs). The MDL is defined as three times the standard deviation of their measured results. The total OC is 0.38 μg/filter; total EC is 0.44 μg/filter; and TC is 0.82 μg/filter.

2）Water-soluble Inorganic Ions

The concentrations of five cations (Na^+, NH_4^+, K^+, Mg^{2+}, Ca^{2+}) and four anions (F^-, Cl^-, NO_3^-, SO_4^{2-}) are determined in aqueous extracts of the $PM_{2.5}$ samples. To extract the water-soluble ions from the Teflon-membrane filters, the portions of the filters used for the gravimetric analysis are placed in a separate 15 mL vial containing 10 mL distilled–deionized water (18.2 MΩ resistivity). The vials are placed in an ultrasonic water bath and shaken with a mechanical shaker for 1 h to extract the ions. The extracts are filtered through 0.45 μm pore size microporous membranes, and the filtrates are stored at 4 °C in clean tubes before instrumental analysis. A Dionex UltiMate 3000 Ion Chromatography (Sunny-vale, CA, USA) is used for the determinations of both cations and anions in the aqueous extracts of the filters. For the cation analyses, the instrument is equipped with an IonPac CS12A column (20 mM methanesulfonic acid as the eluent), while for anions, an IonPac AS14A column (8 mM Na_2CO_3/ 1 mM $NaHCO_3$ as the eluent) is used. The MDLs are as follows: 4.6 mg L^{-1} for Na^+, 4.0 mg L^{-1} for NH_4^+, 10.0 mg L^{-1} for K^+, Mg^{2+} and Ca^{2+}, 0.5 mg L^{-1} for F^-, Cl^- and Br^-, 15 mg L^{-1} for NO_2^- and NO_3^-, and 20 mg L^{-1} for SO_4^{2-}. Standard reference materials produced by the National Research Center for Certified Reference Materials (Beijing, China), are analyzed for quality control and assurance purposes. All the reported ion concentrations are corrected with field blanks, i.e., filters brought to the field and installed in the samplers without pumped air.

3）Element Analysis

Energy Dispersive X-Ray Fluorescence (ED-XRF) spectrometry (Epsilon 5 ED-XRF, PANalytical B. V., Netherlands) is used to determine the concentrations of selected elements on the $PM_{2.5}$ quartz fiber filters. Each sample is analyzed for 30 mins to obtain a spectrum of X-ray counts versus photon energies, in which the individual peak energies matched specific elements, and the peak areas varied with elemental concentrations. Laboratory filter blanks also are analyzed to evaluate analytical bias. The elements that are determined by the ED-XRF method include Al, Si, Cd, Ni, Mg, Na, K, Ca, Ti, Cr, Mn, Fe, Ni, Cu, Zn, Ga, As, Se, Rb, Mo, Sn, Ba, La, Hg and Pb. National Institute of Standards and Technology (NIST) Standard Reference Material (SRM) are employed to validate the accuracy of measurement.

4）$PM_{2.5}$-bound PAHs

The PAHs on the quartz filters are quantified using solvent extraction-gas chromatography/mass spectrometry (SE-GC/MS). The final solution is then mixed with

25 mL injection internal standard (fluoranthene-d10, 20 ng/mL) to a total volume of 1 mL. One microliter of each extract is injected into a GC system (Agilent Technology, Model: 7890N, Santa Clara, CA) at 280 °C with an autosampler (Agilent Technology, Model: 7693, Santa Clara, CA). The operating temperature of the injector is set at 250 °C in a splitless mode. The GC oven temperature is initially set at 50 °C, ramps to 150 °C in 4 mins and holds at this temperature for 10 mins, and then increases to 300 °C in 30 mins and holds at this final temperature for 5 mins. The target PAHs are scanned and detected by a mass selective detector (MSD) (Agilent Technology, Model: 5975C, Santa Clara, CA) in the selective ion monitoring (SIM) mode. Calibration curves are established by plotting the peak area ratios (analytes/injection internal standard) versus the amounts of the analytes per injection. Target PAHs are identified and quantified using comparison of retention times and chromatographic peaks with those of known calibration curves. The MDLs for the target PAHs represent the amounts of the compounds that generate detectable signals plus three times the standard deviation of the blank signal. When no peaks is detected in the blank calibration samples, the blank signal is estimated by the calibration line intercept and the blank standard deviation is the standard error of the intercept. The MDLs range from 0.11 – 2.28 ng per sample. All the detected and analyzed PAH chemicals from the $PM_{2.5}$ samples are summarized in Table 3-3.

Table 3-3 Summary of the PAHs analyzed in the $PM_{2.5}$ samples

PAHs Congener	**Abbv.**	**Ring**	**Mass Class**	**Formular**	**MW (g/mol)**	**LOD (ng/m^3)**
Acenaphthylene	Acy	2	LM	$C_{12}H_8$	152	0.0031
Naphthalane	Nap	3	LM	$C_{10}H_8$	128	0.0460
Acenapthene	Ace	3	LM	$C_{12}H_8$	154	0.0050
Fluorene	Flu	3	LM	$C_{13}H_{10}$	166	0.0061
Phenanthrene	Phe	3	LM	$C_{14}H_{10}$	178	0.0104
Anthracene	Ant	3	LM	$C_{14}H_{10}$	178	0.0076

Fluoranthene	Fln	4	MM	$C_{16}H_{10}$	202	0.0088
Pyrene	Pyr	4	MM	$C_{16}H_{10}$	202	0.0098
Benzo[a]anthracene	BaA	4	MM	$C_{18}H_{12}$	228	0.0080
Chrysene	Chr	4	MM	$C_{18}H_{12}$	228	0.0076
Benzo[b]fluoranthene	BbF	5	MM	$C_{20}H_{12}$	252	0.0040
Benzo[k]fluoranthene	BkF	5	MM	$C_{20}H_{12}$	252	0.0038
Benzo[a]fluoranthene	BaF	5	MM	$C_{20}H_{12}$	252	0.0054
Perylene	Per	5	MM	$C_{20}H_{12}$	252	0.0054
Dibenzo[a,h]anthracene	DBA	5	HM	$C_{22}H_{14}$	278	0.0042
Benzo[e]pyrene	BeP	6	MM	$C_{20}H_{12}$	252	0.0058
Benzo[a]pyrene	BaP	6	MM	$C_{20}H_{12}$	252	0.0032
Indeno[1,2,3-cd]pyrene	InD	6	HM	$C_{22}H_{12}$	276	0.0010
Benzo[ghi]perylene	BghiP	6	HM	$C_{22}H_{12}$	276	0.0069
Dibenzo[a,e]pyrene	Dip	6	HM	$C_{24}H_{14}$	302	0.0070
Coronene	Cor	7	HM	$C_{24}H_{12}$	300	0.0031

3.2.7 Analysis of VOCs

Certified PAMS and Air Toxic standard mixtures (100 ppbv for each of the target VOCs) (Restek Corporation, Bellefonte, PA, USA) are used for calibration and performance tests and all these targeted VOCs are listed in Table 3-4. A 3-Liter Tedlar bag (Restek Corporation, USA) is filled with high-purity nitrogen gas and evacuated with a pump three times before each experiment. The standard gas is diluted with high-purity nitrogen gas to the desired concentrations (i.e., 0.08 – 1.67 ppbv for calibration and 2 ppbv for performance tests). These mixtures are drawn through the absorbents with a low-flow pump (1 – 350 mL min^{-1}; ACTI-VOC, Markes, UK), calibrated with a mass flow calibrator (Defender 510, Bios, Torrance, CA, USA) with a stability of ± 2.7% at 50 mL min^{-1}. A certified reference standard (CRS) (C-TO17XX-10, Markes) containing 100 ng each of benzene, toluene, o-xylene, 1,2,4-trimethylbenzene, dichloromethane, 1,1,1-trichloroethane, methyl tertbutyl ether, methyl ethyl ketone, and ethyl acetate is used to evaluate the desorption accuracy.

The samples are analyzed using a thermo-desorption (TD) unit (Series 2 UNITY-xr system with ULTRA-xr, Markes) coupled with a gas chromatograph/mass spectrometric detector (TD-GC/MS, Models 7890A/5977B, Agilent Technology, Santa Clara, CA, USA). The absorbent tube is connected to the TD unit at room temperature (~20 °C) and purged with ultra-high purity He gas at a flow rate of 40 mL min^{-1} for 10 s to eliminate air and oxygen intrusion. For the first desorption stage, the analytes are desorbed at 330 °C for 8 mins and refocused onto a cryogenic-trap (U-T1703P-2S, Markes) to capture high volatility target compounds at −15 °C. For the secondary desorption stage, the trap is dry-purged for 10 s and rapidly heated from −15 °C to 320 °C and maintains for 5 mins. The analytes are passed via a heated transfer line at 160 °C and refocused again onto a cold GC capillary column head (Rtx®-1, 105 m × 0.25 mm× 1 mm film thickness, Restek Corporation, USA) at −45 °C with liquid N_2 in the GC oven. After the second desorption, the oven temperature remains at −45 °C for 4 mins, ramps to 230 °C at a rate of 6 °C min^{-1}, and stabilizes at 230 °C for 5 mins. The helium carrier gas flow rate is 1.0 mL min^{-1} for the duration of GC analysis. The selective ion monitoring (SIM) mode is applied to scan and identify the target analytes with the MSD in electron impact (EI) ionization (70 eV) mode. Multi-point calibration curves are established to quantify each of the target compounds with linearity > 0.999. The method detection limits (MDLs) are in the range of 0.003 - 0.808 ppbv with a sampling volume of 3 L. The precision of the measurement for the analysis of eight replicates of standard samples at 2 ppbv is < 5%.

Table 3-4 Summary of the detected and analyzed VOCs

Chemical	**LOD**	**MW (g/mol)**	**Formular**	**Carbon Number**	**Detection Method**
Alkane					
ethane	0.0534	30.070	C_2H_6	2	FID
propane	0.0154	44.10	C_3H_8	3	FID
isobutane	0.0202	58.12	C_4H_{10}	4	MSD
butane	0.0167	58.12	C_4H_{10}	4	MSD

cyclopentane	0.0084	70.14	C_5H_{10}	5	MSD
isopentane	0.0047	72.15	C_5H_{12}	5	MSD
pentane	0.0016	72.15	C_5H_{12}	5	MSD
2,2-dimethylbutane	0.0021	86.18	C_6H_{14}	6	MSD
2,3-dimethylbutane	0.0017	86.18	C_6H_{14}	6	MSD
isohexane	0.0086	86.18	C_6H_{14}	6	MSD
3-methylpentane	0.0074	86.18	C_6H_{14}	6	MSD
hexane	0.0068	86.18	C_6H_{14}	6	MSD
2,4-dimethylpentane	0.0107	100.21	C_7H_{16}	7	MSD
methylcyclopentane	0.0089	84.16	C_6H_{12}	6	MSD
2-methylhexane	0.0013	100.21	C_7H_{16}	7	MSD
2,3-dimethylpentane	0.0024	100.21	C_7H_{16}	7	MSD
cyclohexane	0.0023	84.16	C_6H_{12}	6	MSD
3-methylhexane	0.0173	100.21	C_7H_{16}	7	MSD
heptane	0.0086	100.21	C_7H_{16}	7	MSD
methylcyclohexane	0.0083	98.19	C_7H_{14}	7	MSD
2,3,4-trimethylpentane	0.0111	114.23	C_8H_{18}	8	MSD
2,2,4-trimethylpentane	0.0164	114.23	C_8H_{18}	8	MSD
2-methylheptane	0.0127	114.23	C_8H_{18}	8	MSD
3-methylheptane	0.0102	114.23	C_8H_{18}	8	MSD
octane	0.0078	114.23	C_8H_{18}	8	MSD
nonane	0.0069	128.26	C_9H_{20}	9	MSD
decane	0.0113	142.29	$C_{10}H_{22}$	10	MSD
undecane	0.0096	156.31	$C_{11}H_{24}$	11	MSD
dodecane	0.0165	170.34	$C_{12}H_{26}$	12	MSD
trichlorofluoromethane	0.032	137.4	CCl_3F	1	MSD
dichlorodifluoromethane	0.026	120.91	CCl_2F_2	1	MSD
1,1,2-trichlorotrifluoroethane	0.040	187.4	$C_2Cl_3F_3$	2	MSD
1,2-dichlorotetrafluoroethane	0.026	170.92	$C_2Cl_2F_4$	2	MSD
Alkene					
ethylene	0.0502	28.054	C_2H_4	2	FID
propylene	0.0231	42.081	C_3H_6	3	FID
trans-2-butene	0.0020	56.11	C_4H_8	4	MSD
1-butene	0.0008	56.11	C_4H_8	4	MSD
cis-2-butene	0.0019	56.11	C_4H_8	4	MSD
1,3-butadiene	0.0167	54.09	C_4H_6	4	MSD
1-pentene	0.0118	70.14	C_5H_{10}	5	MSD
trans-2-pentene	0.0019	70.14	C_5H_{10}	5	MSD
isoprene	0.0164	68.12	C_5H_8	5	MSD
cis-2-pentene	0.0018	70.14	C_5H_{10}	5	MSD
1-hexene	0.0065	84.16	C_6H_{12}	6	MSD
1,4-dioxane	0.0267	88.11	$C_4H_8O_2$	4	MSD
Aromatics					
benzene	0.002	78.11	C_6H_6	6	MSD

toluene	0.003	92.14	C_7H_8	7	MSD
ethylbenzene	0.003	106.17	C_8H_{10}	8	MSD
dimethylbenzene	0.003	106.17	C_8H_{10}	8	MSD
1,2-dimethylbenzene	0.002	106.17	C_8H_{10}	8	MSD
styrene	0.002	104.15	C_8H_8	8	MSD
cumene	0.002	120.20	C_9H_{12}	9	MSD
N-propylbenzene	0.002	120.20	C_9H_{12}	9	MSD
3-ethyltoluene	0.002	120.20	C_9H_{12}	9	MSD
4-ethyltoluene	0.002	120.20	C_9H_{12}	9	MSD
mesitylene	0.001	120.20	C_9H_{12}	9	MSD
1-ethyl-2-methylbenzene	0.002	120.20	C_9H_{12}	9	MSD
pseudocumene	0.001	120.20	C_9H_{12}	9	MSD
1,2,3-trimethylbenzene	0.009	120.20	C_9H_{12}	9	MSD
1,3-diethylbenzene	0.010	134.22	$C_{10}H_{14}$	10	MSD
1,4-diethylbenzene	0.002	134.22	$C_{10}H_{14}$	10	MSD
naphthalene	0.003	128.17	$C_{10}H_8$	10	MSD
Halogenated Hydrocarbons					
methyl chloride	0.025	50.49	CH_3Cl	1	MSD
vinyl chloride	0.016	62.50	C_2H_3Cl	2	MSD
methyl bromide	0.020	94.94	CH_3Br	1	MSD
chloroethane	0.012	64.51	C_2H_5Cl	2	MSD
1,1-dichloroethylene	0.012	96.94	$C_2H_2Cl_2$	2	MSD
methylene chloride	0.016	84.93	CH_2Cl_2	1	MSD
1,1-dichloroethane	0.021	98.95	$C_2H_4Cl_2$	2	MSD
cis-1,2-dichloroethylene	0.009	96.94	$C_2H_2Cl_2$	2	MSD
chloroform	0.007	119.4	$CHCl_3$	1	MSD
1,1,1-trichloroethane	0.011	133.4	$C_2H_3Cl_3$	2	MSD
carbon tetrachloride	0.023	153.8	CCl_4	1	MSD
trans-1,2-dichloroethylene	0.020	96.94	$C_2H_2Cl_2$	2	MSD
trichloroethylene	0.017	131.4	C_2HCl_3	2	MSD
1,2-dichloropropane	0.008	112.98	$C_3H_6Cl_2$	3	MSD
bromodichloromethane	0.017	163.82	$CHBrCl_2$	1	MSD
trans-1,3-dichloropropene	0.009	110.97	$C_3H_4Cl_2$	3	MSD
cis-1,3-dichloropropylene	0.008	110.97	$C_3H_4Cl_2$	3	MSD
1,1,2-trichloroethane	0.010	133.4	$C_2H_3Cl_3$	2	MSD
tetrachloroethylene	0.008	165.8	C_2Cl_2	2	MSD
ethylene dibromide	0.020	187.86	$C_2H_4Br_2$	2	MSD
chlorobenzene	0.006	112.56	C_6H_5Cl	6	MSD
m-dichlorobenzene	0.023	147.00	$C_6H_4Cl_2$	6	MSD
p-dichlorobenzene	0.021	147.00	$C_6H_4Cl_2$	6	MSD
chlorotoluene	0.023	126.58	C_7H_7Cl	7	MSD
1,2,4-trichlorobenzene	0.023	181.4	$C_6H_3Cl_3$	6	MSD
hexachlorobutadiene	0.024	260.7	C_4Cl_6	4	MSD
dichlorobenzene	0.010	147.00	$C_6H_4Cl_2$	6	MSD

Others					
acetylene	0.035	26.038	C_2H_2	2	FID
acetonitrile	0.024	41.053	CH_3CN	1	MSD
isopropyl alcohol	0.033	60.10	C_3H_8O	3	MSD
ethyl acetate	0.030	88.11	$C_4H_8O_2$	4	MSD
vinyl acetate	0.015	86.09	$C_4H_6O_2$	4	MSD
methyl tert-butyl ether	0.031	88.15	$C_5H_{12}O$	5	MSD
tetrahydrofuran	0.030	72.11	C_4H_8O	4	MSD
methyl methacrylate	0.030	100.12	$C_5H_8O_2$	5	MSD
methyl isobutyl ketone	0.023	100.16	$C_6H_{12}O$	6	MSD
n-butyl methyl ketone	0.030	100.16	$C_6H_{12}O$	6	MSD

3.2.8 Analysis of OVOCs

A total of 16 carbonyls (listed in Table 3-5) are quantified, including formaldehyde, acetaldehyde, acetone, propionaldehyde, 2-butanone (MEK), iso+n-butyraldehyde, benzaldehyde, iso-valeraldehyde, n-valeraldehyde, o-tolualdehyde, mtolualdehyde, p-tolualdehyde, hexanal, and 2,5-dimethylbenzaldehyde. Each DNPH-coated cartridge is eluted with 2.0 mL of acetone-free acetonitrile (HPLC grade, J&K Scientific Ltd., Ontario, Canada) to a volumetric flask. Certified calibration standards of the monocarbonyl DNP-hydrazones are purchased from Supelco (Bellefonte, PA, USA) and diluted into concentration ranges of 0.015 – 3.0 μg mL^{-1}. The final volume of each calibration mixture is made to be 2.0 mL with 8:2 (v/v) of acetonitrile/pyridine (HPLC/GCMS grade, Sigma). Linearity is indicated by a correlation of determination (r^2) of at least 0.999.

The cartridge extracts and calibration standards are analyzed by injecting 20 μL of the samples to a high-performance liquid chromatography (HPLC) system (Series 1200; Agilent Technology, Santa Clara, CA, USA) equipped with a photodiode array detector (PAD). The column for separation is a 4.6 × 250 mm Spheri-5 ODS 5-μm C-18 reversed-phase column (PerkinElmer, Norwalk, CT, USA) operated at room temperature. The mobile phase consists of three solvent mixtures: mixture A, 6:3:1 (v/v/v) of water/acetonitrile/tetrahydrofuran; mixture B, 4:6 (v/v) of water/acetonitrile; and mixture C, acetonitrile. The gradient program is 80% A/ 20% B for 1 min, followed by linear gradients to 50% A/ 50% B for the next 8 mins, and to 100% B for the next 10 mins and to 100% C for the next 6 mins, and final 100% C for the next 5 mins. The flow rate is 2.0 mL/min. The absorption peaks at 360 s and 390 s are used for the identification of the aliphatic carbonyls and aromatic carbonyls (benzaldehyde and tolualdehydes), respectively. Identification and quantification of carbonyl compounds are based on the retention times and peak areas of the corresponding calibration standards. The MDLs are done by analyzing a minimum of seven replicates of a standard solution containing the analytes at a concentration of 0.015 μg/mL. The MDLs of the target carbonyls range from 0.002 to 0.010 μg/mL, which can be translated to 0.016 – 0.12 parts per billion by volume (ppbv) with a sampling volume of 2.02 m^3. The measurement precision for the analysis of ten replicates of a standard solution containing the analytes at a concentration of 1.0 μg/mL ranges from 0.5% to 3.2%.

Table 3-5 Summary of the detected and analyzed carbonyls

Chemical	**LOD**	**MW (g/mol)**	**Formular**	**Carbon Number**	**Detection Method**
formaldehyde	0.028	30.026	CH_2O	1	HPLC
acetaldehyde	0.043	44.053	C_2H_4O	2	HPLC
acetone	0.039	58.08	C_3H_6O	3	HPLC
acrolein	0.035	56.064	C_3H_4O	3	HPLC
propionaldehyde	0.038	58.08	C_3H_6O	3	HPLC
crotonaldehyde	0.020	70.09	C_4H_6O	4	HPLC
methyl ethyl ketone	0.020	72.11	C_4H_8O	4	HPLC
isobutyraldehyde	0.038	72.11	C_4H_8O	4	HPLC
benzaldehyde	0.036	106.12	C_7H_6O	7	HPLC
isovaleraldehyde	0.040	86.13	$C_5H_{10}O$	5	HPLC
valeraldehyde	0.045	86.13	$C_5H_{10}O$	5	HPLC
2-methylbenzaldehyde	0.049	120.15	C_8H_8O	8	HPLC
3-methylbenzaldehyde	0.079	120.15	C_8H_8O	8	HPLC
4-methylbenzaldehyde	0.079	120.15	C_8H_8O	8	HPLC

caproic aldehyde	0.046	100.16	$C_6H_{12}O$	6	HPLC
2,5-dimethylbenzaldehyde	0.067	134.18	$C_9H_{10}O$	9	HPLC

3.3 COFs Impact Assessment and Model Configuration

3.3.1 VOCs Hydroxyl Radical Loss Rate (L_{OH})

The L_{OH} of VOCs is commonly used to quantify the contribution of reactivity of various VOCs in the atmosphere (Wang et al., 2014; X. X. Zhang et al., 2019). The chemical reactivity is calculated by the mixing ratio level of VOCs and its •OH rate constant using the equation 3-1 shown below:

$$L_{OH}\,(j) \;=\; [VOC]\,(j) \;\times\; k^{OH}\,(j) \qquad \text{(Eq. 3-1)}$$

where $L_{OH}\,(j)$ is the •OH loss rate for the specific VOC j; $[VOC](j)$ is the concentration of the VOC specie j (in molecules/cm^3); and $k^{OH}(j)$ is the constant of •OH loss rate of specie j (in cm^3 molecule^{-1}·s^{-1}), which has been reported by Atkinson and Arey (2003).

3.3.1 VOCs Hydroxyl Radical Loss Rate (L_{OH})

The L_{OH} of VOCs is commonly used to quantify the contribution of reactivity of various VOCs in the atmosphere (Wang et al., 2014; X. X. Zhang et al., 2019). The chemical reactivity is calculated by the mixing ratio level of VOCs and its •OH rate constant using the equation 3-1 shown below:

$$L_{OH}\,(j) \;=\; [VOC]\,(j) \;\times\; k^{OH}\,(j) \qquad \text{(Eq. 3-1)}$$

where $L_{OH}\,(j)$ is the •OH loss rate for the specific VOC j; $[VOC](j)$ is the concentration of the VOC specie j (in molecules/cm^3); and $k^{OH}(j)$ is the constant of •OH loss rate of specie j (in cm^3 molecule^{-1}·s^{-1}), which has been reported by Atkinson and Arey (2003).

3.3.2 VOCs Ozone Formation Potential

The maximum incremental reactivity (MIR) method established by Carter (2010) was used to evaluate the O_3 formation potential (OFP) of an individual VOC by the following equation 3-2:

$$OFP\,(j) \;=\; Concentration\,(j) \;\times\; MIR\,(j) \qquad \text{(Eq. 3-2)}$$

where $OFP\,(j)$ is the OFP for the specific VOCj; $Concentration\,(j)$ is the concentration of the specific VOC j (in μg/m^3); and $MIR\,(j)$ (in gram of O_3 per gram of an organic compound) is the maximum incremental reactivity coefficient of the specific VOCj.

3.3.3 Secondary Organic Aerosol Formation Potential

The formation of secondary organic aerosol (SOA) is a complex process and several approaches or methods for calculating the SOA formation potential have been developed. In this study, the widely applied fraction aerosol coefficient (FAC) method (J. Li et al., 2022; Z. J. Zhang et al., 2017) has been used to estimate the SOA formation potential (SOAFP), which uses the published FAC values reflecting the ratio of aerosol yield from a specific VOC (Grosjean, 1992; Grosjean & Seinfeld, 1989). The SOAFP can be calculated by the following equation 3-3:

$$SOAFP_{VOC(j)} \;=\; Concentration\,(j) \;\times\; FAC\,(j) \qquad \text{(Eq. 3-3)}$$

where $SOAFP_{VOC(j)}$ is the SOAFP of the specific VOCj, $Concentration\,(j)$ is the concentration of the specific VOCj (in μg/m^3); and $FAC(j)$ (in %) is the fractional aerosol coefficient of species VOCj.

3.3.4 Health Risk Assessment Model

To determine the carcinogenic risks and other health issues posed by PAHs and VOCs of COFs from the cooking activities, a chronic risk exposure assessment has been performed referring to the assessment guidance stimulated by US EPA (U.S. EPA, 2009). The detailed calculation processes are listed below, and the exposure concentration (EC) (g/m^3) of a specific substance can be calculated as below Eq. 3-4:

$$EC = \frac{CA \times ET \times EF \times ED}{AT} \qquad \text{(Eq. 3-4)}$$

where CA is the specific VOC concentration (in g/m^3), ET is the exposure time (in hours/day), EF is the exposure frequency (in days/year), ED is the exposure duration (in years), and AT is the averaging time (in hours).

The linear low-dose method can be used to evaluate the incremental lifetime cancer risks (ILCR) for people exposed via the inhalation pathway with the following Eq. 3-5:

$$ILCR = IUR \times EC \qquad \text{(Eq. 3-5)}$$

where IUR is the inhalation unit risk (in (μg/m^3)$^{-1}$) and the IUR values could be obtained from the Integrated Risk Information System (IRIS) (U.S.EPA, 2004) and California office of environmental health hazard assessment (OEHHA) (OEHHA, 2023). A value higher than 1×10^{-6} denotes a possible carcinogenic effect by the inhalation exposure, and a value less than or equal to 1×10^{-6} represents no carcinogenic effects occurring.

The dimensionless hazard quotient (HQ) is used to reflect the non-cancer risk of roadside exposure, which can be calculated by below Eq. 3-6:

$$HQ = \frac{EC}{TV} \qquad \text{(Eq. 3-6)}$$

where TV is the toxicity value (in g/m^3) of the inhalation Reference Concentration (RfC) which is available in the IRIS system (U.S. EPA, 2018). When the HQ is higher than

1, possible adverse non-cancer effects exist, and when the HQ is less than or equal to 1, the adverse effects are not likely to occur.

3.3.5 Density Functional Theory Model Calculation

DFT calculations are conducted using the Vienna ab initio simulation package (code VASP 5.3.5) (Kresse and Furthmüller, 1996a; Kresse and Furthmüller, 1996b), which uses a generalized gradient correlation function (Perdew, Burke and Ernzerhof, 1996) with the projector-augmented wave method. The plane wave cutoff and the convergence criterion for total energy were set to 400 eV. All atoms were relaxed until Hellmann–Feynman forces on each atom reduced to less than 0.02 eV $Å^{-1}$. The $SrTiO_3$/$SrCO_3$ heterojunction model with interfaces composed of the 2 × 1 × 2 $SrTiO_3$ (001) and the 2 × 1 × 1 $SrCO_3$ (001) lattice planes were built. The bulk supercell of 2 × 1 × 2 $SrTiO_3$ (001) and 2 × 1 × 2 $SrCO_3$ (001) were also applied for $SrTiO_3$ and $SrCO_3$, respectively. The simulated surfaces were modeled using the slabs of seven atomic layers separated by a 40 Å vacuum. The calculated bond lengths are consistent with the published values (Bhatia & Myers, 2006).

3.4 Evaluation of COF Purification Scrubber and Photocatalyst

3.4.1 Setup of HiGee Rotating Packed Bed Scrubber

A miniatured movable high gravity rotating packed bed equipment (HiGee Co. Ltd, Taiwan, China) was developed and installed as the COF purification device. The operation principle and components are illustrated in Fig. 3-3, where the rotating packed bed, gas inlet and outlet control system, and liquid circulation system are included. The untreated COF emissions will pass through the HiGee system and cleaned air will be discharged directly to the hood.

The radius of the inner rotating packed bed and outer casing are 0.165 m and 0.28 m, respectively. The axial height of the scrubber is 0.66 m and the thickness of the casing and the distance between the casing and RPB are 0.008 m and 0.011 m, respectively. The RPB is driven by a motor, and the rotating speed can be adjusted from 300 to 1600 rpm, which provides centrifugal force for mass transfer process. The packing material is made of grade 304 stainless-steel wires in the shape of annular rings, which comprise interconnected wires with a mean diameter of 0.22 mm. High-voidage packing (0.954 m^3/m^3) of the wire mesh is used to lower the air pressure drop and to reduce the tendency for fouling issues (Singh et al., 1992). The circulation of liquid absorbent is controlled by a base-mounted solenoid-driven dosing pump (Tekba, Model: EML-803. Italy) with adjustable flow rate from 0 to 62 L/h.

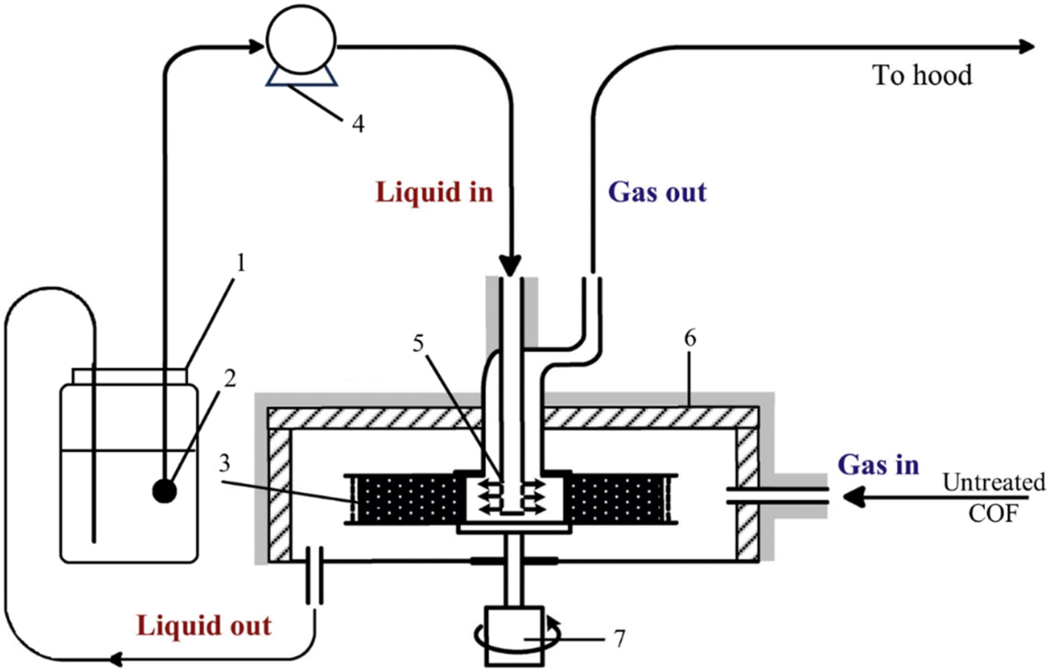

Figure 3-3 Operation principle and components of the HiGee RPB scrubber for the application of COF control

The components in the figure are illustrated below. 1. Water tank for storage of liquid absorbent, 2. Water filter for circulation of liquid absorbent, 3. Rotating packed bed, 4. Water pump 5. Liquid nozzle, 6. Casing of HiGee RPB scrubber, 7. Rotating motor.

In order to evaluate the purification efficiency of the HiGee scrubber, two sampling points as shown in Fig 3-1 were set at the inlet and outlet of the scrubber, respectively. By comparing the differences of chemical concentrations, the purification efficiency (η) of specific pollutants can be calculated using below equation 3-7.

$$Purification\,efficiency\ (\eta) = \frac{c_{in} - c_{out}}{c_{in}} \times 100\% \qquad \text{(Eq. 3-7)}$$

where C_{in} is the concentration of the typical pollutant at the inlet point, and C_{out} represents its outlet concentration.

3.4.2 Characterization of Nanomaterial

The crystal phase was analyzed via X-ray diffraction (XRD) with Cu Kα radiation at a scan rate of 0.05°2θ/s (λ = 1.5406 Å, 40 kV, 40 mA, PANalytical X' Pert PRO X-ray diffractometer). Samples were embedded in KBr pellets and then subjected to Fourier-transform infrared spectroscopy (FT-IR) on an FT-IR absorption spectrometer (Magna-IR 750, Nicolet, USA). X-ray photoelectron spectroscopy (XPS) with Al Kα X-rays (hm = 1486.6 eV) radiation operated at 150 W (Nexsa, Thermo Scientific) was used to investigate the surface properties. All binding energies were calibrated by C 1s at 284.8 eV as a reference. The spectra were fitted using XPSPEAK41 software, and the different valent species were quantified by the peak area. Scanning electron microscopy (SEM, JEOL JSM-6490, Japan) was used to characterize the morphology and elemental distribution maps of the obtained products. High-resolution transmission electron microscopy (TEM) images were acquired via a JEOL-Model-JEM-2100F field-emission electron microscope at an accelerating voltage of 200 kV. The Brunauer-Emmett-Teller surface area and pore structure were determined by measuring the nitrogen adsorption-desorption isotherms at 77 K using the Micrometrics ASAP2020 equipment. All the samples were degassed at 200 ^{o}C prior to measurements. A Varian Cary 100 Scan UV–vis system equipped with a labsphere diffuse reflectance accessory was used to obtain the reflectance spectra of the catalysts over a range of 200–800 nm. The room-temperature photoluminescence (PL) spectra of the as-prepared samples were investigated by using a fluorescence spectrophotometer (Edinburgh Instruments, FLSP-920) equipped with a xenon (Xe) lamp with an excitation wavelength of 310 nm. Labsphere USRS-99-010 was employed as a reflectance standard. Samples for electron spin-resonance spectroscopy (ESR, ER200-SRC, Bruker, Germany) were prepared by mixing 0.05 g of the as-prepared photocatalyst in a 25 mM 5,5′-dimethyl-1-pirroline-N-oxide (DMPO) solution with a 50 mL aqueous dispersion for DMPO-•OH or a 50 mL alcohol dispersion for DMPO-•O_2^- under irradiation with 420 nm visible light. Photoelectrochemical properties of the as-prepared samples were evaluated using a Parstat 4000 electrochemical workstation (USA) in a conventional three-electrode cell, with a platinum plate and an Ag/AgCl electrode as the counter and reference electrodes, respectively. The photocurrent-time curves were measured at 0.2 V versus Ag/AgCl in 0.5 mol/L Na_2SO_3 at ambient temperature under a 300 W Xe lamp (Microsolar 300, Perfectlight, China) with 420 nm. Electrochemical impedance spectroscopy (EIS) was measured at a frequency range of 0.1 Hz to 100 kHz with an 5 mV voltage amplitude under an open-circuit voltage in a 1 mmol/L $K_3Fe(CN)_6$ and $K_4Fe(CN)_6$ solution.

3.4.3 Evaluation of Photocatalytic Activity

The efficiencies of the photocatalytic removal of the as-prepared catalysts for HCHO and NO were evaluated using two well-designed continuous-flow reactors as shown in Fig. 3-4. The volumes of the reactors were 0.4 L (20 cm × 10 cm × 2 cm) for HCHO reaction and 4.5 L (30 cm × 15 cm × 10 cm) for NO reaction with the distances between sample surface and the optical path window of about 5.0 mm and 80.0 mm, respectively. The optical path window is made of quartz glass and the reaction gas can only pass between the surface of the sample and the window. A 300 W commercial Xe arc lamp (Microsolar 300, Perfectlight, China) was vertically placed outside the reactor. 0.1 g of catalyst was added into 2 mL distilled water and then coated onto a glass dish with a diameter of 8 cm. After being treated at 60 °C, the coated dish was placed in the center of the reactor to evaporate water and then cooled down to room temperature. The standard HCHO gas was supplied by a compressed gas cylinder with the HCHO concentration at 50 ppm (N_2 balance), whilst NO was acquired from another gas cylinder with the NO concentration at 49.6 ppm (N_2 balance) conforming to the standard of the National Institute of Standards and Technology (NIST). A zero-air initiator (Model 111, Thermo Environmental Instruments Inc., USA) generated an air stream that was separately mixed in a gas dilution calibrator (Model T700, Teledyne Technologies Inc., USA) with HCHO or NO. The preset concentrations of HCHO and NO were diluted to 1 ppm and 400 ppb with the controlled flow rate of 1 L/min, respectively. Once the equilibrium of adsorption–desorption was achieved, the lamp was then turned on to initiate the photocatalytic reaction. The concentration of HCHO was measured by an online Photoacoustic IR multi-gas monitor (Model 1412, INNOVA Air Tech Instruments, Denmark). Chemiluminescence NO/NO_2/NO_X analyzer (Model T200, Teledyne Technologies Inc., USA) was used to continuously measure the NO concentration. The removal efficiency (η) of each typical pollutant (HCHO or NO) was calculated by Equation (3-8):

$$Purification\ efficiency\ (\eta) = \frac{c_0 - c_t}{c_0} \times 100\% \qquad \text{(Eq. 3-8)}$$

where C_t is the outlet concentration of the typical pollutant at the reaction time of t, and C_0 represents the initial outlet concentration.

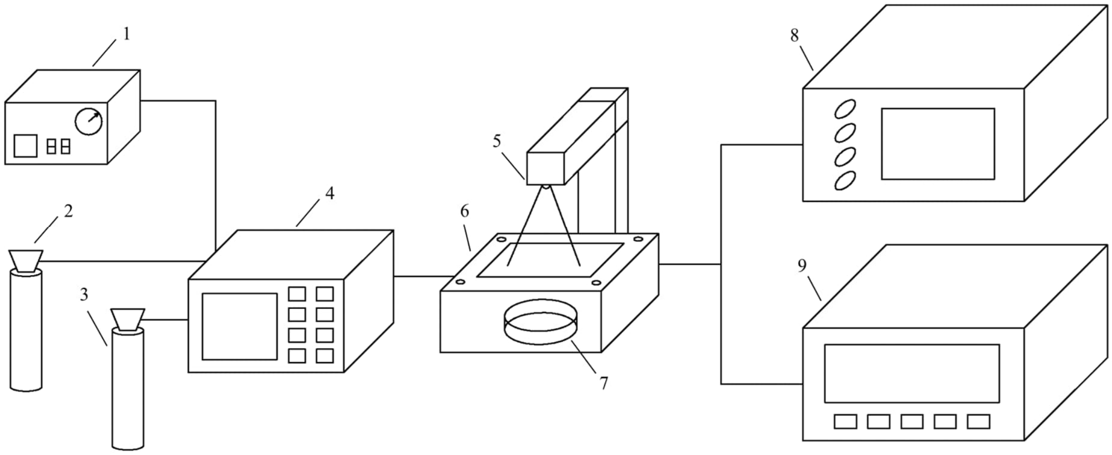

Figure 3-4 Schematic chart of the on-line photocatalytic activity evaluation system

The components in the figure are illustrated below: 1. Zero-air generator, 2. Standard gas of HCHO, 3. Standard gas of NO, 4. Gas dilution controller 5. Xe lamp system, 6. Photocatalytic reaction chamber, 7. Photocatalyst holder, 8. Chemiluminescence $NO/NO_2/NO_X$ analyzer, 9. Photoacoustic IR multi gas monitor (HCHO)

Chapter 4 Characteristics and Chemical Compositions of Cooking Oil Fumes from Different Cooking Processes

4.1 Introduction

Both the $PM_{2.5}$ and VOCs samples of the COFs were collected from the in-lab simulation kitchens to study the specific emission characteristics of different cooking methods. A total of 92 sample sets were collected covering five common cooking methods in Hong Kong including stir-frying, pan-frying, deep-frying, steaming, and boiling, which were detailed listed in Table 3-1 together with their main dishes, energy types and raw ingredients of each cooking method. Their detailed chemical compositions and featured emission factors were analyzed and summarized, which would serve as the baseline for future COFs investigation and study in real commercial restaurants.

4.2 Chemical Characterization of $PM_{2.5}$ Samples

4.2.1 $PM_{2.5}$ Mass Concentration and Chemical Profiles

The average concentrations of the total detected $PM_{2.5}$ chemical profiles from the five different cooking methods were listed in Table 4-1 and the overall mass concentrations and mass fractions of each species were illustrated in Fig. 4-1. The $PM_{2.5}$ concentrations emitted from different cooking processes were 381.66 $\mu g/m^3$, 146.87 $\mu g/m^3$, 235.88 $\mu g/m^3$, 88.13 $\mu g/m^3$ and 38.58 $\mu g/m^3$ for stir-frying, pan-frying, deep-frying, boiling, and steaming, respectively. The $PM_{2.5}$ concentrations from cooking processes were 1.49 to 14.78 times higher than the ambient concentrations at their corresponding sampling time, which implied the greater influences and contributions from cooking activities to the indoor air quality. In general, oil-based frying cooking methods (stir-frying, pan-frying and deep-frying) generated more $PM_{2.5}$ emissions than water-based methods (boiling and steaming). As shown in Fig. 4-1 (a)**,** stir-frying, the oil-based cooking method, released the highest concentration of $PM_{2.5}$ among the five different cooking styles, whose concentration was 1.62 to 9.89 times higher than others. While water-based steaming released the lowest concentration of $PM_{2.5}$ due to the reduction of the oil consumption and lower opportunities of food mixing with less human actions. At the same time, the use of a cover lid with limited emission holes during the whole heating processes inhibited the emission of particulate pollutants. In addition, great deviations among sampled results from the same cooking method were observed mainly from these oil-based cooking methods, where deep-frying stood out. Although the cooking conditions, as well as the selection and quantity of the raw food materials were well controlled in each cooking simulation test, variations still existed between these cooking tests. The results were due to the uneven distribution of the food materials, especially for those protein-containing and fat-containing meat and oils and the unstable distribution of COFs inside the emission flue gases. While for the results from water-based cooking methods with relative stable and mild cooking environments, the range variations were quite small, since most of the raw food materials were fully or partially soaked into the water bath, where cooking oil fumes were emitted evenly with the evaporation of water.

Unsurprisingly, organic carbon (OC), accounting from 39.27% to 48.26% of the total $PM_{2.5}$ chemical profiles, constituted the largest portion of $PM_{2.5}$ in all the studied cooking styles as shown in Fig 4-1 (b), due to the rich organic contents in raw food materials. This was also observed in other published cooking processes and the proportions of OC were at the similar compositional levels reported by Abdullahi, Delgado-Saborit and Harrison (2013) and Wang et al. (2015). Besides, as displayed in Fig. 4-1 (b), the percentages of elemental carbon (EC), water-soluble ions and elements ranged at 2.11% - 7.52%, 4.75% - 8.91% and 3.41% - 4.08% of the total $PM_{2.5}$ mass concentration, respectively. In comparison with those studies of COFs from similar cooking methods conducted by other groups, the $PM_{2.5}$ concentration levels and chemical compositions in this study were not quite identical with these results. The proportions of EC and measured elements was higher than Zhao, Chen and Zhao (2019)'s work, which ranged at 1.0% – 1.3% and 1.0% – 1.9%, respectively, while the percentages of ions and elements were lower than those results from See and Balasubramanian (2008). These inconsistences were because that multiple parameters beyond cooking methods could still affect the $PM_{2.5}$ emission patterns during cooking activities at the same time. Cooking methods, food ingredients, oil types, fuel energies and even sampling and chemical analysis methods have been proved to be the important factors affecting the concentration and composition of $PM_{2.5}$ emissions (Olson & Burke, 2006; Xu et al., 2020).

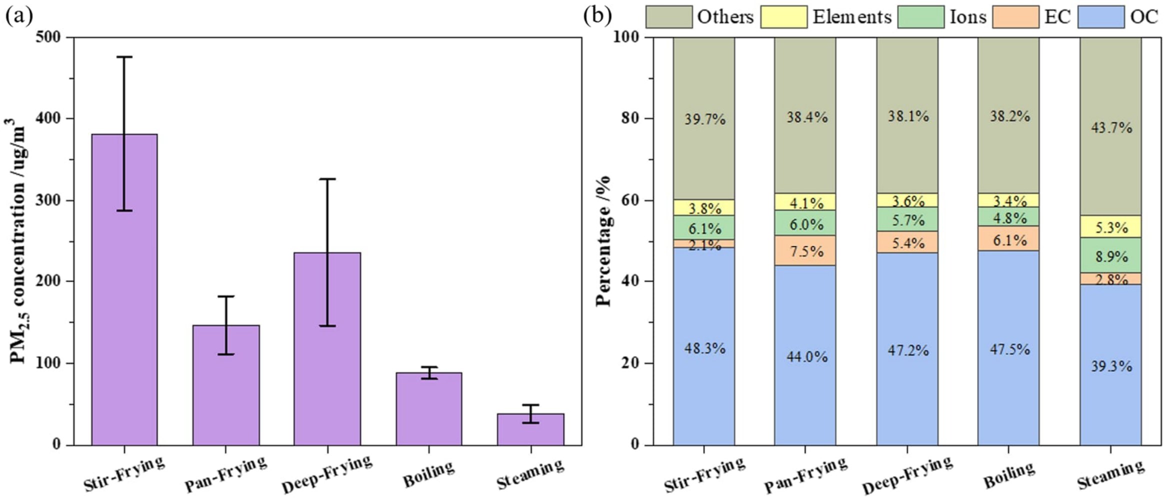

Figure 4-1 (a) Average concentrations of $PM_{2.5}$, vertical bars indicate the standard deviation and (b) Percentage of chemical profiles of $PM_{2.5}$ emitted from different commercial cooking processes

Table 4-1 Summary of the concentrations of the detected chemicals in the $PM_{2.5}$ samples from the five different cooking methods

Chemicals	**Stir-Frying**	**Pan-Frying**	**Deep-Frying**	**Boiling**	**Steaming**
∑$PM_{2.5}$ (μg/m^3)	**381.66 ± 93.94**	**146.87 ± 35.33**	**235.88 ± 90.01**	**88.13 ± 7.21**	**38.58 ± 10.98**
$PM_{2.5}$ emission rate (mg/min)	7.61 ± 1.85	2.91 ± 0.68	4.69 ± 1.78	1.74 ± 0.12	0.75 ± 0.19
OC (μg/m^3)	184.19 ± 43.38	64.62 ± 14.5	111.37 ± 47.55	41.89 ± 3.71	15.15 ± 4.68
EC (μg/m^3)	8.05 ± 5.32	11.05 ± 1.16	12.69 ± 8.37	5.39 ± 3.52	1.09 ± 1.07
Water-soluble Ions (μg/m^3)					
Na^+	0.13 ± 0.07	0.33 ± 0.32	0.28 ± 0.35	0.01 ± 0	0.02 ± 0.01
NH_4^+	3.21 ± 1.14	1.24 ± 0.21	1.74 ± 0.62	0.61 ± 0.06	0.45 ± 0.2
K^+	0.82 ± 0.24	0.48 ± 0.28	0.72 ± 0.53	0.2 ± 0.03	0.11 ± 0.05
Mg^{2+}	0.08 ± 0.05	0.02 ± 0.01	0.04 ± 0.02	0.01 ± 0	0.01 ± 0.01
Ca^{2+}	3.2 ± 0.9	1.01 ± 0.23	1.34 ± 0.51	0.57 ± 0.08	0.41 ± 0.2
F^-	0.1 ± 0.06	0.54 ± 0.53	0.82 ± 0.87	0.01 ± 0	0.01 ± 0.01
Cl^-	1.5 ± 0.53	0.55 ± 0.25	0.81 ± 0.34	0.28 ± 0.05	0.27 ± 0.15
NO_3^-	5.46 ± 1.38	2.78 ± 0.66	4.25 ± 2.14	1.12 ± 0.07	0.59 ± 0.23
SO_4^{2-}	8.61 ± 3.33	1.93 ± 0.41	3.53 ± 0.9	1.38 ± 0.08	1.56 ± 0.86
∑Ions	**23.1 ± 7.42**	**8.87 ± 2.22**	**13.52 ± 4.53**	**4.19 ± 0.36**	**3.44 ± 1.67**
Elements (ng/m^3)					
Al	192.98 ± 56.13	71.48 ± 23.07	105.93 ± 32.21	43.44 ± 0.77	25.36 ± 9.01
Si	617.53 ± 210.47	137.99 ± 55.07	227.79 ± 101.19	102.73 ± 5.67	97.7 ± 47
Cd	BDL	13.28 ± 1.6	19.74 ± 6.18	BDL	BDL
Ni	26.65 ± 8.57	39.1 ± 29.27	41.91 ± 46.1	7.44 ± 0.38	3.58 ± 0.91
Mg	211.76 ± 62.72	61 ± 10.94	88.37 ± 18.93	47.88 ± 5.2	33.62 ± 12.75
Na	183.19 ± 83.01	730.58 ± 720.73	734.9 ± 1010.22	26.78 ± 2.95	24.44 ± 13.26
K	1035.72 ± 319.33	615.55 ± 315.36	810.46 ± 562.48	213.46 ± 27.63	133.16 ± 48.28
Ca	10091.6 ± 2782.5	2485.3 ± 642.7	4017.6 ± 1086.4	2189.1 ± 323.0	1444.1 ± 570.0
Ti	15.67 ± 6.26	153.69 ± 150.9	174.8 ± 253.06	2.57 ± 0.29	2.09 ± 1.07
Cr	59.36 ± 21.5	53.71 ± 30.69	65.45 ± 56.55	20.3 ± 0.94	8.39 ± 2.86
Mn	74.08 ± 32.96	28.88 ± 16.61	51.86 ± 40.31	9.66 ± 0.39	8.51 ± 4.78
Fe	1101.2 ± 484.02	564.64 ± 309.39	806.89 ± 536.7	174.59 ± 13.12	127.85 ± 61.15
Co	9.45 ± 3.05	34.35 ± 32.33	35.79 ± 47.32	2.08 ± 0.45	1.17 ± 0.43
Cu	25.09 ± 8.59	357.35 ± 349.08	384.11 ± 554.17	7.88 ± 0.11	2.91 ± 0.78
Zn	650.15 ± 359.39	501.11 ± 419.18	630.2 ± 565.65	71.45 ± 4.13	101.09 ± 62.35
Ga	35.96 ± 13.96	14.16 ± 6.16	19.93 ± 9.76	7.14 ± 0.03	4.68 ± 2.35
As	40.93 ± 13.14	13.57 ± 2.95	21.43 ± 7.8	9.49 ± 1.57	6.18 ± 1.97
Se	1.73 ± 0.54	0.64 ± 0.18	0.88 ± 0.21	0.38 ± 0.01	0.25 ± 0.1
Rb	2.65 ± 0.91	0.82 ± 0.12	1.35 ± 0.34	0.81 ± 0.06	0.37 ± 0.11
Mo	6.52 ± 2.99	2.81 ± 1.09	3.27 ± 1.25	2.53 ± 0.19	0.72 ± 0.28
Sn	25.78 ± 11.21	10.91 ± 2.92	15.12 ± 6.3	10.29 ± 0.6	3.42 ± 0.97
Ba	50.26 ± 18.92	26.38 ± 3.46	31.12 ± 10.95	16.96 ± 1.99	5.87 ± 1.84
La	59.48 ± 19.07	25.44 ± 6.82	32.86 ± 11.49	20.25 ± 1.71	7.93 ± 2.28
Pb	102.12 ± 28.51	55.99 ± 25.95	85.38 ± 59.29	20.79 ± 0.5	13.08 ± 5.41

∑Elements	**14619.9 ± 4255.2**	**5992.1 ± 2125.8**	**8394.0 ± 3722.6**	**3008.0 ± 380.8**	**2056.5 ± 838.6**
PAHs (ng/m^3)					
Nap	1.65 ± 0.57	0.56 ± 0.37	1.04 ± 0.65	0.63 ± 0.01	0.15 ± 0.06
Acy	0.46 ± 0.15	0.64 ± 0.52	0.62 ± 0.55	0.11 ± 0.01	0.04 ± 0.01
Ace	1.1 ± 0.96	1.32 ± 0.49	1.55 ± 1.16	0.66 ± 0	0.11 ± 0.12
Flu	0.24 ± 0.07	0.94 ± 0.82	1.22 ± 1.57	0.08 ± 0	0.02 ± 0.01
Phe	0.24 ± 0.08	2.53 ± 2.47	4.3 ± 6.37	0.08 ± 0	0.02 ± 0.01
Ant	0.22 ± 0.08	0.2 ± 0.15	0.25 ± 0.23	0.03 ± 0	0.02 ± 0.01
Fln	1.36 ± 0.36	0.93 ± 0.54	1.32 ± 0.94	0.33 ± 0.04	0.12 ± 0.04
Pyr	1.21 ± 0.44	0.89 ± 0.28	1.33 ± 0.92	0.45 ± 0.04	0.11 ± 0.04
BaA	0.66 ± 0.22	0.32 ± 0.1	0.47 ± 0.21	0.21 ± 0.01	0.06 ± 0.02
Chr	1.41 ± 0.44	0.71 ± 0.21	1.07 ± 0.62	0.35 ± 0.03	0.13 ± 0.04
BbF	4.55 ± 1.32	1.38 ± 0.33	2.1 ± 0.6	0.95 ± 0.04	0.41 ± 0.13
BkF	1.61 ± 0.62	0.68 ± 0.31	0.97 ± 0.39	0.24 ± 0	0.13 ± 0.05
BaF	0.59 ± 0.18	0.12 ± 0.12	0.23 ± 0.17	0.16 ± 0.01	0.05 ± 0.01
BeP	1.9 ± 0.74	0.42 ± 0.11	0.81 ± 0.25	0.31 ± 0.04	0.13 ± 0.04
BaP	1.79 ± 0.69	0.48 ± 0.14	0.78 ± 0.2	0.31 ± 0.05	0.14 ± 0.05
Per	0.2 ± 0.05	0.06 ± 0.04	0.09 ± 0.07	0.06 ± 0.01	0.02 ± 0.01
InD	0.51 ± 0.19	0.89 ± 0.63	1.76 ± 2.18	0.15 ± 0.01	0.06 ± 0.02
DBA	0.17 ± 0.05	0.29 ± 0.23	0.61 ± 0.76	0.04 ± 0	0.02 ± 0
BghiP	0.17 ± 0.05	0.76 ± 0.72	1.96 ± 2.74	0.05 ± 0.01	0.02 ± 0.01
Cor	0.18 ± 0.04	0.45 ± 0.38	0.67 ± 0.88	0.05 ± 0	0.02 ± 0.01
Dip	0.02 ± 0.01	0.05 ± 0.04	0.97 ± 1.42	BDL	BDL
∑PAH	**20.25 ± 5.51**	**14.61 ± 7.54**	**24.14 ± 20.15**	**5.26 ± 0.21**	**1.78 ± 0.55**

*BDL: below detection limit.
**Unit of elements and PAHs is ng/m^3, and unit of others is μg/m^3.

4.2.2 Carbonaceous Particles

As discussed in previous section, carbonaceous fraction (OC + EC) was the dominant component in $PM_{2.5}$ emissions from all these cooking processes. The concentration levels of the carbonaceous particles were listed in Table 4-1. The averaged total emission concentrations of OC and EC in decreasing order were stir-frying (192.24 μg/m^3), deep-frying (124.06 μg/m^3), pan-frying (75.67 μg/m^3), boiling (47.28 μg/m^3), and steaming (16.24 μg/m^3). The total measured carbonaceous fractions (OC + EC) contributed about 42.10% to 53.65% of the $PM_{2.5}$ mass concentrations from the five different cooking methods. The large amounts of carbonaceous particles suggested that cooking activities consumed large amount of carbon-containing materials, especially for the OC component, which was the primary composition in the $PM_{2.5}$ accounting for 85% to 96% of carbonaceous particles. The total quantified OC concentrations ranged from 15.15 $\mu g/m^3$ to 184.19 $\mu g/m^3$, while the highest OC concentration was seen from the stir-frying process, which was nearly 13-fold higher than the lowest OC concentration from the steaming process. The OC concentrations from the oil-based cooking methods were 1.54 – 12.61 times higher than those from water-based cooking samples, which was due to the release of organic compounds from the precursors of edible oils and raw meat components (Rogge et al., 1991), indicating the major contribution from oil consumptions and fat contents in food ingredients to the OC emissions (Huboyo, Tohno, & Cao, 2011). In addition, the OC concentration from boiling process was 2.77 times higher than that from steaming method, which indicated that more OC contents produced by oils and fats would be brought out by the water vapours during the boiling process.

Besides, significant differences in EC concentrations and proportions were observed from different cooking methods, which were not consistent with the emission patterns of OC from these cooking processes. The mass fractions of EC contents in $PM_{2.5}$ samples showed greatly differences among these cooking methods, i.e., stir-frying (4.19%), deep-frying (14.60%), pan-frying (10.23%), boiling (11.39%), and steaming (6.74%). While the OC/EC ratios for stir-frying, pan-frying, deep-frying, boiling, and steaming were 22.87, 5.85, 8.78, 7.78 and 13.84, respectively. As shown in Fig. 4-2, these OC/EC ratios from cooking oil fumes were larger than other anthropogenic sources including industrial emissions, biomass burning and vehicular combustion, which could be used to identify the sources of $PM_{2.5}$ (Y. C. Li et al., 2015). The OC/EC ratios from these COFs results in this study were consistent with the results reported by See and Balasubramanian (2008) and somehow showed a bit lower than those published by Y. C. Li et al. (2015). As the major cooking energy source in their study was natural gas, which could provide higher heating temperature to cooking oils, more organic matters could be decomposed and released from the oil-based cooking processes. In addition, the ratios from industrial processes and biomass burning were around 4 – 5; (Cheng et al., 2021; Dejchanchaiwong et al., 2020; Merico et al., 2020; G. Q. Zhang et al., 2020), which was similar to water-based cooking methods, while the lower OC/EC ratios from road transportation and diesel vehicles were 1.35, and 0.67, respectively (Pongpiacha, Kudo, & Sekiguchi, 2014; Wang et al., 2021). Overall, the measured OC/EC ratios from cooking processes were higher than those from other different common emission sources in cities, which suggested COFs became major contributors to the OC components in densely urban areas.

4.2.3 Water-soluble Ions

All sample extracts showed the presence of water-extractable ions, aligning with previous research that also detected these substances in cooking oil fumes both from laboratory cooking tests and actual restaurants (Wang et al., 2015; Zhao & Zhao, 2018). As shown in Table 4-1, the highest concentration of water-soluble ions was generated from stir-frying method, while steaming styles generated the least concentration of ions due to its less mass concentration of total $PM_{2.5}$ emissions. Thereinto, SO_4^{2-}, NO_3^-, NH_4^+ and Ca^{2+} were the major components from all these different cooking processes, which could be directly emitted from the added water and cooking ingredients (Bandowe et al., 2021) as well as produced from the reactions and transformations during heating process by other common gaseous pollutants such as SO_2, NO_X and NH_3 (Bandowe et al., 2021; See & Balasubramanian, 2008).

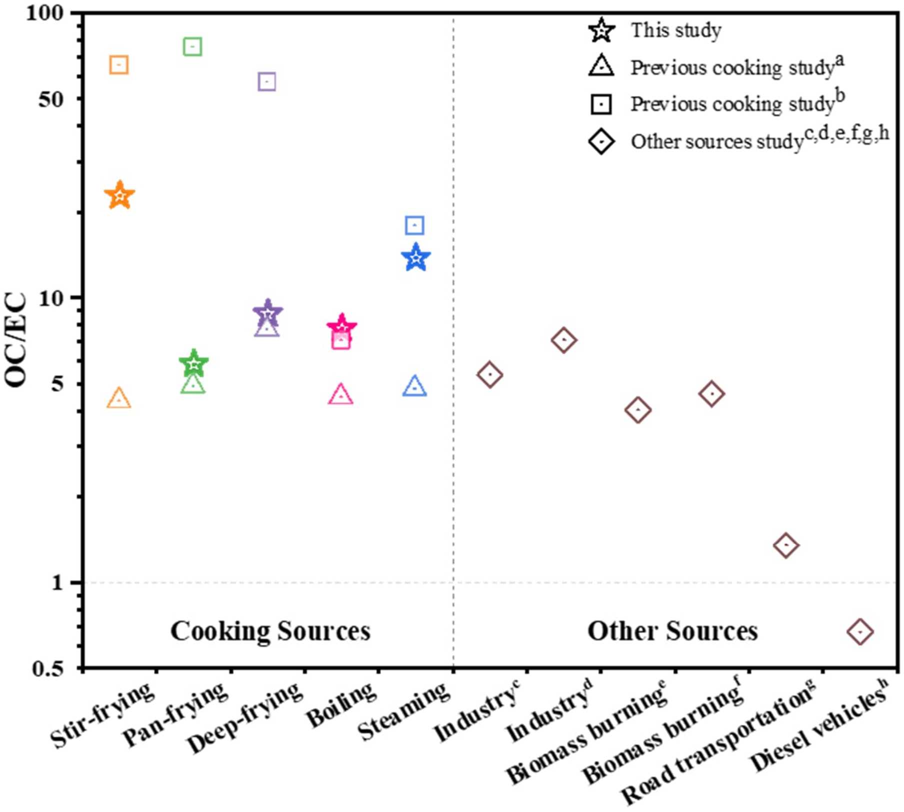

Figure 4-2 Comparison of OC/EC ratios of $PM_{2.5}$ in our cooking oil fumes samples and from cooking and other anthropogenic sources (a: See and Balasubramanian (2008), b: Y. C. Li et al. (2015), c: G. Q. Zhang et al. (2020), d: Merico et al. (2020), e: Cheng et al. 0014(2021), f: Dejchanchaiwong et al. (2020), g: Pongpiacha, Kudo and Sekiguchi (2014), h: Wang et al. (2021))

It could be concluded from Fig 4-3 (a) that highest water-soluble ions were detected from stir-frying, because of its largest amounts of $PM_{2.5}$ emissions and easy release due to the continuous stirring motions (Sun et al., 2020). Water-based boiling and steaming produced the most concentrated SO_4^{2-} ion which should be ascribed to the evaporation of sulphate from the large amount of added tap water (Y. C. Li et al., 2015). While NO_3^- was the most emitted component for both pan-frying and deep-frying styles because of the transformation from NO_X which was emitted from oil heating process (Zhao & Zhao, 2018). In addition, the concentration of F^- and Na^+ were particularly notable for oil-based pan-frying and deep-frying compared with the ranks of other ions, which were basically dominated by the stir-frying. And similar situations were also reported by several studies of ions from cooking exhausts (Y. C. Li et al., 2015; Wei See, Karthikeyan, & Balasubramanian, 2006), since the pre-treated meats and salted raw materials could emit F^- and Na^+ when they were placed onto hot surface of cookers or put into the heated oils.

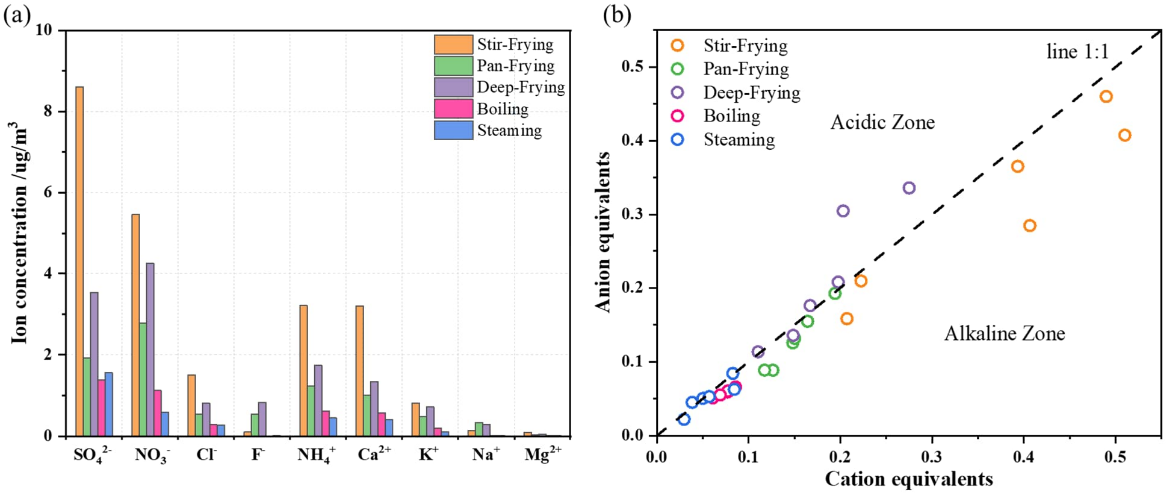

Figure 4-3 (a) Emission concentrations of $PM_{2.5}$-bound ions from different cooking methods and (b) Scatter plot of the ratios of total cation equivalents (CE) and anion equivalents (AE) of $PM_{2.5}$ filter samples from various cooking methods

Furthermore, the ion balances of the $PM_{2.5}$ particles from the COFs can be calculated to evaluate the acid-base balance (Shen et al., 2007) and to further compare and analyse the differences among these cooking processes. The detailed cation equivalent (CE) and anion equivalent (AE) of the $PM_{2.5}$ particle samples from COFs were calculated by equation 4-1 and 4-2 as follows:

$$CE = NH_4^{+}/18 + Ca^{2+}/20 + K^{+}/39 + Na^{+}/23 + Mg^{2+}/12 \qquad \text{(Eq. 4-1)}$$

$$AE = SO_4^{2-}/48 + NO_3^{-}/62 + Cl^{-}/35.5 + F^{-}/19 \qquad \text{(Eq. 4-2)}$$

Fig 4-3 (b) displays the relations between the anion equivalents and cation equivalents of all samples from all these cooking processes. Most of the $PM_{2.5}$ samples except samples from stir-frying dispersed around the 1:1 - AE: CE line, showing that the contents of both anion and cation were close and possessing the neutral characteristic. However, weakly alkaline $PM_{2.5}$ samples were obtained from all the COFs by the stir-frying cooking method, as the used vegetables and added seasonings such as baking soda, which would release some alkaline components like carbonate (CO_3^{2-}) to improve the alkalinity (Shen et al., 2007; Shen et al., 2011). On the contrary, several $PM_{2.5}$ emission samples from deep-frying process were scattered inside the acidic zone, which could be attributed to the generated free fatty acid and other organic acids during the persistent oil heating periods (Yoon et al., 1987; Zhao et al., 2019). By exploring the acid-base balances of these particulate samples from cooking process, it would be helpful and instructive for us to design the liquid absorbents and fine-tune the COFs control system to suit for different cooking scenarios.

4.2.4 Elements

As shown in Table 4-1, the highest emission concentration of $PM_{2.5}$-bound elements was from stir-frying, which was 14.62 μg/m^3, while the lowest elemental concentration was 2.06 μg/m^3, which was emitted from steaming process. The concentration sequence of the elemental emissions from various cooking methods was consistent with the sequence of the concentration of total $PM_{2.5}$ emissions. As displayed in Fig 4-1 (b), elements accounted for around 3.5% of the total $PM_{2.5}$ compositions for most of cooking processes, whereas the proportion of elements increased to 5.3% in water-based steaming process since its relative lower emission concentration of carbonaceous compounds.

Fig. 4-4 illustrated the emission concentration of each $PM_{2.5}$-bound element from different cooking styles. Ca, K and Fe were found to be the most abundant metal elements emitted from all cooking processes, which was similar to the previous reported cooking emission profiles (Wang et al., 2015; Zhao, Chen, & Zhao, 2019), and these top-three emitted metals accounted for about 85% mass concentration of the total measured elements, no matter what the cooking methods were. In addition, some of the major elements including Ca, Na, K, Al and Mg were derived from water, oil, raw materials and other food ingredients (Kumar, Srivastava, & Srivastava, 1994; See & Balasubramanian, 2008), while trace elements like Fe, Cr and Ni might be released from the cooking utensils under very high temperature (Anwar et al., 2004). Besides, outstanding emission of Cu, Ti, Co and Cd were observed in oil-based pan-frying and deep-frying, which might be attributed to the inherent trace metal elements in the edible vegetable oils from production, transportation and storage (Shah & Soylak, 2022).

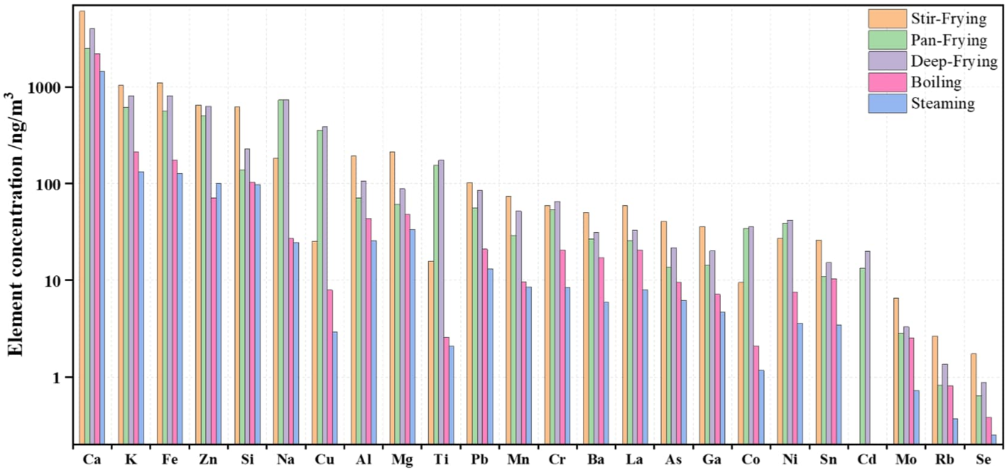

Figure 4-4 Emission concentrations of the $PM_{2.5}$-bound elements from five different cooking methods

4.2.5 $PM_{2.5}$-bound PAHs

The total concentrations of the 21 detected PAHs from $PM_{2.5}$ samples as displayed in Table 4-1 from stir-frying, pan-frying, deep-frying, boiling, and steaming were 20.24, 14.62, 24.12, 5.25 and 1.78 ng/m^3, respectively. Although the most concentrated total $PM_{2.5}$ was emitted from stir-frying method, the $PM_{2.5}$-bound PAHs with the highest mass concentration was released from deep-frying. As shown in Fig. 4-5 (a), higher PAH/$PM_{2.5}$ ratios were observed from deep-frying and pan-frying processes, meaning that more PAHs existed in the unit concentration of $PM_{2.5}$ emissions from these methods. This was also consistent with previous reported results (See & Balasubramanian, 2008), as PAHs were mainly produced by the fat contents under high handling temperature, which was in line with the cooking styles of oil-based pan-frying and deep-frying. The highest BpF was detected from the stir-frying and boiling process, which could be affected and released by the heating of beef and beef offal (Zhu et al., 2019), which were less used in other cooking methods. Phe was the major PAH from deep-frying and pan-frying processes, while Nap was the main PAH from water-based cooking methods of boiling and steaming. Fig 4-5 (b) demonstrated the distributions of PAHs by the number of their aromatic rings in different cooking methods. The dominant PAHs in pan-frying and deep-frying were three-ring (Nap, Ace, Flu, Ant) with over 30% of the total PAHs. Five-ring PAHs (BbF, BkF, BaF, Per, DBA) were the most abundant fraction (28% - 35%) for stir-frying, boiling and steaming. More PAHs with less rings were emitted from deep-frying and pan-frying than those from stir-frying, because high-molecular-weight-PAHs (HM-PAHs, PAHs containing six or seven rings) and middle-molecular-weight-PAHs (MM-PAHs, containing four or five ring PAHs) could be destroyed or decomposed to low-molecular-weight-PAHs (LM-PAHs, PHAs with two or three rings) under high heating temperatures during deep-frying or pan-frying processes (Li et al., 2018). The most abundant PAHs from water-based boiling and steaming were the middle-molecular-weight-PAHs (MM-PAHs), accounting for 54% and 59%, respectively.

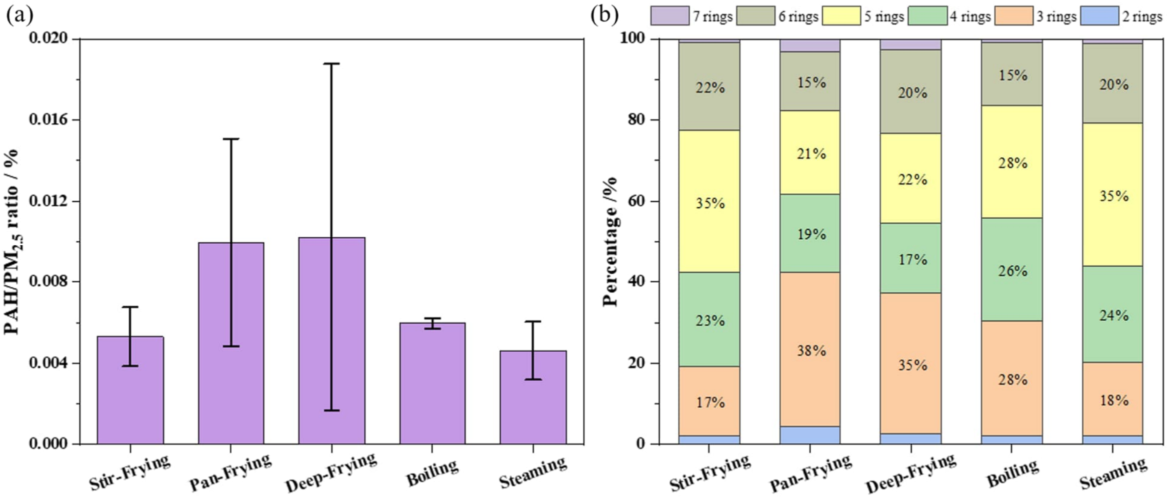

Figure 4-5 Mass concentration ratios of $PM_{2.5}$-bound PAHs and total $PM_{2.5}$ in different cooking methods, vertical bars indicate the standard deviation and (b) Percentage of different rings in composition of PAHs for each cooking process

In addition, since several PAHs are defined as hazardous chemicals to human beings, it is critical to take into account of these harmful PAHs compounds. The carcinogenic PAHs (C-PAHs), which include Chr, BbF, BkF, BaP, InD and Dip belong to the groups of MM-PAHs and HM-PAHs in our study. The ratios of C-PAHs of the total detected PAHs in $PM_{2.5}$ ranged from 29% to 49%, where the emission from stir-frying ranked the highest although its PAHs/$PM_{2.5}$ ratios was relatively low. This result was caused by the easy release of both MM-PAHs and HM-PAHs during the food mixing process, and also pointed out that additional attentions and protections should be taken when flipping the heated food materials inside the hot cookers. While the lowest ratio was observed in pan-frying, as most of these PAHs with higher molecular weights were decomposed before emission in the long-time heating process under high temperature. Although less C-PAHs particles were released into ambient air from the pan-frying cooking process, high PAH concentrations were still detected being deposited onto the surface of the well-cooked meat through the pan-frying cooking method (Kılıç Büyükkurt et al., 2017).

4.3 Chemical Characterization of Gaseous Samples

4.3.1 Overview of VOC emissions from Different Cooking Methods

A total of 81 kinds of VOCs chemical species were detected from cooking emissions samples including 33 alkanes, 11 akenes, 17 aromatic hydrocarbons, 16 carbonyls and 9 other VOCs by their functional groups. The emission patterns of the total volatile organic compounds (TVOC) were similar to the $PM_{2.5}$ emission based on these cooking methods, where oil-based cooking styles emitted much more VOCs than water-based boiling and steaming. As shown in Table 4-2, the TVOC concentrations released from cooking oil fumes were 897.3 ± 203.8 $\mu g/m^3$, 937.0 ± 322.5 $\mu g/m^3$, 1166.2 ± 552.5 $\mu g/m^3$, 692.4 ± 137.8 $\mu g/m^3$ and 133.4 ± 33.5 $\mu g/m^3$ by stir-frying, pan-frying, deep-frying, steaming, and boiling, respectively. Although stir-frying emitted the most $PM_{2.5}$ pollutants, the highest TVOC concentration was emitted from deep-frying process, which was 8.7 times higher than steaming as demonstrated in Fig. 4-6. This could be attributed to the gasification and hydrolysis of fat contents from edible oils, meats and even ingredients under high cooking temperature. In a laboratory-based sunflower oil boiling test, D. C. Zhang et al. (2019) found that when the cooking temperature increased from 130 °C to 260 °C, the mass concentration of VOCs would increase for over 7 times. This finding also confirmed that more VOCs were emitted from deep-frying than stir-frying and pan-frying, which always underwent the highest heating temperature up to 220 °C in our test. Besides, the similar patterns of $PM_{2.5}$ variation ranges were also observed in the concentration of TVOC, where the concentrations from oil-based cooking methods fluctuated more evident than water-based cooking methods. And steaming showed the least variations due to its lowest VOC concentrations and fixed emission locations from the holes of the cover lid.

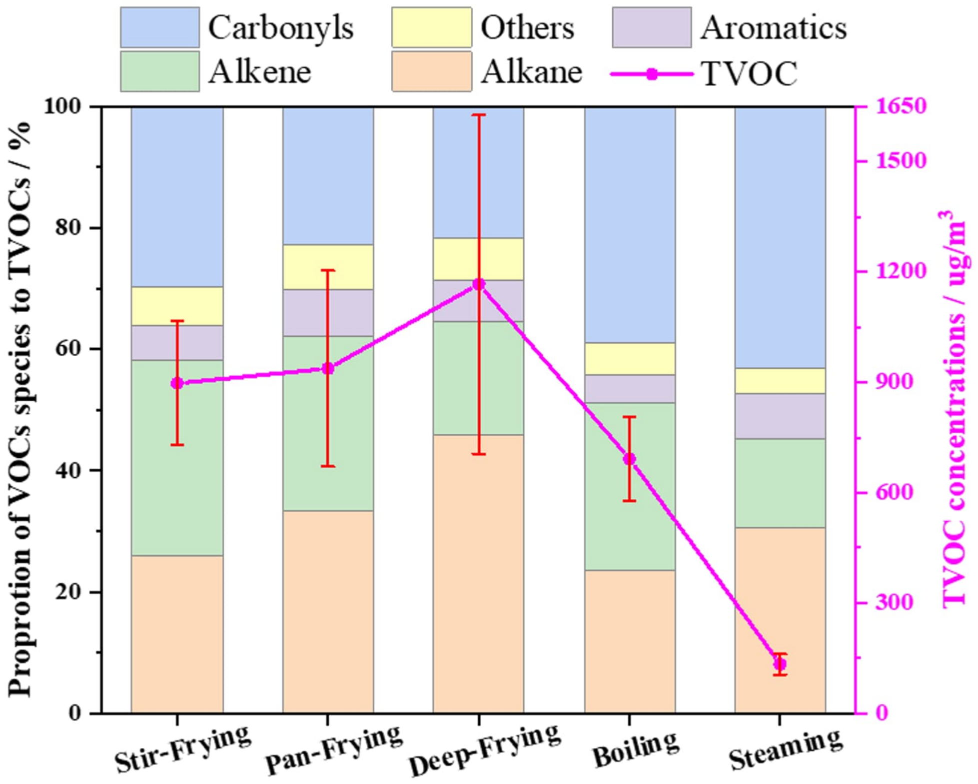

Figure 4-6 Mass concentrations of TVOC emissions, vertical bars indicate the standard deviation and the proportion of VOC species from different cooking methods

In addition to the different TVOC emission concentrations, the variations in the VOC species and components were also significant, because of the use of different raw food materials and oil contents (Tao et al., 2023). The bar chart in Fig. 4-6 demonstrates the mass proportions of each VOC group to TVOCs in different cooking methods. Pan-frying and deep-frying generated the most alkanes, which accounted for 33% and 46% of the total

VOCs, respectively, while carbonyls and alkenes were the dominant products from stir-frying despite its nature of oil-based cooking process. The greater emission number of alkanes might come from the pyrolysis of meat-fat and oils in pan-frying and deep-frying (H. Zhang et al., 2023), while the carbonyls and alkenes might be a consequence of the decomposition and evaporation of the added ingredients of cooking wines and sauces. As for water-based cooking methods, carbonyls were the predominant VOC components with the ratios of 39% in boiling and 43% in steaming, which were higher than those from oil-based cooking methods and other reported integrated Chinese cooking activities (X. Liang et al., 2022). Aromatic hydrocarbons were the least emitted VOCs for all kinds of cooking methods except steaming due to its very different raw food materials usage of aromatic rice with less employ of meats and oil contents.

Table 4-2 Summary of the concentrations of the detected VOCs from the five different cooking methods

Cooking Methods	**Stir-Frying**	**Pan-Frying**	**Deep-Frying**	**Boiling**	**Steaming**
Alkane					
ethane	35.56 ± 15.86	35.02 ± 15.9	47.42 ± 30.4	18.55 ± 4.49	7.69 ± 3.1
propane	11.82 ± 4.26	13.55 ± 3.77	17.58 ± 9.52	9.03 ± 2.64	3.4 ± 2.07
isobutane	11.24 ± 1.09	13.32 ± 7.07	17.89 ± 8.83	9.53 ± 0.71	3.66 ± 0.91
butane	18.55 ± 3.64	21.9 ± 4.55	27.04 ± 12.11	16.26 ± 1.49	7.24 ± 1.99
cyclopentane	0.3 ± 0.07	0.4 ± 0.12	0.48 ± 0.23	0.24 ± 0.06	0.1 ± 0.03
isopentane	3.91 ± 1.03	4.55 ± 1.25	5.53 ± 2.71	3.36 ± 0.06	1.4 ± 0.7
pentane	21.77 ± 4.13	22.34 ± 3.31	29.21 ± 11.34	18.39 ± 3.97	7.69 ± 2.55
2,2-dimethylbutane	0.29 ± 0.08	0.37 ± 0.08	0.45 ± 0.21	0.3 ± 0.03	0.09 ± 0.04
2,3-dimethylbutane	9.01 ± 1.66	11.85 ± 3.9	14.17 ± 7.5	6.46 ± 0.48	2.91 ± 0.97
isohexane	10.6 ± 1.72	12.65 ± 3.37	15.78 ± 6.19	8.26 ± 2.16	3.67 ± 0.92
3-methylpentane	12.8 ± 2.98	15.2 ± 4.27	18.43 ± 7.78	8.02 ± 0.09	3.86 ± 1.73
hexane	31.47 ± 5.05	34.79 ± 13.34	46.78 ± 21.87	21.66 ± 6	12.26 ± 1.84
2,4-dimethylpentane	0.62 ± 0.19	0.68 ± 0.3	0.84 ± 0.36	0.37 ± 0.15	0.2 ± 0.1
methylcyclopentane	0.42 ± 0.08	0.52 ± 0.27	0.68 ± 0.35	0.35 ± 0.08	0.15 ± 0.03
2-methylhexane	2.37 ± 0.57	3.13 ± 1.84	3.4 ± 1.71	1.46 ± 0.29	0.6 ± 0.17
2,3-dimethylpentane	0.41 ± 0.16	0.46 ± 0.12	0.52 ± 0.23	0.25 ± 0.08	0.1 ± 0.03
cyclohexane	3.78 ± 0.92	3.98 ± 1.04	5.24 ± 2.45	2.79 ± 0.69	1.27 ± 0.6

3-methylhexane	3.27 ± 0.8	4.65 ± 2.11	4.69 ± 2.31	1.86 ± 0.67	1.09 ± 0.52
heptane	15.6 ± 5.41	16.04 ± 4.59	24.57 ± 14.41	9.9 ± 2.42	4.31 ± 1.85
methylcyclohexane	2.07 ± 0.78	3.44 ± 2.14	3 ± 1.86	0.74 ± 0.27	0.53 ± 0.2
2,3,4-trimethylpentane	1.14 ± 0.18	1.37 ± 0.66	1.8 ± 0.94	0.8 ± 0.02	0.37 ± 0.13
2,2,4-trimethylpentane	8.09 ± 1.09	10.63 ± 3.62	11.48 ± 5.93	5.27 ± 0.25	2.58 ± 1.04
2-methylheptane	0.43 ± 0.13	0.52 ± 0.18	0.65 ± 0.28	0.31 ± 0.13	0.13 ± 0.06
3-methylheptane	0.39 ± 0.11	0.45 ± 0.19	0.54 ± 0.2	0.33 ± 0.15	0.12 ± 0.07
octane	6.16 ± 2.78	6.54 ± 1.7	9.77 ± 5.79	4.37 ± 0.73	1.79 ± 1.1
nonane	1.32 ± 0.57	1.68 ± 0.53	1.9 ± 1.1	0.8 ± 0.04	0.31 ± 0.15
decane	4.46 ± 0.86	5.43 ± 2.1	6.32 ± 3.15	2.77 ± 0.07	1.2 ± 0.4
undecane	4.79 ± 1.22	7.31 ± 4.37	7.29 ± 4.45	2.77 ± 0.17	1.38 ± 0.16
dodecane	2.84 ± 1.06	3.48 ± 1.73	4.31 ± 2.36	1.65 ± 0.79	0.77 ± 0.24
trichlorofluoromethane	1.97 ± 0.24	1.51 ± 0.62	2.07 ± 0.15	2.02 ± 0.06	1.62 ± 0.15
dichlorodifluoromethane	3.69 ± 0.25	2.8 ± 1.04	3.8 ± 0.21	3.64 ± 0.11	3.45 ± 0.36
1,1,2-trichlorotrifluoroethane	0.72 ± 0.05	0.57 ± 0.23	0.98 ± 0.11	0.89 ± 0.2	0.86 ± 0.1
1,2-dichlorotetrafluoroethane	0.17 ± 0.03	0.14 ± 0.05	0.18 ± 0.01	0.16 ± 0.02	0.15 ± 0.01
$\sum_{\mathbf{Alkane}}$	**232.03 ± 56.1**	**313.5 ± 103.0**	**534.7 ± 254.6**	**163.61 ± 28.07**	**40.79 ± 12.33**
Alkene					
ethylene	169.73 ± 21.8	153.27 ± 39.52	222.6 ± 98.1	146.52 ± 8.27	50.47 ± 13.8
propylene	26.54 ± 3.15	33.61 ± 12.45	39.4 ± 19.86	18.92 ± 1.68	8.65 ± 2.35
trans-2-butene	2.04 ± 0.72	2.33 ± 0.4	2.65 ± 1.62	0.93 ± 0.04	0.57 ± 0.15
1-butene	1.83 ± 0.71	2.12 ± 0.8	2.71 ± 1.3	1.1 ± 0.22	0.56 ± 0.24
cis-2-butene	0.42 ± 0.11	0.52 ± 0.14	0.59 ± 0.28	0.29 ± 0.1	0.13 ± 0.08
1,3-butadiene	19.94 ± 3.69	19.95 ± 4.93	28.41 ± 10.38	14.39 ± 2.92	7.51 ± 2.91
1-pentene	49.17 ± 5.95	53.04 ± 14.91	73.86 ± 30.03	34.23 ± 7.12	16.59 ± 6.3
trans-2-pentene	0.98 ± 0.2	0.97 ± 0.27	1.54 ± 0.72	0.6 ± 0.03	0.26 ± 0.1
isoprene	8.8 ± 1.72	12.63 ± 6.05	12.73 ± 6.2	5.95 ± 0.31	2.38 ± 0.81
cis-2-pentene	0.53 ± 0.12	0.69 ± 0.25	0.8 ± 0.42	0.38 ± 0.02	0.16 ± 0.04
1-hexene	10.78 ± 3.66	12.97 ± 4.44	14.67 ± 7.07	5.6 ± 0.62	3.94 ± 1.66
$\sum_{\mathbf{Alkene}}$	**290.76 ± 37.65**	**268.8 ± 71.9**	**218.6 ± 86.8**	**189.8 ± 17.2**	**19.44 ± 5.46**
Aromatics					
benzene	9.03 ± 3.72	11.89 ± 3.55	12.64 ± 7.61	5.06 ± 0.38	2.1 ± 0.5
toluene	10.04 ± 3.03	10.69 ± 3.82	14.6 ± 5.91	7.34 ± 3.71	3.58 ± 1.84
ethylbenzene	2.29 ± 0.7	2.97 ± 1.43	3.71 ± 2.09	1.67 ± 0.91	0.67 ± 0.25
dimethylbenzene	3.65 ± 1.27	4.59 ± 3.03	5.08 ± 2.15	2.93 ± 2.15	1.24 ± 0.63
1,2-dimethylbenzene	1.66 ± 0.76	1.8 ± 0.95	2.46 ± 1.55	1.07 ± 0.39	0.55 ± 0.31
styrene	1.13 ± 0.63	1.35 ± 0.79	1.69 ± 1.02	0.65 ± 0.33	0.28 ± 0.12
cumene	0.38 ± 0.12	0.38 ± 0.13	0.54 ± 0.17	0.27 ± 0.18	0.13 ± 0.08
N-propylbenzene	0.64 ± 0.17	0.73 ± 0.32	0.98 ± 0.41	0.41 ± 0.16	0.21 ± 0.1
3-ethyltoluene	0.45 ± 0.14	0.5 ± 0.28	0.66 ± 0.23	0.43 ± 0.31	0.18 ± 0.12
4-ethyltoluene	0.37 ± 0.1	0.39 ± 0.11	0.55 ± 0.21	0.29 ± 0.18	0.13 ± 0.08
mesitylene	0.36 ± 0.09	0.43 ± 0.17	0.57 ± 0.26	0.26 ± 0.14	0.12 ± 0.06
1-ethyl-2-methylbenzene	1.07 ± 0.82	1.28 ± 1.09	1.52 ± 1.32	0.51 ± 0.03	0.19 ± 0.12
pseudocumene	2.39 ± 0.43	2.45 ± 1.19	3.5 ± 0.76	2.28 ± 1.48	1.01 ± 0.4

1,2,3-trimethylbenzene	0.6 ± 0.16	0.73 ± 0.33	0.85 ± 0.31	0.52 ± 0.35	0.23 ± 0.14
1,3-diethylbenzene	3.01 ± 1.54	2.86 ± 1.39	4.81 ± 2.23	2.56 ± 1.78	1.08 ± 0.95
1,4-diethylbenzene	0.5 ± 0.34	0.44 ± 0.26	0.78 ± 0.29	0.65 ± 0.51	0.27 ± 0.23
naphthalene	11.91 ± 5.62	15.34 ± 6.61	18.5 ± 11.4	5.06 ± 1.43	3.17 ± 2.4
$\sum_{\mathbf{Aromatics}}$	**49.48 ± 17.67**	**70.59 ± 27.48**	**77.82 ± 37.36**	**31.96 ± 12.97**	**10.09 ± 5**
Others					
acetylene	18.77 ± 4.2	20.96 ± 5.28	26.85 ± 8.7	15.1 ± 3.49	7.85 ± 5.73
acetonitrile	5.46 ± 1.5	6.77 ± 1.97	7.71 ± 3.84	1.75 ± 0.47	1.25 ± 1.24
isopropyl alcohol	16.63 ± 5.38	14.74 ± 4.54	19.98 ± 8.85	10.66 ± 2.8	3 ± 2.19
ethyl acetate	1.91 ± 0.45	2.09 ± 0.62	2.76 ± 0.95	1.24 ± 0.21	0.3 ± 0.18
vinyl acetate	2.29 ± 0.49	1.98 ± 0.51	2.98 ± 1	1.68 ± 0.57	0.29 ± 0.12
methyl tert-butyl ether	1.82 ± 0.62	2.19 ± 0.68	2.61 ± 1.05	0.94 ± 0.22	0.24 ± 0.17
tetrahydrofuran	2.33 ± 0.5	2.41 ± 1.16	3.03 ± 0.99	1.47 ± 0.43	0.37 ± 0.28
methyl methacrylate	5.69 ± 2	5.63 ± 1.57	8.09 ± 3.13	2.77 ± 0.71	0.74 ± 0.53
methyl isobutyl ketone	2.62 ± 0.51	2.95 ± 1.39	3.61 ± 1.07	1.48 ± 0.31	0.33 ± 0.21
$\sum_{\mathbf{Others}}$	**57.53 ± 14.08**	**71.66 ± 19.14**	**82 ± 29.22**	**37.08 ± 8.29**	**5.39 ± 3.63**
Carbonyls					
formaldehyde	45.39 ± 13.97	40.7 ± 14.86	45.45 ± 21.85	24.7 ± 6.4	10.85 ± 1.02
acetaldehyde	42.77 ± 8.38	36.72 ± 13.52	49.58 ± 18.65	27.16 ± 3.64	10.55 ± 0.37
acetone	27.34 ± 4.41	23.6 ± 6.87	32.92 ± 15.24	17.03 ± 2.03	5.8 ± 0.6
acrolein	44.53 ± 14.31	41.51 ± 13.73	49.02 ± 22.29	25.24 ± 9.49	9.79 ± 1.41
propionaldehyde	5.57 ± 1.4	4.84 ± 1.51	5.69 ± 2.45	3.81 ± 1.53	1.38 ± 0.06
crotonaldehyde	9.89 ± 2.14	8.72 ± 3.08	12.27 ± 5.66	6.67 ± 1.3	1.84 ± 0.07
methyl ethyl ketone	10.38 ± 1.85	10.37 ± 5.06	11.22 ± 4.88	6.41 ± 0.07	1.65 ± 0.04
isobutyraldehyde	15.39 ± 3.26	14.12 ± 8.31	16.3 ± 7.2	11.79 ± 2.52	2.65 ± 0.08
benzaldehyde	3.35 ± 0.87	3.02 ± 0.85	3.56 ± 1.52	2.13 ± 0.48	0.64 ± 0.09
isovaleraldehyde	0.86 ± 0.07	0.75 ± 0.31	0.81 ± 0.29	0.49 ± 0.04	0.17 ± 0.04
valeraldehyde	1.08 ± 0.21	0.83 ± 0.31	1.17 ± 0.54	0.62 ± 0.14	0.23 ± 0.01
2-methylbenzaldehyde	1.6 ± 0.34	1.86 ± 0.95	2.07 ± 0.87	1.18 ± 0.08	0.3 ± 0.01
3-methylbenzaldehyde	1.91 ± 0.36	1.65 ± 0.52	2.23 ± 0.82	1.37 ± 0.23	0.36 ± 0.05
4-methylbenzaldehyde	1.41 ± 0.25	1.49 ± 1.0	1.39 ± 0.61	0.96 ± 0.16	0.19 ± 0.03
caproic aldehyde	52.26 ± 15.18	54.13 ± 23.38	57.5 ± 28.48	29.68 ± 10.63	10.44 ± 0.89
2,5-dimethylbenzaldehyde	3.87 ± 0.64	3.48 ± 1.8	4.12 ± 1.72	2.75 ± 0.56	0.79 ± 0.08
$\sum_{\mathbf{Carbonyls}}$	**267.59 ± 60.89**	**212.4 ± 74.12**	**253.1 ± 102.7**	**269.95 ± 58.94**	**57.66 ± 4.36**
$\sum_{\mathbf{TVOC}}$	**897.4 ± 167.8**	**937.0 ± 266.1**	**1166.2 ± 459.6**	**692.4 ± 112.9**	**133.38 ± 27.71**
TVOC emission rate (mg/min)	17.92 ± 3.33	18.72 ± 5.3	23.3 ± 9.17	13.82 ± 2.23	2.64 ± 0.53

**Unit of all VOCs is μg/m^3

4.3.2 Emission Profiles and Significant VOCs from Cooking Oil Fumes

The detailed averaged VOC emission concentrations with their standard deviations from the five different kinds of cooking methods were listed in Table 4-2. It could be found that ethane, pentane and hexane as well as ethylene and 1-pentene were the major contributors to alkanes and alkenes, while formaldehyde and toluene were the dominant chemicals in carbonyls and aromatic hydrocarbons for most of these cooking methods. In order to investigate the typical distribution profiles of these VOCs with high emission concentrations from different cooking methods, the double-bar charts illustrating both the mass concentrations and VOC percentages of TOVC were shown in Fig. 4-7. It was clear that formaldehyde was the most emitted VOC in steaming with a proportion of 8.1%, while ethylene showed the highest emitted concentrations in all the other cooking methods with the proportion of 10.2% - 18.9%. The similar mass percentages could be observed for the emissions of alcohols and aldehydes including isopropyl alcohol, formaldehyde acetaldehyde and acrolein from these three oil-based cooking styles, while formaldehyde, acetaldehyde and acrolein were the representative VOCs of water-based boiling and steaming, which all accounted for over 6% of the total VOCs. Alkanes involving ethane, pentane and hexane were found to be the typical peak chemical compounds for deep-frying with the emission concentrations of 48.7 $\mu g/m^3$ to 79.0 $\mu g/m^3$. Alkene was also identified as the featured characteristic VOC group from oil-based processes, where ethylene and 1-pentene were the distinct alkenes for stir-frying and pan-frying, respectively. These fully measured VOCs and significant emission characteristics would assist to complement the anthropogenic VOC emission inventories of cooking oil fumes from different common cooking methods and to further help to distinguish the emission sources in integrated kitchens and even in complex polluted ambient environments. Moreover, these particular and gaseous emission features would help to set targets for COF control and provide theoretic guidelines for better design of control systems.

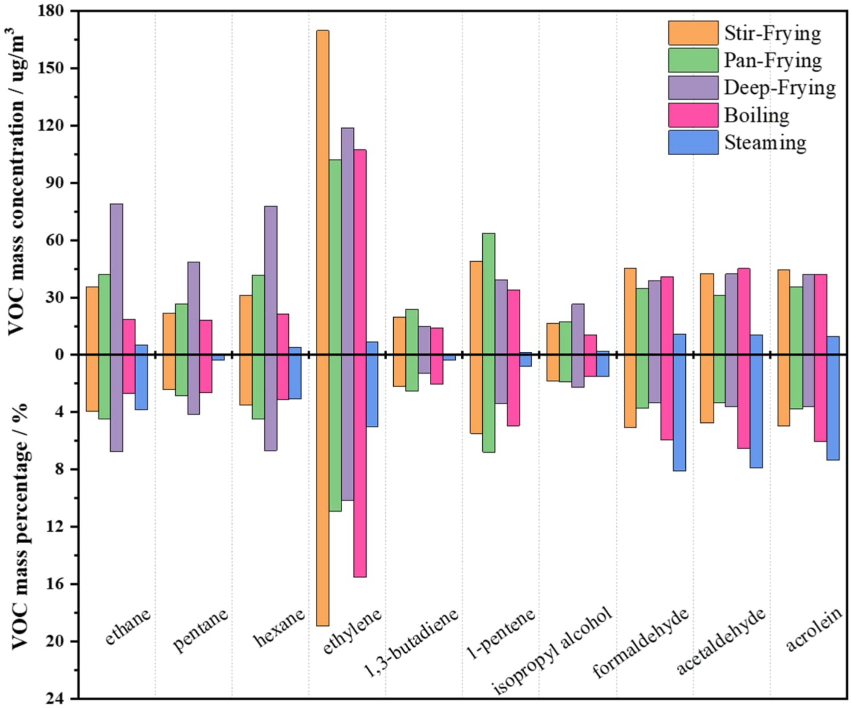

Figure 4-7 Mass concentrations and mass percentages of significant VOC emissions from different cooking methods

4.4 Chapter Summary

The concentrations and detailed chemical compositions of the $PM_{2.5}$ and VOCs were determined for all these five cooking methods in a lab-based simulation kitchen. In general, the concentration trend of stir-frying > deep-frying > pan-frying > boiling > steaming for the $PM_{2.5}$ from COF was identified, while for the VOCs concentration trend, deep-frying > pan-frying > stir-frying > boiling > steaming was observed, indicating the oil-based cooking methods emitted higher concentrations of both $PM_{2.5}$ and VOCs than those from water-based cooking styles. Significant deviations of the total concentrations of $PM_{2.5}$ and TVOC were found in the results from same cooking method, especially for those oil-based cooking processes, which was because of the uneven distribution of the exhaust flue and uncontrollable fat and protein contents in raw food materials. OC was found to be the dominant component in all cooking styles, accounting for 39.3% to 49.3% of the total $PM_{2.5}$, due to the rich organic contents in food materials, which was also supported by the high OC/EC ratios from cooking sources. Water-soluble ions contributed to 4.8% - 8.9% mass concentration of the $PM_{2.5}$, where SO_4^{2-}, NO_3^-, NH_4^+ and Ca^{2+} were detected as the major components from all these cooking processes. The mass concentration of elements ranged from 2.06 $\mu g/m^3$ to 14.62 $\mu g/m^3$ which occupied small proportions (3.4% - 5.3%) in $PM_{2.5}$, and Ca, K and Fe were the major components. C-PAHs accounted for 29% to 49% of the total detected PAHs, where stir-frying emitted the highest ratios of C-PAHs though highest PAHs/$PM_{2.5}$ ratio was observed from deep-frying. Alkane and alkene were the main species of VOCs for oil-based cooking methods while carbonyls were the dominant species for water-based cooking methods, because of their different cooking temperatures and food materials. Ethylene, acetaldehyde, acrolein and formaldehyde were the common high-emission VOCs in all the cooking methods. The above results provided the updated emission inventory from cooking process, and will complement the emission data for anthropogenic sources, and these emission concentrations/rates and significant features will assist for better identification of pollutants and source apportionment of cooking emissions from integrated kitchens.

Chapter 5 Characterization of Cooking Oil Fumes from Commercial Kitchens and Impacts Evaluation

5.1 Introduction

In this chapter, the detailed characteristics of cooking of fumes from typical commercial kitchens in Hong Kong including Chinese fast food, Western fast food, Cantonese cuisine, and Chongqing hot pot will be analyzed and discussed. The chemical compositions of $PM_{2.5}$ and VOCs will be investigated, and emission features will be compared with the results from our studied COFs in different cooking methods discussed in the previous chapter and from other reported studies. In addition, evaluation of both the environment and health impacts of the COFs from commercial kitchens will be conducted to reflect the influence of cooking emissions and guide the development of emission control strategies. These results will complement the emission inventory from anthropogenic activities in Hong Kong and Asian urban areas.

5.2 Emission Profiles and Chemical Compositions

5.2.1 Overview of COFs from Commercial Kitchens

In order to thoroughly study the characterization of COFs based on the results from cooking methods by in-lab simulation tests, sampling and analysis work were conducted in real commercial kitchens in Hong Kong. The indoor ambient concentrations of the most representative restaurants in Hong Kong including Chinese fast food (CFF), Western fast food (WFF), Cantonese cuisine (CAN) and Chongqing hot pot (CHP) were measured. The continuous variations of these critical parameters ($PM_{2.5}$, NO_X and TVOC) were recorded in those sampled kitchens by portable mini air station and handheld TVOC analyzer. The

3-hour concentration variations of those pollutants from cooking processes during the peak hours of each kitchen were displayed in Fig. 5-1. Although the cooking methods and material types were different among these studied restaurants, the pollutant concentrations of $PM_{2.5}$, NO_X and TVOC all exhibited high concentration levels during the whole cooking periods in comparison with those concentrations from the normal residential indoor and outdoor environments (Lin et al., 2018; Paterson et al., 2021).

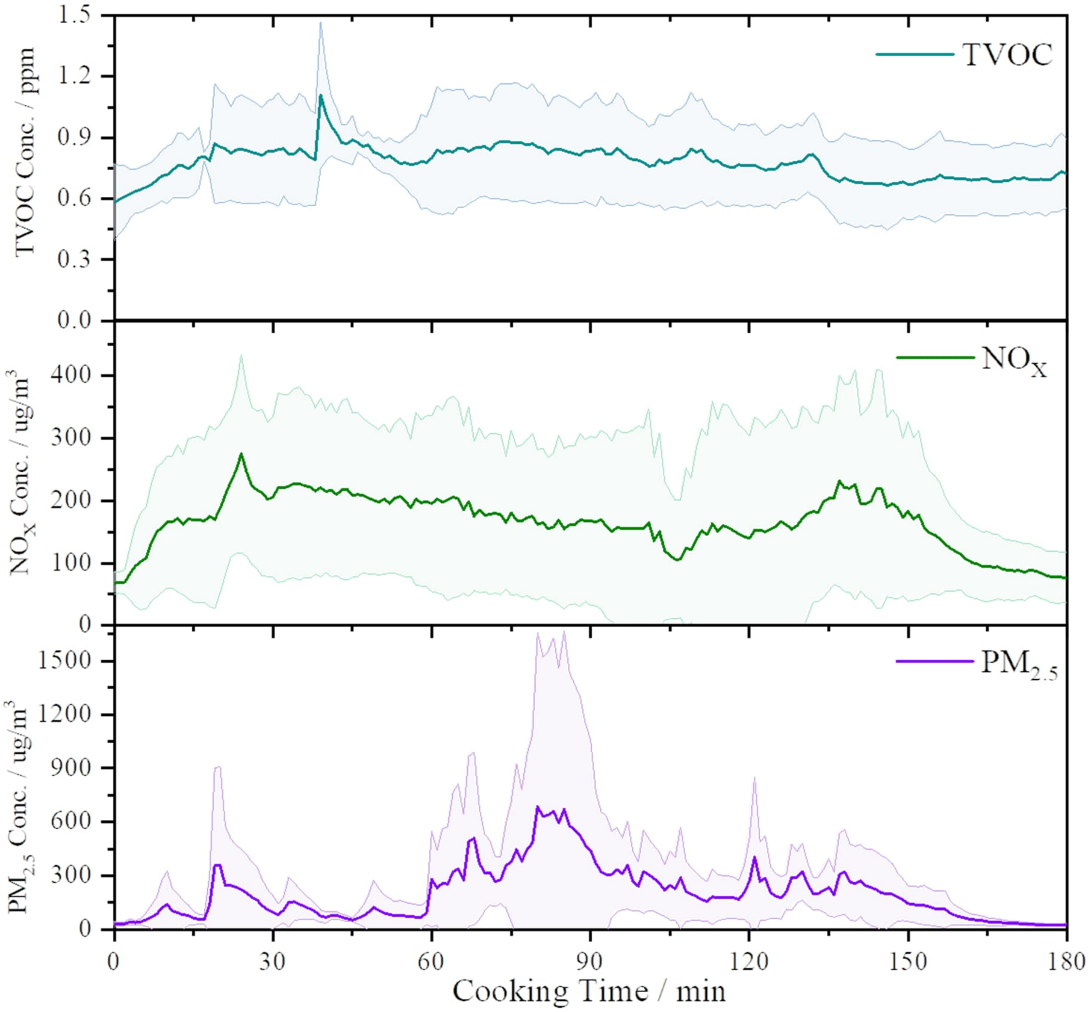

Figure 5-1 Average concentration variations of TVOC, NO_X and $PM_{2.5}$ during cooking process in different investigated restaurants (n = 16)

The averaged $PM_{2.5}$ concentration was around 200 μg/m^3, which greatly exceeded the WHO air quality standard and was considered to be harmful to human health (WHO, 2021). The $PM_{2.5}$ concentration showed evident fluctuation during the cooking processes as the sedimentation effects happened during the cooking intervals (Kim et al., 2023). As the TVOC and NO_X were both gaseous pollutants with longer floating time in the indoor ambience, the variations of concentration were quite stable during the whole cooking process. And concentration spikes were observed at the start of the cooking process with significant increases of 0.6 ppm for TVOC and 150 μg/m^3 for NO_X. The average concentrations of TVOC and NO_X during the cooking periods were around 0.7 ppm and 180 μg/m^3, respectively, which exceeded the air quality standards stipulated by WHO as well (WHO, 2021). Thus, it become necessary to investigate the detailed chemical compositions of COFs to determine their individual impacts and to further guide the development of control strategies.

5.2.2 $PM_{2.5}$ Compositions of COFs from Commercial Kitchens

The averaged mass concentrations of the $PM_{2.5}$ species and their chemical profiles from the four commercial kitchens were listed in Tabel 5-1. As shown in Fig. 5-2 (a), the total $PM_{2.5}$ mass concentrations in decreasing order were 269.85 μg/m^3, 232.11 μg/m^3, 199.95 μg/m^3, and 85.69 μg/m^3 for CAN, CFF, WFF, and CHP restaurants, respectively. The range of the total mass concentration from 38.58 μg/m^3 to 381.66 μg/m^3 was similar to those results from 5 cooking methods study as discussed in Chapter 4. However, the deviations of $PM_{2.5}$ concentration were at similar levels in all 4 commercial kitchens as they are integrated kitchens with more than one cooking method and evenly distributed exhausts. Cantonese cuisine and Chinese fast-food restaurants were the top two in $PM_{2.5}$

emissions since stir-frying with the highest $PM_{2.5}$ emissions among all these studied cooking methods was their dominant cooking style at all times. While pan-frying and deep-frying were the main cooking styles for WFF kitchen, which also produced higher $PM_{2.5}$ emissions compared to the situation from CHP. All these major cooking styles in the three kitchens with high $PM_{2.5}$ emissions were oil-based cooking methods, which could also be confirmed by their higher proportions of OC emission as illustrated in Fig 5-2 (b). Boiling was the primary and almost the only cooking method in CHP causing the COFs emission profiles largely depending on their raw food materials and ingredients. The concentration of $PM_{2.5}$ from CHP was the lowest one due to its water-based nature, which was also equivalent to that from the in-lab boiling study. Furthermore, a relatively high percentage of water-soluble ions was observed from the CHP kitchens due to its widely use of salts and food dressings, which was probably emitted with the continuous evaporation of boiled water (Sun et al., 2020; Taner, Pekey, & Pekey, 2013).

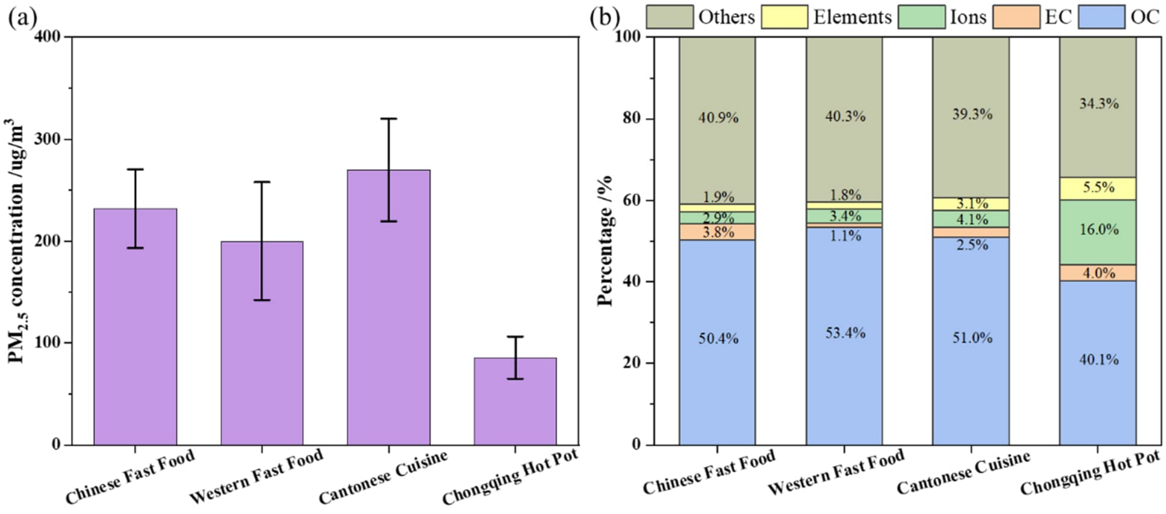

Figure 5-2 (a) Average concentrations of $PM_{2.5}$, vertical bars indicate the standard deviation and (b) Percentage of chemical profiles of $PM_{2.5}$ emitted from different commercial cooking processes

As discussed in the previous chapter, the OC/EC ratios showed great variations from different cooking methods and processes. Normally, higher OC/EC ratios were observed in oil-based cooking methods. As shown in Fig. 5-3, the calculated OC/EC ratios were 13.19, 48.12, 20.70 and 9.95 for CFF, WFF, CAN and CHP, respectively. The large variations were due to the different amounts of oil usage and raw food materials. The ratios of stir-frying-based CFF and CAN were found to be close to the results of the in-lab stir-frying process, confirming their major cooking methods. The OC/EC ratio from CAN was still found to be consistent with the results from Cantonese restaurants reported by He et al. (2004), as both studies focused on the specified Cantonese cuisine with similar dishes and food materials. However, the ratio from the oil-based WFF was much higher than those from pan-frying and deep-frying, but was very similar to the ratio from the cafeteria frying reported by See and Balasubramanian (2008). This could be attributed to the use of different types of frying oils with diverse smoke temperatures (Sankhyan et al., 2022) and the commercial fryer used in kitchens with higher and more stable heating temperatures than the simulated induction cooker (Al-Harbi & Al-Kahtani, 1993). In addition, the CHP emission exhibited slightly higher OC/EC ratio compared to the results from our in-lab boiling study and the cafeteria boiling study (See & Balasubramanian, 2008), as large amounts of beef tallow and vegetable oils would be added into the boiling pot rather than those soup boiling and porridge cooking with little oils added.

The $PM_{2.5}$-bound PAHs chemical profiles from COFs has been used to identify the main cooking styles based on their emission signatures (N. Zhang et al., 2017). The total PAHs were further divided into three categories, i.e., LWM, MWM and HMW according to their number of rings as described in Chapter 4. Fig. 5-4 shows the diagnostic contributions of these three categories from the four investigated kitchens, five simulated cooking methods and two typical indoor and outdoor environments in Hong Kong (Z. Z. Zhang et al., 2023). In general, all the COFs samples from cooking processes exhibited the significant high percentages in both LMW- and MMW-PAHs compared with the PAH contributors of the typical indoor and outdoor environment, since the PAHs with more rings would be decomposed by the high heating temperatures from cookers to form PAHs with less rings (Cai et al., 2019). Higher proportions of LMW-PAHs were found in the restaurants of WFF (47.0%) and CHP (40.9%), and in the cooking methods of pan-frying (42.3%) and deep-frying (37.3%). WFF owned the largest proportions of PAHs with low molecular weight, which was consistent with its main cooking methods of deep-frying and pan-frying, indicating the generation of LMW-PAHs from the oil boiling process under high cooking temperatures (Li et al., 2018). Unlike the results from in-lab soup boiling test, CHP released more LWM-PAHs due to the chemical transformations from fat contents of the added beef tallow and vegetable oils during continuous water boiling processes (Gysel et al., 2018). MMW-PAHs were observed to be dominant group in both CFF (55%) and CAN (48%), which were close to the diagnostic chemical profiles of stir-frying, boiling, and steaming methods, suggesting these common cooking methods were used in the Chinese food-related restaurants. On the other hand, as HMW-PAHs compounds were more likely to be originated and released from industrial processes such as crude oil refining (Wolska et al., 2012), least HWM-PAHs components were detected from all these cooking related emissions, which were below 25% for all these results of COFs samples.

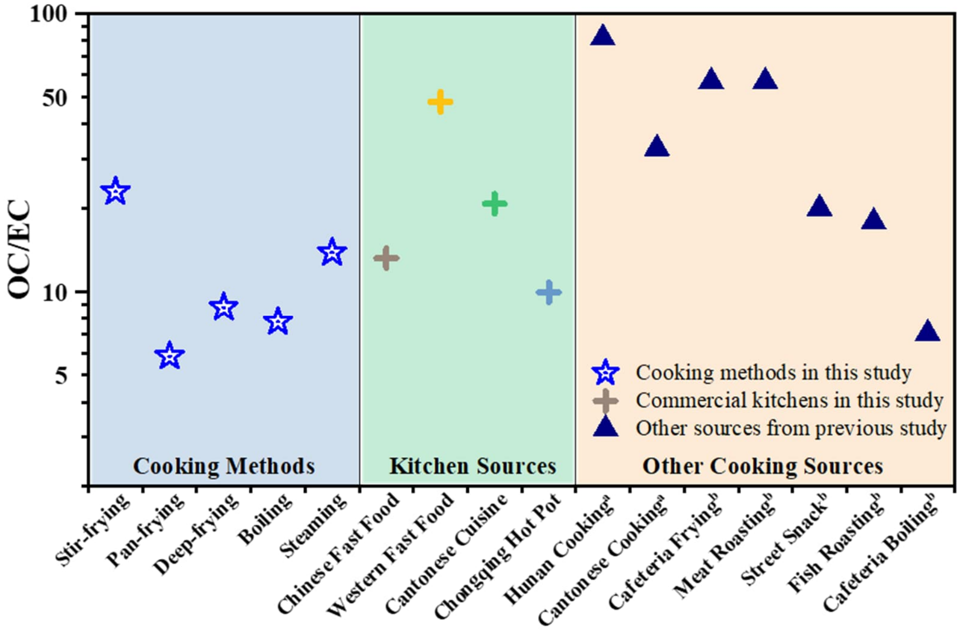

Figure 5-3 Comparison of OC/EC ratios of $PM_{2.5}$ in the COFs samples from the study of five cooking methods and four kitchens with other related cooking sources (a: (He et al., 2004) and b: See and Balasubramanian (2008))

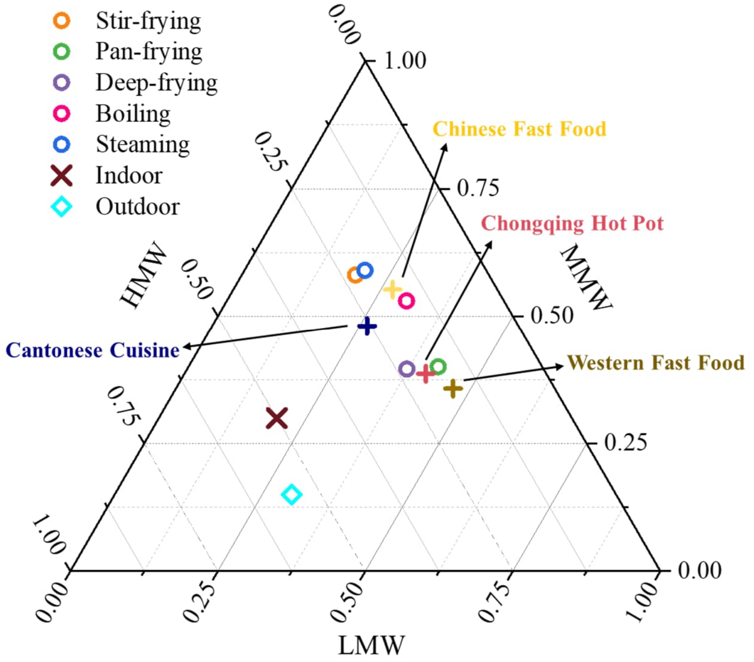

Figure 5-4 Contributions of different molecular-weight groups to the PAHs in $PM_{2.5}$

5.2.3 VOCs Compositions of COFs from Commercial Kitchens

The detailed 81 kinds of VOC species from the four investigated kitchens in Hong Kong were listed in Table 5-1. The concentrations of the total VOC emissions were 832.1 ± 200.4 μg/m^3, 998.9 ± 205.0 μg/m^3, 847.9.3 ± 347.0 μg/m^3 and 654.5 ± 270.0 μg/m^3 from the restaurants of CFF, WFF, CAN and CHP, respectively, which demonstrated the similar VOC levels with the results in the aforementioned cooking methods studies. The deviations of TVOC concentration showed similar patterns as those from PM$_{2.5}$ in commercial kitchens without significant differences. As shown in Fig. 5-5, the largest VOC emission was recorded from the WFF, which only ranked in the third place for PM$_{2.5}$ emission concentrations, which could be attributed to the intensive VOC emissions from deep-frying process as discussed before. The least VOC emission from the CHP restaurant was more than half of the concentration from the highest emission of WFF, while its PM$_{2.5}$ emission concentration was only 1/3 of the highest one from CAN kitchens. This result meant that the VOC emission was increased compared with its PM$_{2.5}$ emission in CHP, indicating that VOCs were easier to be generated and released from the boiling process of oil-water mixtures where fewer particulate pollutants formed due to its relatively low heating temperatures.

As shown in Fig. 5-5, alkane and alkene were the dominant products from CFF, WFF and CAN, while carbonyls were the major components from the water-based CHP. This was also supported by the results from cooking methods study, as organics with higher molecular weight and long chains might be decomposed under high heating temperatures. In addition, although the TVOC concentrations from the kitchens were below their relevant cooking methods due to their longer cooking intervals, the concentrations of some short-chain alkanes such as propane and butane were found to be higher in CFF, WFF and

CAN than those from the in-lab simulation tests. Since these commercial kitchens applied natural gas as one of their heating energy sources and the abundant alkane compounds might escape from the gas stove (Sun et al., 2022). Naphthalene was found to be the most emitted aromatic hydrocarbon from all cooking methods which was identical to the results from a recent study on cooking emissions (Huang et al., 2021). Moreover, Hexane, ethylene, and formaldehyde were detected to have significantly high VOC emission levels in COFs samples from all these commercial kitchens.

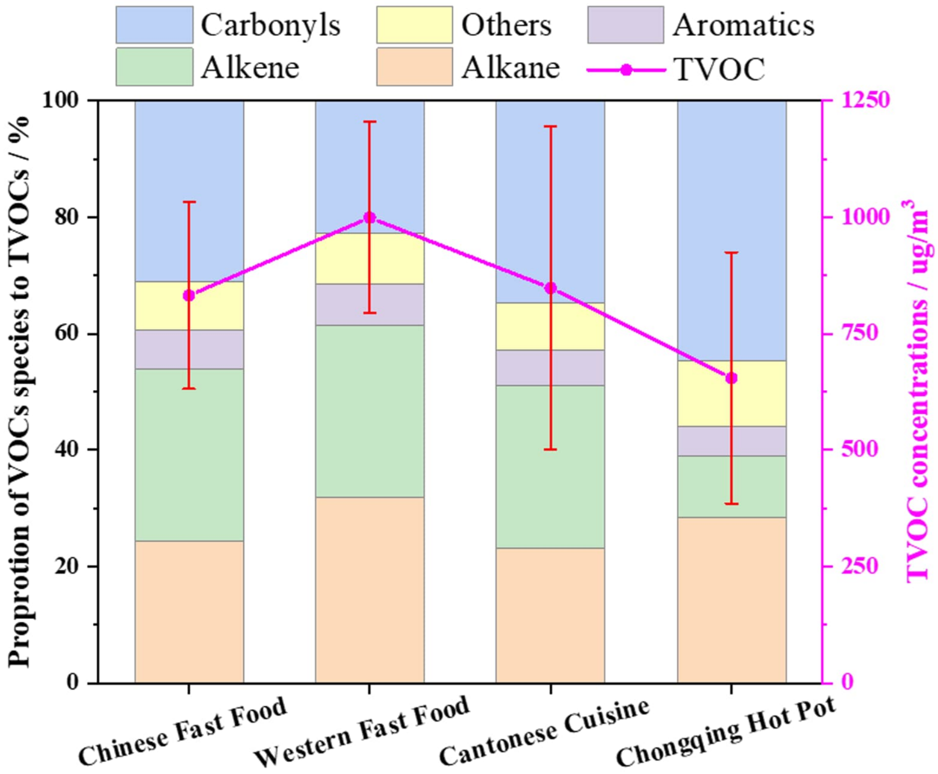

Figure 5-5 Mass concentration of TVOC emissions, vertical bars indicate the standard deviation and the proportion of VOC species from different kitchens

Table 5-1 Summary of the concentrations of the detected particulate and gaseous compounds from kitchen COF emission and scrubber-controlled emissions in the four restaurants

	Kitchen COF Emission (N=30)				COF Scrubber Control (N=26)			
	CFF	**WFF**	**CAN**	**CHP**	**CFF**	**WFF**	**CAN**	**CHP**
				$PM_{2.5}$ (μg/m^3)				
∑$PM_{2.5}$	**232.11 ± 38.64**	**199.95 ± 58.01**	**269.85 ± 50.23**	**85.69 ± 20.65**	**31.03 ± 9.13**	**33.78 ± 5.44**	**38.96 ± 6.4**	**29.54 ± 0.57**
OC	117.05 ± 23.37	106.75 ± 36	137.63 ± 31.05	34.39 ± 8.53	15.45 ± 5.56	15.96 ± 3.59	18.4 ± 5.35	15.02 ± 1
EC	8.87 ± 2.67	2.22 ± 0.7	6.65 ± 4.23	3.46 ± 2.62	1.2 ± 0.28	0.32 ± 0.12	0.84 ± 0.65	1.15 ± 0.37
				Water-soluble Ions (μg/m^3)				
Na+	0.02 ± 0.01	0.2 ± 0.07	0.2 ± 0.28	0.31 ± 0.18	BDL	BDL	BDL	0.02 ± 0.01
NH4+	0.9 ± 0.19	0.7 ± 0.19	1.59 ± 0.66	1.8 ± 0.52	0.12 ± 0.02	0.11 ± 0.02	0.15 ± 0.09	0.24 ± 0.08
K+	0.26 ± 0.05	1.12 ± 0.33	0.37 ± 0.11	0.71 ± 0.4	BDL	0.07 ± 0.01	0.06 ± 0.03	0.08 ± 0.05
Mg2+	0.02 ± 0.01	0.04 ± 0.01	0.06 ± 0.05	0.07 ± 0.02	BDL	BDL	BDL	BDL
Ca2+	1.16 ± 0.19	0.44 ± 0.12	1.42 ± 0.17	0.47 ± 0.26	0.1 ± 0.07	0.12 ± 0.01	0.14 ± 0.09	0.12 ± 0.05
F-	0.01 ± 0.01	0.07 ± 0.02	0.02 ± 0.03	0.32 ± 0.28	BDL	BDL	BDL	0.1 ± 0.02
Cl-	0.42 ± 0.08	0.48 ± 0.14	0.74 ± 0.31	0.79 ± 1.34	0.08 ± 0.03	0.05 ± 0.01	0.09 ± 0.09	0.09 ± 0.04
NO3-	1.63 ± 0.32	0.4 ± 0.13	2.48 ± 0.76	2.92 ± 0.76	0.15 ± 0.04	0.2 ± 0.01	0.21 ± 0.07	0.3 ± 0.21
SO42-	2.43 ± 0.86	3.37 ± 1.03	4.29 ± 3.36	6.58 ± 3.11	0.31 ± 0.1	0.28 ± 0.06	0.4 ± 0.12	0.56 ± 0.11
∑Ions	**6.85 ± 1.61**	**6.82 ± 2**	**11.17 ± 4.77**	**13.72 ± 3.47**	**0.76 ± 0.09**	**0.83 ± 0.05**	**1.06 ± 0.32**	**1.52 ± 0.66**
				Elements (ng/m^3)				
Al	69.53 ± 14.41	195.95 ± 51.94	302.59 ± 391.63	394.8 ± 227.57	16 ± 6.51	9.52 ± 3.17	19.38 ± 1.25	12.55 ± 11.39
Si	200.15 ± 48.64	189.74 ± 56.76	708.26 ± 754.69	436.4 ± 245.33	69.37 ± 28.62	24.99 ± 4.81	86.94 ± 21.74	22.65 ± 9.18
Ni	11.54 ± 1.32	2.1 ± 0.48	30.13 ± 26.57	22.92 ± 6.03	2.7 ± 0.6	1.54 ± 0.16	2.83 ± 0.36	7.67 ± 9.39
Mg	82.53 ± 11.97	203.55 ± 67.84	267.11 ± 299.14	150.33 ± 84.04	20.89 ± 8.66	11.4 ± 3.51	24.88 ± 2.7	9.99 ± 5.75
Na	40.13 ± 13.58	281.93 ± 81.16	257.14 ± 343.4	646.56 ± 638.5	16.88 ± 9.04	4.19 ± 0.33	21.95 ± 2.8	162.38 ± 25.66
K	353.8 ± 59.08	1546.9 ± 427.2	645.33 ± 447.65	819.9 ± 439.9	82.81 ± 11.45	41.78 ± 5.48	96.31 ± 10.98	121.7 ± 37.23

Ca	3055.3 ± 932.6	838.6 ± 214.49	4863.2 ± 2473.1	1352.2 ± 337.5	1056.9 ± 150.7	383.4 ± 54.25	1296.5 ± 111.96	380.43 ± 115.94
Ti	3.95 ± 1.06	10.41 ± 3.31	83.51 ± 134.6	68.14 ± 28.8	1.43 ± 0.74	0.43 ± 0.04	1.82 ± 0.09	28.44 ± 9.79
Cr	25.96 ± 3.4	4.37 ± 1.41	64.89 ± 52.79	30.66 ± 7.39	6.43 ± 1.63	3.34 ± 0.82	7.02 ± 0.5	12.49 ± 4.32
Mn	15.54 ± 5.3	38.26 ± 7.62	20.53 ± 6.37	14.12 ± 5.12	5.37 ± 3	1.88 ± 0.43	6.84 ± 1.16	4.23 ± 1.6
Fe	280.43 ± 95.24	117.42 ± 37.29	742.37 ± 640.86	469.8 ± 134.73	87.03 ± 13.09	34.77 ± 9.66	107.08 ± 26.9	104.37 ± 18.2
Co	2.56 ± 0.56	0.47 ± 0.09	3.97 ± 1.44	7.25 ± 10.6	0.73 ± 0.37	0.33 ± 0.09	0.95 ± 0.02	7.23 ± 10
Cu	10.83 ± 1.22	6.11 ± 1.82	23.49 ± 17.91	74.79 ± 77.97	2.04 ± 0.33	1.48 ± 0.43	2.12 ± 0.08	68.35 ± 25.4
Zn	115.13 ± 60.73	48.29 ± 8.79	201.29 ± 148.42	186.65 ± 255.8	67.14 ± 13.12	12.67 ± 4.32	95.31 ± 15.55	81.69 ± 28.8
Ga	8.95 ± 2.18	6.41 ± 1.39	10.09 ± 8.27	1.73 ± 3	3.69 ± 1.74	1.11 ± 0.1	4.4 ± 0.54	2.57 ± 2.58
As	12.66 ± 2.15	1.18 ± 0.31	20.39 ± 7.2	16.64 ± 4.06	4.17 ± 1.98	1.87 ± 0.57	5.35 ± 0.37	1.89 ± 1.56
Se	0.6 ± 0.15	0.34 ± 0.1	0.62 ± 0.46	BDL	0.17 ± 0.07	0.11 ± 0.1	0.2 ± 0.01	BDL
Rb	1.04 ± 0.19	3 ± 0.93	0.99 ± 0.63	BDL	0.26 ± 0.08	0.13 ± 0.07	0.3 ± 0.02	BDL
Mo	3.35 ± 0.75	10.94 ± 3.37	2.6 ± 1.98	BDL	0.51 ± 0.09	0.46 ± 0.22	0.4 ± 0.03	BDL
Sn	14.52 ± 1.91	0.45 ± 0.16	11.68 ± 7.71	1.21 ± 2.09	2.45 ± 0.42	2.07 ± 0.26	2.1 ± 0.18	1.87 ± 0.51
Ba	26.53 ± 3.33	24.76 ± 5.92	20.6 ± 12.63	3.61 ± 6.25	4.15 ± 0.32	4.01 ± 0.4	3.64 ± 0.29	4.5 ± 2.67
La	35.39 ± 5.75	13.41 ± 4.33	27.52 ± 18.68	6.6 ± 11.43	4.77 ± 0.98	4.87 ± 0.54	4.37 ± 0.71	4.58 ± 1.55
Pb	33.23 ± 3.77	11.33 ± 3.25	43.3 ± 7.37	13.06 ± 3.15	8.54 ± 3.35	4.49 ± 0.7	9.72 ± 1.18	10.2 ± 2.63
∑Elements	**4403.6 ± 1237**	**3556.9 ± 941.1**	**8351.6 ± 4349.1**	**4717.4 ± 1440**	**1464.5 ± 222.47**	**550.7 ± 79.48**	**1800.4 ± 162.21**	**1050.5 ± 117.17**
PAHs (ng/m^3)								
Nap	0.88 ± 0.1	0.54 ± 0.17	0.79 ± 0.28	0.34 ± 0.11	0.07 ± 0.01	0.08 ± 0.03	0.1 ± 0.04	0.13 ± 0.02
Acy	0.16 ± 0.03	1.46 ± 0.36	0.2 ± 0.06	0.05 ± 0.07	0.03 ± 0	0.08 ± 0.09	0.03 ± 0	0.02 ± 0
Ace	0.8 ± 0.1	2.98 ± 0.94	0.85 ± 0.42	0.21 ± 0.32	0.02 ± 0	0.18 ± 0.16	0.05 ± 0.04	0.11 ± 0.01
Flu	0.11 ± 0.02	2.71 ± 0.66	0.23 ± 0.23	0.44 ± 0.48	0.01 ± 0	0.13 ± 0.16	0.02 ± 0	0.02 ± 0
Phe	0.1 ± 0.02	8.7 ± 2.11	0.52 ± 0.75	1.03 ± 1.67	0.01 ± 0	0.44 ± 0.62	0.01 ± 0	0.01 ± 0.01
Ant	0.06 ± 0.01	0.56 ± 0.18	0.09 ± 0.03	0.05 ± 0.07	0.01 ± 0	0.03 ± 0.03	0.01 ± 0	0.01 ± 0
Fln	0.49 ± 0.1	2.63 ± 0.82	0.64 ± 0.23	0.33 ± 0.47	0.08 ± 0.01	0.13 ± 0.14	0.08 ± 0.02	0.06 ± 0.02
Pyr	0.66 ± 0.1	2.34 ± 0.82	0.92 ± 0.61	0.35 ± 0.35	0.06 ± 0.01	0.14 ± 0.11	0.08 ± 0.03	0.09 ± 0.02
BaA	0.25 ± 0.02	0.61 ± 0.16	0.27 ± 0.06	0.08 ± 0.11	0.03 ± 0	0.05 ± 0.04	0.03 ± 0	0.03 ± 0
Chr	0.57 ± 0.1	1.72 ± 0.55	0.54 ± 0.1	0.23 ± 0.37	0.07 ± 0.01	0.11 ± 0.08	0.08 ± 0.01	0.09 ± 0.03

BbF	1.57 ± 0.23	2.02 ± 0.42	1.51 ± 0.35	0.43 ± 0.1	0.27 ± 0.03	0.18 ± 0.09	0.26 ± 0.06	0.22 ± 0.04
BkF	0.39 ± 0.08	1.26 ± 0.47	0.35 ± 0.07	0.26 ± 0.08	0.08 ± 0.02	0.08 ± 0.07	0.07 ± 0.03	0.05 ± 0.01
BaF	0.22 ± 0.02	0.02 ± 0.01	0.21 ± 0.04	0.02 ± 0.01	0.03 ± 0	0.02 ± 0.01	0.03 ± 0.01	0.03 ± 0.01
BeP	0.5 ± 0.15	0.76 ± 0.18	0.52 ± 0.11	0.36 ± 0.11	0.1 ± 0.01	0.07 ± 0.03	0.11 ± 0.01	0.06 ± 0.01
BaP	0.46 ± 0.12	0.72 ± 0.24	0.56 ± 0.13	0.41 ± 0.13	0.11 ± 0.01	0.06 ± 0.03	0.09 ± 0.03	0.06 ± 0.01
Per	0.1 ± 0.02	0.03 ± 0.01	0.11 ± 0.04	0.17 ± 0.11	0.01 ± 0	0.01 ± 0	0.01 ± 0	0.01 ± 0
InD	0.28 ± 0.06	2.31 ± 0.88	0.45 ± 0.28	0.2 ± 0.22	0.03 ± 0	0.11 ± 0.13	0.03 ± 0	0.04 ± 0.02
DBA	0.06 ± 0.01	0.87 ± 0.23	0.1 ± 0.05	0.05 ± 0.01	0.01 ± 0	0.05 ± 0.06	0.01 ± 0	0.01 ± 0
BghiP	0.08 ± 0.01	2.29 ± 0.65	0.37 ± 0.5	0.14 ± 0.21	0.01 ± 0	0.13 ± 0.17	0.01 ± 0	0.01 ± 0
Cor	0.08 ± 0.01	1.43 ± 0.36	0.57 ± 0.86	0.04 ± 0.01	0.01 ± 0	0.08 ± 0.1	0.01 ± 0	0.01 ± 0
Dip	0.01 ± 0.01	0.14 ± 0.05	0.42 ± 0.71	BDL	BDL	BDL	BDL	BDL
∑PAHs	**7.84 ± 0.81**	**36.08 ± 10.07**	**10.19 ± 4.09**	**5.17 ± 4.13**	**1.06 ± 0.1**	**2.14 ± 2.13**	**1.13 ± 0.14**	**1.05 ± 0.16**
Alkane (μg/m^3)								
ethane	19.09 ± 5.87	34.16 ± 5.32	20.71 ± 11.69	15.44 ± 4.91	6.03 ± 2.23	12.51 ± 1.94	6.23 ± 1.68	6.74 ± 0.86
propane	13.09 ± 3.95	17.03 ± 5.33	10.53 ± 7.2	0.21 ± 0.05	3.19 ± 1.66	3.08 ± 0.18	3.26 ± 1.36	1.66 ± 0.06
isobutane	18.11 ± 6.36	15.79 ± 1.31	14.79 ± 10.19	0.72 ± 0.18	4.41 ± 3.09	2.09 ± 0.35	4.68 ± 2.71	1.77 ± 0.68
butane	21.76 ± 6.55	27.94 ± 9.35	17.68 ± 11.95	0.37 ± 0.09	6.6 ± 3.26	3.74 ± 0.49	6.06 ± 3.22	3.55 ± 1.24
cyclopentane	0.27 ± 0.08	0.43 ± 0.08	0.27 ± 0.09	0.67 ± 0.35	0.09 ± 0.03	0.07 ± 0.01	0.08 ± 0.03	0.05 ± 0.01
isopentane	3.39 ± 1.18	6.01 ± 1.99	2.98 ± 1.64	1.21 ± 0.63	1.13 ± 0.45	0.87 ± 0.08	1.04 ± 0.46	0.67 ± 0.13
pentane	27.3 ± 9.39	32.59 ± 10.46	25.13 ± 11.52	16.39 ± 3.92	7.75 ± 4.39	3.97 ± 0.59	7.75 ± 3.91	3.31 ± 1.45
2,2-dimethylbutane	0.28 ± 0.09	0.45 ± 0.13	0.25 ± 0.12	0.21 ± 0.05	0.08 ± 0.04	0.05 ± 0.01	0.08 ± 0.03	0.04 ± 0.01
2,3-dimethylbutane	7 ± 1.92	11.91 ± 2.24	6.45 ± 2.6	9.31 ± 2.48	2.14 ± 0.68	2.7 ± 0.33	1.9 ± 0.75	1.92 ± 0.14
isohexane	9.3 ± 3.42	15.59 ± 5.32	8.7 ± 3.96	12.32 ± 3.56	2.93 ± 1.1	2.25 ± 0.69	2.59 ± 1.16	2.05 ± 0.35
3-methylpentane	7.6 ± 2.74	17.65 ± 7.47	9.44 ± 2.9	15.69 ± 5.08	2.81 ± 0.89	2.69 ± 0.44	2.5 ± 1.03	2.25 ± 0.46
hexane	30.22 ± 10.15	50.49 ± 10.53	27.63 ± 13.64	17.31 ± 4.85	9.71 ± 3.43	9.7 ± 1.15	8.66 ± 3.45	6.48 ± 1.5
2,4-dimethylpentane	0.78 ± 0.25	1.27 ± 0.39	0.68 ± 0.34	0.37 ± 0.13	0.18 ± 0.09	0.16 ± 0.02	0.2 ± 0.07	0.12 ± 0.02
methylcyclopentane	0.48 ± 0.14	0.61 ± 0.12	0.41 ± 0.24	0.11 ± 0.04	0.15 ± 0.08	0.12 ± 0.02	0.14 ± 0.08	0.08 ± 0.02
2-methylhexane	2.29 ± 0.62	3.09 ± 1.07	3.51 ± 1.77	10.93 ± 3.35	0.62 ± 0.38	0.67 ± 0.13	0.62 ± 0.34	0.48 ± 0.05
2,3-dimethylpentane	0.35 ± 0.09	0.46 ± 0.1	0.33 ± 0.12	0.31 ± 0.09	0.08 ± 0.03	0.1 ± 0.02	0.08 ± 0.03	0.06 ± 0

cyclohexane	3.45 ± 0.81	4.96 ± 0.79	3.06 ± 1.45	2.3 ± 1.08	1.05 ± 0.47	0.81 ± 0.09	0.98 ± 0.46	0.54 ± 0.09
3-methylhexane	2.63 ± 0.92	4.63 ± 0.96	4.1 ± 2.41	10.93 ± 3.02	0.81 ± 0.26	0.64 ± 0.12	0.76 ± 0.26	0.56 ± 0.14
heptane	11.45 ± 3.36	19.27 ± 8.55	12.41 ± 3.34	16.55 ± 3.87	3.69 ± 1.67	5.51 ± 0.65	3.35 ± 1.72	3.01 ± 0.06
methylcyclohexane	1.03 ± 0.37	1.87 ± 0.45	1.92 ± 1.36	5.21 ± 1.22	0.39 ± 0.12	0.61 ± 0.13	0.34 ± 0.14	0.37 ± 0.02
2,3,4-trimethylpentane	0.91 ± 0.32	1.68 ± 0.39	0.96 ± 0.31	1.42 ± 0.34	0.27 ± 0.09	0.23 ± 0.03	0.26 ± 0.08	0.17 ± 0.06
2,2,4-trimethylpentane	4.15 ± 1.51	10.8 ± 1.75	4.79 ± 1.59	12.36 ± 3.19	1.71 ± 0.41	1.55 ± 0.05	1.48 ± 0.57	1.21 ± 0.4
2-methylheptane	0.39 ± 0.15	0.8 ± 0.28	0.4 ± 0.15	0.42 ± 0.11	0.11 ± 0.05	0.12 ± 0.03	0.11 ± 0.05	0.09 ± 0
3-methylheptane	0.66 ± 0.2	0.66 ± 0.21	0.64 ± 0.25	0.61 ± 0.15	0.2 ± 0.17	0.12 ± 0.02	0.2 ± 0.15	0.07 ± 0.01
octane	5.1 ± 1.44	9.87 ± 1.76	5.03 ± 1.7	6.68 ± 1.59	1.58 ± 0.75	2.11 ± 0.38	1.59 ± 0.62	1.2 ± 0.13
nonane	0.83 ± 0.27	1.48 ± 0.33	1 ± 0.37	2.39 ± 0.59	0.22 ± 0.06	0.41 ± 0.1	0.2 ± 0.07	0.29 ± 0.04
decane	3.33 ± 0.96	6.64 ± 2.44	3.11 ± 1.22	3.93 ± 1.51	0.92 ± 0.33	1.24 ± 0.09	0.84 ± 0.33	0.76 ± 0.21
undecane	2.92 ± 0.79	4.78 ± 0.62	2.97 ± 0.87	4.16 ± 1.02	0.94 ± 0.24	1.57 ± 0.19	0.81 ± 0.25	1.03 ± 0.16
dodecane	2.16 ± 0.62	3.38 ± 1.04	2.52 ± 0.85	4.38 ± 1.21	0.6 ± 0.22	0.96 ± 0.1	0.57 ± 0.2	0.55 ± 0
Trichloro fluoromethane	0.91 ± 0.35	3.53 ± 0.31	1.29 ± 0.66	3.81 ± 0.98	1.33 ± 0.49	2.84 ± 1.06	1.04 ± 0.57	1.42 ± 0.2
Dichloro difluoromethane	1.73 ± 0.69	6.12 ± 0.29	2.29 ± 1.02	7.33 ± 1.86	2.86 ± 1.11	5.65 ± 1.99	2.29 ± 1.29	2.73 ± 0.36
1,1,2-trichlorotri fluoroethane	0.35 ± 0.14	1.72 ± 0.21	0.56 ± 0.31	1.71 ± 0.42	0.66 ± 0.21	1.17 ± 0.34	0.51 ± 0.26	0.61 ± 0.08
1,2-dichlorotetra fluoroethane	0.07 ± 0.02	0.3 ± 0.03	0.1 ± 0.04	0.32 ± 0.08	0.12 ± 0.05	0.25 ± 0.06	0.1 ± 0.06	0.13 ± 0.01
∑Alkane	**203.36 ± 62.44**	**317.96 ± 77.52**	**196.65 ± 93.02**	**186.09 ± 49.39**	**65.37 ± 27.13**	**70.58 ± 11.3**	**61.28 ± 26.02**	**46.01 ± 8.52**
Alkene (μg/m^3)								
ethylene	112.71 ± 33.57	135.99 ± 15.67	122.17 ± 76.09	18.79 ± 5.95	44.87 ± 20.49	41.69 ± 9.67	42.57 ± 19.24	30.82 ± 3.48
propylene	25.53 ± 7.43	32.09 ± 15.26	20.49 ± 13.96	0.38 ± 0.1	7.72 ± 3.85	4.73 ± 0.55	7.19 ± 3.73	4.21 ± 2.11
trans-2-butene	0.53 ± 0.15	1.61 ± 0.38	0.45 ± 0.25	0.19 ± 0.05	0.29 ± 0.04	0.67 ± 0.11	0.2 ± 0.09	0.38 ± 0.04
1-butene	1.6 ± 0.54	2.81 ± 0.69	1.37 ± 0.76	0.77 ± 0.2	0.45 ± 0.17	0.56 ± 0.07	0.42 ± 0.17	0.36 ± 0.04
cis-2-butene	0.42 ± 0.11	0.74 ± 0.25	0.42 ± 0.13	0.58 ± 0.14	0.11 ± 0.05	0.11 ± 0.01	0.12 ± 0.04	0.07 ± 0
1,3-butadiene	26.84 ± 6.45	36.08 ± 11.17	22.36 ± 12.62	7.04 ± 2.16	6.77 ± 3.18	3.1 ± 0.29	6.53 ± 2.91	2.74 ± 1.29
1-pentene	63.57 ± 18.39	64.18 ± 24.68	54.37 ± 29.21	21.8 ± 5.11	15.62 ± 8.29	10.96 ± 2.28	15.1 ± 7.62	8.39 ± 1.66
trans-2-pentene	0.74 ± 0.27	1.31 ± 0.41	0.73 ± 0.3	0.5 ± 0.13	0.25 ± 0.14	0.29 ± 0.04	0.24 ± 0.13	0.17 ± 0.01

isoprene	7.35 ± 1.9	10.66 ± 2.57	6.69 ± 3.02	4.3 ± 1.26	2.36 ± 1.35	2.06 ± 0.36	2.18 ± 1.34	1.44 ± 0.41
cis-2-pentene	0.51 ± 0.15	0.65 ± 0.09	0.54 ± 0.15	0.56 ± 0.27	0.15 ± 0.08	0.14 ± 0.01	0.14 ± 0.07	0.1 ± 0.02
1-hexene	4.89 ± 1.93	9.4 ± 3.34	6.29 ± 2.61	14.38 ± 3.74	2.2 ± 0.22	3.35 ± 0.58	1.75 ± 0.68	2.42 ± 0.35
∑Alkene	**244.68 ± 63.81**	**295.53 ± 67.05**	**235.88 ± 125.21**	**69.28 ± 17.19**	**80.8 ± 34.07**	**67.67 ± 12.59**	**76.45 ± 32.42**	**51.1 ± 8.48**
Aromatic Hydrocarbon ($\mu g/m^3$)								
benzene	4.55 ± 1.38	6.12 ± 1.19	4.15 ± 1.88	3.98 ± 1.48	1.68 ± 0.64	2.47 ± 0.45	1.49 ± 0.67	1.62 ± 0.1
toluene	10.13 ± 3.66	13.45 ± 4.57	9.86 ± 4.44	5.91 ± 1.79	4.16 ± 2.72	3.63 ± 0.74	3.98 ± 2.57	2.24 ± 0.26
ethylbenzene	2.94 ± 0.88	2.89 ± 0.64	2.94 ± 0.95	2.68 ± 1.15	0.81 ± 0.56	0.84 ± 0.23	0.86 ± 0.48	0.56 ± 0.06
dimethylbenzene	6.13 ± 1.93	6.49 ± 1.71	5.62 ± 2.58	2.56 ± 1.29	1.95 ± 1.65	0.67 ± 0.11	1.96 ± 1.51	0.54 ± 0.23
1,2-dimethylbenzene	1.75 ± 0.45	1.92 ± 0.3	1.71 ± 0.6	1.25 ± 0.38	0.62 ± 0.41	0.61 ± 0.16	0.64 ± 0.35	0.41 ± 0.07
styrene	1.3 ± 0.45	1.06 ± 0.31	1.16 ± 0.59	0.7 ± 0.17	0.35 ± 0.25	0.42 ± 0.08	0.37 ± 0.21	0.26 ± 0.04
cumene	0.4 ± 0.16	0.84 ± 0.26	0.36 ± 0.19	0.19 ± 0.07	0.12 ± 0.05	0.09 ± 0.01	0.12 ± 0.04	0.06 ± 0.01
N-propylbenzene	0.73 ± 0.24	1.17 ± 0.29	0.66 ± 0.31	0.47 ± 0.12	0.2 ± 0.11	0.19 ± 0.02	0.21 ± 0.09	0.12 ± 0.01
3-ethyltoluene	0.79 ± 0.3	1.17 ± 0.26	0.72 ± 0.36	0.42 ± 0.21	0.24 ± 0.18	0.1 ± 0.01	0.24 ± 0.16	0.07 ± 0.01
4-ethyltoluene	0.48 ± 0.15	0.61 ± 0.13	0.44 ± 0.21	0.2 ± 0.05	0.15 ± 0.1	0.11 ± 0.04	0.15 ± 0.08	0.08 ± 0
mesitylene	0.41 ± 0.14	0.74 ± 0.28	0.37 ± 0.19	0.24 ± 0.06	0.13 ± 0.07	0.1 ± 0.02	0.12 ± 0.07	0.07 ± 0.01
1-ethyl-2-methylbenzene	0.44 ± 0.14	0.88 ± 0.08	0.39 ± 0.19	0.51 ± 0.36	0.15 ± 0.07	0.5 ± 0.07	0.16 ± 0.05	0.29 ± 0.13
pseudocumene	3.83 ± 1.05	4.6 ± 1.22	3.55 ± 1.57	2.1 ± 1.16	1.14 ± 0.72	0.52 ± 0.13	1.19 ± 0.62	0.48 ± 0.15
1,2,3-trimethylbenzene	0.86 ± 0.26	1.43 ± 0.54	0.77 ± 0.37	0.43 ± 0.2	0.22 ± 0.13	0.14 ± 0.02	0.23 ± 0.1	0.12 ± 0.02
1,3-diethylbenzene	5.41 ± 1.42	6.71 ± 1.86	5.92 ± 1.53	6.26 ± 3.42	1.48 ± 1.12	0.97 ± 0.23	1.64 ± 0.88	0.56 ± 0.13
1,4-diethylbenzene	1.69 ± 0.57	2.06 ± 0.76	1.5 ± 0.85	0.45 ± 0.24	0.47 ± 0.41	0.08 ± 0.02	0.52 ± 0.35	0.07 ± 0.02
naphthalene	14.2 ± 4.61	19.73 ± 4.72	12.42 ± 7.1	4.43 ± 1.24	4.93 ± 3.97	4.5 ± 0.93	5.26 ± 3.39	2.38 ± 0.78
∑Aromatics	**56.03 ± 16**	**71.86 ± 17.2**	**52.53 ± 21.53**	**32.78 ± 12.06**	**18.8 ± 11.84**	**15.93 ± 2.93**	**19.13 ± 10.47**	**9.93 ± 1.83**
Others ($\mu g/m^3$)								
acetylene	21.64 ± 7.65	27.19 ± 10.93	18.28 ± 11.73	5.21 ± 2.29	7.05 ± 3.48	5.62 ± 1.08	6.78 ± 3.24	3.61 ± 0.12
acetonitrile	4.24 ± 1.45	9.02 ± 2.16	3.56 ± 2.09	1.83 ± 0.51	1.31 ± 0.82	1.89 ± 0.3	1.42 ± 0.6	0.85 ± 0.33
isopropyl alcohol	12.72 ± 3.67	24.36 ± 10.24	17.88 ± 8.6	45.51 ± 11.67	3.44 ± 2.25	2.17 ± 0.33	3.85 ± 1.69	1.4 ± 0.15
ethyl acetate	3.47 ± 1.36	3.23 ± 0.17	3.06 ± 1.73	2.65 ± 1.61	0.76 ± 0.75	0.41 ± 0.07	0.91 ± 0.64	0.23 ± 0.04
vinyl acetate	3.33 ± 1	4.1 ± 1.7	3.31 ± 1.18	3.02 ± 0.71	0.98 ± 1.06	0.57 ± 0.08	1.07 ± 0.95	0.34 ± 0.08

methyl tert-butyl ether	2.32 ± 0.9	2.65 ± 0.83	2.05 ± 1.14	2.34 ± 1.78	0.48 ± 0.44	0.63 ± 0.14	0.59 ± 0.36	0.34 ± 0.14
tetrahydrofuran	5.65 ± 1.57	3.75 ± 1.68	5.93 ± 1.59	6.1 ± 2.3	1.38 ± 1.51	0.57 ± 0.13	1.7 ± 1.27	0.33 ± 0.1
methyl methacrylate	9.03 ± 3.16	7.79 ± 0.62	7.95 ± 4.33	4.58 ± 1.34	1.86 ± 1.85	1.43 ± 0.07	2.22 ± 1.55	0.77 ± 0.26
methyl isobutyl ketone	6.76 ± 2.14	4.85 ± 1.49	6.02 ± 3.01	3.22 ± 1.08	1.46 ± 1.65	0.4 ± 0.04	1.75 ± 1.42	0.23 ± 0.04
∑Others	**69.15 ± 20.61**	**86.92 ± 26.83**	**68.04 ± 31.86**	**74.48 ± 20.97**	**18.74 ± 12.44**	**13.69 ± 2.02**	**20.3 ± 10.54**	**8.1 ± 1.13**
Carbonyls (μg/m^3)								
formaldehyde	88.72 ± 18.37	40.36 ± 10.1	96.31 ± 33.38	41.39 ± 12.69	35.88 ± 18.83	22.3 ± 1.69	39.65 ± 20.8	39.93 ± 14.95
acetaldehyde	46.9 ± 11.22	37.24 ± 4.38	62.04 ± 19.85	67.74 ± 50.9	24.33 ± 5.59	24.88 ± 8.77	22.94 ± 6.42	28.95 ± 7.96
acetone	27.55 ± 9	21.9 ± 3.29	26.73 ± 14.52	27.36 ± 29.56	13.28 ± 2.71	13.66 ± 4.02	12.85 ± 3.97	17.08 ± 3.73
acrolein	21.26 ± 6.9	31.37 ± 4.34	31.73 ± 15.39	37.83 ± 14.55	18.53 ± 2.75	16.41 ± 5.68	15.12 ± 6.12	21.04 ± 2.63
propionaldehyde	9.5 ± 2.78	3.73 ± 0.66	10.7 ± 4	9.3 ± 6.07	3.94 ± 1.67	3.86 ± 1.01	4.18 ± 1.9	4.72 ± 1.58
crotonaldehyde	10.03 ± 1.99	7.34 ± 1.72	13.42 ± 4.16	30.82 ± 27.03	4.42 ± 1.14	6.62 ± 2.75	4.36 ± 1.31	6.19 ± 1.62
methyl ethyl ketone	4.24 ± 1.2	10.2 ± 2.89	8.22 ± 5.87	13.23 ± 3.69	3.21 ± 1	4.61 ± 2.11	2.34 ± 0.79	3.83 ± 0.4
isobutyraldehyde	8.6 ± 2.7	12.93 ± 3.91	7.78 ± 4.96	7.64 ± 9.04	5.33 ± 1.24	8.19 ± 3.71	4.38 ± 1.15	6.42 ± 1.15
benzaldehyde	5.96 ± 1.62	3.14 ± 0.28	5.12 ± 3.6	7.51 ± 10.18	1.5 ± 0.29	1.34 ± 0.44	1.64 ± 0.29	1.67 ± 0.49
isovaleraldehyde	2.04 ± 0.63	0.76 ± 0.04	1.82 ± 1.18	1.7 ± 1.89	0.44 ± 0.11	0.54 ± 0.16	0.5 ± 0.12	0.67 ± 0.28
valeraldehyde	1.98 ± 0.36	1.13 ± 0.43	1.69 ± 1.16	1.27 ± 1.62	0.53 ± 0.13	0.6 ± 0.19	0.47 ± 0.15	0.84 ± 0.22
2-methylbenzaldehyde	2.34 ± 0.56	1.44 ± 0.23	2 ± 1.39	2.3 ± 2.98	0.7 ± 0.18	0.94 ± 0.46	0.65 ± 0.19	0.82 ± 0.15
3-methylbenzaldehyde	2.14 ± 0.49	2.24 ± 0.45	1.86 ± 1.24	2.07 ± 2.68	0.73 ± 0.09	0.74 ± 0.27	0.69 ± 0.11	0.87 ± 0.19
4-methylbenzaldehyde	1.27 ± 0.37	1.73 ± 0.22	1.12 ± 0.74	2.25 ± 2.94	0.4 ± 0.04	0.99 ± 0.49	0.36 ± 0.11	0.74 ± 0.28
caproic aldehyde	22.84 ± 7.56	47.5 ± 9.83	20.04 ± 13.77	28.09 ± 34.21	17.06 ± 7.64	11.43 ± 2.15	11.45 ± 6.94	21.98 ± 1.73
2,5-dimethylbenzaldehyde	3.47 ± 0.67	3.63 ± 0.79	4.22 ± 1.42	11.39 ± 12.66	1.45 ± 0.32	1.79 ± 0.59	1.15 ± 0.44	2.22 ± 0.34
∑Carbonyls	**258.83 ± 59.78**	**226.66 ± 39.2**	**294.81 ± 113.96**	**291.9 ± 200.4**	**131.72 ± 39.36**	**118.9 ± 31.03**	**122.76 ± 45.73**	**157.98 ± 33.93**
∑TVOC	**832.1 ± 200.4**	**998.9 ± 205.0**	**847.9 ± 347.0**	**654.5 ± 270.0**	**283.88 ± 112.4**	**258.1 ± 53.9**	**269.93 ± 112.7**	**245.81 ± 48.5**

5.3 Environment and Health Impacts of COFs

Due to the high emission levels and complexity of various pollutants from COFs, it is necessary to conduct impact assessments and quantify the influences on environment and health. In addition to the air pollution caused by the direct emissions, VOC can still react with other chemicals in ambient air to form secondary pollutants such as ozone and SOA (Han et al., 2023). Many VOC and PAH species have been defined as toxic compounds in causing cancer and other severe health issues (David & Niculescu, 2021), which should be well studied and evaluated.

5.3.1 Chemical Reactivity and Ozone Formation Potential

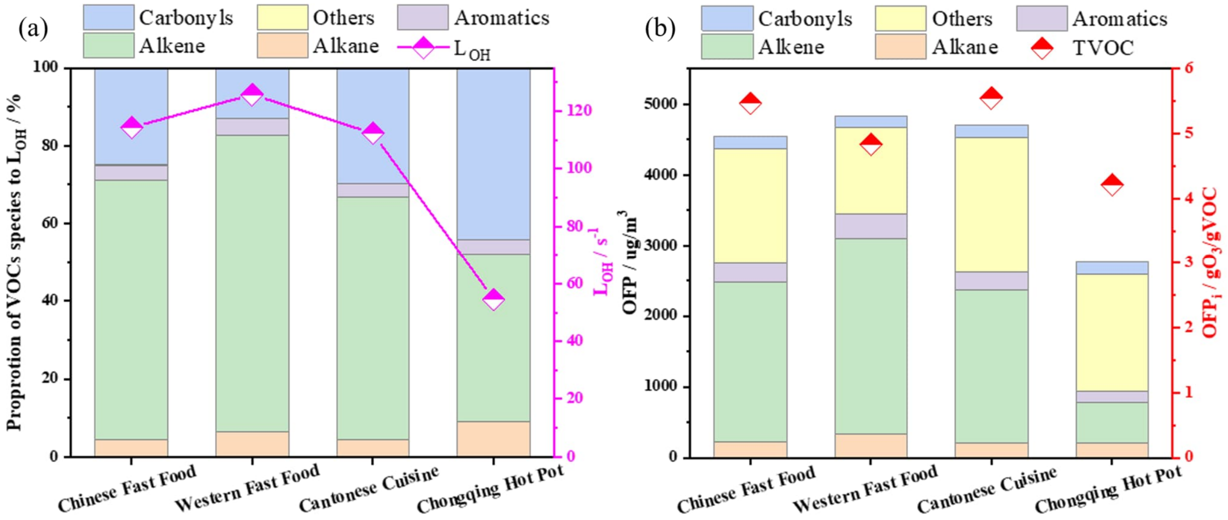

Figure 5-6 (a) Contribution of VOC species to L_{OH} and the total L_{OH} and (b) accumulative contribution of VOC species to OFP and the mass O_3 (g) generation from 1 g of VOCs in the COFs from different kitchens

The chemical reactivity of VOC reflects the ability of an individual VOC to participate in atmospheric chemical reactions. The tropical O_3 formation process is principally influenced by the chemical reaction between VOCs and radical ·OH in the atmosphere (Atkinson & Arey, 2003; Whalley et al., 2021). While the OFP is used to represent and reflect the ability of O_3 generation in the VOC-limited regime (Tan et al., 2021). The high concentrations of NO_X were released from all the cooking processes as shown in Fig. 5-1 and high ambient NO_X concentrations were also reported in urban Hong Kong (Tan et al., 2023). Thus, the VOC-limited regime could be confirmed, and VOCs played a dominating factor in the O_3 formation processes (Jin & Holloway, 2015). Fig 5-6 (a) shows the contributions and total L_{OH} from the emitted VOCs of the four sampled commercial kitchens. The highest L_{OH} of 125 s^{-1} was from WFF and the lowest one was from CHP of 54 s^{-1}, which were consistent with their TVOC emission concentrations. While alkene was the dominant VOC species in all kitchen emissions which contributed 42% to 76% of the total hydroxyl radical loss rate. Fig. 5-6 (b) displays the total OFP concentrations of 4,550 $\mu g/m^3$, 4,825 $\mu g/m^3$, 4,705 $\mu g/m^3$ and 2,757 $\mu g/m^3$ for CFF, WFF, CAN and CHP, respectively. Both the total OFP concentrations and percentages of the VOC species exhibited very similar contribution patterns as the results of L_{OH} except for the methyl methacrylate and methyl isobutyl ketone assigned to the category of other VOCs. They both demonstrated significant OFP contributions rather than their chemical reactivities as their L_{OH} factors were not available in the previous studies. Although WFF had the highest total OFP value, Chinese food-related CFF and CAN owned higher unit OFP values (OFP_i), which were 5.47 g O_3/g VOCs and 5.55 g O_3/g VOCs, respectively. This was due to the higher emission concentrations from CFF and CAN of the OFP-beneficial VOCs such as formaldehyde, acetaldehyde and methyl methacrylate which possessed high MIR values and chemical reactivities. The unit OFP values ranged from 4.21 to 5.55 g O_3/g VOCs was similar to those reported OFP_i from Si Chuan restaurants which was 3.87 g O_3/g VOCs (X.

Huang et al., 2020) and higher than some OFPi reported by other studies (range from 2-3 g O_3/g VOCs) (X. Liang et al., 2022; H. L. Wang et al., 2018), which was due to the differences in cooking methods, food ingredients and serving capacities.

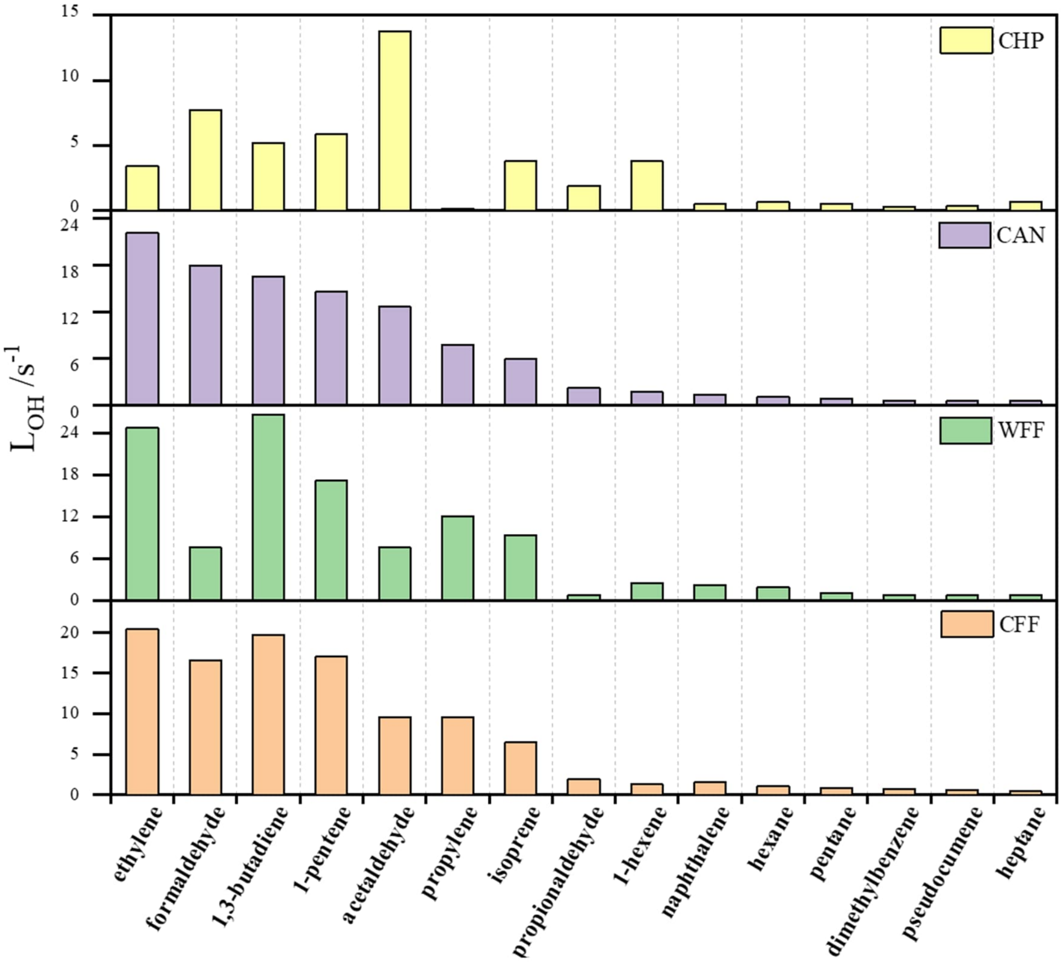

Figure 5-7 The top 15 VOC species of the L_{OH} in four different kitchens

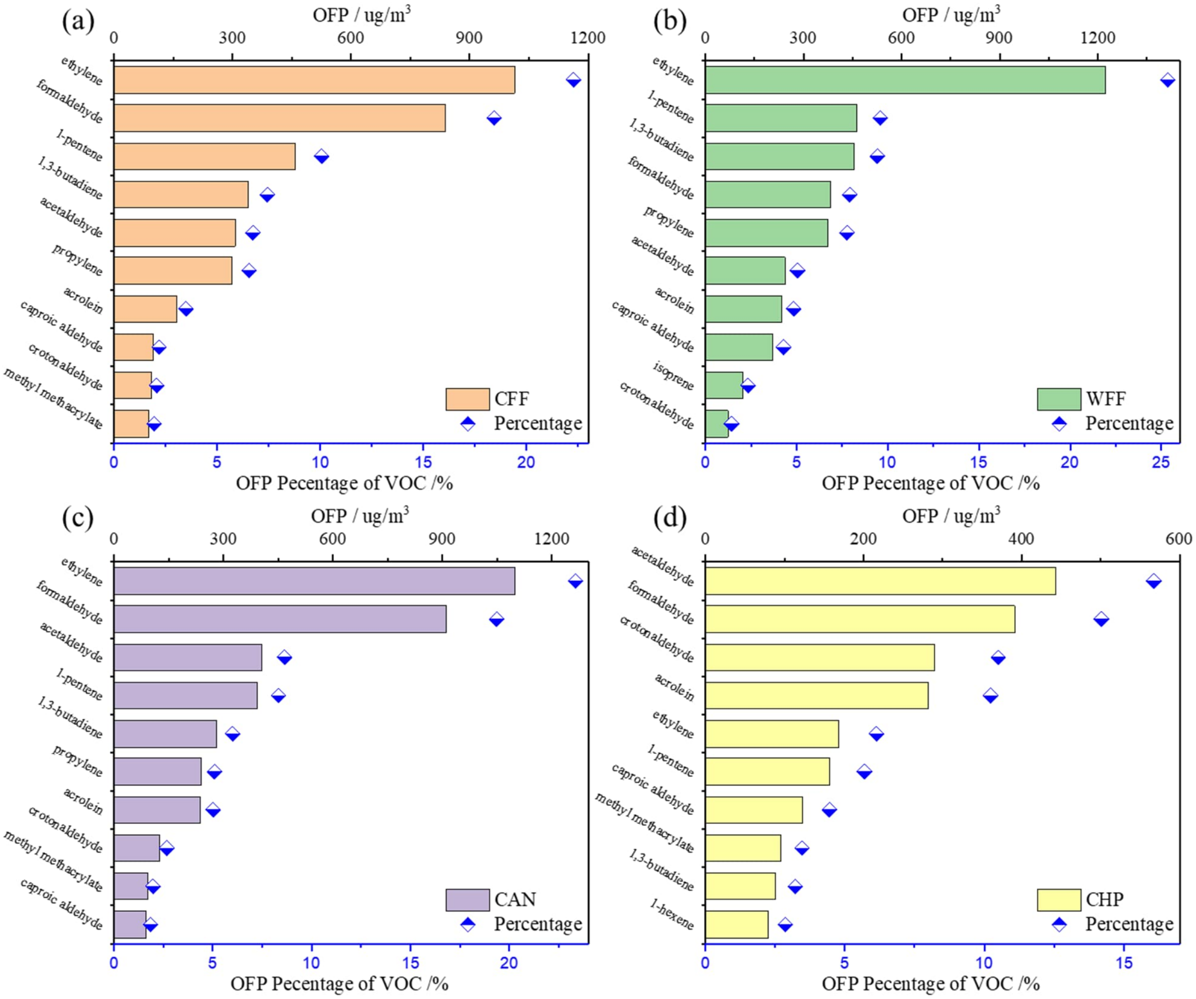

Figure 5-8 The top 10 VOC species of the OFP and their contribution percentages in four different kitchens

The L_{OH} of individual VOC ranged from 0.003 s^{-1} to 26.6 s^{-1}, and Fig. 5-7 presented the top-fifteen VOC species to L_{OH} in all the four kitchens, which accounted for 88.8% - 94.4% of the total L_{OH} in all the detected VOCs. In addition, obvious differences were observed among those kitchens with different serving food and cooking methods. Acetaldehyde was the highest L_{OH} in CHP with the value of 13.8 s^{-1}, while 1,3-butadiene contributed the most in WFF of 26.6 s^{-1}. Ethylene was observed to have the highest L_{OH} in both CAN and CFF as 20.5 s^{-1} and 22.2 s^{-1}, respectively. Besides, formaldehyde, 1-pentene and isoprene were all representatives VOCs with high chemical reactivity from COFs in all restaurants. The calculated OFP of individual VOC ranged from -5.0 $\mu g/m^3$ to 1223.3 $\mu g/m^3$, and the top-ten VOC species with their OFP concentrations and proportions were shown in Fig 5-8. Ethylene was the largest contributor to CFF (22.2%), WFF (25.3%) and CAN (23.3%) with OFP values of 1,013.8 $\mu g/m^3$, 1,223.3 $\mu g/m^3$ and 1,098.9 $\mu g/m^3$, respectively, while acetaldehyde with the OFP value of 443.0 $\mu g/m^3$ made up the largest proportion in WCP (16.1%). Carbonyls including acetaldehyde, formaldehyde and crotonaldehyde were the major OFP contributors in water-based CHP since they had both the higher emission concentrations with over 40% of the TVOC and relativly larger MIR values. In addition, due to the dominant VOC emissions of alkane and alkene, 1-pentene, 1,3-butadiene and ethylene together with formaldehyde occupied over 50% of the total OFP concentrations in these CFF, WFF and CAN kitchens primarily using oil-based cooking methods.

5.3.2 Secondary Organic Aerosol Formation Potential

A total of 29 VOCs with carbon numbers of 6-12 were identified as the compounds in promoting the formation of SOA based on the provided coefficients by Grosjean (1992), which comprised of 11 alkanes, 15 aromatic hydrocarbons and 3 carbonyls. As shown in Fig. 5-9, the highest SOAFP was from WFF of 2,167.7 $\mu g/m^3$, followed by CAN of 1,740.8 $\mu g/m^3$, CFF of 1,769.2 $\mu g/m^3$ and CHP of 604.0 $\mu g/m^3$. And the unit mass SOAFP value ($SOAFP_i$) had the same order as the total SOAFP ranging from 0.92 g SOAFP/g VOCs to 2.17 g SOAFP/g VOCs. The VOC species with the carbon numbers of 7 and 9 were the major contributors for SOAFP in COFs from all commercial kitchens, which could account for as high as 83.3% of the total SOAFP in CAN. Although VOCs with low carbon numbers were dominant in COF emissions, their contribution to SOAs was negligible. As the high saturated vapor pressures of the low-carbon-number VOCs prevented them from condensing into aerosol phases and in turn contributed less to SOAFP (Ait-Helal et al., 2014). Aromatics, on the other hand, accounted for 80.2% - 92.5% of the total SOAFP as demonstrated in Fig. 5-10. The largest two contributors observed in all studied commercial kitchens were toluene (16.8% - 34.9%) and 1,2,4-trimethylbenzene (22.9% - 27.7%), followed by ethylbenzene (6.4% to 8%) in CFF, WFF and CAN, and 1,3-diethylbezene (6.2%) in CHP.

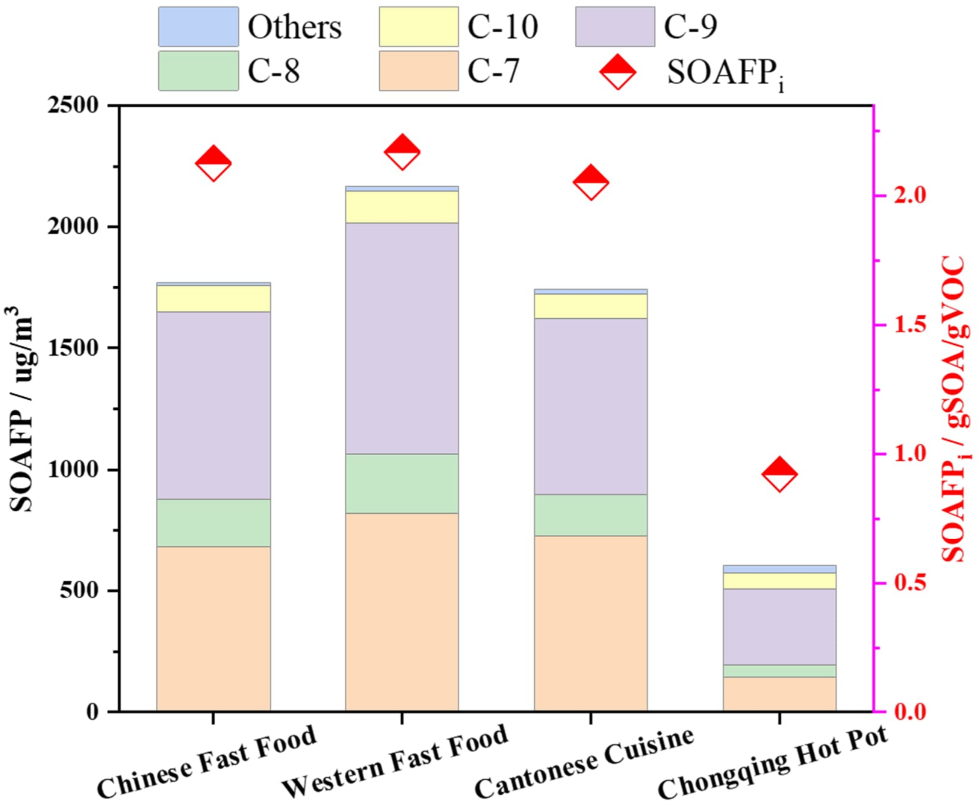

Figure 5-9 Accumulative contributions of VOCs with various carbon numbers to SOAFP and the mass SOAFP (g) generation from 1 g of VOCs in the COFs in different kitchens

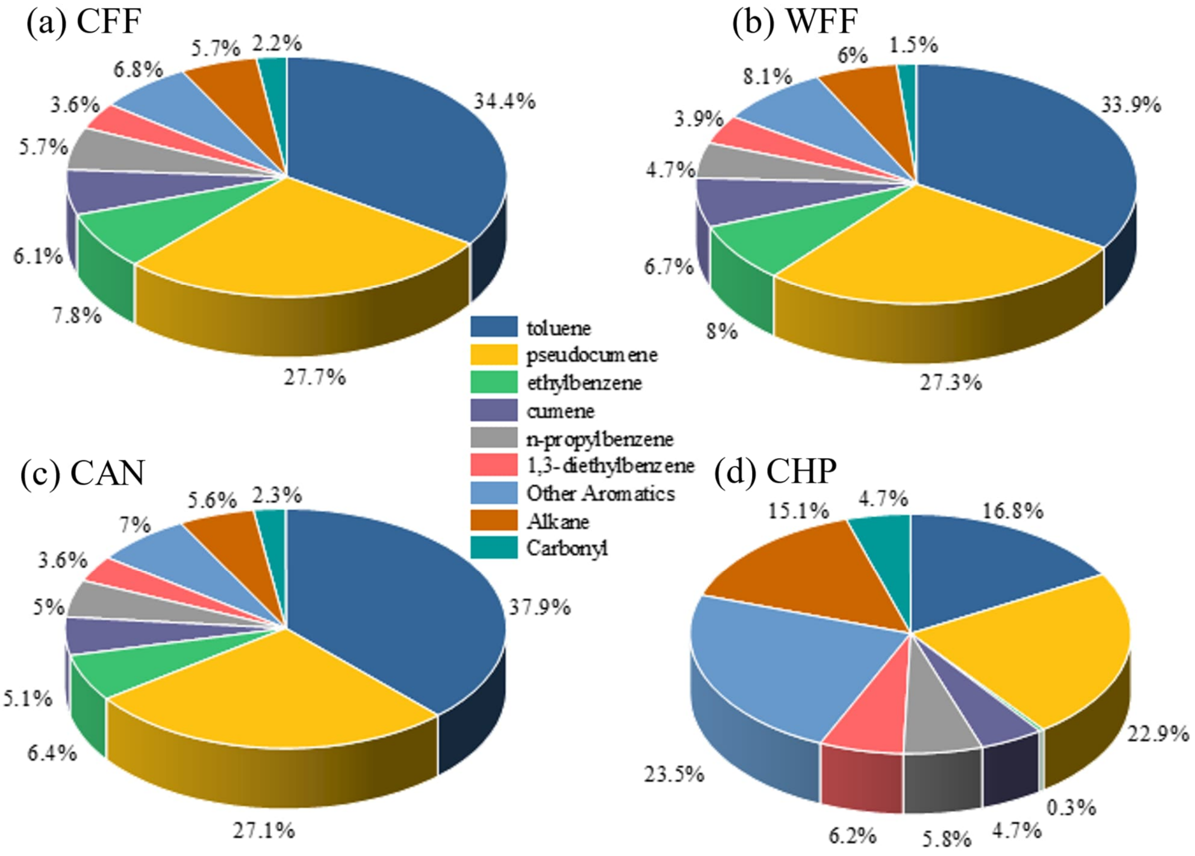

Figure 5-10 Contribution of SOAFP from major VOC species and groups in four different restaurants

5.3.3 Health Risk Assessment of Cooking Oil Fumes

A total of 21 non-carcinogenic chemicals (19 VOCs and 2 PAHs) and 12 carcinogenic chemicals (6 VOCs and 6 PAHs) were sorted out to evaluate the health risks from COFs in the four investigated kitchens to human beings through inhalation exposure. The chronic daily intake and the lifetime hazardous cancer risk are determined by inhalation exposure frequency, duration, and activity patterns based on the nature of exposure. Two common scenarios for kitchen staffs and restaurant customers, respectively, were proposed and the detailed inhalation exposure parameters were listed in Table 5-2. Both the possible carcinogenic effects and potential harmful effects were conducted. As a result, the non-cancer risk was not prominent for both kitchen staffs and customers in all these restaurants, and only 2 toxic chemicals with potential risks were obtained and listed here: acrolein (Staff: CFF: 13.52, WFF: 19.95, CAN: 20.18, CHP: 24.06, Customer: CFF: 2.08, WFF: 3.06, CAN: 3.10, CHP: 37.02) and BaF (Staff: CFF: 1.41, WFF: 0.12, CAN: 1.31, CHP: 0.11, Customer: CFF: 0.22, WFF: 0.02, CAN: 0.20, CHP: 0.16), where only acrolein exhibited the risk for both groups in all these restaurants, while the risk posed by BaF was only observed for staff in WFF and CAN. In addition, the non-carcinogenic risk values (HQ) of all other chemicals were lower than 1 for each group in all scenarios, meaning their insignificant health risks.

Table 5-2 Exposure assumption parameters values for the two scenarios

Parameters (Abbreviation)	Unit	Kitchen Staff	Restaurant Customer
Exposure Time (ET)	h/day	1 (Peak working hour)	2 (Eat and stay 2 hour every time)
Exposure Frequency (EF)	days/year	260 (Assume 5-day work week)	120 (Assume eat once every 3 days)
Exposure Duration (ED)	years	30 (Assume work for 30 years)	50 (Assume visit restaurants for 50 years)
Average Time (AT)	h	613200 (Assume 70-years life)	613200 (Assume 70-years life)
Dilution Factor (DF)	-	1 (No Dilution)	0.2 (Obtained from ratio of TVOC), expect for CHP (DF=1) cooked by customer

On the contrary, the evident severe cancer risks existed in all these investigated scenarios for all restaurants. When the value was higher than the value of 1×10^{-6}, it meant the presence of potential cancer risks. The total cancer risks for kitchen staff in decreasing order were 5.11×10^{-5}, 4.95×10^{-5}, 4.29×10^{-5} and 2.12×10^{-5} in WFF, CAN, CFF and CHP, respectively, the lowest cancer risk from CHP was about half of the highest one from WFF. 1,3-butadiene, naphthalene, formaldehyde, and BaP all exhibited high cancer risk to kitchen staff in all those four restaurants. Most of these toxic chemicals were found to have cancer risks in at least one kind of restaurant. However, when considering the cancer risks to restaurant customers, the total risks were 3.27×10^{-5}, 7.86×10^{-6}, 7.62×10^{-6} and 6.60×10^{-6} in descending order from CHP, WFF, CAN and CFF, respectively. In contrast, the total cancer risk from CHP was recorded as the highest one, which was about 5 times more than the lowest value from CFF. This was because of the special dining method in CFF, where the raw food materials were self-cooked by the customers. In addition, a dilution factor of 0.2 obtained by the differential ratio of TVOC ($TVOC_{kitchen\ area}/TVOC_{dining\ area}$) was applied to other dining scenarios (WFF, CFF and CAN) as the cooking areas were often located inside kitchens and physically isolated from the dining areas. 1,3-butadiene and formaldehyde were still found to have elevated cancer risks for customers in all the restaurants. It could be concluded that the complicated toxic COFs had potential cancer risks in all those restaurants if there was no proper personal protection and not enough ventilation system. As a result, public attention must be drawn to the potentially harmful effects on humans and effective control techniques should be developed to eliminate the COFs emissions from cooking processes as well.

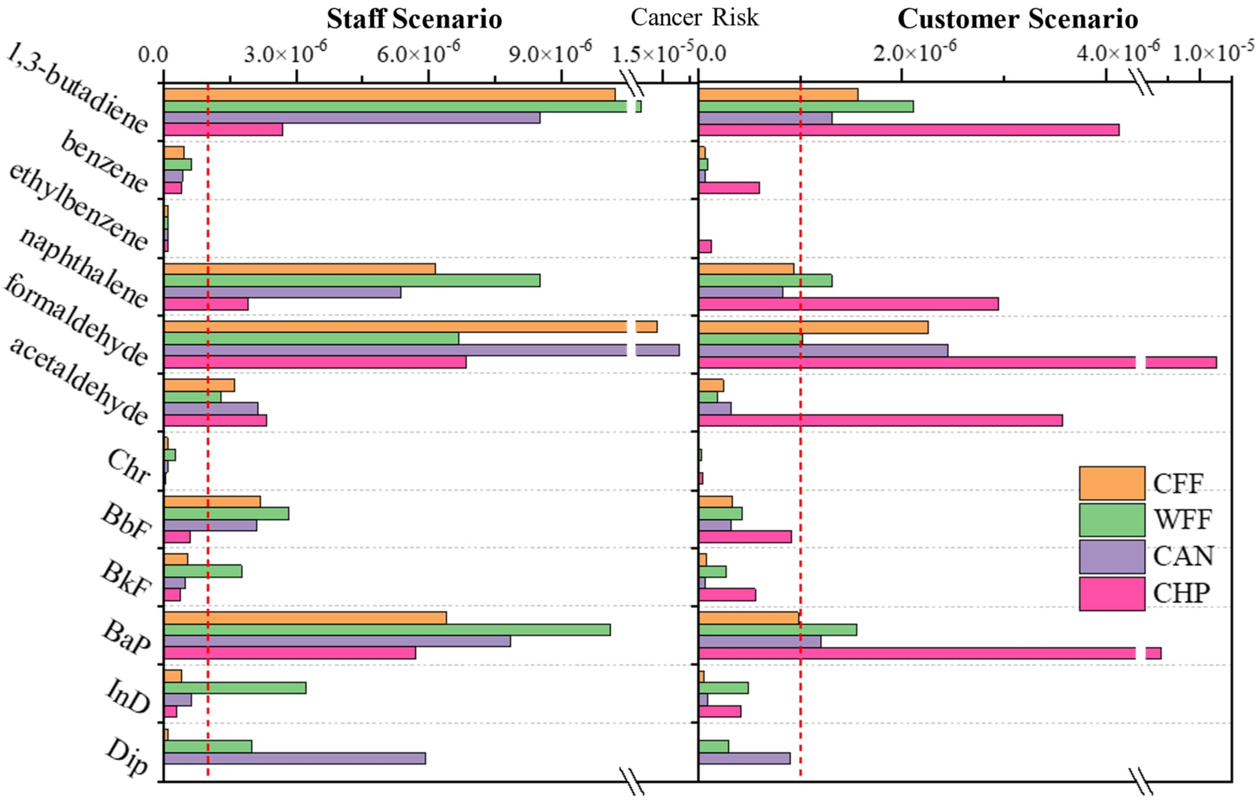

Figure 5-11 The cancer risk values of the 6 VOC species and 6 PAH species detected for the 4 restaurants in two scenarios

5.4 Chapter Summary

Both the chemical characteristics and environment and health impacts of the COFs from four integrated commercial kitchens in Hong Kong were analyzed in detail. The mass concentrations of $PM_{2.5}$ in decreasing order were 269.85 μg/m^3, 232.11 μg/m^3, 199.95 μg/m^3, and 85.69 μg/m^3 for CAN, CFF, WFF, and CHP restaurants, respectively, with the similar ranges of those from cooking methods study. The dominant cooking methods could be confirmed by the ratios of OC/EC and diagnostic analysis of PAH with different molecular weights and rings. The VOC emission levels and composition profiles from commercial kitchens were consistent with their major cooking methods, while hexane, ethylene, and formaldehyde were detected to have significantly high VOC emission levels in COFs from all kitchens. Significant adverse environmental effects on the formation of O_3 and secondary organic aerosol were revealed by the results of their high chemical reactivity, OFP, and SOAFP. The highest unit formation rates for ozone and SOA were obtained from CAN as 5.55 g OFP/g VOCs and WFF as 2.17 g SOAFP/ g VOCs. In addition, significant induvial VOC contribution came from ethylene, formaldehyde and 1,3-butadiene with a total of over 50% contribution to the OFP concentrations, while the largest two contributors for SOAFP were toluene (16.8% - 34.9%) and 1,2,4-trimethylbenzene (22.9% - 27.7%). Health risk assessment by inhalation exposure suggested that significant carcinogenic risks existed to both kitchen staffs and customers if there was no proper personal protection and not enough ventilation system. All these characteristic and evaluation results pointed out the critical pollution situations from commercial kitchens and the necessity in application and development of effective control techniques towards the severe COFs emissions from cooking process.

Chapter 6 Investigation and Application of High Gravity Rotating Packed Bed Scrubber for Control of Cooking Oil Fumes

6.1 Introduction

As HiGee technology has been widely used in different chemical and environmental processes by enhancing and intensifying the mass transfer processes, it has also been developed and applied for air and wastewater pollution control and mostly targets on single pollutant such as NO_X, H_2S, SO_2 and NH_3. These successful applications also demonstrate their outstanding performance, easy operation and other economic or social advantages. HiGee exerts strong force on the liquid surface and improves the mass transfer process by increasing the interfacial areas without selection. It would be considered suitable to deal with various pollutants from complex exhausts simultaneously such as cooking oil fumes, which have been identified as mixed and complicated air pollution containing large amounts of particulate matter and VOCs. In this chapter, the COF removal efficiency driven by the high gravity rotating packed bed scrubber will be thoroughly studied and tested. The optimal working conditions will be determined in the lab-based simulation kitchen. In addition, in order to fully understand its capability and performance, an on-stie efficiency test for $PM_{2.5}$ and VOCs will also be carried out in our selected four different commercial kitchens.

6.2 Study and Optimize the Operation Conditions of High Gravity Rotating Packed Bed Scrubber

Before the HiGee scrubber can be applied to exhausts from real kitchen, the optimal operation conditions with best performance should be explored through lab studies. The concentration of $PM_{2.5}$ was chosen as the indicator to evaluate its purification efficiency due to its critical position in COFs. In addition, in order to reduce the uncertainty and deviations of the cooking emissions, COFs fumes were generated by heating the well mixed corn oil (200 mL) and distilled water (100 mL) on the induction cooker in each test. The $PM_{2.5}$ concentration was measured by TSI DustTrak II Aerosol Monitor (Model 8532), and other environmental parameters were measured by TSI Q-Trak Indoor Air Quality (Model 7575). The $PM_{2.5}$ concentrations at the inlet and outlet of HiGee scrubber will be measured after 10 mins to ensure the stable generation of cooking oil fumes and the smooth operation of purification equipment. And the $PM_{2.5}$ removal efficiency (η) could be calculated by the following Eq 6-1.

$$\text{PM}_{2.5}\text{ removal efficiency }(\eta) = \frac{c_{in} - c_{out}}{c_{in}} \times 100\% \qquad \text{(Eq. 6-1)}$$

Where c_{in} and c_{out} are the $PM_{2.5}$ concentrations at the inlet and outlet of the purification equipment, respectively.

6.2.1 Span/Tween-6 and Effect of its Added Concentration

As analyzed and discussed in Chapter 4 and 5, the COFs consist large amounts of particulate and gaseous organic matters and water-soluble ions, which could not be easily washed away by water-based (hydrophilic) absorbent or oil-based (lipophilic) absorbent only. Considering the co-exist of the hydrophilic and lipophilic pollutants, surfactants are proposed and designed to increase the absorption abilities of both water and oil. In this study, two commercial surfactants Span 80 and Tween 80 are adopted based on the previous study from our research partner for the control of fried-food in Taiwan (C. Y. Liang et al., 2022). Both Span 80 (sorbitan monooleate) and Tween 80 (polyethylene glycol sorbitan monooleate) are nonionic and bio-based surfactants derived from sorbitol and natural fatty acid (oleic acid). They have been widely used as additives in personal care, cosmetic and food industries, due to their low toxicity, high bio-degradable and low foaming level (Chatzidaki et al., 2015; Doshi, Sillanpaa, & Kalliola, 2018; Garti et al., 2005). The hydrophilic-lipophilic balance (HLB) value of Span 80 and Tween 80 are 4.3 and 15, respectively, and the HLB value of the mixed Span 80 and Tween 80 could be calculated by Eq. 6-2. The optimal HLB for HiGee COFs scrubber was examined by the emulsion contents by adding cooking oil into water containing surfactant mixtures with different HLB values (C. Y. Liang et al., 2022). When the HLB was 6, i.e., mixture with 76.9% of Span 80 and 23.1% of Tween 80, the least oil content layer could be identified in the mixture, indicating its best adsorption capability.

$$HLB\ (surfactant\ mixture) = \frac{4.3 \times M_{Span80} + 15 \times M_{Tween80}}{M_{Span80} + M_{Tween80}} \qquad \text{(Eq. 6-2)}$$

Where M_{Span80} is the weight of Span 80 and $M_{Tween80}$ represents the weight of Tween 80 in the surfactant mixture.

In a mixed Span 80/Tween 80 emulsion system, the Span 80 molecules have fatty acyl chains and a larger hydrophobic area per molecule, allowing the monolayer film to better accommodate oily droplets at the air-water interface. The nonionic hydrophilic surfactant Tween 80, an ethoxylated derivative of Span 80, improves the water hydrogen-bond networks that are weak in Span 80. While Span 80 molecules form a dense and narrow peak in hydrogen-bond density, Tween 80 has a wider and dispersed hydrogen-bond network, improving interactions with other molecules in the system (Kopanichuk et al., 2018). In the formation of micelles, Span 80 molecules are primarily located on the micelle surface, while Tween 80 headgroups form a stable network with water inside the micelles. These properties explain why the mixed Span 80/Tween 80 system has advantages over using a single surfactant. The developed Span 80/Tween 80 surfactant mixture with HLB of 6 is named as ST-6 and will be applied for future tests.

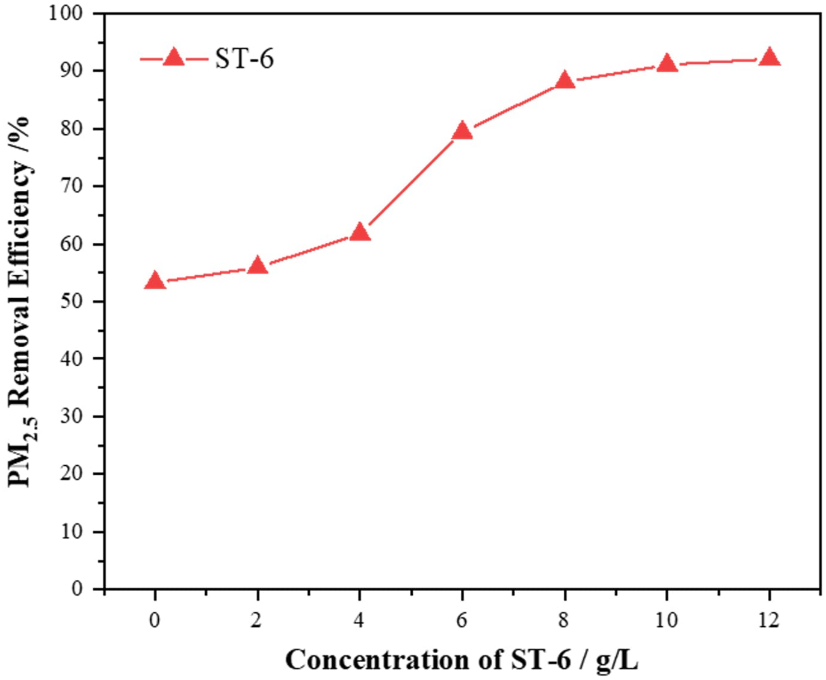

Figure 6-1 Effect of different concentrations of ST-6 absorbent in water on $PM_{2.5}$ removal efficiency

The $PM_{2.5}$ removal efficiency test was conducted to investigate the best dosage for ST-6 as the surfactant for COF purification. The concentrations of ST-6-water mixed surfactant were adjusted from 0-12 g/L. As shown in Fig. 6-1, the $PM_{2.5}$ removal efficiency increased significantly from around 50% to over 90%, as the ST-6 surfactant was added gradually. When the concentration of ST-6 was below 4 g/L, the removal efficiency did not show clear increase. This was because that the added ST-6 did not reach the critical micelle concentration (CMC), where the surfactant molecules were integrated loosely into the water structure and no thermodynamically stable micelles were formed. While the noticeable rise was identified in the concentration range of 4-8 g/L, and the removal efficiency could reach to around 90% with the concentration of 8 g/L. Although the removal efficiency kept rising when more ST-6 was added, the slight increase could be neglected. In addition, when the ST-6 concentration was over 8 g/L, mild grease scent and higher foam layer were observed in the liquid tank, which negatively impacted the adsorption capability and efficiency of the mass transfer process. Furthermore, in considering the operation cost of adding ST-6 surfactant, the ST-6 concentration of 8 g/L could achieve the balance of both economy and efficiency. Therefore. ST-6 concentration of 8 g/L was selected as the optimal liquid condition for COF purification.

6.2.2 Effect of Different Added Liquid Absorbents

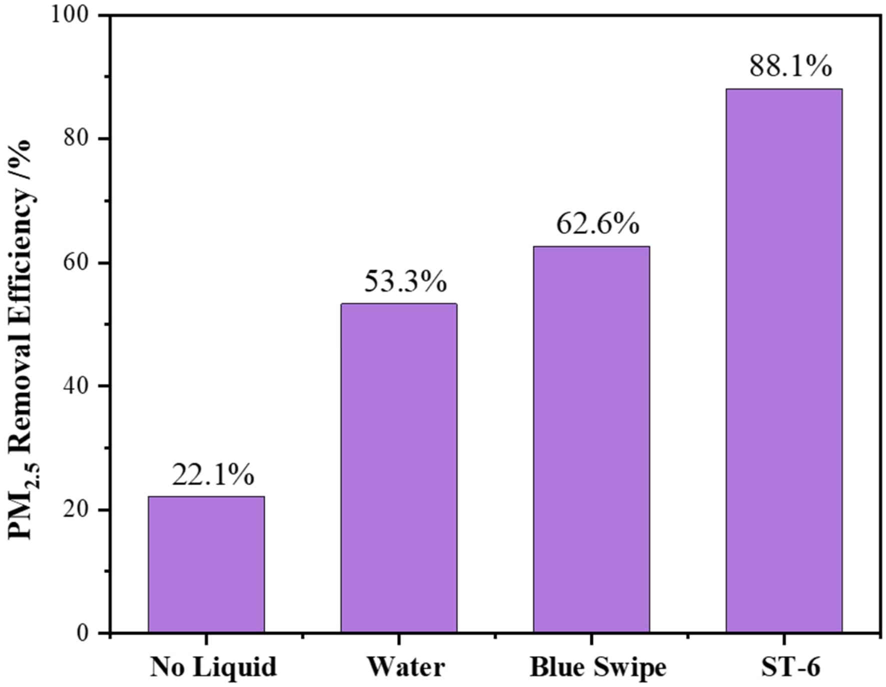

Figure 6-2 Effect of different added liquid absorbents on $PM_{2.5}$ removal efficiency

The purification efficiency of the selected surfactant ST-6 and other cleaning products from the market will be investigated. Blue Swipe (BS) is selected as the targeted liquid absorbent, which has the active ingredients of anionic surfactants alkylbenzene sulfonates and is wildly used to handle with oil and grease cleaning work in Hong Kong. As shown in Fig. 6-2, the highest removal efficiency was achieved by ST-6 with the removal efficiency of 88.1%, while Blue Swipe also demonstrated an enhanced ability of 20% more than that of water in trapping particulate matters. Both ST-6 and BS are surfactants, which increase the contact between the air and the liquid surface by decreasing the tension on the water surface (Zhou & Qin, 2021). At the same time, the empty machine without liquid added was also tested, and the removal rate of 22.1% was observed, which is due to the direct impact between the air flue and inside packed bed rotator and air ducts. ST-6 was confirmed to have highest purification rate and was suitable for future application in the control of COFs.

6.2.3 Effect of the Gas-Liquid Ratio

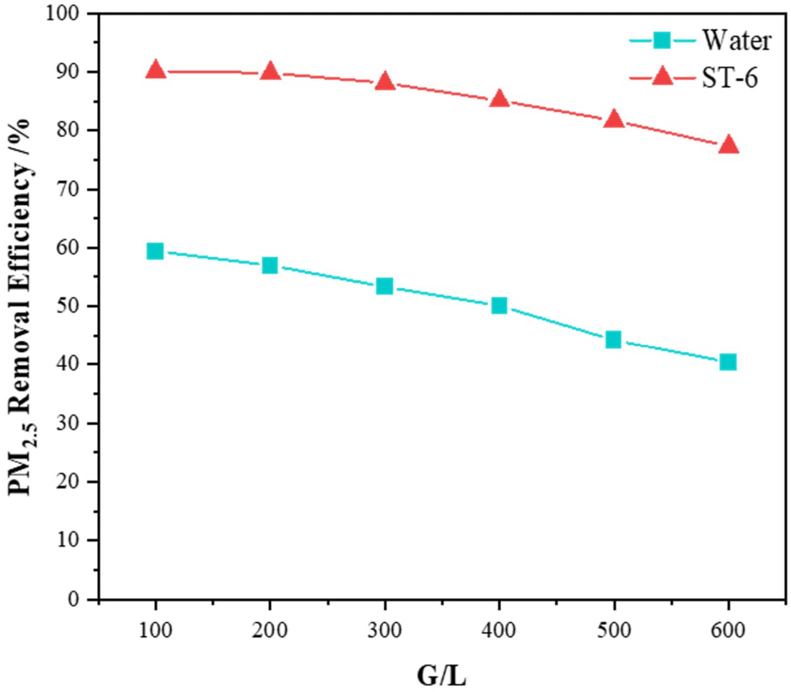

Figure 6-3 Effect of gas-liquid ratios on $PM_{2.5}$ removal efficiency by water and ST-6 absorbents

The gas-liquid ratio is determined by the total air flow rate and water circulation rate. Normally, the water circulation rate is fixed due to the operation requirement for droplets being uniformly sprayed from the central nozzle (Rao, 2022). Thus, it would be practical to consider the adjustment of the flow rate at the air side, which would directly affect the capacity and volumes for COF treatment as well as the running cost. The removal efficiencies under different G/L ratios with water and ST-6 as absorbents are displayed in Fig 6-3. As the G/L value increased from 100 to 600, the $PM_{2.5}$ removal efficiency decreased for both water absorbent and ST-6 surfactants. When the air flow rate increases, the surface renewal rate will increase which helps to enhance the mass transfer coefficient in gas phase. At the same time, disturbance may happen in the gas phase to improve the capture of pollutants in flue gas. Although both factors may promote the removal efficiency of $PM_{2.5}$ to some extent, the actual efficiency shows a definite decrease. This is because the increased gas flow rate reduces the gas retention time inside the packed bed which is not benefit to the mass transfer processes. Furthermore, higher G/L ratio means lower liquid amounts and higher liquid absorption concentrations in the packed bed, further reducing the capture probability. The latter two negative factors will be more influential than these positive factors in the actual results.

When it comes to the operation conditions for real applications, many other factors should be considered such as air handling capacity, running cost and so on. From the lab test and analysis, lower G/L values will lead to higher PM removal efficiency. And as shown in Fig. 6-3, when the G/L value increases to above 400, the efficiency shows an apparent decrease for both absorbents. Hence, it is suggested that the G/L ratio of 300 will be adopted for future study and application.

6.2.4 Effect of the Rotating Speed

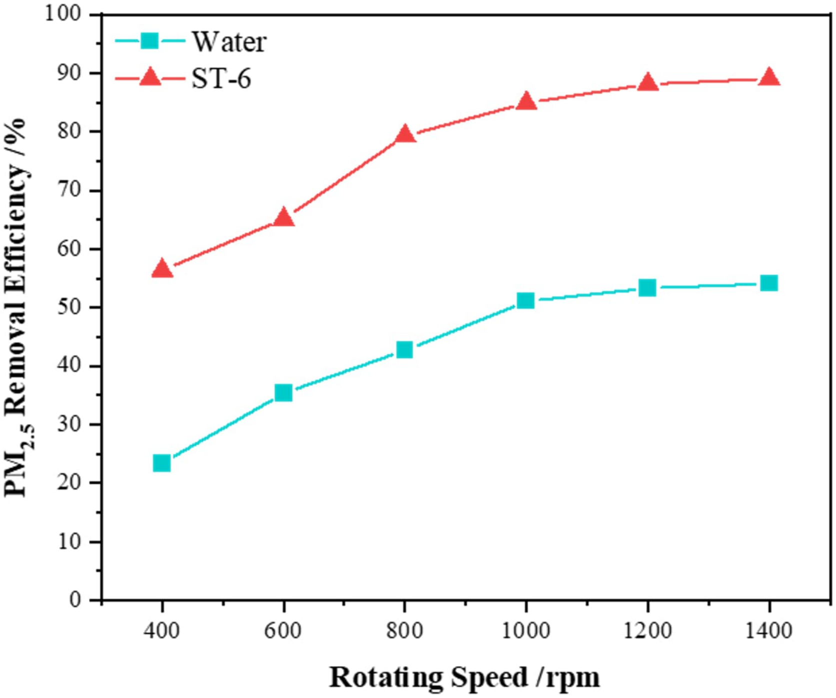

Figure 6-4 Effect of rotating speeds of packed bed on $PM_{2.5}$ removal efficiency by water and ST-6 absorbents

Rotating speed of the packed bed is the key factor to the strength of the generated gravity field represented by the high gravity factor (β), which is a dimensionless parameter that represents the ratio of centrifugal acceleration to gravitational acceleration at any point within a high gravity field (Duan et al., 2021). The relationship between the rotational speed and high gravity factor is shown in the below Eq. 6-3.

$$High\ gravity\ factor\ (\beta) = \frac{\omega^2 r}{g} \qquad \text{(Eq. 6-3)}$$

Where ω is the rotational speed, s^{-1}, r is the radius, m, and g is the gravitational acceleration (i.e., 9.8 m/s^2). The rotating speed is adjusted from 400 rpm to 1400 rpm and the results were demonstrated in Fig 6-4. The $PM_{2.5}$ removal efficiency became higher with the increase of rotational speed. When the rotating speed increased from 200 rpm to 1200 rpm, the removal efficiency by ST-6 promoted significantly from 56% to 90%, and the increase trend was similar for the situation of using water as absorbent. When the rotating speed was higher than 1,000 rpm, the variation of $PM_{2.5}$ removal efficiency became relatively stable and kept above 85% for ST-6 surfactant. It can be concluded from the experimental results that the removal efficiency is positively correlated to the rotating speed. The main reason for the improvement of mass transfer process is that the inner liquid is driven by the centrifugal force induced by the high-speed rotation of packed bed and will be cut and broken up by the filaments of the packed bed into droplets and liquid films. When the rotation speed increases, the size of the droplets becomes smaller and the liquid film becomes thinner, which will enlarge the contact surface areas between liquid and gas phases making the pollutants in gas phase to be captured by these liquid microelements easily. In addition, the increased rotating speed will pose greater acceleration onto the liquid droplets. The relative speed between the accelerated droplets and particles will become large and further lead to the increase of Stoke drag force on particulate matters (Darbandi, Risberg, & Westerlund, 2021), which contributes to the improvement of the removal efficiency. On the other side, the increased rotational speed would reduce the liquid retention time inside the packed bed and further shorten the contact time between liquid and gas pollutants. This adverse factor may offset the improvement from these positive elements, which makes the efficiency promotion inconspicuous when the rotating speed is above 1,000 rpm.

As for the HiGee real application in kitchens, other relevant issues should also be considered including safety issues, vibration, and long-term satiability. During our in-lab experiment, slight vibration and noise were found from the RBP equipment when the rotating speed is over 1,200 rpm. In addition, a large number of bubbles and abnormal foaming issues from the absorbent liquid could be detected when the speed exceeded 1,400 rpm. In considering the test results and different operation conditions, the rotational speed of 1,200 rpm is suggested to be applied in the pilot test with acceptable efficiency and stable operation state.

6.2.5 Effect of the Oil Boiling Temperature

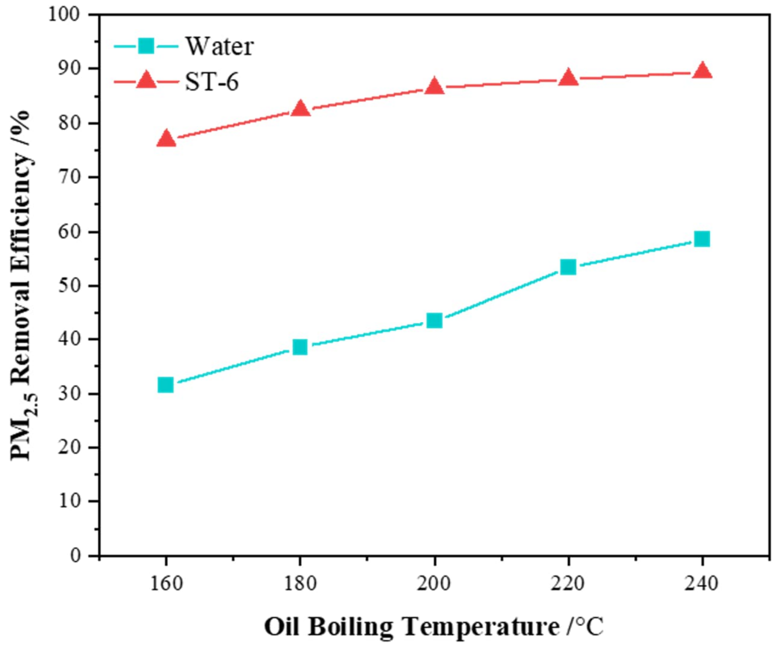

Figure 6-5 Effect of oil boiling temperatures on $PM_{2.5}$ removal efficiency by water and ST-6 absorbents

The high gravity rotating packed bed is designed to tackle the different cooking scenarios, and it is necessary to know its performance with different cooking temperatures. Fig. 6-5 demonstrates the variation of $PM_{2.5}$ removal efficiencies under different oil boiling temperatures ranging from 160 °C to 240 °C through in-lab simulation tests, and the efficiencies of water absorbent and ST-6 surfactant show the positive relationship with boiling temperature. The highest efficiencies for water and ST-6 were recorded at the oil boiling temperature of 240 °C, which were 58.5% and 89.4%, respectively. The main reason for the variation of the removal efficiency is due to the different generated concentrations of particulate matters under different temperatures. When the temperature is low, less PM pollutants will be produced from the cooking source. Hence, the impacts and capture processes inside the packed bed will be less and the efficiency will be reduced, and vice versa. In addition, both heat transfer and mass transfer will happen simultaneously (Bao et al., 2013), when the high-temperature gas enters the RPB system. This means that the inlet gas will contact the liquid with lower temperature, which will cause liquid evaporation and lead to the increase of moisture contents in gas phase. These water vapors will become small droplets and then condense with dust in gas phase to form larger particles. The newly formed large particles are inclined to settle and are easily captured by liquid phase, which in turn helps to promote the $PM_{2.5}$ removal efficiency. In conclusion, the removal efficiency does not change significantly with temperature, but it still shows good performance especially for the gas flue with higher temperature. These features further confirm the promising application of HiGee technology in control and elimination of cooking oil fumes.

6.2.6 Effect of ST-6 Changing Mode for Long-term Operation

In addition to the high COFs purification efficiency in a single test by the HiGee RPB scrubber, a long-term operation test has been carried out to study the operation mode and durability of ST-6 surfactant in real applications as well. In this experiment, a total of 3 L of the ST-6 solutions were filled into the container as the initial liquid absorbent. Two changing modes were set for this simulation test, one was no change of the liquid during the whole test period with only addition of water if the liquid level fell below 3 L, which was denoted as no change. While the other mode was to replace half of the used liquid (1.5 L) with the same amount of new ST-6 solutions every day before the test (denoted as ST-6 + ST-6). Considering the operation time in the commercial kitchens, the in-lab cooking emissions were generated by oil boiling for a consecutive of three hours every day, and the scrubber was turned on during the whole cooking period.

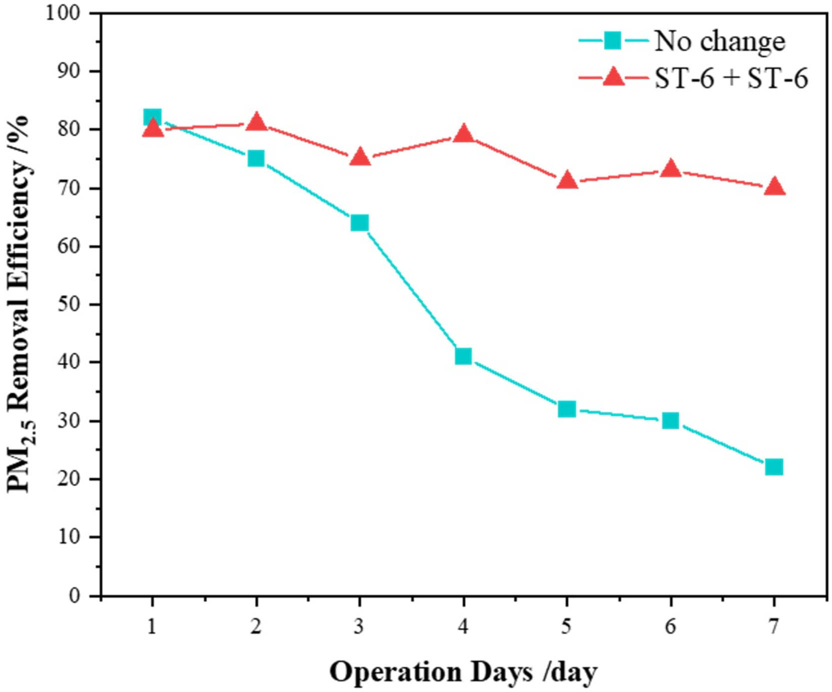

Figure 6-6 Effect of ST-6 changing mode on the 7-day $PM_{2.5}$ removal efficiency

The long-term $PM_{2.5}$ removal efficiencies under two different changing modes of the liquid absorbent are shown in Fig. 6-6. The absolute decrease of the removal efficiency was observed for the case without changing ST-6, where only a few efficiency declines happened in the first three days. However, a sharp efficiency drop occurred in the 4th day of operation with the purification efficiency below 40%, meaning the saturation of the ST-6 liquid. After that the efficiency became lower to around 20% with rare absorption abilities, which was even lower than that by using water only. For the half-half changing mode, although a slight decrease was seen between each testing day, the final removal efficiency still remained higher than 70%, which maintained enough activity in handling $PM_{2.5}$ pollutants. This experiment result suggested the consistent purification performance and the durability of the ST-6 surfactant for control of COFs emissions. In addition, an alternative liquid absorbent changing mode could be proposed on a weekly basis to reduce the usage and cost of the surfactant.

6.3 Field Trails of High Gravity Rotating Packed Bed Scrubber

The investigated optimal operation parameters (i.e., liquid flow rate of 36 L/h, gas flow rate of 180 L/min, G/L ratio of 300, rotational speed of 1200 rpm) with 3 L of 8 g/L ST-6 absorbent liquid were adopted for field trails of the HiGee RPB scrubber in commercial restaurants. The absorbent liquid was prepared and blended right before the commencement of each test to avoid pollution and stratification, and the liquid was completely replaced after each experiment. The removal efficiency of $PM_{2.5}$ and VOCs were evaluated and detailed improvements of environmental impacts were also assessed in the following sections.

6.3.1 Removal of Particulate Pollutants

As shown in Fig. 6-7, the mass concentrations of the scrubber-controlled emissions all demonstrated significant declines compared with the direct COFs emissions from cooking processes. The final reduced $PM_{2.5}$ concentrations were 31.03 $\mu g/m^3$, 33.78 $\mu g/m^3$, 38.96 $\mu g/m^3$ and 29.54 $\mu g/m^3$ for CFF, WFF, CAN and CHP, respectively, which basically met the $PM_{2.5}$ standard of 35 $\mu g/m^3$ set by the National Ambient Air Quality Standards (NAAQS) (USEPA, 2023) from environmental protection agency of the United States

(USEPA). The $PM_{2.5}$ removal efficiencies were observed to have outstanding values ranging from 80% to 86% in all these kitchens even in CHP with its original lower emissions concentrations, indicating its high purification efficiency with non-selective removal on particulate matters. The total $PM_{2.5}$ removal by the HiGee scrubber demonstrated superior performance compared to other studies, where COFs removal efficiencies was 73.8 – 90.2% by a traditional wet scrubber with large areas occupied reported by Zhao et al. (2021). In addition, Cho et al. (2020) reported an in-lab study by using wet scrubber, which had very similar results of 89% removal of $PM_{1-2.5}$ and 99.7% removal of PM over 2.5 μm, further confirming the effectiveness of COFs control by wet scrubber system.

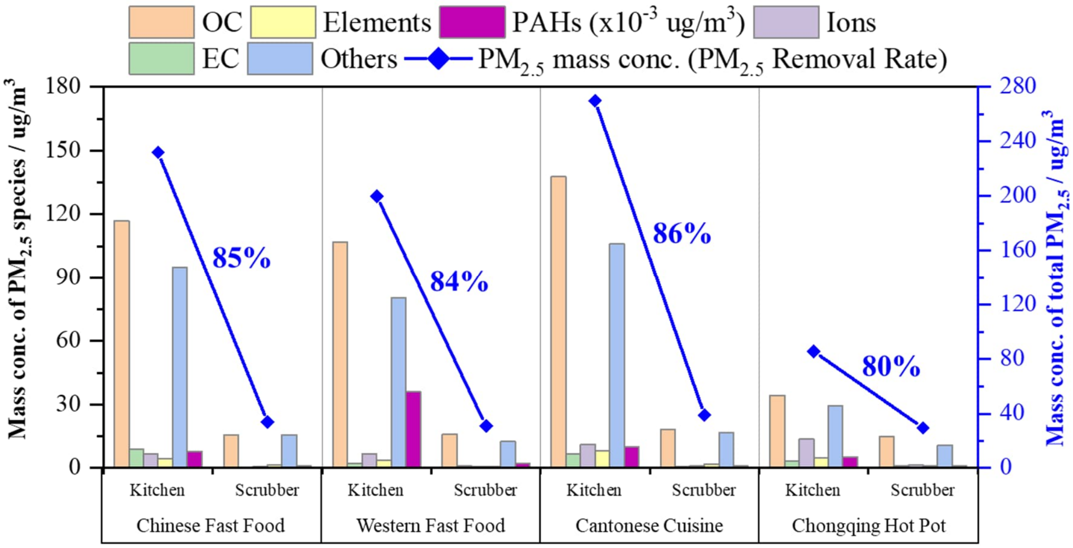

Figure 6-7 Mass concentrations of $PM_{2.5}$-bound species and $PM_{2.5}$ mass concentration and removal rates of COF emissions and scrubber-controlled emissions in four kitchens

The detailed and averaged removal efficiencies of the specific compounds were listed in Table 6-1, the removal of ions ranked 1st place with the average removal rate of 89.03%, as water-soluble ions were quickly dissolved in water-surfactant scrubbing liquid and easily washed away (Hsieh et al., 2011). While the removal of PAHs ranked the second place with an averaged removal rate of 87.28%, which was due to their organic property that was soluble in surfactant treated water and also due to their higher molecular weights which tended to be captured by the stretched water surface (Ali, Plaza, & Mann, 2018). However, elements showed a relatively low removal rate of 76.83%, because of their low molecular weight, small in size and no solubility in water. All these removal results demonstrated its purification capability in handling the $PM_{2.5}$ from COFs and exhibited promising prospect in future application.

6.3.2 Removal of Gaseous Pollutants and Improvement of Environment Impacts

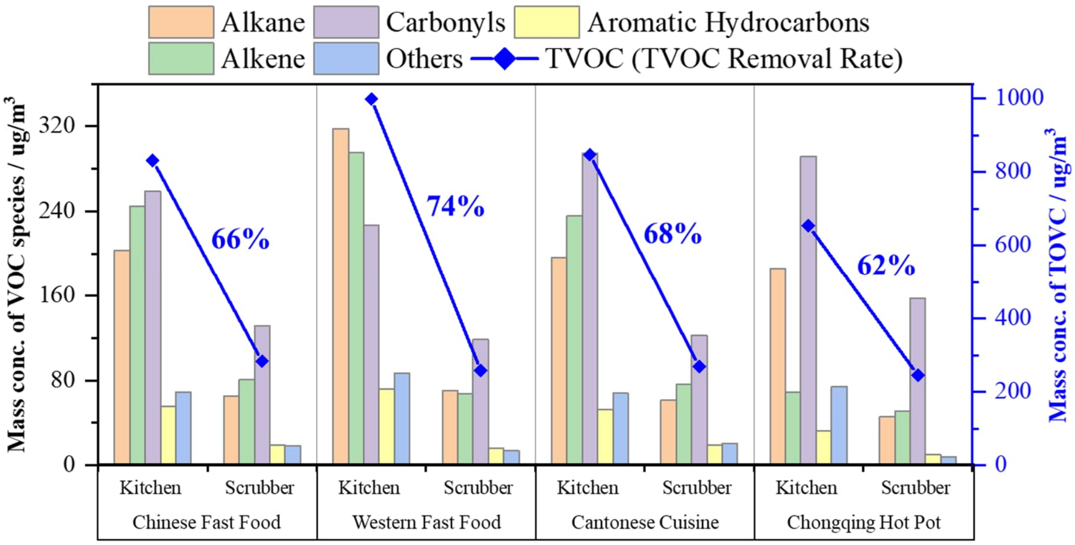

Figure 6-8 Mass concentrations of VOC species and TVOC mass concentrations and removal rates from COF emissions and scrubber-controlled emissions in four kitchens

Fig. 6-8 shows the mass concentrations of the scrubber-controlled emissions and the TVOC purification rates for all the four investigated commercial kitchens. The TVOC showed the clear decline rates of 66%, 74%, 68% and 62% for CFF, WFF, CAN and CHP, respectively, which was lower than the removal rates of $PM_{2.5}$. All the VOC species from the COFs showed evident reductions ranging from 50.23% to 79.10%, where alkanes demonstrated the highest removal rate of 72.45%, due to their higher emission concentrations. And higher VOC removal efficiencies were found from the cooking scenarios with higher initial VOC concentrations. This was because of the limitation of the performance of ST-6 absorbents with the final exhaust VOC concentrations around 200 $\mu g/m^3$ in spite of their initial concentrations. In addition, higher removal efficiencies were observed from those VOC species with higher molecular weights, which was because that these VOC species might receive higher capture power due to their enhanced centrifugal force on the rotating packed bed. While for those VOCs with smaller and lighter molecules, the probability for liquid capture would become lower, which lead to decrease in their removal efficiency by HiGee scrubber compared with $PM_{2.5}$ in particle phase and VOCs with higher molecular weight. The working principle of HiGee RPB scrubber was wet adsorption and washing with enhanced mass transfer (C. Y. Liang et al., 2022), which would not produce any additional by-product pollutants. Unlike some other COF control methods including electrostatic precipitator, ultraviolet (UV) light, which could even increase the final VOC concentrations as they decomposed some large organic compounds or VOCs large carbon numbers to small VOC species (He et al., 2020; H. Zhang et al., 2023). By comparing the VOCs removal rates with other reported studies with the rates of only 14% - 23% (Tao et al., 2023) and 29% - 54.4% (H. Zhang et al., 2023), let alone those situations with increased VOCs concentrations (He et al., 2020), our investigated HiGee RPB scrubber system coupled with ST-6 surfactant absorbent could provide ideal purification for VOCs in COFs, especially for those alkane and other VOCs with higher molecular weights.

As some of VOCs were not completed removed after the HiGee scrubber system, the environment impacts caused by the excessive emission of VOCs from cooking processes were also reassessed As listed in Table 6-1, the average decrease rates of the L_{OH}, OFP and SOAFP were 62.95%, 60.35%, and 61.05%, respectively, which was consistent with the removal rates of VOCs after the COFs was controlled by application of HiGee RPB scrubber. The highest reducing rates of over 70% were all observed from the WFF as it had the highest VOCs emission concentrations. The improvement of the environmental impacts confirmed the necessity in application of air purification system with effective VOC control. The simultaneous purification of particulate matters and gaseous pollutants in the trail test verified the capability of the all-in-one scrubber, which could be applied for the control of COF emissions. In addition, due to the remaining VOCs after the HiGee system, advanced technologies such as photocatalytic oxidation degradation for control of VOCs with lower molecular weight and higher environment and health impacts including formaldehyde, 1,3-butadiene should be taken into consideration for further development and integration.

Table 6-1 Reducing Rates of Chemicals and Impacts by the HiGee RPB Scrubber in four studies kitchens

Chemical Species or Impacts	HiGee RPB Scrubber Reducing Rate				
	CFF	WFF	CAN	CHP	Average
			Particulate Pollutants		
$PM_{2.5}$	86.6 ± 4.4%	83.1 ± 4.4%	85.6 ± 7.2%	65.5 ± 5.5%	80.2 ± 5.4%
OC	86.8 ± 7.1%	85.1 ± 7.0%	86.6 ± 7.3%	56.3 ± 3.7%	78.7 ± 6.3%
EC	86.5 ± 8.0%	85.5 ± 6.8%	87.4 ± 7.8%	66.8 ± 3.9%	81.6 ± 6.6%
Ions	88.9 ± 5.0%	87.8 ± 7.4%	90.5 ± 7.7%	88.9 ± 6.4%	89.0 ± 6.6%
Elements	66.7 ± 5.1%	84.5 ± 6.0%	78.4 ± 5.7%	77.7 ± 5.2%	76.8 ± 5.5%
PAHs	86.4 ± 6.3%	94.1 ± 6.8%	88.9 ± 8.6%	79.7 ± 5.6%	87.3 ± 6.8%
			Gaseous Pollutants		
TVOC	62.1 ± 4.9%	71.3 ± 3.7%	64.6 ± 6.2%	58.3 ± 3.4%	64.1 ± 4.6%
Alkane	67.9 ± 4.5%	77.8 ± 4.2%	68.8 ± 6.7%	75.3 ± 4.8%	72.5 ± 5.1%
Alkene	67.0 ± 4.0%	77.1 ± 6.6%	67.6 ± 6.1%	26.2 ± 1.6%	59.5 ± 4.6%
Aromatics	66.5 ± 6.2%	77.8 ± 6.7%	63.6 ± 3.7%	69.7 ± 6.8%	69.4 ± 5.9%
Carbonyls	49.1 ± 4.3%	47.5 ± 3.0%	58.4 ± 5.8%	45.9 ± 4.4%	50.2 ± 4.4%
Other VOC	72.9 ± 6.6%	84.2 ± 5.8%	70.2 ± 3.9%	89.1 ± 5.4%	79.1 ± 5.4%
			Environment Impacts		
L_{OH}	65.8 ± 5.6%	75.3 ± 6.5%	66.0 ± 4.9%	44.7 ± 3.0%	63.0 ± 5.0%
OFP	61.5 ± 4.0%	70.4 ± 6.1%	64.1 ± 3.2%	45.4 ± 4.3%	60.4 ± 4.4%
SOAFP	65.6 ± 4.9%	76.3 ± 5.6%	66.8 ± 5.0%	35.5 ± 2.6%	61.1 ± 4.5%

6.4 Chapter Summary

The selected high gravity rotating packed bed scrubber was tested and developed for the application of COFs control. The developed surfactant made by the mixture of span 80 and Tween 80 were proved to be effective in removing $PM_{2.5}$ and VOC pollutants with the mixed concentration of 8 g/L. Besides, the detailed operation conditions including air flow rate, rotating speed and long-term operation mode were further investigated. The surfactant together with the optimal operation parameter obtained by the in-lab simulation tests were used to conduct the trail test to evaluate the real removal efficiency in these four investigated kitchens. The $PM_{2.5}$ removal efficiency could reach as high as 86%, while the rate of 74% in TVOC removal could be achieved. Due to the non-selective operation theories, all these chemical species in $PM_{2.5}$ and VOCs exhibited effective removal efficiency. Removal efficiencies of $PM_{2.5}$ were kept at high levels with over 80% for all these restaurants, while higher VOCs removal efficiencies were observed from those scenarios with higher initial VOCs concentrations. Besides, VOCs with higher molecular weight exhibited increased removal efficiencies in HiGee scrubber, due to the enhanced liquid capture with higher centrifugal force compared with lighter VOCs. In addition, the evaluation results of environmental impacts including L_{OH}, OFP and SOAFP all exhibited superior improvement of 62.95%, 60.35%, and 61.05%, respectively, suggesting its effectiveness in control of the COF emissions especially for $PM_{2.5}$ and those VOCs with higher molecular weights from real cooking processes and promising application abilities in food industries.

Chapter 7 Development of Functional Nanomaterials for Degradation of Typical Gaseous Pollutants from COFs

7.1 Introduction

The developed HiGee rotating packed bed scrubber could remove most of the $PM_{2.5}$ pollutants and large amounts of VOCs from the COFs in real kitchen trials as discussed in Chapter 6. However, some typical gaseous VOCs pollutants which have critical environment and health impact even at low concentrations such as formaldehyde and water-insoluble trace gases which has lower removal efficiency in HiGee scrubber system such as nitrogen oxide still need to be taken seriously. In order to further enhance the gaseous purification effects of COFs, novel nanomaterial composite for photocatalytic degradation of gaseous pollutants has been developed, and the photocatalytic system can be operated in series after the HiGee scrubber system. In this chapter, the detailed development works from design and characterization of photocatalyst to activity evaluation and degradation mechanism are introduced.

7.2 Synthesis and Characterization of $SrTiO_3/SrCO_3$ Heterojunction Nanomaterials

7.2.1 Synthesis of $SrTiO_3/SrCO_3$ Composites

g-C_3N_4 (CN) was synthesized through the pyrolysis method by using an analytical grade urea. In a general process, a total of 10 g of urea and 30 mL of deionized water were placed in a crucible and stirred evenly. The sample is oven-dried at 60 °C, and then heated at 550 °C in a muffle furnace for 2 h. Subsequently, the obtained light yellow powder CN sample was grounded and properly stored for future use.

$SrTiO_3/SrCO_3$ composites (STO/SCO for short) were synthesized through the hydroxide-mediated hydrothermal method. Normally, 0.30 mL of tetrabutyl titanate ($C_{16}H_{36}O_4Ti$, Aladdin Co., ltd, Chemical Grade, China) was added to 25 mL of absolute ethyl alcohol (C_2H_5OH, Analytical Grade, Sinopharm Chemical Reagent Co., Ltd, China). Then, a semi-transparent light-white solution was obtained by continuous mixing using a magnetic stirrer. 1 mmol of strontium nitrate ($Sr(NO_3)_2$, Analytical Grade, Sinopharm Chemical Reagent Co., Ltd, China) was added to the mixed liquid with persistent stirring. Subsequently, a total of 10 mL of 0.4 $mol \cdot L^{-1}$ sodium hydroxide (NaOH, Analytical Grade, Sinopharm Chemical Reagent Co., Ltd, China) solution was mixed into the liquid with continuous stirring for 30 mins. Afterwards, 0.018 g of prepared CN powder sample was added with continuous stirring for another 60 mins. Then, the mixture was transferred and sealed into a 100 mL Teflon-lined autoclave to be heated at 160 °C for 24 hours. After cooling down to room temperature, the synthesized $SrTiO_3/SrCO_3$ heterojunction (denoted as STO/SCO-1) was obtained after rinsing with absolute ethanol and water thrice. STO/SCO composites with different CN weight ratios (denoted as STO/SCO-2, STO/SCO-3) were fabricated by changing the added weights of CN (0.046 g and 0.092 g), respectively. The pure $SrTiO_3$ (STO) sample was also prepared by following the same process without adding CN. The pure $SrCO_3$ (SCO) of analytical grade was purchased from Aladdin. Fig. 7-1 shows the schematic illustration of the synthesis processes of STO/SCO heterojunctions.

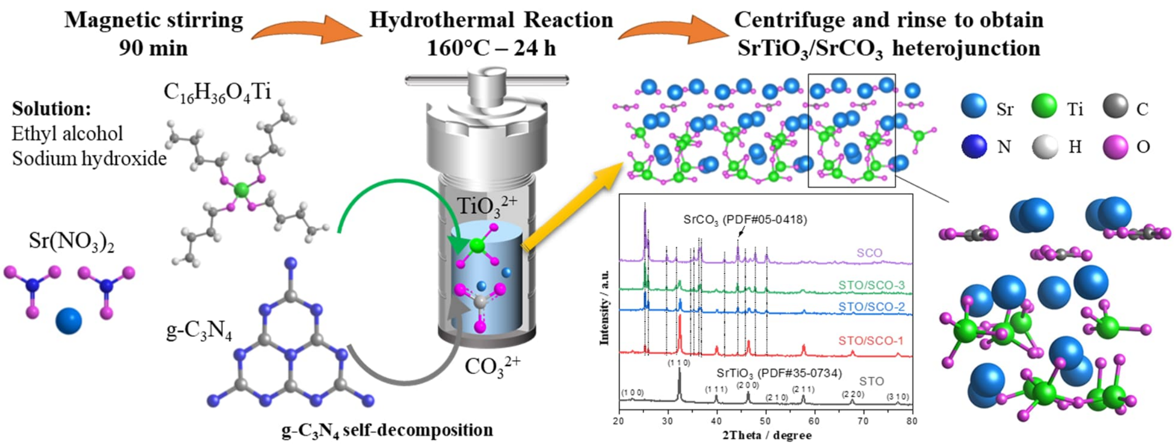

Figure 7-1 Schematic illustration of the synthesis processes of STO/SCO heterojunctions

7.2.2 Structural Characterization of $SrTiO_3/SrCO_3$ nanoparticles

The phase compositions of synthesized STO, STO/SCO - 1, 2, 3, and SCO samples were characterized by X-ray diffraction (XRD). Fig. 7-2 shows the XRD pattern of STO that matches well with the standard $SrTiO_3$ (PDF#35 – 0734) and no other diffraction peak is detected, indicating the pristine $SrTiO_3$ structure of the STO sample. The diffraction peaks of $SrTiO_3$ are also detected in synthesized STO/SCO-1,2,3 heterojunction samples. Another group of distinct peaks at 25.2°, 25.8°, 29.6°, 31.3°, 34.5°, 35.1°, 36.2°, 36.5°, 41.3°, 44.1°, 45.6°, 47.7° and 49.9°, which could be indicated to the (1 1 1), (0 2 1), (0 0 2), (1 2 1), (1 0 2), (2 0 0), (1 1 2), (1 3 0), (2 2 0), (2 2 1), (0 4 1), (1 3 2) and (1 1 3) crystal planes of orthorhombic $SrCO_3$ (PDF#05 – 0418), are indexed respectively. The two crystal groups of STO and SCO in STO/SCO samples are independent phases without any position shift of diffraction peaks, suggesting that there was no lattice distortion occurred. With the increasing addition contents of CN, the XRD patterns of $SrCO_3$ become prominent in STO/SCO heterojunctions. Further XRD phase quantitative analysis (Degen et al., 2014) results of STO/SCO-1,2,3 samples shown in Table 7-1 demonstrate that 71.5% contents of SCO are found in STO/SCO-3 sample based on XRD Rietveld refinement (O'Donnell et al., 2008; Wang et al., 1999). It was followed by STO/SCO-2 and STO/SCO-1 samples with 66.7% and 17.3% contents of SCO, respectively. The weight ratio of SCO is positively related to the additional contents of CN.

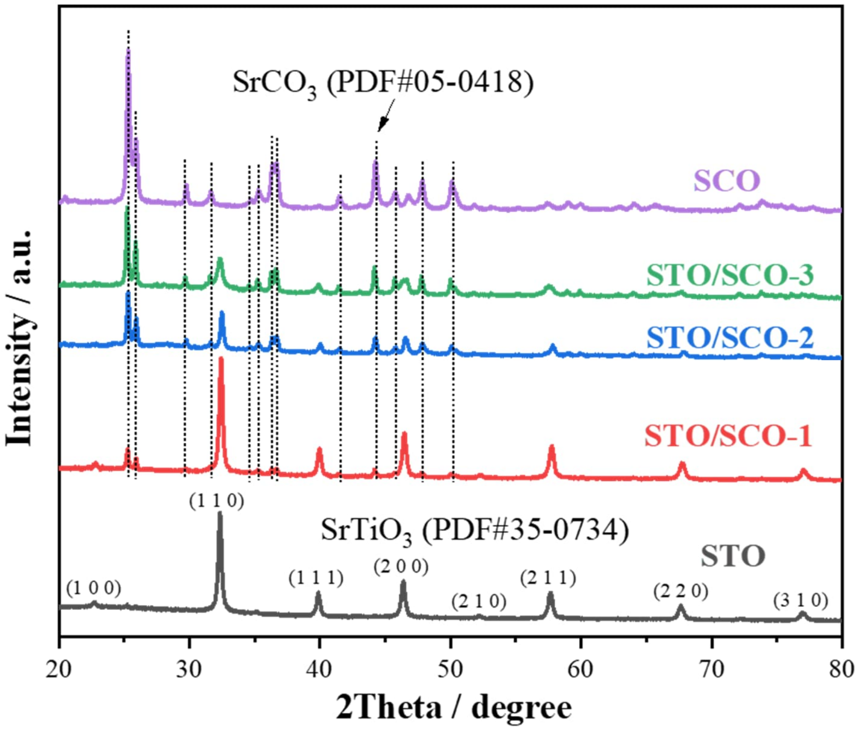

Figure 7-2 XRD patterns of SCO, STO/SCO - 1, 2, 3 and STO samples

As visualized by the SEM images in Fig. 7-3 (a) and (b), a typical STO sample is composed of various nanoparticle structures stacked together. While in STO/SCO heterojunctions samples (Fig. 7-3 (c-h)), two types of characteristics morphologies are identified, namely nanoparticles and nanorods, which are attributed to the formation of STO/SCO heterojunction structures. In photocatalytic reactions, the rough surface and crack structure amongst nanoparticles would be assumed to be beneficial for the adsorption processes (Shawabkeh et al., 2022). In addition, related SEM elements mappings displayed in Fig. 7-4 indicate that these elements are evenly distributed on the STO/SCO-2 sample. Table 7-2 shows the lists of the atomic ratios of Sr/Ti based on the EDS analysis, and the Sr/Ti ratio increases from 1/0.89 to 1/0.66 for STO/SCO-2 compared with the original STO. The decrease of the Ti element implies that there are other compounds engaged to react with the precursor of Sr.

Table 7-1 XRD phase analyses of STO/SCO compounds

Compounds	$SrTiO_3$ Weight Fraction (%)	$SrCO_3$ Weight Fraction (%)
STO/SCO-1	82.7	17.3
STO/SCO-2	33.3	66.7
STO/SCO-3	28.5	71.5

The TEM and HRTEM images of both STO and STO/SCO-2 samples were obtained to view the detailed morphology and the interface of the as constructed STO/SCO heterojunction. The TEM image presented in Fig. 7-5 (a) and (b) further confirms the pileup of nanostructure of STO. In addition to the similar nanostructure of STO, another kind of rod-like nanostructures are viewed in STO/SCO-2 sample, as previewed in SEM image. The HRTEM image of STO sample in Fig. 7-5 (c) displays clear lattice spacing of 0.277 nm, which are well agreed with the (1 1 0) crystal plane of STO. For the corresponding HRTEM image of STO/SCO-2 sample in Fig. 7-5 (d), lattice spacings viewed of 0.277 nm and 0.352 nm are referred to the (1 1 0) crystal plane of STO and (1 1 1) crystal plane of SCO, respectively. The HRTEM images of the STO/SCO-2 sample evidence the formation of heterojunction interface with intimate contact, which promotes the transmission and separation of photo-generated carriers. In addition, as demonstrated in Fig. 7-6 (a), the specific surface areas detected by BET methods are found to be increased with the gradual addition of CN contents. And as shown in Fig. 7-6 (b), no obvious change of the crystal sizes among different STO/SCO combinations can be observed by BJH pore size distribution.

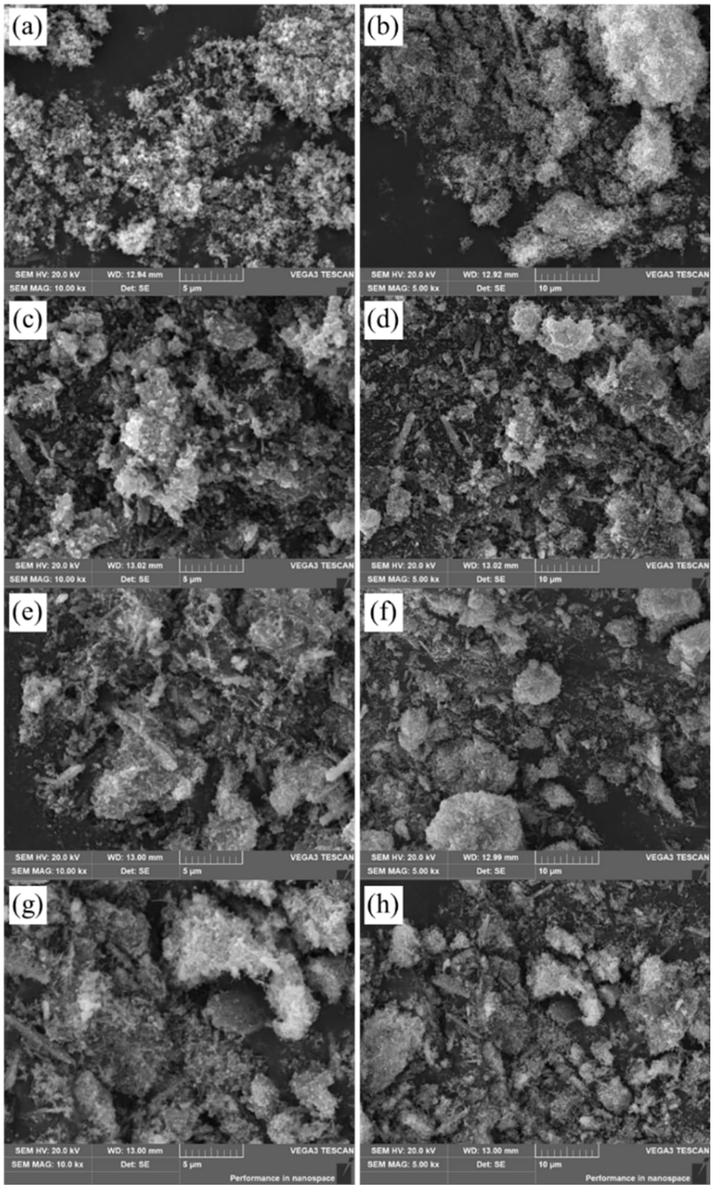

Figure 7-3 SEM images of STO (a, b) and STO/SCO-1 (c, d), 2 (e, f), and 3 (g, h)

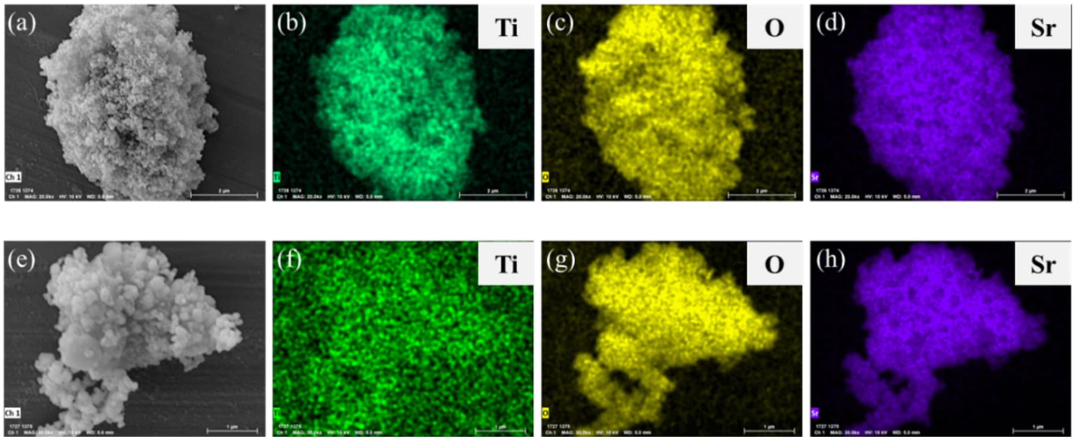

Figure 7-4 SEM images of STO/SCO-2 and their spatial elemental distribution maps of Ti, O and Sr

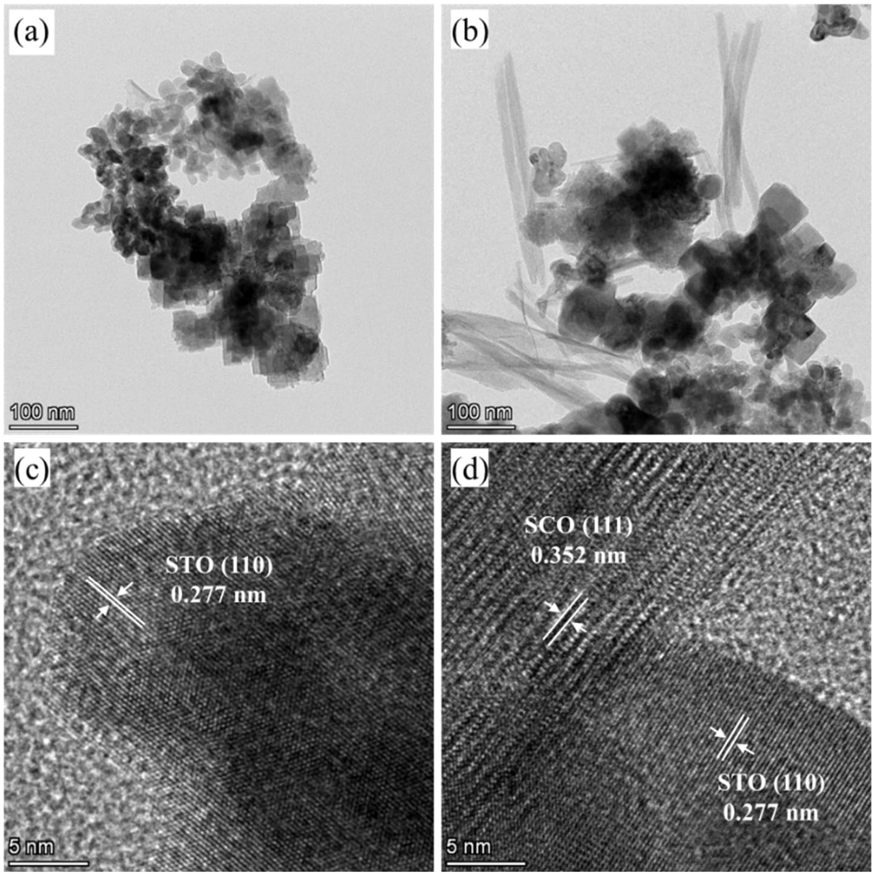

Figure 7-5 TEM images of the (a) STO and (b) STO/SCO-2 and HRTEM images of the (c) STO and (d) STO/SCO-2

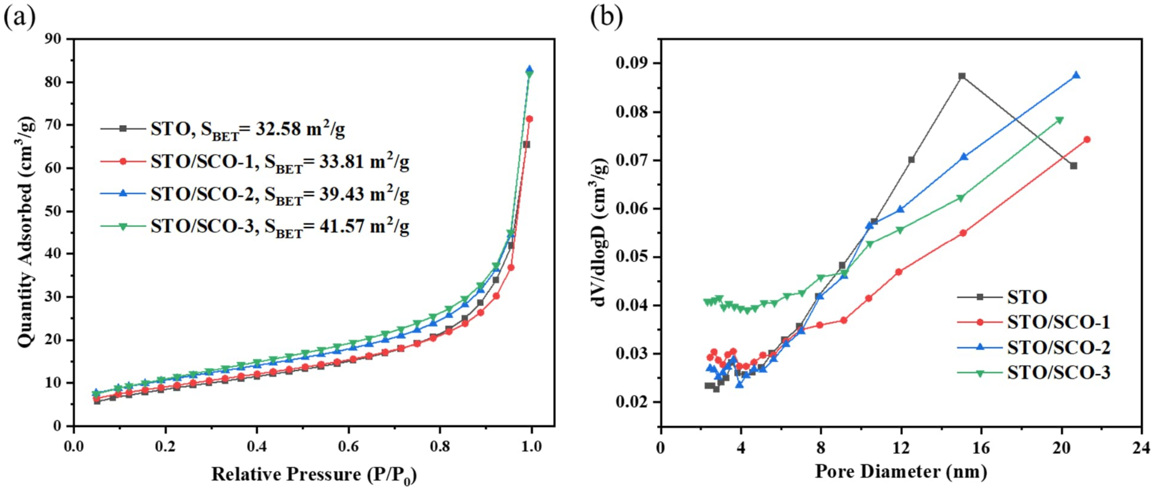

Figure 7-6 (a) Nitrogen adsorption–desorption isotherm and (b) corresponding BJH pore size distribution curve of STO and STO/SCO-1,2,3 samples

Table 7-2 Elemental analyses of the STO/SCO-2, STO and SCO compounds by EDS

Element	Atomic of STO/SCO-2 (%)	Atomic of STO (%)	Atomic of SCO (%)
Sr	20.79	15.18	25.05
Ti	13.65	17.08	0.00
O	65.56	67.74	74.95
Sr: Ti	1: 0.66	1: 0.89	-

7.2.3 Interfacial Characterization of $SrTiO_3$/$SrCO_3$ nanoparticles

Fig. 7-7 (a) shows the FT-IR spectra of the STO and STO/SCO-1,2,3. Four distinct absorption bands at 820 cm^{-1}, 1067 cm^{-1}, 1468 cm^{-1} and 1756 cm^{-1} in STO/SCO samples are identified as functional groups of CO_3^{2-} at out-of-plane bending mode, symmetric stretching mode, corresponding anti-symmetric vibration and both out-of-plane bending mode and in-plane deformation, respectively (Dong et al., 2012). Therefore, confirming the existence of CO_3^{2-} in STO/SCO components. In addition, no feature peak of CN (Wang et al., 2016) was found in STO/SCO samples, implying that CN was completely decomposed during the hydroxide-mediated hydrothermal process.

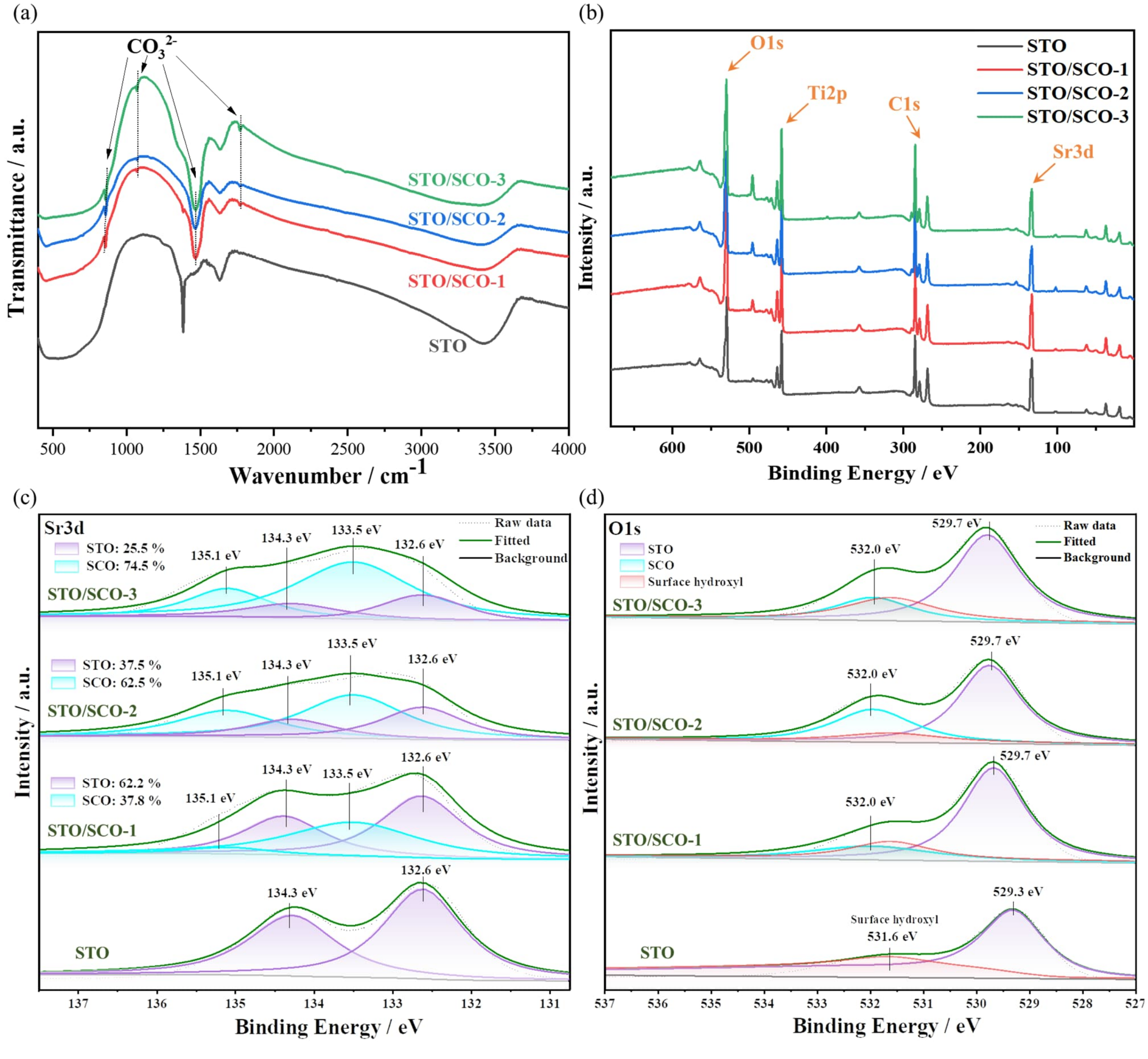

Figure 7-7 (a) FT-IR spectra of STO and STO/SCO-1,2,3, (b) XPS spectra survey of STO and STO/SCO-1,2,3 samples and XPS spectra of (c) Sr3d and (d) O1s for STO and STO/SCO-1,2,3

The surface chemical states of as-prepared samples were further investigated by the XPS profiles. Fig. 7-7 (b) displays the full-scan spectra of Sr, Ti, O and C elements in STO and STO/SCO heterojunction samples as expected. For the Sr 3d spectra of pristine STO sample in Fig. 7-7 (c), the binding energy at 132.6 eV (Sr $3d_{5/2}$) and 134.3 eV (Sr $3d_{3/2}$) are attributed to Sr^{2+} state of $SrTiO_3$ (Sosulnikov & Teterin, 1991). While Sr 3d XPS spectra of the STO/SCO-1,2,3 samples are fitted into four characteristic peaks with binding energy at the 132.6 eV (Sr $3d_{5/2}$) and 134.3 eV (Sr $3d_{3/2}$) attributed to $SrTiO_3$, and at the 133.5 eV (Sr $3d_{5/2}$) and 135.1 eV (Sr $3d_{3/2}$) referred to Sr^{2+} of $SrCO_3$ (Sosulnikov & Teterin, 1991), respectively. Also, the Sr^{2+} ratio of SCO part in STO/SCO samples increases from 37.5% in STO/SCO-1 to 62.5% in STO/SCO-2, and then to 74.5% in STO/SCO-3, which indicates the addition of CN promotes the formation of SCO in crystal growth. This constitution results are consistent with the previous XRD and FTIR analysis. The O 1s spectrum of STO shown in Fig. 7-7 (d) is fitted into two peaks at around 529.7 eV, and 531.6 eV, which are ascribed to Sr-O-Ti in $SrTiO_3$ and surface hydroxyl species, respectively. The O 1s of STO/SCO samples are divided into three peaks at 532.0 eV, 531.6 eV and 529.7, which are attributed to Sr-O-C in SCO, surface hydroxyl species, and Sr-O-Ti in $SrTiO_3$ respectively. There is a slight peak deviation observed in STO/SCO samples for oxygen bound to Sr and Ti, owing to the construction of heterojunction between $SrTiO_3$ and $SrCO_3$. Ti $2p_{1/2}$ and Ti $2p_{3/2}$ peaks indicating the existence of Ti^{4+} (Tan et al., 2014) are identified in Fig. 7-8 (a). The binding energy of Ti 2p for STO/SCO samples shifts to higher energy direction compared with STO sample due to the surface interaction between the STO and SCO counterparts of the heterojunction structure (Ouyang et al., 2012). C 1s in Fig. 7-8 (b) is fitted into two distinct peaks. The peak at 284.8 eV is attributed to the adventurous carbon compounds, whereas the peak at 289.4 eV corresponds to O-C=O of the carbonate in $SrCO_3$ (Shtarev et al., 2021). The enhancement of O-C=O peaks confirms the gradual increase of SCO from STO/SCO-1 sample to STO/SCO-3 sample. All these above XPS results indicate the formation of STO/SCO heterojunction with strong chemical bonds interactions.

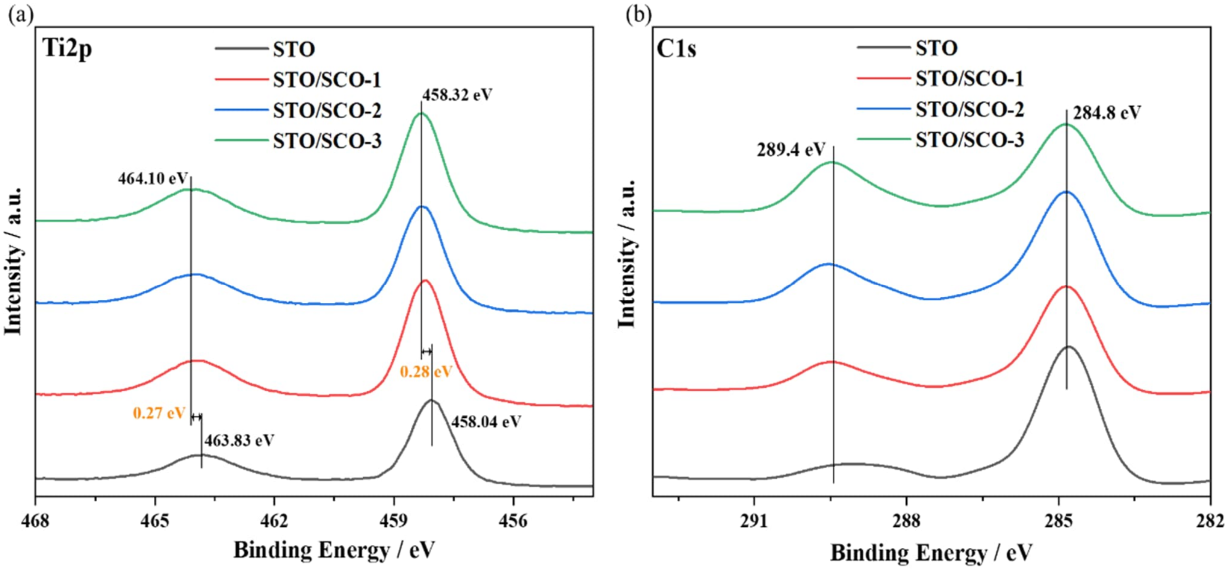

Figure 7-8 XPS spectra of (a) Ti2p and (b) C1s for STO and STO/SCO-1,2,3

Based on the results from the characterization of nanophotocatalysts, the formation process of STO/SCO heterojunction is deduced as follows. Firstly, TiO_3^{2-} hydrolyzed from the precursor of tetrabutyl titanate and uncombined Sr^{2+} that originated from $Sr(NO_3)_2$ will crystalize to STO during the hydrothermal process. Considering that CO_3^{2-} producing from hydrolyzed CN participates in the reaction system, the precursor of Sr would also react with this C source to generate SCO simultaneously under alkaline conditions and finally contributes to the construction of STO/SCO heterojunctions interface (Deng et al., 2023; H. Wang et al., 2018).

7.3 Photocatalytic Degradation of HCHO and NO

The photocatalytic air purification potentiality of the as-prepared STO and STO/SCO-X (X = 1,2,3) samples were evaluated in continuous reaction systems under simulated solar light irradiation. HCHO and NO were chosen as the representative target air pollutants. Fig. 7-9 (a) displays the time-varying concentrations of HCHO (C/C_0%) with the as-prepared photocatalysts under light irritation. The HCHO concentrations sharply decline in the first 6 mins and become steady as the equilibration of the photocatalytic reaction. After irradiating for 30 mins, the removal efficiencies of HCHO by STO, STO/SCO-1. STO/SCO-2 and STO/SCO-3 samples are 7.1%, 32.2%, 40.3% and 20.5%, respectively, while there is rare degradation for pristine SCO under similar conditions. As for the degradation of NO shown in Fig. 7-9 (b), the STO/SCO heterojunctions all exhibit improved capacities compared with both pristine STO and SCO. The removal case of NO is similar to that of the HCHO, STO/SCO-2 sample presents the highest removal efficiency of NO of 44%. Considering SCO cannot be activated under visible light irritation because of its wide band gap (H. Wang et al., 2018), pristine SCO showed limited photocatalytic activity for both HCHO and NO degradation. The reaction rates of NO and HCHO photooxidation were calculated to quantitatively compare their capabilities. The early stage of photocatalytic degradation progress follows the mass-transfer-controlled pseudo-first-order rate reaction (Ai et al., 2009). The reaction kinetics based on the Langmuir-Hinshelwood model is used and defined as Eq. 7-1 (Shie et al., 2008).

$$- \ln (C / C_0) = k\,t \qquad \text{(Eq. 7-1)}$$

where C and C_0 represent the concentrations after and before irradiation, respectively, k represents the apparent reaction rate constant, and t is the irradiation time.

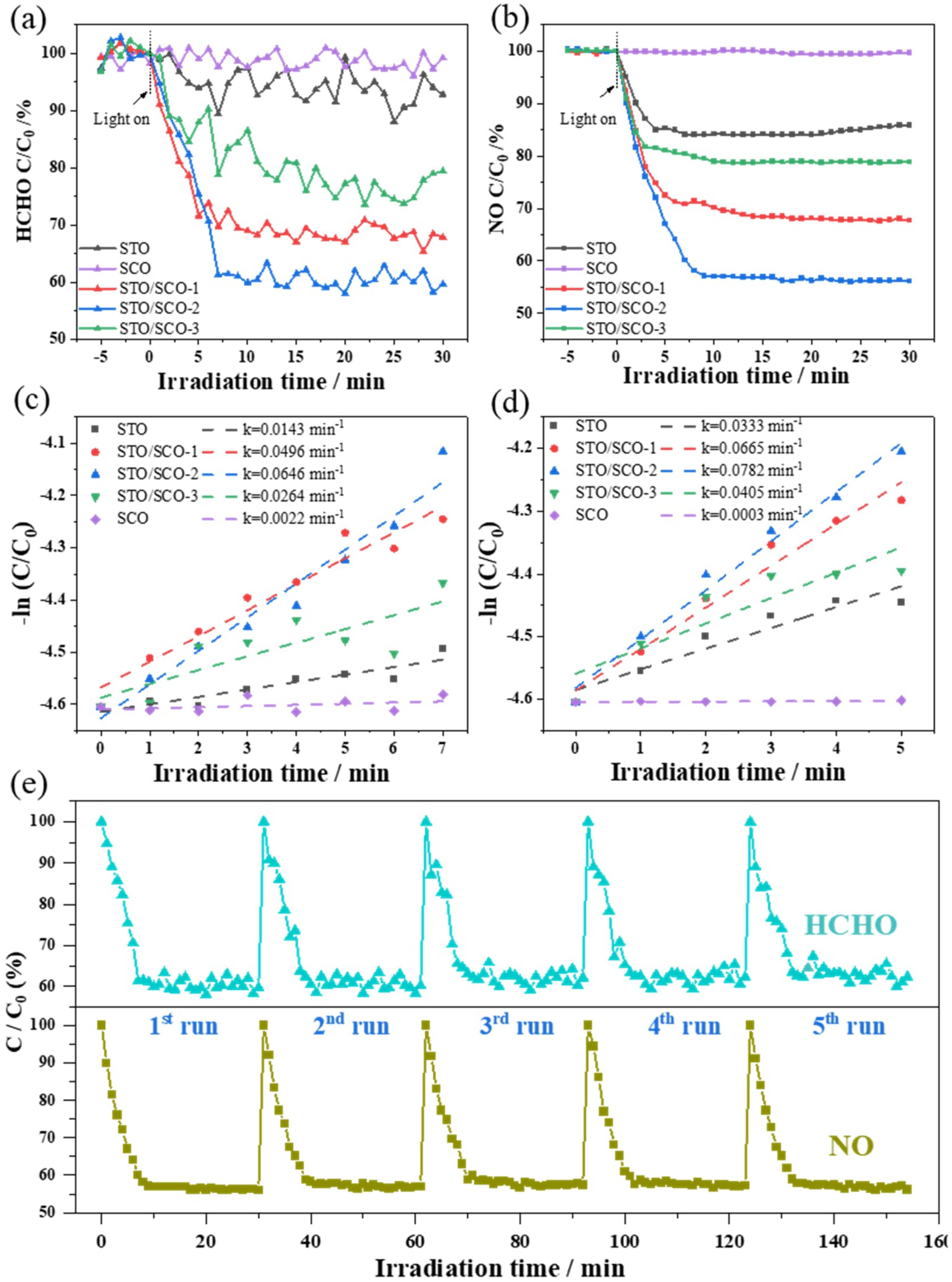

Figure 7-9 Photocatalytic activities of STO, SCO and STO/SCO-1,2,3 for removal of (a) HCHO and (b) NO, reaction rate constant k of STO, SCO and STO/SCO-1,2,3 for removal of (c) HCHO and (d) NO, and (e) cycling runs for the photocatalytic removal of HCHO and NO over STO/SCO-2

The apparent reaction rate constant k is the slope of the plot of -ln (C/C_0) versus irradiation time t (min), which is demonstrated in Fig. 7-9 (c) and 7-9 (d) for HCHO degradation and NO degradation, respectively. The apparent reaction rate constants of STO/SCO-2 are the largest for both degradation of HCHO (0.0646 min^{-1}) and NO (0.0782 min^{-1}) among all these samples, which are 4.5 and 2.3 times higher for HCHO and NO than those of pristine STO. Photodegradation experiments with different initial pollutant concentrations for both NO and HCHO were conducted to thoroughly study their photocatalytic effects. As shown in Fig. 7-10, The SCO/STO-2 sample with the best removal performances exhibits almost the identical reaction rates and degradation efficiencies under various initial concentrations for both NO and HCHO pollutants. Thus, the effectiveness of air purification can be confirmed for both high and low pollution situations. The above results indicate the STO/SCO-2 heterojunction is the most effective photocatalyst in removing both NO and HCHO amongst all samples.

Moreover, in order to evaluate the potential applications for continuous purification of COFs emissions, the photocatalytic stability and reusability of STO/SCO-2 for degradation of both HCHO and NO were evaluated by repeated cyclic experiments. As shown in Fig. 7-9 (e), after five cycled degradation runs, the removal efficiency of HCHO keeps the initial value of nearly 40%. Likewise, the efficiency for NO degradation also remains over 40% and consistent with almost the same level in all these five test runs. These results verify its outstanding reproducibility and stability for purification of two typical contaminants in practice and provide a promising application ability for control of typical gaseous pollutants from COFs.

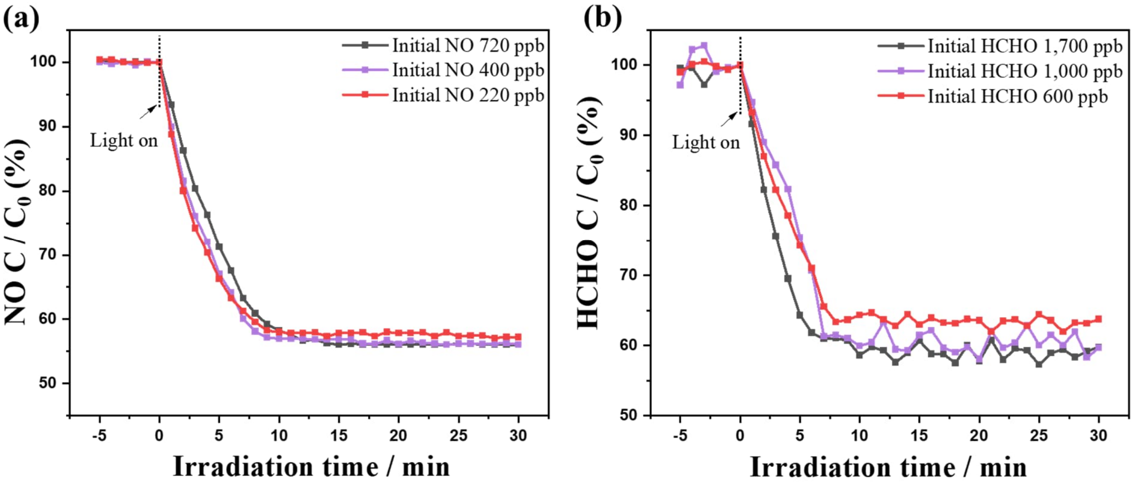

Figure 7-10 Photocatalytic activities of STO/SCO-2 under different initial pollutant concentrations for both (a) NO and (b) HCHO

7.4 Mechanism of Oxidation Degradation

7.4.1 O_2 Activation and Adsorption Behavior

The O_2 activation is generally considered the key step in photocatalytic reaction in environmental remediation application (Yang et al., 2022). In this case, O_2 activation adsorption models are revealed by DFT calculation on the surfaces of STO, SCO and STO/SCO heterojunction (Shown in Fig. 7-11). Table 7-3 lists the summary of the main calculation results. The bond length of O-O observed at the surface of STO is 1.32 Å while the O-O bond on STO/SCO surface is stretched to 1.45 Å. The adsorption energies of the O_2 molecule (E_{ads}) on the three composites are in the order of STO/SCO (−4.91 eV) < SCO (−4.72 eV) < STO (−1.14 eV) despite the O_2 bond length on SCO is 1.50 Å. The STO/SCO is determined to be more effective for O_2 activation than STO with lower E_{ads} and elongated O-O bond which is the same as SCO.

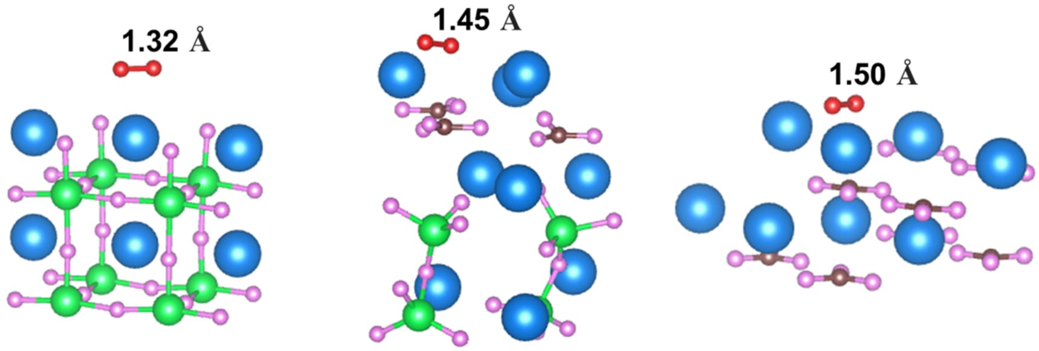

O_2 on STO
E_{ads} = -1.14 eV
Δq = -0.58 e

O_2 on STO/SCO
E_{ads} = -4.91 eV
Δq = -1.40 e

O_2 on SCO
E_{ads} = -4.72 eV
Δq = -1.54 e

Figure 7-11 Optimised O_2 adsorption on STO, STO/SCO and SCO configuration, Δq and E_{ads} represent the carried electrons and adsorption energy

Table 7-3 Summary of bond length (N-O for NO and O-O for O_2), E_{ads} and Δq of adsorption on STO, SCO and STO/SCO, respectively

Sample	HCHO		NO			O_2		
	E_{ads} (eV)	Δq (e)	N-O Length (Å)	E_{ads} (eV)	Δq (e)	O-O Length (Å)	E_{ads} (eV)	Δq (e)
STO	-0.47	-0.17	1.19	-0.42	-0.24	1.32	-1.14	-0.58
SCO	-1.66	-1.08	1.25	-1.15	-0.75	1.50	-4.72	-1.54
STO/SCO	-1.92	-0.94	1.29	-2.80	-1.11	1.45	-4.91	-1.40

The HCHO and NO adsorption behaviors on the catalyst surface are before their photocatalytic reactions, and the adsorption/desorption performances are extremely necessary to determine the photocatalytic reaction (X. W. Li et al., 2019). The temperature-programmed desorption (TPD) was employed to investigate the behavior between HCHO and the as-synthesized photocatalysts. The adsorption process of HCHO on the catalyst was conducted at room temperature till equilibrium. As illustrated in Fig. 7-12, there is one distinguished desorption peak for the STO/SCO-2 sample at the temperature of nearly 500 °C representing the cleavage of the C=O bond of the intermediates formate (HCOOH) from HCHO oxidation (Y. F. Zhang et al., 2020). However, no peak can be identified from STO catalyst, indicating the HCHO chemisorption process does not occur on STO.

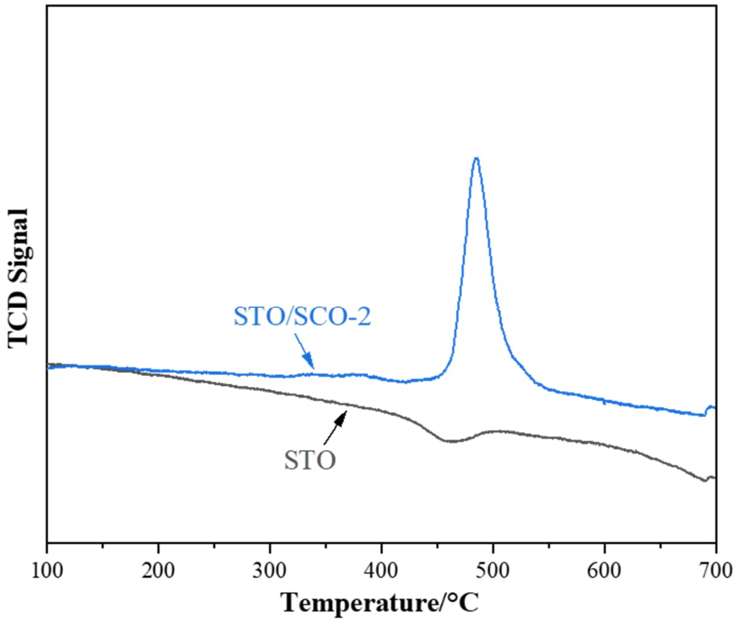

Figure 7-12 HCHO-TPD profiles of STO/SCO-2 and STO

The adsorption configurations of HCHO (Fig. 7-13 (a)) and NO (Fig. 7-13 (b)) onto STO, SCO and STO/SCO were calculated through DFT, respectively, to further explore the interactions between the gas pollutant molecules and the catalysts. The adsorption energy E_{ads} of HCHO molecules onto STO/SCO structure is calculated to be −1.92 eV, which is 4 times and 1.2 times lower than those on the pristine STO and SCO structures, respectively, while the charge depletion (Δq) also decreases from −0.17 e on STO to −0.94 e on STO/SCO by the Bader method (Henkelman, Arnaldsson, & Jonsson, 2006). The heterojunction structure of STO/SCO in line with HCHO-TPD would facilitate and support the HCHO chemisorption process. In the NO adsorption process, the E_{ads} and Δq of NO on STO/SCO structure are found to be −2.80 eV and −1.11 e, which are about 6.7 times lower than those on STO structure of −0.42 eV and 4.6 times lower for Δq of −0.24 e, respectively. In addition, the N-O bond length of adsorbed NO varies from 1.19 Å on STO to 1.29 Å on STO/SCO, respectively. This indicates that the NO adsorption process would also be influenced by constructing the heterojunction. Both experimental and DFT calculation results validate the STO/SCO heterojunction surface promotes both the O_2 activation and air pollutants adsorption process.

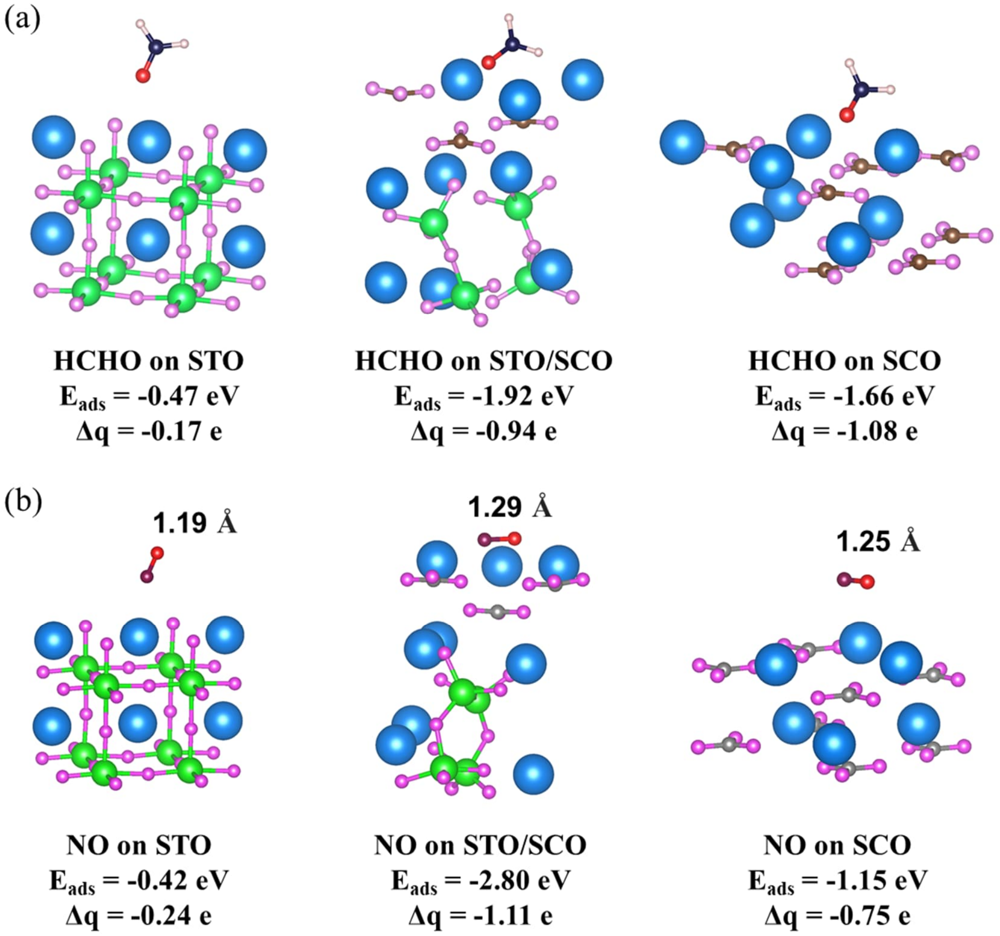

Figure 7-13 Optimised (a) HCHO and (b) NO adsorption on STO, STO/SCO and SCO configurations, Δq and E_{ads} represent the carried electrons and adsorption energy

]

7.4.2 Band Structure and Photocatalytic Degradation Mechanism

The surface work functions of SCO and STO were obtained as 5.41 eV and 4.81 eV by theoretical calculation, respectively, to further understand the effects of STO/SCO heterojunction as shown in Fig. 7-14 (a) and (b). The unequal work functions of SCO and STO spontaneously induce the charge migration at the interface by Colombian force, thereby effectively inhibiting the recombination of photoexcited carriers (Kobayashi et al., 2018; Ran et al., 2018). When the STO/SCO heterojunction is formed, electrons will transfer from the STO to the SCO’s side with a lower work function to achieve the equilibrium of the Fermi levels (Fig. 7-15 (a)). Consequently, the charge distribution of the optimized STO/SCO geometry was also obtained as shown in Fig. 7-14 (c). The value of total charges (Δq) calculated through the Bader method for SCO is −1.74 e, indicating that SCO will receive 1.74 e electrons from STO, further confirming the direction of electron transfer is from STO to SCO (Fig. 7-14 (c)). The main agent of reactant adsorption is the electron transportation at the STO/SCO interface and tends to reinforce the separation rate between photogenerated holes and electrons. The transient photocurrent was tested to probe the migration of photocatalytic electrons. The photocurrent signal excited over the STO/SCO-2 heterojunction (7×10^{-7} A·cm^{-2}) is the highest among the three prepared STO/SCO samples and is about 4 times higher than that of the STO sample as demonstrated in Fig. 7-14 (d). The SCO sample exhibits nearly no photocurrent because of its dielectric properties. Moreover, the photoluminescence (PL) spectra were tested to investigate the transmission and recombination rate of the photogenerated carriers. The excitation wavelength was set as 310 nm. As observed in Fig. 7-15 (b), all the STO/SCO samples exhibit much lower PL peaks compared with pristine STO sample, which is caused by the formation of heterojunction interface that inhibiting the recombination of the photo-generated carriers. These results are consistent with our hypothesis of the formation of STO/SCO heterojunction.

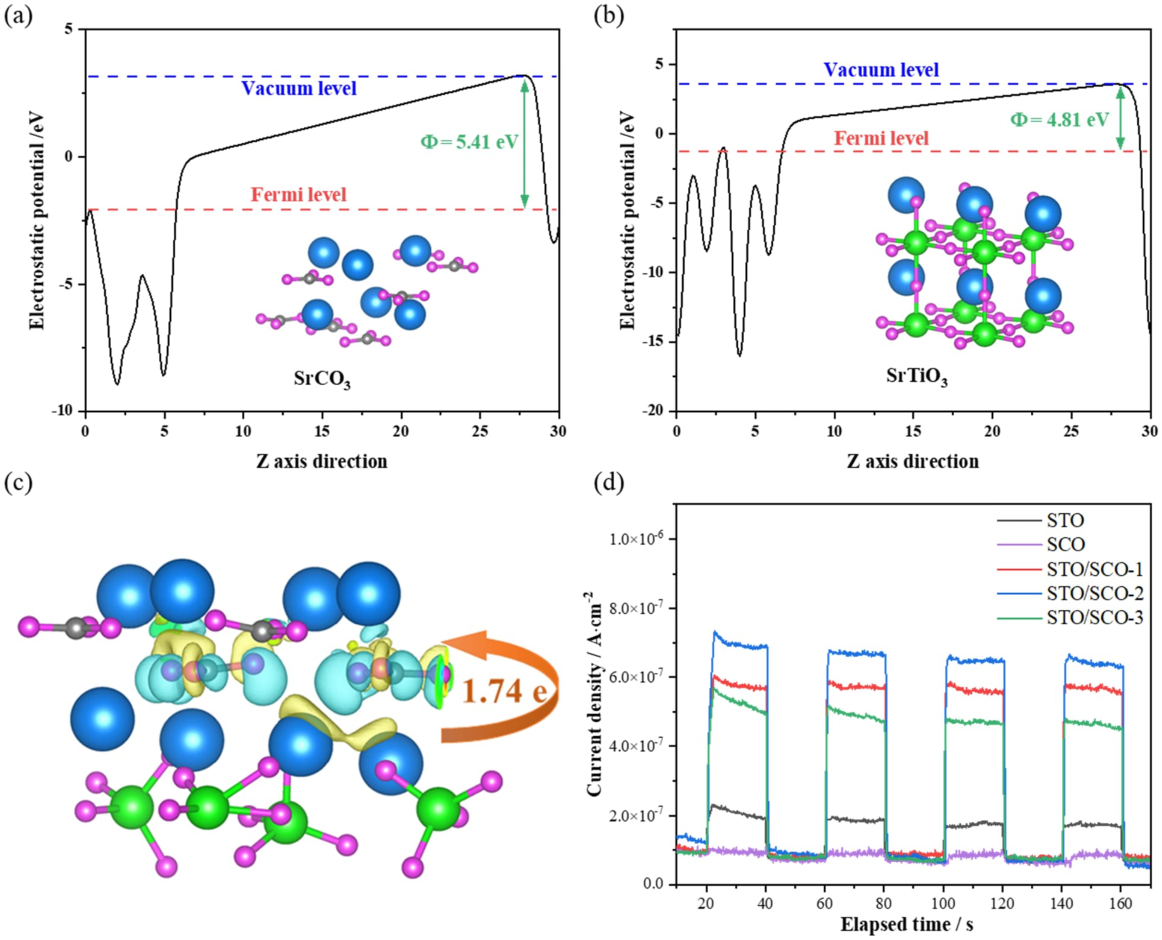

Figure 7-14 Work functions of (a) SrCO$_3$ (001) surface; (b) SrTiO$_3$ (001) surface; (c) charge difference distribution of the STO/SCO interfacial structure (blue represents charge accumulation and yellow represents charge depletion); and (d) transient photocurrent responses

Measurements of ESR on STO, SCO and STO/SCO samples were performed under both simulated solar light irradiation and dark conditions by identifying the intensity of DMPO signals to ascertain the generation of ROS that are key elements in the photocatalytic purification process. Fig. 7-16 (a) demonstrated the characteristic signals of

DMPO-$\cdot O_2^-$ which can be recognized over STO/SCO-2 and STO samples after being irradiated, and the signals of STO/SCO-2 is much stronger than those of STO. Fig. 7-16 (b) shows the characteristic peaks of DPMO-·OH for STO/SCO-2 and STO samples which exhibit the same patterns as $\cdot O_2^-$. The STO/SCO-2 heterojunction enhances the generation of both ·OH and $\cdot O_2^-$, however, both the DMPO-$\cdot O_2^-$ and DMPO-·OH are not detected for SCO because the insulator materials cannot respond to simulated solar light.

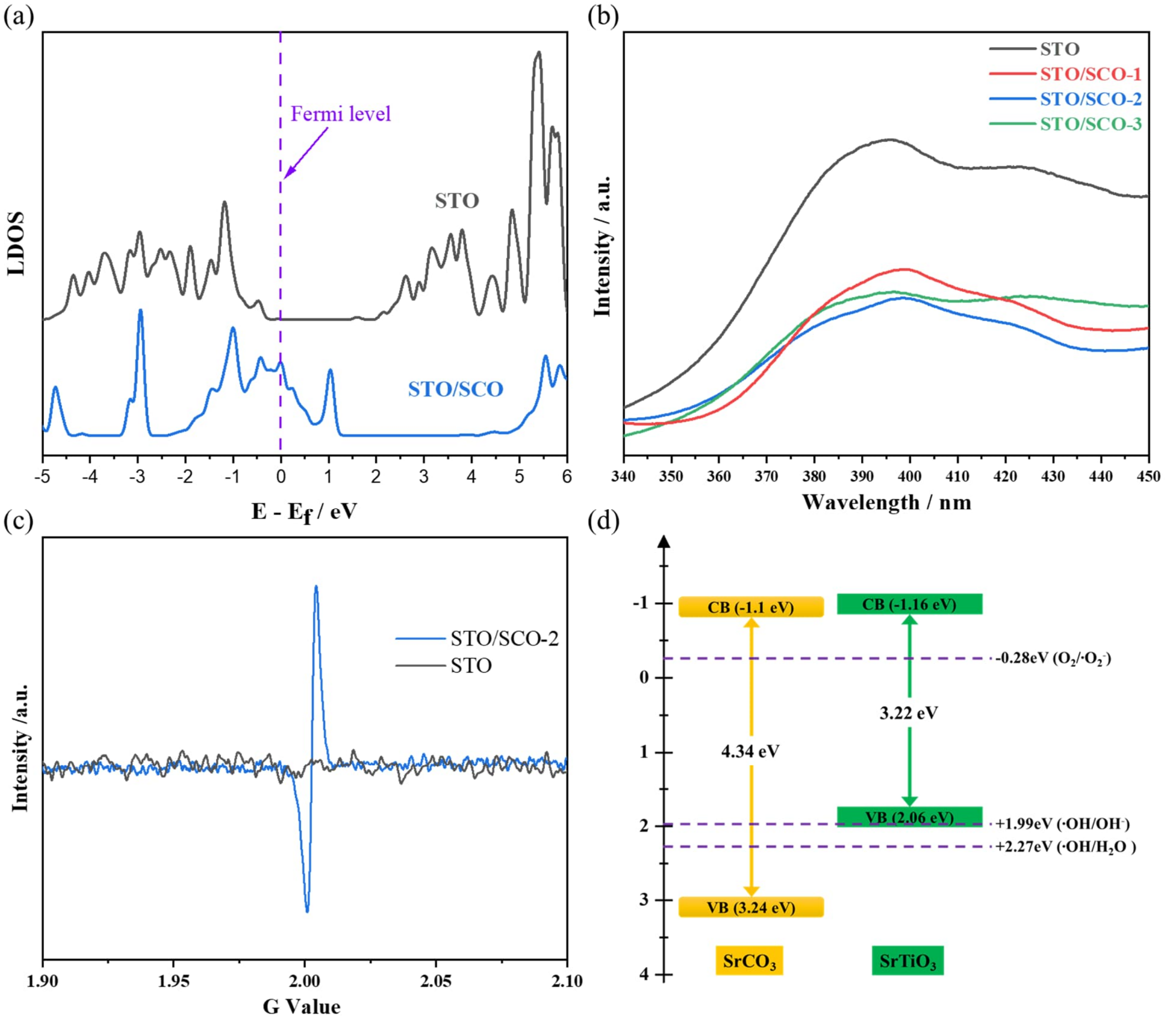

Figure 7-15 (a) Density of state of STO and STO/SCO, (b) photoluminescence spectrum of STO and STO/SCO-1,2,3 (c) electron paramagnetic resonance of STO/SCO and STO and (d) schematic diagram of band gap and energy structure

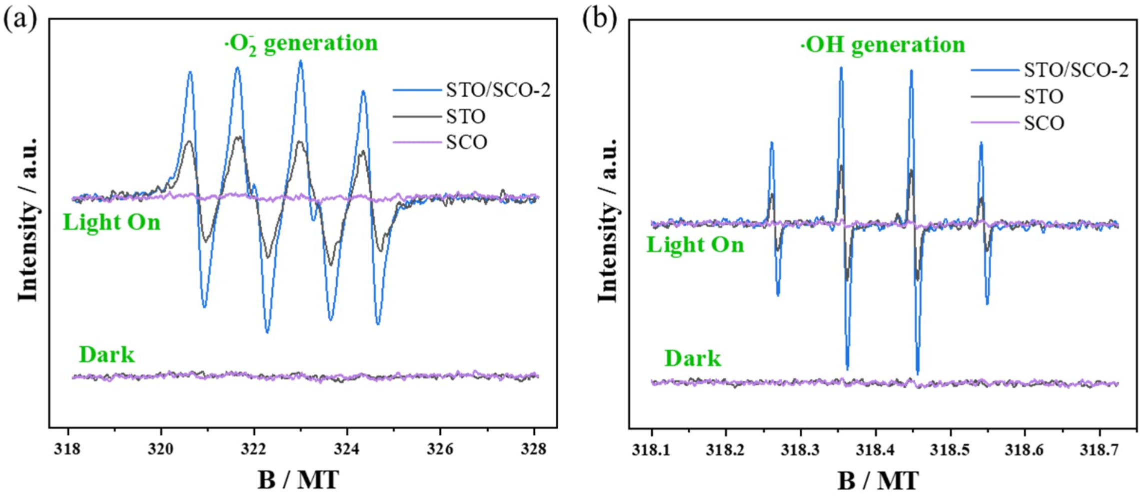

Figure 7-16 DMPO spin-trapping ESR spectra of STO, STO/SCO and SCO samples in methanol dispersion for (a) DMPO-•O_2^-; and in aqueous dispersion for (b) DPMO-•OH

As for the band structure, the STO sample has a band gap energy of 3.22 eV with its absorption edge at 380 nm, whilst the absorption edge for the typical insulator of the SCO sample is at 285 nm with a band gap of 4.34 eV. The valence band (VB) and conduction band (CB) of STO and SCO are calculated to further seek insights by the following Eq. (7-2) and (7-3) (Xu & Schoonen, 2000):

$$E_{\mathrm{VB}} = X - E^{e} + 0.5E_g \qquad \text{(Eq. 7-2)}$$

$$E_{\mathrm{CB}} = E_{VB} - E_g \qquad \text{(Eq. 7-3)}$$

Where E_{VB}, E_{CB} and E_g are the VB, CB and the band gap of the compound. And X is the electronegativity of the compound, which can be calculated from the electronegativity of each constituent atom. E^e is the energy of free electrons on hydrogen scale (~ 4.5 eV). For the STO, the electronegativity X and band gap E_g are obtained to be 4.95 eV and 3.22 eV, respectively. The E_{VB} and E_{CB} are further calculated to be 2.06 eV and -1.16 eV.

Meanwhile, the electronegativity X and band gap E_g for SCO are determined to be 5.57 eV and 4.34 eV, respectively. The E_{VB} and E_{CB} for constituent SCO are 3.24 eV and −1.1 eV, respectively, as shown in Fig. 7-15 (d). In addition, the solid ESR spectrum was used to determine the oxygen vacancy (OV) defects of STO/SCO-2 and STO. Two distinct symmetrical ESR signal peaks can be identified for the STO/SCO-2 sample at g = 2.002, while the STO sample shows no significant peak as demonstrated in Fig. 7-15 (c). Restricted to its band structure, pristine insulator SCO cannot be excited by the simulated solar light because of its wide band gap, while the pristine STO is able to be excited in producing only limited photocatalytic charges. As a result, the existence of oxygen vacancies induces intermediate levels which render the opportunity to be excited by solar energy (Xiong et al., 2018).

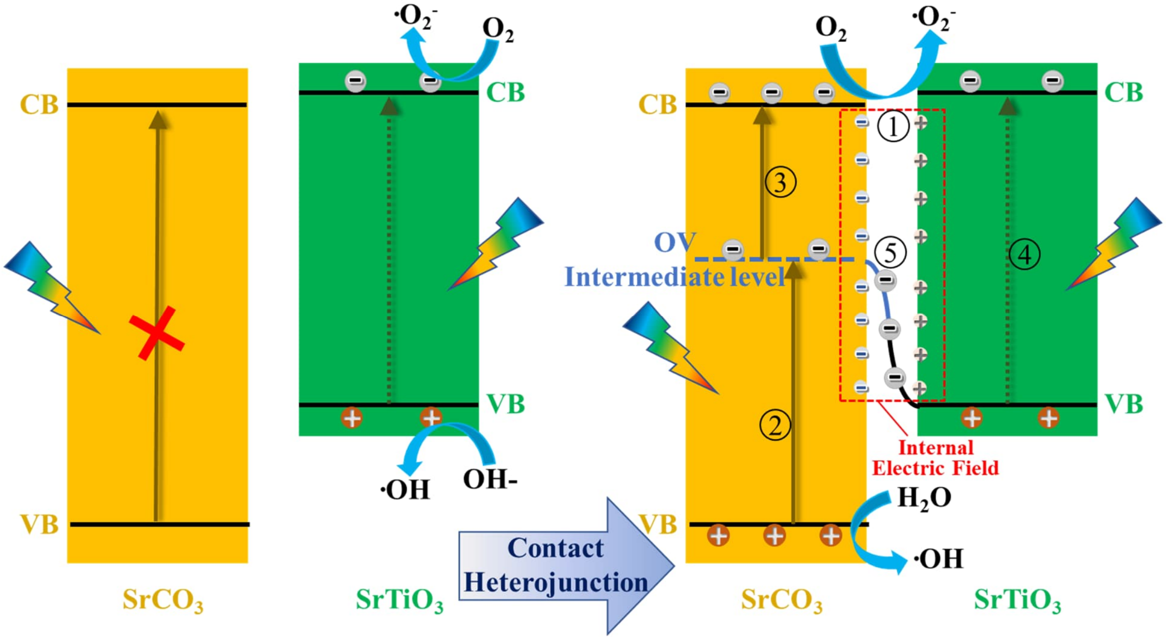

Figure 7-17 Proposed photocatalytic mechanism to enhance photocatalytic activity over STO/SCO heterojunctions

According to the results from the experimental analysis and theoretical calculation, the corresponding mechanism of photocatalytic air purification over STO/SCO heterojunction could be proposed in the following five processes demonstrated in Fig. 17-17. With the building of STO/SCO insulator heterojunction, electrons would be inclined to transfer from the STO to the SCO side at the interface in absence of light irradiation. This is because of the different potentials between the two parts that causes uneven distribution of charges, thereby promoting the construction of an internal electric field (process ①). The OVs were simultaneously generated during the formation of heterojunction rendering the possibility of direct transition from VB to intermediate level over SCO part to take large utilization of solar light (process ②) and subsequently allows the photoexcited electrons transfer from intermediate level to the CB of SCO (process ③). Thus, the insulator-based STO/SCO heterojunction exhibits photocatalytic activities under simulated solar light irradiation. There will also be certain photoexcited electrons migrating from VB to CB as its weak light utilization of STO (process ④). The existence of an internal electric field from process ① was beneficial in separating the photoexcited electron-hole pairs (process ⑤). The accumulated holes at the VB of SCO will react with surface H_2O and hydroxy to generate ·OH. In addition, the electrons gathered at the CB of SCO and STO react with O_2 to produce $\cdot O_2^-$. Consequently, the robust ROS generation of both radical ·OH and $\cdot O_2^-$ would react with pre-adsorbed air pollutants NO or HCHO to achieve the target of air purification.

7.5 Chapter Summary

Insulator-based STO/SCO nano-heterojunctions constructed by using the CN self-sacrificing hydrothermal synthesis method have been applied for the first time to purify the representative indoor air pollutants of NO and HCHO. The ideal photocatalytic activities (44% and 40%) and reaction rates (0.0782 min^{-1} and 0.0646 min^{-1}) towards both NO and HCHO can be achieved by optimizing the ratio of counterparts of STO/SCO heterojunctions. A certain level of oxygen vacancies and the internal electric field were formed at the interface of the insulator-based STO/SCO heterojunction, which maximized the utilization of solar energy to excite photocarriers and enhanced the transfer efficiency on the surface. Molecular O_2 is validated to be beneficially activated at the STO/SCO heterojunction surface with reduced adsorption energy from −1.14 eV to −4.91 eV and enlarged O_2 bond from 1.32 Å to 1.45 Å based on the DFT calculation. The abundant ROS was generated with the combined effects of efficient photocarriers and stimulative O_2 activation for the photo-degradation of NO and HCHO. This study provides a feasible strategy for the design and fabrication of insulator-based photocatalysts as a supplementary to the developed HiGee scrubber in focus on dealing with the gaseous pollutants from the COF emissions.

Chapter 8 Conclusions and Suggestions for Future Research

8.1 Conclusions

The cooking oil fumes from the are the exhaust emissions from cooking processes with complicated particulate and gaseous compositions and have sever impacts on the environment and human health. A comprehensive study from the laboratory simulations to field trails in commercial kitchens was conducted to better understand the detailed emission characteristics and features. Sampling and chemical analysis were conducted in the five different common cooking methods including stir-frying, pan-frying, deep-frying, boiling and steaming simulated. The concentrations and detailed chemical compositions of the $PM_{2.5}$ and VOCs were determined for all these five cooking methods in a lab-based simulation kitchen. In general, the concentration trend of stir-frying > deep-frying > pan-frying > boiling > steaming for the $PM_{2.5}$ from COF was identified, while for the VOCs concentration trend, deep-frying > pan-frying > stir-frying > boiling > steaming was observed, indicating the oil-based cooking methods emitted higher concentration of $PM_{2.5}$ and VOCs than those from water-based cooking styles. Significant deviations of the total concentrations of $PM_{2.5}$ and TVOC were found in the results from same cooking method, especially for those oil-based cooking processes, which was because of the uneven distribution of the exhaust flue and uncontrollable fat and protein contents in raw food materials. OC was found to be the dominant component in all cooking styles, accounting for 39.3% to 49.3% of the total $PM_{2.5}$, due to the rich organic contents in food materials, which was also supported by the high OC/EC ratios from cooking sources. Water-soluble ions contributed to 4.8% - 8.9% mass concentration of the $PM_{2.5}$, where SO_4^{2-}, NO_3^-, NH_4^+ and Ca^{2+} were detected as the major components from all these cooking processes. The mass concentration of elements ranged from 2.06 μg/m^3 to 14.62 μg/m^3 which occupied the small proportion (3.4% - 5.3%) in $PM_{2.5}$, and Ca, K and Fe were the major components. C-PAHs accounted for 29% to 49% of the total detected PAHs, and stir-frying emitted the highest ratios of C-PAHs while highest PAHs/$PM_{2.5}$ ratio was emitted from deep-frying. Alkane and alkene were the main species of VOCs for oil-based cooking methods while carbonyls were the dominant species for water-based cooking methods, because of their different cooking temperatures and food materials. Ethylene, acetaldehyde, acrolein and formaldehyde were the common high emission VOCs in all the cooking methods. The above results provided the updated emission inventory from cooking process, and will complement the emission data for anthropogenic sources, and these emission features will assistant for better identification and source apportionment of cooking emissions from integrated kitchens.

Further sampling work was carried out in four typical commercial kitchens in Hong Kong to reveal the real COF emissions. Both the chemical characteristics and environmental health impacts of the COFs from four integrated commercial kitchens in Hong Kong were analyzed in detail. The mass concentrations of $PM_{2.5}$ in decreasing order were 269.85 μg/m^3, 232.11 μg/m^3, 199.95 μg/m^3, and 85.69 μg/m^3 for CAN, CFF, WFF, and CHP restaurants, respectively, with the similar ranges of those from cooking methods study. The dominant cooking methods could be confirmed by the ratios of OC/EC and diagnostic analysis of PAH with different molecular weights and rings. The VOC emission levels and composition profiles from commercial kitchens were consistent with their major cooking methods, while Hexane, ethylene, and formaldehyde were detected to have significantly high VOC emission levels in COFs from all kitchens. Significant adverse environmental effects on the formation of O_3 and secondary organic aerosol were revealed by the results of their high chemical reactivity, OFP, and SOAFP. The highest unit formation rates for ozone and SOA were obtained from CAN as 5.55 g OFP/g VOCs and WFF as 2.17 g SOAFP/ g VOCs. In addition, significant induvial VOC contribution came from ethylene, formaldehyde and 1,3-butadiene with the total of over 50% contribution to the total OFP concentrations, while the largest two contributors for SOAFP were toluene (16.8% - 34.9%) and 1,2,4-trimethylbenzene (22.9% - 27.7%). Health risk assessment by inhalation exposure suggested that significant carcinogenic risks existed to both kitchen staff and customers if there was not proper personal protection and enough ventilation system. All these characteristic and evaluation results pointed out the critical pollution situations from commercial kitchens and the necessity in application and development of effective control techniques towards the severe COFs emissions from cooking process.

Based on the sampling results, the high gravity rotating packed bed scrubber was selected for the control of COFs due to its non-selective pollutant removal features, and absorbent surfactant was further developed and tested in laboratory. The developed surfactant made by the mixture of Span-80 and Tween-80 were proved to be effective in removing $PM_{2.5}$ pollutants with the mixed concentration of 8 g/L. Besides, the detailed operation conditions including air flow rate, rotating speed and long-term operation mode were further investigated. The surfactant together with the optimal operation parameter obtained by the in-lab simulation test were used to conduct the trail test to evaluate the real removal efficiency in these four investigated kitchens. The $PM_{2.5}$ removal efficiency could reach as high as 86%, while the rate of 74% in TVOC removal could be achieved. Due to the non-selective operation theories, all these chemical species in $PM_{2.5}$ and VOCs exhibited effective removal efficiency. Removal efficiencies of $PM_{2.5}$ were kept at high levels with over 80% for all these restaurants, while higher VOCs removal efficiencies were observed from those scenarios with higher initial VOCs concentrations. Besides, VOCs with higher molecular weight exhibited increased removal efficiencies in HiGee scrubber, due to the enhanced liquid capture with higher centrifugal force compared with lighter VOCs. In addition, the evaluation results of environmental impacts including L_{OH}, OFP and SOAFP all exhibited superior improvement of 62.95%, 60.35%, and 61.05%, respectively, suggesting its effectiveness in control of the COF emissions from real cooking processes and promising application abilities in food industries.

In considering the relative low removal efficiency of the HiGee scrubber on gaseous pollutants from COFs and the severe environment and health impacts posed by some VOCs such as formaldehyde. Supplementary control technique focused on the photocatalytic degradation of excessive gaseous pollutants from the outlet of the scrubber was investigated. Insulator-based STO/SCO nano-heterojunctions constructed by using the CN self-sacrificing hydrothermal synthesis method have been applied for the first time to purify the representative indoor air pollutants of NO and HCHO. The ideal photocatalytic activities (44% and 40%) and reaction rates (0.0782 min^{-1} and 0.0646 min^{-1}) towards both NO and HCHO can be achieved by optimizing the ratio of counterparts of STO/SCO heterojunctions. A certain level of oxygen vacancies and the internal electric field were formed at the interface of the insulator-based STO/SCO heterojunction, which maximized the utilization of solar energy to excite photocarriers and enhanced the transfer efficiency on the surface. Molecular O_2 is validated to be beneficially activated at the STO/SCO heterojunction surface with reduced adsorption energy from −1.14 eV to −4.91 eV and enlarged O_2 bond from 1.32 Å to 1.45 Å based on the DFT calculation. The abundant ROS was generated with the combined effects of efficient photocarriers and stimulative O_2 activation for the photo-degradation of NO and HCHO. The HiGee scrubber associated with photocatalytic degradation can achieve high purification efficiency for both particulate and gaseous pollutants from COF emissions and provide promising purification abilities for application in real kitchens.

8.2 Limitations and Suggestions for Future Research Work

In the present work, the investigation of the emission characteristics and supplement of emission inventory from cooking process has been conducted, and effective control strategies including HiGee scrubber and photocatalysis has been developed and verified. Several limitations and improvements should still be addressed in future studies:

1) The detailed $PM_{2.5}$ and VOCs have been investigated, other chemicals from COFs such as fatty acid from acid-base balance results, mercaptan from odour control aspects should also be sampled and analyzed for better understanding and control of COFs emissions;
2) Besides the investigated 5 common cooking methods and 4 commercial kitchens in Hong Kong, other rare used cooking methods and unconventional kitchens could be included as well;
3) In the study of HiGee scrubber, all research focused on control and removal of gas-phase pollutants, the used surfactant should also be characterized to study the adsorption and transformation processes in liquid phase;
4) The lifespan of photocatalyst and long-term evaluation for HiGee system should be carried out in future study regarding their practical application;
5) A feasible unit could be designed and integrated with HiGee scrubber as a complete system by adopting the as-developed photocatalyst in support of the degradation of COFs directly from the outlet of the scrubber.

References

Abdullahi, K. L., Delgado-Saborit, J. M., & Harrison, R. M. (2013). Emissions and indoor concentrations of particulate matter and its specific chemical components from cooking: A review. *Atmospheric Environment*, *71*, 260-294. https://doi.org/10.1016/j.atmosenv.2013.01.061

Acciai, C., Zhang, Z. Y., Wang, F. J., Zhong, Z. X., & Lonati, G. (2017). Characteristics and source Analysis of trace Elements in PM2.5 in the Urban Atmosphere of Wuhan in Spring. *Aerosol and Air Quality Research*, *17*(9), 2224-2234. https://doi.org/10.4209/aaqr.2017.06.0207

Ai, Z., Ho, W., Lee, S., & Zhang, L. (2009). Efficient photocatalytic removal of NO in indoor air with hierarchical bismuth oxybromide nanoplate microspheres under visible light. *Environ Sci Technol*, *43*(11), 4143-4150. https://doi.org/10.1021/es9004366

Ait-Helal, W., Borbon, A., Sauvage, S., de Gouw, J. A., Colomb, A., Gros, V., Freutel, F., Crippa, M., Afif, C., Baltensperger, U., Beekmann, M., Doussin, J. F., Durand-Jolibois, R., Fronval, I., Grand, N., Leonardis, T., Lopez, M., Michoud, V., Miet, K., . . . Locoge, N. (2014). Volatile and intermediate volatility organic compounds in suburban Paris: variability, origin and importance for SOA formation. *Atmospheric Chemistry and Physics*, *14*(19), 10439-10464. https://doi.org/10.5194/acp-14-10439-2014

Al-Harbi, M. M., & Al-Kahtani, H. A. (1993). Chemical and biological evaluation of discarded frying palm oil from commercial restaurants. *Food Chemistry*, *48*(4), 395-401. https://doi.org/10.1016/0308-8146(93)90324-9

Ali, H., Plaza, F., & Mann, A. (2018). Numerical Prediction of Dust Capture Efficiency of a Centrifugal Wet Scrubber. *AIChE Journal*, *64*(3), 1001-1012.

https://doi.org/10.1002/aic.15979

Amegah, A. K., Jaakkola, J. J., Quansah, R., Norgbe, G. K., & Dzodzomenyo, M. (2012). Cooking fuel choices and garbage burning practices as determinants of birth weight: a cross-sectional study in Accra, Ghana. *Environ Health*, *11*, 78. https://doi.org/10.1186/1476-069X-11-78

Amouei Torkmahalleh, M., Gorjinezhad, S., Unluevcek, H. S., & Hopke, P. K. (2017). Review of factors impacting emission/concentration of cooking generated particulate matter. *Science of the Total Environment*, *586*, 1046-1056. https://doi.org/10.1016/j.scitotenv.2017.02.088

Anwar, F., Kazi, T. G., Saleem, R., & Bhanger, M. I. (2004). Rapid determination of some trace metals in several oils and fats. *Grasas y Aceites*, *55*(2), 160-168. <Go to ISI>://WOS:000227726200009

Arı, A., Ertürk Arı, P., Yenisoy-Karakaş, S., & Gaga, E. O. (2020). Source characterization and risk assessment of occupational exposure to volatile organic compounds (VOCs) in a barbecue restaurant. *Building and Environment*, *174*, 106791. https://doi.org/10.1016/j.buildenv.2020.106791

Atamaleki, A., Zarandi, S. M., Massoudinejad, M., Samimi, K., Fakhri, Y., Ghorbanian, M., & Khaneghah, A. M. (2021). The effect of frying process on the emission of the volatile organic compounds and monocyclic aromatic group (BTEX). *International Journal of Environmental Analytical Chemistry*, 1-14. https://doi.org/10.1080/03067319.2021.1950148

Atkinson, R., & Arey, J. (2003). Atmospheric degradation of volatile organic compounds. *Chem Rev*, *103*(12), 4605-4638. https://doi.org/10.1021/cr0206420

Bandowe, B. A. M., Lui, K. H., Jones, T., BeruBe, K., Adams, R., Niu, X., Wei, C., Cao,

J. J., Lee, S. C., Chuang, H. C., & Ho, K. F. (2021). The chemical composition and toxicological effects of fine particulate matter (PM(2.5)) emitted from different cooking styles. *Environ Pollut*, *288*, 117754. https://doi.org/10.1016/j.envpol.2021.117754

Bao, J. J., Yang, L. J., Yan, J. P., Xiong, G. L., Lu, B., & Xin, C. Y. (2013). Experimental study of fine particles removal in the desulfurated scrubbed flue gas. *Fuel*, *108*, 73-79. https://doi.org/10.1016/j.fuel.2010.12.037

Bhatia, S. K., & Myers, A. L. (2006). Optimum conditions for adsorptive storage. *Langmuir*, *22*(4), 1688-1700. https://doi.org/10.1021/la0523816

Bian, Y., Wang, R., Ting, S. H., Chen, C., & Zhang, L. (2018). Electrospun SF/PVA Nanofiber Filters for Highly Efficient PM $_{2.5}$ Capture. *IEEE Transactions on Nanotechnology*, *17*(5), 934-939. https://doi.org/10.1109/tnano.2018.2824343

Bianchi, C. L., Gatto, S., Pirola, C., Naldoni, A., Di Michele, A., Cerrato, G., Crocella, V., & Capucci, V. (2014). Photocatalytic degradation of acetone, acetaldehyde and toluene in gas-phase: Comparison between nano and micro-sized TiO2. *Applied Catalysis B-Environmental*, *146*, 123-130. https://doi.org/10.1016/j.apcatb.2013.02.047

Borhani, T. N., Oko, E., & Wang, M. H. (2018). Process modelling and analysis of intensified CO2 capture using monoethanolamine (MEA) in rotating packed bed absorber. *Journal of Cleaner Production*, *204*, 1124-1142. https://doi.org/10.1016/j.jclepro.2018.09.089

Brook, R. D., Rajagopalan, S., Pope, C. A., 3rd, Brook, J. R., Bhatnagar, A., Diez-Roux, A. V., Holguin, F., Hong, Y., Luepker, R. V., Mittleman, M. A., Peters, A., Siscovick, D., Smith, S. C., Jr., Whitsel, L., Kaufman, J. D., American Heart Association Council on, E., Prevention, C. o. t. K. i. C. D., Council on Nutrition, P. A., & Metabolism. (2010). Particulate matter air pollution and cardiovascular disease: An update to the scientific statement from the American Heart Association. *Circulation*, *121*(21), 2331-2378. https://doi.org/10.1161/CIR.0b013e3181dbece1

Burns, J. R., & Ramshaw, C. (1996). Process intensification: Visual study of liquid maldistribution in rotating packed beds. *Chemical Engineering Science*, *51*(8), 1347-1352. https://doi.org/Doi 10.1016/0009-2509(95)00367-3

Cai, C., Chen, L., Huang, H., Liu, Y., Yu, S., Liu, Y., Tao, S., & Liu, W. (2019). Effects of temperature on the emission of particulate matter, polycyclic aromatic hydrocarbons, and polybrominated diphenyl ethers from the thermal treatment of printed wiring boards. *J Hazard Mater*, *380*, 120849. https://doi.org/10.1016/j.jhazmat.2019.120849

Carter, W. P. L. (2010). Development of the SAPRC-07 chemical mechanism. *Atmospheric Environment*, *44*(40), 5324-5335. https://doi.org/10.1016/j.atmosenv.2010.01.026

Chang, E. E., Pan, S. Y., Chen, Y. H., Tan, C. S., & Chiang, P. C. (2012). Accelerated carbonation of steelmaking slags in a high-gravity rotating packed bed. *J Hazard Mater*, *227-228*, 97-106. https://doi.org/10.1016/j.jhazmat.2012.05.021

Chang, L. W., Lo, W. S., & Lin, P. P. (2005). Trans, trans-2,4-decadienal, a product found in cooking oil fumes, induces cell proliferation and cytokine production due to reactive oxygen species in human bronchial epithelial cells. *Toxicological sciences*, *87*(2), 337-343. https://doi.org/10.1093/toxsci/kfi258

Chatzidaki, M. D., Mitsou, E., Yaghmur, A., Xenakis, A., & Papadimitriou, V. (2015). Formulation and characterization of food-grade microemulsions as carriers of natural phenolic antioxidants. *Colloids and Surfaces a-Physicochemical and Engineering Aspects*, *483*, 130-136. https://doi.org/10.1016/j.colsurfa.2015.03.060

Che, W. W., Frey, H. C., Fung, J. C. H., Ning, Z., Qu, H. M., Lo, H. K., Chen, L., Wong, T. W., Wong, M. K. M., Lee, O. C. W., Carruthers, D., Cheung, F., Chan, J. W. M., Yeung,

D. W., Fung, Y. H., Zhang, X. G., Stocker, J., Hood, C., Hohenberger, T. L., . . . Lau, A. K. (2020). PRAISE -HK: A personalized real-time air quality informatics system for citizen participation in exposure and health risk management. *Sustainable Cities and Society, 54*, 101986. https://doi.org/10.1016/j.scs.2019.101986

Chen, C., Zhao, Y., & Zhao, B. (2018). Emission Rates of Multiple Air Pollutants Generated from Chinese Residential Cooking. *Environ Sci Technol*, *52*(3), 1081-1087. https://doi.org/10.1021/acs.est.7b05600

Chen, C. Y., Kuo, Y. C., Wang, S. M., Wu, K. R., Chen, Y. C., & Tsai, P. J. (2019). Techniques for Predicting Exposures to Polycyclic Aromatic Hydrocarbons (PAHs) Emitted from Cooking Processes for Cooking Workers. *Aerosol and Air Quality Research*, *19*(2), 307-317. https://doi.org/10.4209/aaqr.2018.09.0346

Chen, H., Li, L., Lei, Y., Wu, S., Yan, D., & Dong, Z. (2020). Public health effect and its economics loss of PM(2.5) pollution from coal consumption in China. *Science of the Total Environment*, *732*, 138973. https://doi.org/10.1016/j.scitotenv.2020.138973

Chen, J., & Shao, L. (2003). Mass production of nanoparticles by high gravity reactive precipitation technology with low cost. *China Particuology*, *1*(2), 64-69. https://doi.org/10.1016/s1672-2515(07)60110-9

Chen, J., Zou, H., Chu, G., Zhao, H., & Shao, L. (2012). High gravity technology and its industrial application. *Sulphur Phosphorus & Bulk Materials Handling Related Engineering*, *1*, 6-10.

Chen, J. F., Zhang, J. Y., Shen, Z. G., Zhong, J., & Yun, J. (2006). Preparation and characterization of amorphous cefuroxime axetil drug nanoparticles with novel technology: high-gravity antisolvent precipitation. *Industrial & Engineering Chemistry Research*, *45*(25), 8723-8727. https://doi.org/10.1021/ie060445h

Chen, J. F., Zhou, M. Y., Shao, L., Wang, Y. Y., Yun, J., Chew, N. Y., & Chan, H. K. (2004). Feasibility of preparing nanodrugs by high-gravity reactive precipitation. *Int J Pharm*, *269*(1), 267-274. https://doi.org/10.1016/j.ijpharm.2003.09.044

Chen, Y. H., Wang, L. C., Tsai, C. H., & Shang, N. C. (2010). Continuous-flow Esterification of Free Fatty Acids in a Rotating Packed Bed. *Industrial & Engineering Chemistry Research*, *49*(9), 4117-4122. https://doi.org/10.1021/ie100112s

Cheng, Y., Yu, Q. Q., Liu, J. M., Du, Z. Y., Liang, L. L., Geng, G. N., Zheng, B., Ma, W. L., Qi, H., Zhang, Q., & He, K. B. (2021). Strong biomass burning contribution to ambient aerosol during heating season in a megacity in Northeast China: Effectiveness of agricultural fire bans? *Science of the Total Environment*, *754*, 142144. https://doi.org/10.1016/j.scitotenv.2020.142144

Cho, K. S., Lee, Y. Y., Jang, S. N., Yun, J., Kwon, J., Park, H. J., & Seo, Y. (2020). Removal of particulate matter from pork belly grilling gas using an orifice wet scrubber. *J Environ Sci Health A Tox Hazard Subst Environ Eng*, *55*(9), 1125-1130. https://doi.org/10.1080/10934529.2020.1773712

Chow, J. C., Watson, J. G., Chen, L. W., Chang, M. C., Robinson, N. F., Trimble, D., & Kohl, S. (2007). The IMPROVE_A temperature protocol for thermal/optical carbon analysis: maintaining consistency with a long-term database. *J Air Waste Manag Assoc*, *57*(9), 1014-1023. https://doi.org/10.3155/1047-3289.57.9.1014

CSD, H. (2023). Statistical Digest of the Services Sector. In: Information Services Department Hong Kong.

Darbandi, T., Risberg, M., & Westerlund, L. (2021). CFD modeling of the forces in the wet scrubber acting on particulate matter released from biomass combustion. *Thermal Science and Engineering Progress, 25,* 100997.

https://doi.org/10.1016/j.tsep.2021.100997

David, E., & Niculescu, V. C. (2021). Volatile Organic Compounds (VOCs) as Environmental Pollutants: Occurrence and Mitigation Using Nanomaterials. *International journal of environmental research and public health*, *18*(24), 13147. https://doi.org/ARTN 13147

10.3390/ijerph182413147

Degen, T., Sadki, M., Bron, E., Konig, U., & Nenert, G. (2014). The HighScore suite. *Powder Diffraction*, *29*, S13-S18. https://doi.org/10.1017/S0885715614000840

Dejchanchaiwong, R., Tekasakul, P., Tekasakul, S., Phairuang, W., Nim, N., Sresawasd, C., Thongboon, K., Thongyen, T., & Suwattiga, P. (2020). Impact of transport of fine and ultrafine particles from open biomass burning on air quality during 2019 Bangkok haze episode. *J Environ Sci (China)*, *97*, 149-161. https://doi.org/10.1016/j.jes.2020.04.009

Deng, Y., Shu, S., Fang, N., Wang, R., Chu, Y., Liu, Z., & Cen, W. (2023). One-pot synthesis of SrTiO3-SrCO3 heterojunction with strong interfacial electronic interaction as a novel photocatalyst for water splitting to generate H2. *Chinese Chemical Letters*, *34*(2), 107323. https://doi.org/10.1016/j.cclet.2022.03.046

Dong, F., Xiong, T., Sun, Y. J., Lu, L. L., Zhang, Y. X., Zhang, H. J., Huang, H. W., Zhou, Y., & Wu, Z. B. (2017). Exploring the photocatalysis mechanism on insulators. *Applied Catalysis B-Environmental*, *219*, 450-458. https://doi.org/10.1016/j.apcatb.2017.07.082

Dong, F., Zheng, A., Sun, Y., Fu, M., Jiang, B., Ho, W.-K., Lee, S., & Wu, Z. (2012). One-pot template-free synthesis, growth mechanism and enhanced photocatalytic activity of monodisperse (BiO) 2 CO 3 hierarchical hollow microspheres self-assembled with single-crystalline nanosheets. *CrystEngComm*, *14*(10), 3534-3544.

Dong, X. A., Zhang, W. D., Sun, Y. J., Li, J. Y., Cen, W. L., Cui, Z. H., Huang, H. W., &

Dong, F. (2018). Visible-light-induced charge transfer pathway and photocatalysis mechanism on Bi semimetal@defective BiOBr hierarchical microspheres. *Journal of Catalysis, 357*, 41-50. https://doi.org/10.1016/j.jcat.2017.10.004

Doshi, B., Sillanpaa, M., & Kalliola, S. (2018). A review of bio-based materials for oil spill treatment. *Water Res*, *135*, 262-277. https://doi.org/10.1016/j.watres.2018.02.034

Du, B. W., Gao, J., Chen, J., Stevanovic, S., Ristovski, Z., Wang, L. N., & Wang, L. (2017). Particle exposure level and potential health risks of domestic Chinese cooking. *Building and Environment*, *123*, 564-574. https://doi.org/10.1016/j.buildenv.2017.07.031

Duan, Q. Q., Yuan, Z. G., Liu, Y. Z., Duan, S. S., & Duan, X. F. (2021). Multilevel cross flow rotating packed bed to enhance gas film control mass transfer process. *Chemical Engineering and Processing-Process Intensification*, *161*, 108321. https://doi.org/ARTN 108321

10.1016/j.cep.2021.108321

Dung, C. H., Wu, S. C., & Yen, G. C. (2006). Genotoxicity and oxidative stress of the mutagenic compounds formed in fumes of heated soybean oil, sunflower oil and lard. *Toxicol In Vitro*, *20*(4), 439-447. https://doi.org/10.1016/j.tiv.2005.08.019

Fraser, M. P., Yue, Z. W., Tropp, R. J., Kohl, S. D., & Chow, J. C. (2002). Molecular composition of organic fine particulate matter in Houston, TX. *Atmospheric Environment*, *36*(38), 5751-5758. https://doi.org/Pii S1352-2310(02)00725-2

Doi 10.1016/S1352-2310(02)00725-2

Gao, Y., Lai, S. C., Lee, S. C., Yau, P. S., Huang, Y., Cheng, Y., Wang, T., Xu, Z., Yuan, C., & Zhang, Y. Y. (2015). Optical properties of size-resolved particles at a Hong Kong urban site during winter. *Atmospheric Research*, *155*, 1-12. https://doi.org/10.1016/j.atmosres.2014.10.020

Garmash, O., Rissanen, M. P., Pullinen, I., Schmitt, S., Kausiala, O., Tillmann, R., Zhao, D. F., Percival, C., Bannan, T. J., Priestley, M., Hallquist, A. M., Kleist, E., Kiendler-Scharr, A., Hallquist, M., Berndt, T., McFiggans, G., Wildt, J., Mentel, T., & Ehn, M. (2020). Multi-generation OH oxidation as a source for highly oxygenated organic molecules from aromatics. *Atmospheric Chemistry and Physics*, *20*(1), 515-537. https://doi.org/10.5194/acp-20-515-2020

Garti, N., Spernath, A., Aserin, A., & Lutz, R. (2005). Nano-sized self-assemblies of nonionic surfactants as solubilization reservoirs and microreactors for food systems. *Soft Matter*, *1*(3), 206-218. https://doi.org/10.1039/b506233k

Ge, D., Zeng, Z., Arowo, M., Zou, H., Chen, J., & Shao, L. (2016). Degradation of methyl orange by ozone in the presence of ferrous and persulfate ions in a rotating packed bed. *Chemosphere*, *146*, 413-418. https://doi.org/10.1016/j.chemosphere.2015.12.058

Grosjean, D. (1992). In situ organic aerosol formation during a smog episode: Estimated production and chemical functionality. *Atmospheric Environment. Part A. General Topics*, *26*(6), 953-963. https://doi.org/10.1016/0960-1686(92)90027-i

Grosjean, D., & Seinfeld, J. H. (1989). Parameterization of the Formation Potential of Secondary Organic Aerosols. *Atmospheric Environment*, *23*(8), 1733-1747. https://doi.org/Doi 10.1016/0004-6981(89)90058-9

Guo, J., Jiao, W. Z., Qi, G. S., Yuan, Z. G., & Liu, Y. Z. (2019). Applications of high-gravity technologies in gas purifications: A review. *Chinese Journal of Chemical Engineering*, *27*(6), 1361-1373. https://doi.org/10.1016/j.cjche.2019.01.011

Gysel, N., Dixit, P., Schmitz, D. A., Engling, G., Cho, A. K., Cocker, D. R., & Karavalakis, G. (2018). Chemical speciation, including polycyclic aromatic hydrocarbons (PAHs), and toxicity of particles emitted from meat cooking operations. *Science of the Total*

Environment, *633*, 1429-1436. https://doi.org/10.1016/j.scitotenv.2018.03.318

Han, S., Tan, Y., Gao, Y., Li, X., Ho, S. S. H., Wang, M., & Lee, S. C. (2023). Volatile organic compounds at a roadside site in Hong Kong: Characteristics, chemical reactivity, and health risk assessment. *Science of the Total Environment*, *866*, 161370. https://doi.org/10.1016/j.scitotenv.2022.161370

He, H. Q., Yuan, S. Q., & Yuan, J. P. (2009). Experiment and analysis of performance parameters for refraction nozzle in vent wash exhaust hood. *Drainage and Irrigation Machinery*, *27*, 247-250.

He, L. Y., Hu, M., Huang, X. F., Yu, B. D., Zhang, Y. H., & Liu, D. Q. (2004). Measurement of emissions of fine particulate organic matter from Chinese cooking. *Atmospheric Environment*, *38*(38), 6557-6564. https://doi.org/10.1016/j.atmosenv.2004.08.034

He, W. Q., Shi, A. J., Shao, X., Nie, L., Wang, T. Y., & Li, G. H. (2020). Insights into the comprehensive characteristics of volatile organic compounds from multiple cooking emissions and aftertreatment control technologies application. *Atmospheric Environment*, *240*, 117646. https://doi.org/ARTN 117646

10.1016/j.atmosenv.2020.117646

He, Z. R., Wang, X. M., Ling, Z. H., Zhao, J., Guo, H., Shao, M., & Wang, Z. (2019). Contributions of different anthropogenic volatile organic compound sources to ozone formation at a receptor site in the Pearl River Delta region and its policy implications. *Atmospheric Chemistry and Physics*, *19*(13), 8801-8816. https://doi.org/10.5194/acp-19-8801-2019

Henkelman, G., Arnaldsson, A., & Jonsson, H. (2006). A fast and robust algorithm for Bader decomposition of charge density. *Computational materials science*, *36*(3), 354-360. https://doi.org/10.1016/j.commatsci.2005.04.010

Hodjati, S., Vaezzadeh, K., Petit, C., Pitchon, V., & Kiennemann, A. (2000). Absorption/desorption of NOx process on perovskites: performances to remove NOx from a lean exhaust gas. *Applied Catalysis B-Environmental*, *26*(1), 5-16. https://doi.org/Doi 10.1016/S0926-3373(99)00143-5

Hou, J., Sun, H., Zhou, Y., Zhang, Y., Yin, W., Xu, T., Cheng, J., Chen, W., & Yuan, J. (2018). Environmental exposure to polycyclic aromatic hydrocarbons, kitchen ventilation, fractional exhaled nitric oxide, and risk of diabetes among Chinese females. *Indoor Air*, *28*(3), 383-393. https://doi.org/10.1111/ina.12453

Hsieh, L. T., Wang, Y. F., Li, P. M., & Chen, K. C. (2011). Removal of Particle-bound Water-soluble Ions from Cooking Fume Using Bio-solution Wet Scrubber. *Aerosol and Air Quality Research*, *11*(5), 508-518. https://doi.org/10.4209/aaqr.2011.02.0012

Hu, T. T., Wang, J. X., Shen, Z. G., & Chen, J. F. (2008). Engineering of drug nanoparticles by HGCP for pharmaceutical applications. *Particuology*, *6*(4), 239-251. https://doi.org/10.1016/j.partic.2008.04.001

Huang, L., Cheng, H., Ma, S., He, R., Gong, J., Li, G., & An, T. (2021). The exposures and health effects of benzene, toluene and naphthalene for Chinese chefs in multiple cooking styles of kitchens. *Environ Int*, *156*, 106721. https://doi.org/10.1016/j.envint.2021.106721

Huang, X., Han, D., Cheng, J., Chen, X., Zhou, Y., Liao, H., Dong, W., & Yuan, C. (2020). Characteristics and health risk assessment of volatile organic compounds (VOCs) in restaurants in Shanghai. *Environ Sci Pollut Res Int*, *27*(1), 490-499. https://doi.org/10.1007/s11356-019-06881-6

Huang, X. F., Zhang, B., Xia, S. Y., Han, Y., Wang, C., Yu, G. H., & Feng, N. (2020). Sources of oxygenated volatile organic compounds (OVOCs) in urban atmospheres in

North and South China. *Environ Pollut*, *261*, 114152. https://doi.org/10.1016/j.envpol.2020.114152

Huang, Y., Ho, S. S., Ho, K. F., Lee, S. C., Yu, J. Z., & Louie, P. K. (2011). Characteristics and health impacts of VOCs and carbonyls associated with residential cooking activities in Hong Kong. *J Hazard Mater*, *186*(1), 344-351. https://doi.org/10.1016/j.jhazmat.2010.11.003

Huang, Y., Wang, P., Wang, Z., Rao, Y., Cao, J.-j., Pu, S., Ho, W., & Lee, S. C. (2019). Protonated g-C3N4/Ti3+ self-doped TiO2 nanocomposite films: Room-temperature preparation, hydrophilicity, and application for photocatalytic NO removal. *Applied Catalysis B: Environmental*, *240*, 122-131. https://doi.org/10.1016/j.apcatb.2018.08.078

Huboyo, H. S., Tohno, S., & Cao, R. Q. (2011). Indoor PM2.5 Characteristics and CO Concentration Related to Water-Based and Oil-Based Cooking Emissions Using a Gas Stove. *Aerosol and Air Quality Research*, *11*(4), 401-411. https://doi.org/10.4209/aaqr.2011.02.0016

Hung, H. S., Wu, W. J., Cheng, Y. W., Wu, T. C., Chang, K. L., & Lee, H. (2007). Association of cooking oil fumes exposure with lung cancer: involvement of inhibitor of apoptosis proteins in cell survival and proliferation in vitro. *Mutat Res*, *628*(2), 107-116. https://doi.org/10.1016/j.mrgentox.2006.12.005

Jiao, W., Liu, Y., Liu, J., Qi, G., & Xie, W. (2005). Pilot study on coking ammonia-nitrogen wastewater by high-gravity rotary bed. *Modern Chemical Industry*, *25*(257), 259.

Jiao, W., Liu, Y., & Zhang, D. (2005). The application of high gravity rotating packed bed in environmental industry. *Sichuan Environ*, *24*, 78-82.

Jiao, W. Z., Luo, S., He, Z., & Liu, Y. Z. (2017). Applications of high gravity technologies for wastewater treatment: A review. *Chemical Engineering Journal*, *313*, 912-927.

https://doi.org/10.1016/j.cej.2016.10.125

Jin, S., Dong, G. H., Luo, J. M., Ma, F. Y., & Wang, C. Y. (2018). Improved photocatalytic NO removal activity of SrTiO3 by using SrCO3 as a new co-catalyst. *Applied Catalysis B-Environmental*, *227*, 24-34. https://doi.org/10.1016/j.apcatb.2018.01.020

Jin, X. M., & Holloway, T. (2015). Spatial and temporal variability of ozone sensitivity over China observed from the Ozone Monitoring Instrument. *Journal of Geophysical Research-Atmospheres*, *120*(14), 7229-7246. https://doi.org/10.1002/2015jd023250

Juntarawijit, C., & Juntarawijit, Y. (2017). Cooking smoke and respiratory symptoms of restaurant workers in Thailand. *BMC Pulm Med*, *17*(1), 41. https://doi.org/10.1186/s12890-017-0385-7

Kang, M. S., Yu, G., Shin, J., & Hwang, J. (2021). Collection and decomposition of oil mist via corona discharge and surface dielectric barrier discharge. *J Hazard Mater*, *411*, 125038. https://doi.org/10.1016/j.jhazmat.2021.125038

Kawashima, L. M., & Soares, L. M. V. (2003). Mineral profile of raw and cooked leafy vegetables consumed in Southern Brazil. *Journal of Food Composition and Analysis*, *16*(5), 605-611. https://doi.org/10.1016/S0889-1575(03)00057-7

Kılıç Büyükkurt, Ö., Aykın Dinçer, E., Burak Çam, İ., Candal, C., & Erbaş, M. (2017). The Influence of Cooking Methods and Some Marinades on Polycyclic Aromatic Hydrocarbon Formation in Beef Meat. *Polycyclic Aromatic Compounds*, *40*(2), 195-205. https://doi.org/10.1080/10406638.2017.1392328

Kim, M., Jeong, S. G., Park, J., Kim, S., & Lee, J. H. (2023). Investigating the impact of relative humidity and air tightness on PM sedimentation and concentration reduction. *Building and Environment*, *241*, 110270. https://doi.org/ARTN 110270

10.1016/j.buildenv.2023.110270

Kleeman, M. J., Robert, M. A., Riddle, S. G., Fine, P. M., Hays, M. D., Schauer, J. J., & Hannigan, M. P. (2008). Size distribution of trace organic species emitted from biomass combustion and meat charbroiling. *Atmospheric Environment*, *42*(13), 3059-3075.

Kobayashi, M., Suzuki, Y., Goto, T., Cho, S. H., Sekino, T., Asakura, Y., & Yin, S. (2018). Low-temperature hydrothermal synthesis and characterization of SrTiO3 photocatalysts for NOx degradation. *Journal of the Ceramic Society of Japan*, *126*(2), 135-138. https://doi.org/10.2109/jcersj2.17195

Kopanichuk, I. V., Vedenchuk, E. A., Koneva, A. S., & Vanin, A. A. (2018). Structural Properties of Span 80/Tween 80 Reverse Micelles by Molecular Dynamics Simulations. *J Phys Chem B*, *122*(33), 8047-8055. https://doi.org/10.1021/acs.jpcb.8b03945

Koppmann, R. (2020). *Chemistry of volatile organic compounds in the atmosphere*.

Kumar, R., Srivastava, P. K., & Srivastava, S. P. (1994). Leaching of heavy metals (Cr, Fe, and Ni) from stainless steel utensils in food simulants and food materials. *Bull Environ Contam Toxicol*, *53*(2), 259-266. https://doi.org/10.1007/BF00192042

Lan, Y., Li, Z., Li, D., Xie, W., Yan, G., & Guo, S. (2020). Visible-light responsive Z-scheme Bi@β-Bi2O3/g-C3N4 heterojunction for efficient photocatalytic degradation of 2,3-dihydroxynaphthalene. *Chemical Engineering Journal*, *392*, 123686. https://doi.org/10.1016/j.cej.2019.123686

Lao, L., Ramshaw, C., & Yeung, H. (2011). Process intensification: water electrolysis in a centrifugal acceleration field. *Journal of applied electrochemistry*, *41*(6), 645-656. https://doi.org/10.1007/s10800-011-0275-2

Lee, T., & Gany, F. (2013). Cooking oil fumes and lung cancer: a review of the literature in the context of the U.S. population. *J Immigr Minor Health*, *15*(3), 646-652. https://doi.org/10.1007/s10903-012-9651-1

Lee, Y. Y., Park, H., Seo, Y., Yun, J., Kwon, J., Park, K. W., Han, S. B., Oh, K. C., Jeon, J. M., & Cho, K. S. (2020). Emission characteristics of particulate matter, odors, and volatile organic compounds from the grilling of pork. *Environ Res*, *183*, 109162. https://doi.org/10.1016/j.envres.2020.109162

Li, C. T., Lin, Y. C., Lee, W. J., & Tsai, P. J. (2003). Emission of polycyclic aromatic hydrocarbons and their carcinogenic potencies from cooking sources to the urban atmosphere. *Environ Health Perspect*, *111*(4), 483-487. https://doi.org/10.1289/ehp.5518

Li, J., Deng, S., Li, G., Lu, Z., Song, H., Gao, J., Sun, Z., & Xu, K. (2022). VOCs characteristics and their ozone and SOA formation potentials in autumn and winter at Weinan, China. *Environ Res*, *203*, 111821. https://doi.org/10.1016/j.envres.2021.111821

Li, R., Wang, X., Jin, S., Zhou, X., Feng, Z., Li, Z., Shi, J., Zhang, Q., & Li, C. (2015). Photo-induced H2 production from a CH3OH-H2O solution at insulator surface. *Sci Rep*, *5*(1), 13475. https://doi.org/10.1038/srep13475

Li, S. S., Zhang, S. Y., Pan, W. X., Long, Z. W., & Yu, T. (2019). Experimental and theoretical study of the collection efficiency of the two-stage electrostatic precipitator. *Powder Technology*, *356*, 1-10. https://doi.org/10.1016/j.powtec.2019.07.107

Li, X., Li, H., Huang, Y., Cao, J., Huang, T., Li, R., Zhang, Q., Lee, S. C., & Ho, W. (2022). Exploring the photocatalytic conversion mechanism of gaseous formaldehyde degradation on TiO(2-x)-OV surface. *J Hazard Mater*, *424*(Pt A), 127217. https://doi.org/10.1016/j.jhazmat.2021.127217

Li, X. W., Zhang, W. D., Cui, W., Li, J. Y., Sun, Y. J., Jiang, G. M., Huang, H. W., Zhang, Y. X., & Dong, F. (2019). Reactant activation and photocatalysis mechanisms on Bi-metal@Bi2GeO5 with oxygen vacancies: A combined experimental and theoretical investigation. *Chemical Engineering Journal*, *370*, 1366-1375.

https://doi.org/10.1016/j.cej.2019.04.003

Li, Y., Liu, Y. Z., Zhang, L. Y., Su, Q., & Jin, G. L. (2010). Absorption of NOx into Nitric Acid Solution in Rotating Packed Bed. *Chinese Journal of Chemical Engineering*, *18*(2), 244-248. https://doi.org/10.1016/S1004-9541(08)60349-3

Li, Y. C., Qiu, J. Q., Shu, M., Ho, S. S. H., Cao, J. J., Wang, G. H., Wang, X. X., & Zhao, X. Q. (2018). Characteristics of polycyclic aromatic hydrocarbons in PM(2.5) emitted from different cooking activities in China. *Environ Sci Pollut Res Int*, *25*(5), 4750-4760. https://doi.org/10.1007/s11356-017-0603-0

Li, Y. C., Shu, M., Ho, S. S. H., Wang, C., Cao, J. J., Wang, G. H., Wang, X. X., Wang, K., & Zhao, X. Q. (2015). Characteristics of PM2.5 emitted from different cooking activities in China. *Atmospheric Research*, *166*, 83-91. https://doi.org/10.1016/j.atmosres.2015.06.010

Liang, C. Y., Hsu, P. T., Yuan, M. H., Chen, Y. H., Chang, C. M., Chang, C. Y., Chou, S. C., & Liang, C. J. (2022). Removal of fine particulate matter from cooking-oil fume using an intensified mobile chemical scrubber based on a rotating packed bed with green surfactants. *Process Safety and Environmental Protection, 164,* 669-677. https://doi.org/10.1016/j.psep.2022.06.054

Liang, X., Chen, L., Liu, M., Lu, Q., Lu, H., Gao, B., Zhao, W., Sun, X., Xu, J., & Ye, D. (2022). Carbonyls from commercial, canteen and residential cooking activities as crucial components of VOC emissions in China. *Science of the Total Environment*, *846*, 157317. https://doi.org/10.1016/j.scitotenv.2022.157317

Lin, L. Y., & Bai, H. L. (2016). Promotional effects of manganese on the structure and activity of Ce-Al-Si based catalysts for low-temperature oxidation of acetone. *Chemical Engineering Journal*, *291*, 94-105. https://doi.org/10.1016/j.cej.2016.01.098

Lin, Y., Zou, J., Yang, W., & Li, C. Q. (2018). A Review of Recent Advances in Research on PM(2.5) in China. *Int J Environ Res Public Health*, *15*(3), 438. https://doi.org/10.3390/ijerph15030438

Liu, J., Wang, P. L., Qu, W. Q., Li, H. R., Shi, L. Y., & Zhang, D. S. (2019). Nanodiamond-decorated ZnO catalysts with enhanced photocorrosion-resistance for photocatalytic degradation of gaseous toluene. *Applied Catalysis B-Environmental*, *257*, 117880. https://doi.org/ARTN 117880
10.1016/j.apcatb.2019.117880

Liu, T. Y., Li, Z. J., Chan, M. N., & Chan, C. K. (2017). Formation of secondary organic aerosols from gas-phase emissions of heated cooking oils. *Atmospheric Chemistry and Physics*, *17*(12), 7333-7344. https://doi.org/10.5194/acp-17-7333-2017

Liu, Y., Li, P., Li, Y., Kang, R., & Diao, J. (2007). Pilot test on treatment of high concentration nitrogen oxides by high gravity technology. *CHEMICAL INDUSTRY AND ENGINEERING PROGRESS*, *26*(7), 1058.

Lombardi-Boccia, G., Lanzi, S., & Aguzzi, A. (2005). Aspects of meat quality: trace elements and B vitamins in raw and cooked meats. *Journal of Food Composition and Analysis*, *18*(1), 39-46. https://doi.org/10.1016/j.jfca.2003.10.007

Lu, S. L., Liu, D. Y., Zhang, W. C., Liu, P. W., Fei, Y., Gu, Y., Wu, M. H., Yu, S., Yonemochi, S., Wang, X. J., & Wang, Q. Y. (2015). Physico-chemical characterization of PM2.5 in the microenvironment of Shanghai subway. *Atmospheric Research*, *153*, 543-552. https://doi.org/10.1016/j.atmosres.2014.10.006

Mandin, P., Cense, J. M., Georges, B., Favre, V., Pauporte, T., Fukunaka, Y., & Lincot, D. (2007). Prediction of the electrodeposition process behavior with the gravity or acceleration value at continuous and discrete scale. *Electrochimica acta*, *53*(1), 233-244.

https://doi.org/10.1016/j.electacta.2007.01.044

Márquez-Herrera, A., Ovando-Medina, V. M., Castillo-Reyes, B. E., Meléndez-Lira, M., Zapata-Torres, M., & Saldaña, N. (2014). A novel synthesis of SrCO3–SrTiO3 nanocomposites with high photocatalytic activity. *Journal of Nanoparticle Research*, *16*(12), 1-10. https://doi.org/10.1007/s11051-014-2804-5

Meng, X., Liu, Y., Jiao, W., & Wang, H. (2008). Study on Treatment Technology for Tail Gas of Nitrophosphate Plant. *M-Sized Nitrogenous Fertilizer Progress*, 41-43.

Merico, E., Grasso, F. M., Cesari, D., Decesari, S., Belosi, F., Manarini, F., De Nuntiis, P., Rinaldi, M., Gambaro, A., Morabito, E., & Contini, D. (2020). Characterisation of atmospheric pollution near an industrial site with a biogas production and combustion plant in southern Italy. *Science of the Total Environment*, *717*, 137220. https://doi.org/10.1016/j.scitotenv.2020.137220

Miller, M. R., & Newby, D. E. (2020). Air pollution and cardiovascular disease: car sick. *Cardiovasc Res*, *116*(2), 279-294. https://doi.org/10.1093/cvr/cvz228

Mizuno, A. (2000). Electrostatic precipitation. *IEEE Transactions on Dielectrics and Electrical Insulation*, *7*(5), 615-624. https://doi.org/10.1109/94.879357

Mosleh, S., Rahimi, M. R., Ghaedi, M., Dashtian, K., & Hajati, S. (2016). BiPO4/Bi2S3-HKUST-1-MOF as a novel blue light-driven photocatalyst for simultaneous degradation of toluidine blue and auramine-O dyes in a new rotating packed bed reactor: optimization and comparison to a conventional reactor. *RSC advances*, *6*(68), 63667-63680. https://doi.org/10.1039/c6ra10385e

Natarajan, T. S., Thampi, K. R., & Tayade, R. J. (2018). Visible light driven redox-mediator-free dual semiconductor photocatalytic systems for pollutant degradation and the ambiguity in applying Z-scheme concept. *Applied Catalysis B-Environmental*, *227*, 296-

311. https://doi.org/10.1016/j.apcatb.2018.01.015

Nikokavoura, A., & Trapalis, C. (2018). Graphene and g-C3N4 based photocatalysts for NOx removal: A review. *Applied Surface Science, 430*, 18-52. https://doi.org/10.1016/j.apsusc.2017.08.192

O'Donnell, M. D., Fredholm, Y., de Rouffignac, A., & Hill, R. G. (2008). Structural analysis of a series of strontium-substituted apatites. *Acta Biomater*, *4*(5), 1455-1464. https://doi.org/10.1016/j.actbio.2008.04.018

OEHHA. (2023). *OEHHA Chemical Database.*

Olson, D. A., & Burke, J. M. (2006). Distributions of PM2.5 source strengths for cooking from the Research Triangle Park particulate matter panel study. *Environ Sci Technol*, *40*(1), 163-169. https://doi.org/10.1021/es050359t

Ouyang, S., Tong, H., Umezawa, N., Cao, J., Li, P., Bi, Y., Zhang, Y., & Ye, J. (2012). Surface-alkalinization-induced enhancement of photocatalytic H2 evolution over SrTiO3-based photocatalysts. *J Am Chem Soc*, *134*(4), 1974-1977. https://doi.org/10.1021/ja210610h

Pan, S. Y., Chen, Y. H., Chen, C. D., Shen, A. L., Lin, M., & Chiang, P. C. (2015). High-Gravity Carbonation Process for Enhancing CO2 Fixation and Utilization Exemplified by the Steelmaking Industry. *Environ Sci Technol*, *49*(20), 12380-12387. https://doi.org/10.1021/acs.est.5b02210

Pan, S. Y., Chiang, P. C., Chen, Y. H., Tan, C. S., & Chang, E. E. (2013). Ex Situ CO2 capture by carbonation of steelmaking slag coupled with metalworking wastewater in a rotating packed bed. *Environ Sci Technol*, *47*(7), 3308-3315. https://doi.org/10.1021/es304975y

Pan, S. Y., Wang, P. C., Chen, Q., Jiang, W. J., Chu, Y. H., & Chiang, P. C. (2017).

Development of high-gravity technology for removing particulate and gaseous pollutant emissions: Principles and applications. *Journal of Cleaner Production*, *149*, 540-556. https://doi.org/10.1016/j.jclepro.2017.02.108

Parul, Kaur, K., Badru, R., Singh, P. P., & Kaushal, S. (2020). Photodegradation of organic pollutants using heterojunctions: A review. *Journal of Environmental Chemical Engineering*, *8*(2), 103666. https://doi.org/10.1016/j.jece.2020.103666

Paterson, C. A., Sharpe, R. A., Taylor, T., & Morrissey, K. (2021). Indoor PM2.5, VOCs and asthma outcomes: A systematic review in adults and their home environments. *Environ Res*, *202*, 111631. https://doi.org/10.1016/j.envres.2021.111631

Peng, C. Y., Lan, C. H., Lin, P. C., & Kuo, Y. C. (2017). Effects of cooking method, cooking oil, and food type on aldehyde emissions in cooking oil fumes. *J Hazard Mater*, *324*(Pt B), 160-167. https://doi.org/10.1016/j.jhazmat.2016.10.045

Peters, A., von Klot, S., Heier, M., Trentinaglia, I., Hormann, A., Wichmann, H. E., Lowel, H., & Cooperative Health Research in the Region of Augsburg Study, G. (2004). Exposure to traffic and the onset of myocardial infarction. *N Engl J Med*, *351*(17), 1721-1730. https://doi.org/10.1056/NEJMoa040203

Pongpiacha, S., Kudo, S., & Sekiguchi, K. (2014). Chemical Characterization of Carbonaceous PM10 in Bangkok, Thailand. *Asian Journal of Applied Sciences*, *7*(5), 325-342. https://doi.org/10.3923/ajaps.2014.325.342

Qi, G., Liu, Y., & Jiao, W. (2008). Desulfurization by high gravity technology. *Chem. Ind. Eng. Prog*, *27*, 1404-1407.

Qu, L., Liu, Y., Chu, S., Zhang, Y., & Jiao, W. (2011). Application of high gravity technology in gas purification. *Natural Gas Chem. Ind*, *2*, 55-59.

Rajagopalan, S., Al-Kindi, S. G., & Brook, R. D. (2018). Air Pollution and Cardiovascular

Disease: JACC State-of-the-Art Review. *J Am Coll Cardiol*, *72*(17), 2054-2070. https://doi.org/10.1016/j.jacc.2018.07.099

Ramshaw, C. (1979). Mass transfer apparatus and its use. *European Patent 0,002,568*.

Ran, J., Guo, W., Wang, H., Zhu, B., Yu, J., & Qiao, S. Z. (2018). Metal-Free 2D/2D Phosphorene/g-C(3) N(4) Van der Waals Heterojunction for Highly Enhanced Visible-Light Photocatalytic H(2) Production. *Adv Mater*, *30*(25), e1800128. https://doi.org/10.1002/adma.201800128

Rao, D. P. (2022). Commentary: Evolution of High Gravity (HiGee) Technology. *Industrial & Engineering Chemistry Research*, *61*(2), 997-1003. https://doi.org/10.1021/acs.iecr.1c04587

Rao, D. P., Bhowal, A., & Goswami, P. S. (2004). Process intensification in rotating packed beds (HIGEE): An appraisal. *Industrial & Engineering Chemistry Research*, *43*(4), 1150-1162. https://doi.org/10.1021/ie030630k

Risto, K., & Panu, M. (2016). Analysis of Capture and Containment Efficiency of a Ventilated Ceiling. *International Journal of Ventilation*, *2*(1), 33-43. https://doi.org/10.1080/14733315.2003.11683651

Robertson, S., & Miller, M. R. (2018). Ambient air pollution and thrombosis. *Part Fibre Toxicol*, *15*(1), 1. https://doi.org/10.1186/s12989-017-0237-x

Rogge, W. F., Hildemann, L. M., Mazurek, M. A., Cass, G. R., & Simonelt, B. R. T. (1991). Sources of Fine Organic Aerosol .1. Charbroilers and Meat Cooking Operations. *Environmental Science & Technology*, *25*(6), 1112-1125. https://doi.org/10.1021/es00018a015

Rosales, C. M. F., Jiang, J., Lahib, A., Bottorff, B. P., Reidy, E. K., Kumar, V., Tasoglou, A., Huber, H., Dusanter, S., Tomas, A., Boor, B. E., & Stevens, P. S. (2022). Chemistry and human exposure implications of secondary organic aerosol production from indoor terpene ozonolysis. *Sci Adv*, *8*(8), eabj9156. https://doi.org/10.1126/sciadv.abj9156

Roy, F., Peter, K., & Russ, C. (2021). *INDOOR AIR QUALITY: RESIDENTIAL COOKING EXPOSURES*.

Sankhyan, S., Zabinski, K., O'Brien, R. E., Coyan, S., Patel, S., & Vance, M. E. (2022). Aerosol emissions and their volatility from heating different cooking oils at multiple temperatures. *Environmental Science-Atmospheres*, *2*(6), 1364-1375. https://doi.org/10.1039/d2ea00099g

Schauer, J. J., Kleeman, M. J., Cass, G. R., & Simoneit, B. R. (2002). Measurement of emissions from air pollution sources. 4. C1-C27 organic compounds from cooking with seed oils. *Environ Sci Technol*, *36*(4), 567-575. https://doi.org/10.1021/es002053m

Schauer, J. J., Kleeman, M. J., Cass, G. R., & Simoneit, B. R. T. (2001). Measurement of Emissions from Air Pollution Sources. 3. C1 −C29 Organic Compounds from Fireplace Combustion of Wood. In: American Chemical Society (ACS).

Schiavoni, S., D'Alessandro, F., Bianchi, F., & Asdrubali, F. (2016). Insulation materials for the building sector: A review and comparative analysis. *Renewable & Sustainable Energy Reviews*, *62*, 988-1011. https://doi.org/10.1016/j.rser.2016.05.045

See, S. W., & Balasubramanian, R. (2008). Chemical characteristics of fine particles emitted from different gas cooking methods. *Atmospheric Environment*, *42*(39), 8852-8862. https://doi.org/10.1016/j.atmosenv.2008.09.011

Shah, N. S., & Soylak, M. (2022). Advanced Methodologies for Trace Elements in Edible Oil Samples: A Review. *Crit Rev Anal Chem*, *52*(7), 1572-1582. https://doi.org/10.1080/10408347.2021.1895710

Shawabkeh, R. A., Faqir, N. M., Rawajfeh, K. M., Hussein, I. A., & Hamza, A. (2022).

Adsorption of CO2 on Cu/SiO2 nano-catalyst: Experimental and theoretical study. *Applied Surface Science*, *586*, 152726. https://doi.org/ARTN 152726

10.1016/j.apsusc.2022.152726

Shen, Z.-g., Chen, J.-f., & Zhong, J. (2004). Properties of cephradine produced by high gravity technology. *CHINESE PHARMACEUTICAL JOURNAL-BEIJING-*, *39*(1), 36-39.

Shen, Z. X., Cao, J. J., Arimoto, R., Zhang, R. J., Jie, D. M., Liu, S. X., & Zhu, C. S. (2007). Chemical composition and source characterization of spring aerosol over Horqin sand land in northeastern China. *Journal of Geophysical Research-Atmospheres*, *112*(D14). https://doi.org/10.1029/2006jd007991

Shen, Z. X., Wang, X., Zhang, R. J., Ho, K. F., Cao, J. J., & Zhang, M. G. (2011). Chemical Composition of Water-soluble Ions and Carbonate Estimation in Spring Aerosol at a Semi-arid Site of Tongyu, China. *Aerosol and Air Quality Research*, *11*(4), 360-368. https://doi.org/10.4209/aaqr.2011.02.0010

Sheng, Y., Zhang, L., Wang, Y. Q., & Miao, Z. Z. (2020). Exploration of a novel three-dimensional knitted spacer air filter with low pressure drop on cooking fume particles removal. *Building and Environment*, *177*, 106903. https://doi.org/ARTN 106903

10.1016/j.buildenv.2020.106903

Shevchenko, N. (2012). Problem of grease and its solutions in commercial kitchens.

Shie, J. L., Lee, C. H., Chiou, C. S., Chang, C. T., Chang, C. C., & Chang, C. Y. (2008). Photodegradation kinetics of formaldehyde using light sources of UVA, UVC and UVLED in the presence of composed silver titanium oxide photocatalyst. *J Hazard Mater*, *155*(1-2), 164-172. https://doi.org/10.1016/j.jhazmat.2007.11.043

Shtarev, D. S., Shtareva, A. V., Kevorkyants, R., & Syuy, A. V. (2021). Synthesis, characterization, optoelectronic and photocatalytic properties of Sr2Bi2O5/SrCO3 and

Sr3Bi2O6/SrCO3 heterostructures with varying SrCO3 content. *Chemosphere*, *267*, 129229. https://doi.org/ARTN 129229

10.1016/j.chemosphere.2020.129229

Singh, S. P., Wilson, J. H., Counce, R. M., Villiersfisher, J. F., Jennings, H. L., Lucero, A. J., Reed, G. D., Ashworth, R. A., & Elliott, M. G. (1992). Removal of Volatile Organic-Compounds from Groundwater Using a Rotary Air Stripper. *Industrial & Engineering Chemistry Research*, *31*(2), 574-580. https://doi.org/10.1021/ie00002a019

Son, J. H., Shi, L., Zhang, W., Bai, Z., Li, L., Wang, L., & Chen, J. (2022). Characteristics of non-methane hydrocarbons emitted from Chinese kitchens and their effect on ozone formation potential. *Air Quality, Atmosphere & Health*, *16*(3), 583-593. https://doi.org/10.1007/s11869-022-01292-y

Song, K., Guo, S., Gong, Y. Z., Lv, D. Q., Zhang, Y., Wan, Z. C., Li, T. Y., Zhu, W. F., Wang, H., Yu, Y., Tan, R., Shen, R. Z., Lu, S. H., Li, S. D., Chen, Y. F., & Hu, M. (2022). Impact of cooking style and oil on semi-volatile and intermediate volatility organic compound emissions from Chinese domestic cooking. *Atmospheric Chemistry and Physics*, *22*(15), 9827-9841. https://doi.org/10.5194/acp-22-9827-2022

Sosulnikov, M. I., & Teterin, Y. A. (1991). X-Ray Photoelectron Study of Calcium, Strontium, Barium and Their Oxides. *Doklady Akademii Nauk SSSR*, *317*(2), 418-421. <Go to ISI>://WOS:A1991FN29200042

Sun, C., Zhao, L., Chen, X., Nie, L., Shi, A., Bai, H., & Li, G. (2022). A comprehensive study of volatile organic compounds from the actual emission of Chinese cooking. *Environmental Science and Pollution Research*, *29*(35), 53821-53830. https://doi.org/10.1007/s11356-022-19342-4

Sun, J., Shen, Z. X., Niu, X. Y., Yu, J. J., Zhang, Y., Liu, S. X., Niu, X. F., Zhang, Y., Xu,

H. M., Li, X. X., & Cao, J. J. (2020). PM2.5 source profiles from typical Chinese commercial cooking activities in northern China and its influences on bioreactivity of vascular smooth muscle cells (VSMCs). *Atmospheric Environment*, *239*, 117750. https://doi.org/ARTN 117750

10.1016/j.atmosenv.2020.117750

Sun, Y., Li, N., Xing, X., Zhang, X., Zhang, Z., Wang, G., Cheng, J., & Hao, Z. (2019). Catalytic oxidation performances of typical oxygenated volatile organic compounds (acetone and acetaldehyde) over MAlO (M = Mn, Co, Ni, Fe) hydrotalcite-derived oxides. *Catalysis Today*, *327*, 389-397. https://doi.org/10.1016/j.cattod.2018.03.002

Svedahl, S. R., Hilt, B., & Svendsen, K. (2020). Work environment factors and respiratory complaints in Norwegian cooks. *Int Arch Occup Environ Health*, *93*(2), 205-212. https://doi.org/10.1007/s00420-019-01473-w

Takhar, M., Li, Y. C., & Chan, A. W. H. (2021). Characterization of secondary organic aerosol from heated-cooking-oil emissions: evolution in composition and volatility. *Atmospheric Chemistry and Physics*, *21*(6), 5137-5149. https://doi.org/10.5194/acp-21-5137-2021

Tan, H., Zhao, Z., Zhu, W. B., Coker, E. N., Li, B., Zheng, M., Yu, W., Fan, H., & Sun, Z. (2014). Oxygen vacancy enhanced photocatalytic activity of pervoskite SrTiO(3). *ACS Appl Mater Interfaces*, *6*(21), 19184-19190. https://doi.org/10.1021/am5051907

Tan, Y., Han, S., Chen, Y., Wu, Z., & Lee, S. C. (2023). Long-term variation and evaluation of air quality across Hong Kong. *J Environ Sci (China)*, *127*, 284-294. https://doi.org/10.1016/j.jes.2022.05.009

Tan, Y., Han, S. W., Chen, Y., Zhang, Z. Z., Li, H. W., Li, W. Q., Yuan, Q., Li, X. W., Wang, T., & Lee, S. C. (2021). Characteristics and source apportionment of volatile organic compounds (VOCs) at a coastal site in Hong Kong. *Science of the Total Environment*, *777*, 146241. https://doi.org/10.1016/j.scitotenv.2021.146241

Taner, S., Pekey, B., & Pekey, H. (2013). Fine particulate matter in the indoor air of barbeque restaurants: elemental compositions, sources and health risks. *Science of the Total Environment*, *454-455*, 79-87. https://doi.org/10.1016/j.scitotenv.2013.03.018

Tao, C., He, L. M., Zhou, X. C., Li, H. J., Ren, Q. Q., Han, H. D., Hu, S., Su, S., Wang, Y., & Xiang, J. (2023). Review of Emission Characteristics and Purification Methods of Volatile Organic Compounds (VOCs) in Cooking Oil Fume. *Processes*, *11*(3), 705. https://doi.org/10.3390/pr11030705

Tian, E. Z., Mo, J. H., & Li, X. F. (2018). Electrostatically assisted metal foam coarse filter with small pressure drop for efficient removal of fine particles: Effect of filter medium. *Building and Environment*, *144*, 419-426. https://doi.org/10.1016/j.buildenv.2018.08.026

Tu, G. M., Song, Q., & Yao, Q. (2017). Experimental and numerical study of particle deposition on perforated plates in a hybrid electrostatic filter precipitator. *Powder Technology*, *321*, 143-153. https://doi.org/10.1016/j.powtec.2017.08.021

Tung, Y. H., Ko, J. L., Liang, Y. F., Yin, L., Pu, Y., & Lin, P. (2001). Cooking oil fume-induced cytokine expression and oxidative stress in human lung epithelial cells. *Environ Res*, *87*(1), 47-54. https://doi.org/10.1006/enrs.2001.4272

U.S.EPA. (2004). *Risk assessment guidance for superfund (RAGS)* (Vol. 1).

USEPA. *Particulate Matter (PM) Basics*. https://www.epa.gov/pm-pollution/particulate-matter-pm-basics

USEPA. (2023). *National Ambient Air Quality Standards*. https://www.epa.gov/criteria-air-pollutants/naaqs-table

Wallace, L. (2006). Indoor sources of ultrafine and accumulation mode particles: Size distributions, size-resolved concentrations, and source strengths. *Aerosol science and technology*, *40*(5), 348-360. https://doi.org/10.1080/02786820600612250

Wan, M. P., Wu, C. L., Szeto, G. N., Chan, T. C., & Chao, C. Y. H. (2011). Ultrafine particles, and PM2.5 generated from cooking in homes. *Atmospheric Environment*, *45*(34), 6141-6148. https://doi.org/10.1016/j.atmosenv.2011.08.036

Wang, B., Lau, Y. S., Huang, Y., Organ, B., Chuang, H. C., Ho, S. S. H., Qu, L., Lee, S. C., & Ho, K. F. (2021). Chemical and toxicological characterization of particulate emissions from diesel vehicles. *J Hazard Mater*, *405*, 124613. https://doi.org/10.1016/j.jhazmat.2020.124613

Wang, C. Y., Liu, L. F., Liu, X. L., Chen, W. J., & He, G. P. (2017). Mechanisms of Lung Cancer Caused By Cooking Fumes Exposure: A Minor Review(big up tri, open). *Chin Med Sci J*, *32*(3), 193-197. https://doi.org/10.24920/J1001-9294.2017.026

Wang, D. N., Guo, Y. Q., Liang, K. M., & Tao, K. (1999). Crystal structure of zirconia by Rietveld refinement. *Science in China Series a-Mathematics*, *42*(1), 80-86. https://doi.org/10.1007/Bf02872053

Wang, G., Bai, Y., Fu, W., Feng, Y., Chen, W., Li, G., Wu, X., Meng, H., Liu, Y., Wei, W., Wang, S., Wei, S., Zhang, X., He, M., Yang, H., & Guo, H. (2019). Daily cooking duration and its joint effects with genetic polymorphisms on lung cancer incidence: Results from a Chinese prospective cohort study. *Environ Res*, *179*(Pt A), 108747. https://doi.org/10.1016/j.envres.2019.108747

Wang, G., Cheng, S. Y., Wei, W., Wen, W., Wang, X. Q., & Yao, S. (2015). Chemical Characteristics of Fine Particles Emitted from Different Chinese Cooking Styles. *Aerosol and Air Quality Research*, *15*(6), 2357-2366. https://doi.org/10.4209/aaqr.2015.02.0079

Wang, H., Sun, Y., Jiang, G., Zhang, Y., Huang, H., Wu, Z., Lee, S. C., & Dong, F. (2018).

Unraveling the Mechanisms of Visible Light Photocatalytic NO Purification on Earth-Abundant Insulator-Based Core-Shell Heterojunctions. *Environ Sci Technol*, *52*(3), 1479-1487. https://doi.org/10.1021/acs.est.7b05457

Wang, H. L., Qiao, Y. Z., Chen, C. H., Lu, J., Dai, H. X., Qiao, L. P., Lou, S. R., Huang, C., Li, L., Jing, S. G., & Wu, J. P. (2014). Source Profiles and Chemical Reactivity of Volatile Organic Compounds from Solvent Use in Shanghai, China. *Aerosol and Air Quality Research*, *14*(1), 301-310. https://doi.org/10.4209/aaqr.2013.03.0064

Wang, H. L., Xiang, Z. Y., Wang, L. N., Jing, S. G., Lou, S. R., Tao, S. K., Liu, J., Yu, M. Z., Li, L., Lin, L., Chen, Y., Wiedensohler, A., & Chen, C. H. (2018). Emissions of volatile organic compounds (VOCs) from cooking and their speciation: A case study for Shanghai with implications for China. *Science of the Total Environment*, *621*, 1300-1309. https://doi.org/10.1016/j.scitotenv.2017.10.098

Wang, Z. Y., Huang, Y., Ho, W. K., Cao, J. J., Shen, Z. X., & Lee, S. C. (2016). Fabrication of Bi2O2CO3/g-C3N4 heterojunctions for efficiently photocatalytic NO in air removal: In-situ self-sacrificial synthesis, characterizations and mechanistic study. *Applied Catalysis B-Environmental*, *199*, 123-133. https://doi.org/10.1016/j.apcatb.2016.06.027

Wei, Q., Qiao, S. F., Sun, B. C., Zou, H. K., Chen, J. F., & Shao, L. (2015). Study on the treatment of simulated coking wastewater by O-3 and O-3/Fenton processes in a rotating packed bed. *RSC advances*, *5*(113), 93386-93393. https://doi.org/10.1039/c5ra14198b

Wei See, S., Karthikeyan, S., & Balasubramanian, R. (2006). Health risk assessment of occupational exposure to particulate-phase polycyclic aromatic hydrocarbons associated with Chinese, Malay and Indian cooking. *J Environ Monit*, *8*(3), 369-376. https://doi.org/10.1039/b516173h

Whalley, L. K., Slater, E. J., Woodward-Massey, R., Ye, C., Lee, J. D., Squires, F., Hopkins,

J. R., Dunmore, R. E., Shaw, M., Hamilton, J. F., Lewis, A. C., Mehra, A., Worrall, S. D., Bacak, A., Bannan, T. J., Coe, H., Percival, C. J., Ouyang, B., Jones, R. L., . . . Heard, D. E. (2021). Evaluating the sensitivity of radical chemistry and ozone formation to ambient VOCs and NO_{<i>x</i>} in Beijing. *Atmospheric Chemistry and Physics*, *21*(3), 2125-2147. https://doi.org/10.5194/acp-21-2125-2021

WHO. (2021). *WHO global air quality guidelines: particulate matter (PM2. 5 and PM10), ozone, nitrogen dioxide, sulfur dioxide and carbon monoxide*. WHO.

Wilhelm, P. C., & Wilhelm, D. S. (1960). Apparatus for intimate contacting of two fluid media having different specific weight. In: Google Patents.

Wolska, L., Mechlinska, A., Rogowska, J., & Namiesnik, J. (2012). Sources and Fate of PAHs and PCBs in the Marine Environment. *Critical Reviews in Environmental Science and Technology*, *42*(11), 1172-1189. https://doi.org/10.1080/10643389.2011.556546

Wu, P. F., Chiang, T. A., Wang, L. F., Chang, C. S., & Ko, Y. C. (1998). Nitro-polycyclic aromatic hydrocarbon contents of fumes from heated cooking oils and prevention of mutagenicity by catechin. *Mutat Res*, *403*(1-2), 29-34. https://doi.org/10.1016/s0027-5107(98)00015-3

Xiang, Z. Y., Wang, H. L., Stevanovic, S., Jing, S. G., Lou, S., Tao, S., Li, L., Liu, J., Yu, M. Z., & Wang, L. N. (2017). Assessing impacts of factors on carbonyl compounds emissions produced from several typical Chinese cooking. *Building and Environment*, *125*, 348-355. https://doi.org/10.1016/j.buildenv.2017.08.045

Ximin, H., Jiaoping, X., & Shuanghong, S. (2008). Use of Ultragravity Separator in Shift Effluent Desulfurization Unit. *HUAFEI GONGYE, 35*(2), 52.

Xing, Y., Liu, Y., & Cui, L. (2007). Experimental study on intensification absorption of carbon dioxide from simulation flue gas by high-gravity rotary packed bed. Mod. *Chem.*

Ind, *27*, 470-473.

Xiong, H., & Zhang, Q. G. (2009). Purifying equipment with self-suction and vortex plate for removing cooking-oil smoke. *Environmental Science and Technology*, *32*(3), 54-56.

Xiong, J., Di, J., Xia, J. X., Zhu, W. S., & Li, H. M. (2018). Surface Defect Engineering in 2D Nanomaterials for Photocatalysis. *Advanced Functional Materials*, *28*(39), 1801983. https://doi.org/ARTN 1801983

10.1002/adfm.201801983

Xu, H., Ta, W., Yang, L., Feng, R., He, K., Shen, Z., Meng, Z., Zhang, N., Li, Y., Zhang, Y., Lu, J., Li, X., Qu, L., Ho, S. S. H., & Cao, J. (2020). Characterizations of PM(2.5)-bound organic compounds and associated potential cancer risks on cooking emissions from dominated types of commercial restaurants in northwestern China. *Chemosphere*, *261*, 127758. https://doi.org/10.1016/j.chemosphere.2020.127758

Xu, J., Chen, J., Zou, H., Chu, G., & Zhao, H. (2013). Application of high-gravity desulfurization technology in sulfuric acid industry. *Sulphur Phosphorus & Bulk Mater. Handl. Relat. Eng. 32e36*.

Xu, Y., & Schoonen, M. A. A. (2000). The absolute energy positions of conduction and valence bands of selected semiconducting minerals. *American Mineralogist*, *85*(3-4), 543-556. https://doi.org/DOI 10.2138/am-2000-0416

Xue, C. F., Liu, Y. Z., & Jiao, W. Z. (2016). Mass transfer of acrylonitrile wastewater treatment by high gravity air stripping technology. *Desalination and Water Treatment*, *57*(27), 12424-12432. https://doi.org/10.1080/19443994.2015.1054314

Xue, J., Liu, J. X., Liu, Y. M., Li, H. L., Wang, Y., Sun, D., Wang, W., Huang, L. J., & Tang, J. G. (2019). Recent advances in synthetic methods and applications of Ag2S-based heterostructure photocatalysts. *Journal of Materials Chemistry C*, *7*(14), 3988-4003.

https://doi.org/10.1039/c9tc00008a

Yamashita, K., Yoshioka, Y., Higashisaka, K., Mimura, K., Morishita, Y., Nozaki, M., Yoshida, T., Ogura, T., Nabeshi, H., Nagano, K., Abe, Y., Kamada, H., Monobe, Y., Imazawa, T., Aoshima, H., Shishido, K., Kawai, Y., Mayumi, T., Tsunoda, S., . . . Tsutsumi, Y. (2011). Silica and titanium dioxide nanoparticles cause pregnancy complications in mice. *Nat Nanotechnol*, *6*(5), 321-328. https://doi.org/10.1038/nnano.2011.41

Yang, Y., Wang, Y., Yao, D., Zhao, S., Yang, S., Ji, D., Sun, J., Wang, Y., Liu, Z., Hu, B., Zhang, R., & Wang, Y. (2020). Significant decreases in the volatile organic compound concentration, atmospheric oxidation capacity and photochemical reactivity during the National Day holiday over a suburban site in the North China Plain. *Environ Pollut*, *263*(Pt A), 114657. https://doi.org/10.1016/j.envpol.2020.114657

Yang, Z., Shi, Y., Li, H., Mao, C., Wang, X., Liu, X., Liu, X., & Zhang, L. (2022). Oxygen and Chlorine Dual Vacancies Enable Photocatalytic O(2) Dissociation into Monatomic Reactive Oxygen on BiOCl for Refractory Aromatic Pollutant Removal. *Environ Sci Technol*, *56*(6), 3587-3595. https://doi.org/10.1021/acs.est.1c08532

Yatera, K., Hsieh, J., Hogg, J. C., Tranfield, E., Suzuki, H., Shih, C. H., Behzad, A. R., Vincent, R., & van Eeden, S. F. (2008). Particulate matter air pollution exposure promotes recruitment of monocytes into atherosclerotic plaques. *American Journal of Physiology-Heart and Circulatory Physiology*, *294*(2), H944-H953. https://doi.org/10.1152/ajpheart.00406.2007

Ye, X., Fangueiro, R., Hu, H., & de Araujo, M. (2007). Application of warp-knitted spacer fabrics in car seats. *Journal of the Textile Institute*, *98*(4), 337-343. https://doi.org/10.1080/00405000701489677

Yi, F., Zou, H. K., Chu, G. W., Shao, L., & Chen, J. F. (2009). Modeling and experimental studies on absorption of CO2 by Benfield solution in rotating packed bed. *Chemical Engineering Journal*, *145*(3), 377-384. https://doi.org/10.1016/j.cej.2008.08.004

Yi, H. H., Huang, Y. H., Tang, X. L., Zhao, S. Z., Xie, X. Z., & Zhang, Y. Y. (2019). Characteristics of non-methane hydrocarbons and benzene series emission from commonly cooking oil fumes. *Atmospheric Environment*, *200*, 208-220. https://doi.org/10.1016/j.atmosenv.2018.12.018

Yoon, S. H., Kim, S. K., Kim, K. H., Kwon, T. W., & Teah, Y. K. (1987). Evaluation of Physicochemical Changes in Cooking Oil during Heating. *Journal of the American Oil Chemists Society*, *64*(6), 870-873. https://doi.org/10.1007/Bf02641496

Yu, G., Qian, J., Zhang, P., Zhang, B., Zhang, W., Yan, W., & Liu, G. (2019). Collective excitation of plasmon-coupled Au-nanochain boosts photocatalytic hydrogen evolution of semiconductor. *Nat Commun*, *10*(1), 4912. https://doi.org/10.1038/s41467-019-12853-8

Yu, I. T. S., Chiu, Y. L., Au, J. S. K., Wong, T. W., & Tang, J. L. (2006). Dose-response relationship between cooking fumes exposures and lung cancer among Chinese nonsmoking women. *Cancer research*, *66*(9), 4961-4967. https://doi.org/10.1158/0008-5472.Can-05-2932

Yuan, M. H., Chen, Y. H., Tsai, J. Y., & Chang, C. Y. (2016). Ammonia removal from ammonia-rich wastewater by air stripping using a rotating packed bed. *Process Safety and Environmental Protection*, *102*, 777-785. https://doi.org/10.1016/j.psep.2016.06.021

Zeng, Z., Zou, H., Li, X., Sun, B., Chen, J., & Shao, L. (2012). Ozonation of Phenol with O3/Fe(II) in Acidic Environment in a Rotating Packed Bed. *Industrial & Engineering Chemistry Research*, *51*(31), 10509-10516. https://doi.org/10.1021/ie300476d

Zeng, Z. Q., Wang, J. F., Li, Z. H., Sun, B. C., Shao, L., Li, W. J., Chen, J. F., & Zou, H. K. (2013). The Advanced Oxidation Process of Phenol Solution by O3/H2O2 in a Rotating

Packed Bed. *Ozone-Science & Engineering*, *35*(2), 101-108. https://doi.org/10.1080/01919512.2013.759869

Zhang, D. C., Liu, J. J., Jia, L. Z., Wang, P., & Han, X. (2019). Speciation of VOCs in the cooking fumes from five edible oils and their corresponding health risk assessments. *Atmospheric Environment*, *211*, 6-17. https://doi.org/10.1016/j.atmosenv.2019.04.043

Zhang, G. Q., Ding, C., Jiang, X. J., Pan, G., Wei, X. F., & Sun, Y. M. (2020). Chemical Compositions and Sources Contribution of Atmospheric Particles at a Typical Steel Industrial Urban Site. *Scientific Reports*, *10*(1), 7654. https://doi.org/10.1038/s41598-020-64519-x

Zhang, H., Wang, X., Shen, X., Li, X., Wu, B., Li, G., Bai, H., Cao, X., Hao, X., Zhou, Q., & Yao, Z. (2023). Chemical characterization of volatile organic compounds (VOCs) emitted from multiple cooking cuisines and purification efficiency assessments. *J Environ Sci (China)*, *130*, 163-173. https://doi.org/10.1016/j.jes.2022.08.008

Zhang, N., Han, B., He, F., Xu, J., Zhao, R., Zhang, Y., & Bai, Z. (2017). Chemical characteristic of PM(2.5) emission and inhalational carcinogenic risk of domestic Chinese cooking. *Environ Pollut*, *227*, 24-30. https://doi.org/10.1016/j.envpol.2017.04.033

Zhang, P., Huang, Y., Rao, Y. F., Chen, M. J., Li, X. W., Ho, W. K., Lee, S. C., & Cao, J. J. (2021). Chemical etching fabrication of uniform mesoporous Bi@Bi2O3 nanospheres with enhanced visible light-induced photocatalytic oxidation performance for NOx. *Chemical Engineering Journal*, *406*, 126910. https://doi.org/ARTN 126910

10.1016/j.cej.2020.126910

Zhang, W., Yu, Y., & Yi, Z. G. (2017). Controllable synthesis of SrCO3 with different morphologies and their co-catalytic activities for photocatalytic oxidation of hydrocarbon gases over TiO2. *Journal of Materials Science*, *52*(9), 5106-5116.

https://doi.org/10.1007/s10853-017-0748-8

Zhang, X. X., Ding, X., Wang, X. M., Talifu, D., Wang, G., Zhang, Y. L., & Abulizi, A. (2019). Volatile Organic Compounds in a Petrochemical Region in Arid of NW China: Chemical Reactivity and Source Apportionment. *Atmosphere*, *10*(11), 641. https://doi.org/ARTN 641

10.3390/atmos10110641

Zhang, Y. F., Huang, Y., Lee, S. C., & Cao, J. J. (2020). The mechanism of room temperature catalytic C-H dissociation and oxygenation of formaldehyde over nano-zirconia phase-junction. *Chemical Engineering Journal*, *380*, 122498. https://doi.org/ARTN 122498

10.1016/j.cej.2019.122498

Zhang, Y. H., Tang, Z. R., Fu, X. Z., & Xu, Y. J. (2011). Nanocomposite of Ag-AgBr-TiO2 as a photoactive and durable catalyst for degradation of volatile organic compounds in the gas phase. *Applied Catalysis B-Environmental*, *106*(3-4), 445-452. https://doi.org/10.1016/j.apcatb.2011.06.002

Zhang, Z. J., Wang, H., Chen, D., Li, Q. Q., Thai, P., Gong, D. C., Li, Y., Zhang, C. L., Gu, Y. G., Zhou, L., Morawska, L., & Wang, B. G. (2017). Emission characteristics of volatile organic compounds and their secondary organic aerosol formation potentials from a petroleum refinery in Pearl River Delta, China. *Science of the Total Environment*, *584*, 1162-1174. https://doi.org/10.1016/j.scitotenv.2017.01.179

Zhang, Z. Z., Yuan, Q., Wang, M., Hu, T. F., Huang, Y., Xiu, G. L., Lai, S. C., Gao, Y., & Lee, S. C. (2023). Exposure and health risk assessment of PM2.5-bound polycyclic aromatic hydrocarbons during winter at residential homes: A case study in four Chinese cities. *Science of the Total Environment*, *895*, 165111. https://doi.org/ARTN 165111

10.1016/j.scitotenv.2023.165111

Zhao, D., & You, X.-Y. (2021). Cooking grease particles purification review and technology combination strategy evaluation for commercial kitchens. *Building Simulation*. https://doi.org/10.1007/s12273-021-0767-x

Zhao, D. F., & You, X. Y. (2021). Cooking grease particles purification review and technology combination strategy evaluation for commercial kitchens. *Building Simulation*, *14*(6), 1597-1617. https://doi.org/10.1007/s12273-021-0767-x

Zhao, H., Shao, L., & Chen, J. F. (2010). High-gravity process intensification technology and application. *Chemical Engineering Journal*, *156*(3), 588-593. https://doi.org/10.1016/j.cej.2009.04.053

Zhao, H., Wang, J., Zhang, H., Shen, Z., Yun, J., & Chen, J. (2009). Facile Preparation of Danazol Nanoparticles by High-Gravity Anti-solvent Precipitation (HGAP) Method. *Chinese Journal of Chemical Engineering*, *17*(2), 318-323. https://doi.org/10.1016/s1004-9541(08)60210-4

Zhao, Q. C., Chen, C., Zhang, J. T., Hu, P. J., & Zhang, X. J. (2021). Performance of Cooking Aerosol Treatment in China Catering: a Review and Assessment [journal article]. *Polish Journal of Environmental Studies*, *30*(2), 1923-1933. https://doi.org/10.15244/pjoes/125939

Zhao, Y. J., Chen, C., & Zhao, B. (2019). Emission characteristics of PM2.5-bound chemicals from residential Chinese cooking. *Building and Environment*, *149*, 623-629. https://doi.org/10.1016/j.buildenv.2018.12.060

Zhao, Y. J., Liu, L., Tao, P. F., Zhang, B., Huan, C., Zhang, X. A., & Wang, M. (2019). Review of Effluents and Health Effects of Cooking and the Performance of Kitchen Ventilation. *Aerosol and Air Quality Research*, *19*(8), 1937-1959.

https://doi.org/10.4209/aaqr.2019.04.0198

Zhao, Y. J., & Zhao, B. (2018). Emissions of air pollutants from Chinese cooking: A literature review. *Building Simulation*, *11*(5), 977-995. https://doi.org/10.1007/s12273-018-0456-6

Zheng, Y., Chen, Q., Cheng, X., Mohr, C., Cai, J., Huang, W., Shrivastava, M., Ye, P., Fu, P., Shi, X., Ge, Y., Liao, K., Miao, R., Qiu, X., Koenig, T. K., & Chen, S. (2021). Precursors and Pathways Leading to Enhanced Secondary Organic Aerosol Formation during Severe Haze Episodes. *Environ Sci Technol*, *55*(23), 15680-15693. https://doi.org/10.1021/acs.est.1c04255

Zhong, J., Shen, Z., Yang, Y., & Chen, J. (2005). Preparation and characterization of uniform nanosized cephradine by combination of reactive precipitation and liquid anti-solvent precipitation under high gravity environment. *Int J Pharm*, *301*(1-2), 286-293. https://doi.org/10.1016/j.ijpharm.2005.06.005

Zhou, Q., & Qin, B. T. (2021). Coal dust suppression based on water mediums: A review of technologies and influencing factors. *Fuel*, *302*, 121196. https://doi.org/ARTN 121196 10.1016/j.fuel.2021.121196

Zhu, H., Wang, L., Liu, C., Stryker, Z., Loganathan, B. G., & Kannan, K. (2019). Phthalate Metabolites, Hydroxy-Polycyclic Aromatic Hydrocarbons, and Bisphenol Analogues in Bovine Urine Collected from China, India, and the United States. *Environ Sci Technol*, *53*(19), 11524-11531. https://doi.org/10.1021/acs.est.9b04178

Ziashahabi, A., Prato, M., Dang, Z., Poursalehi, R., & Naseri, N. (2019). The effect of silver oxidation on the photocatalytic activity of Ag/ZnO hybrid plasmonic/metal-oxide nanostructures under visible light and in the dark. *Sci Rep*, *9*(1), 11839. https://doi.org/10.1038/s41598-019-48075-7

Ziemann, P. J., & Atkinson, R. (2012). Kinetics, products, and mechanisms of secondary organic aerosol formation. *Chem Soc Rev*, *41*(19), 6582-6605. https://doi.org/10.1039/c2cs35122f

Zou, Z., Wu, H., & Huang, C. (2010). Application research of electrostatic purification device in clean air conditioning system. *Contamination Control & Air-Conditioning Technology*, *2010*(1), 35-37.